

COORDINATION OF GEOLOGICAL AND ENGINEERING RESEARCH IN SUPPORT
OF GULF COAST CO-PRODUCTION PROGRAM

ANNUAL REPORT

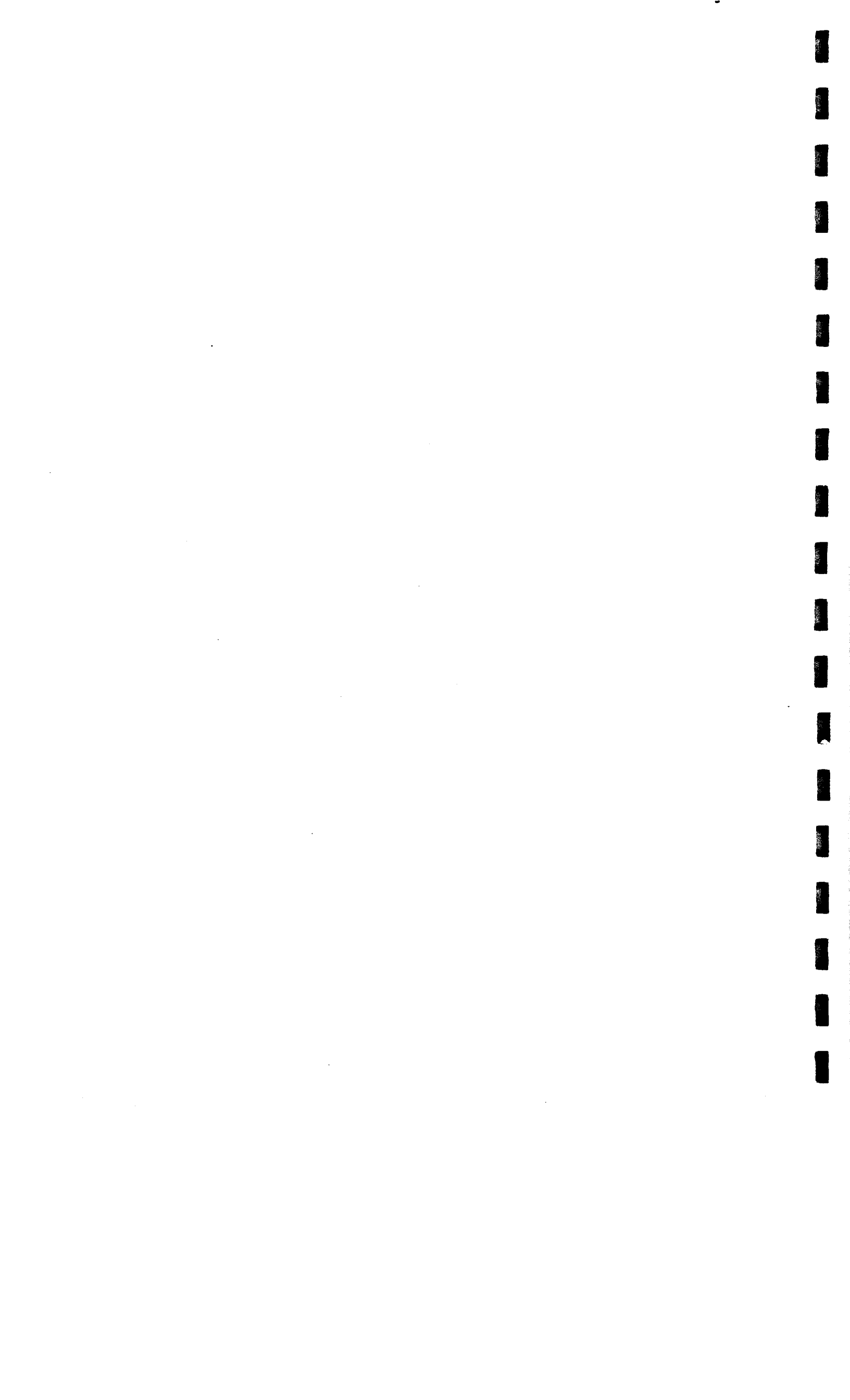
(August 1, 1985 - May 31, 1986)

Prepared by
Malcolm P. R. Light, Mary L. W. Jackson,
and Walter B. Ayers, Jr.

Bureau of Economic Geology
and
Center for Energy Studies
The University of Texas at Austin
Austin, Texas 78713

For
GAS RESEARCH INSTITUTE
Contract No. 5084-212-0924
Scot C. Hathaway, GRI Project Manager

May 1986



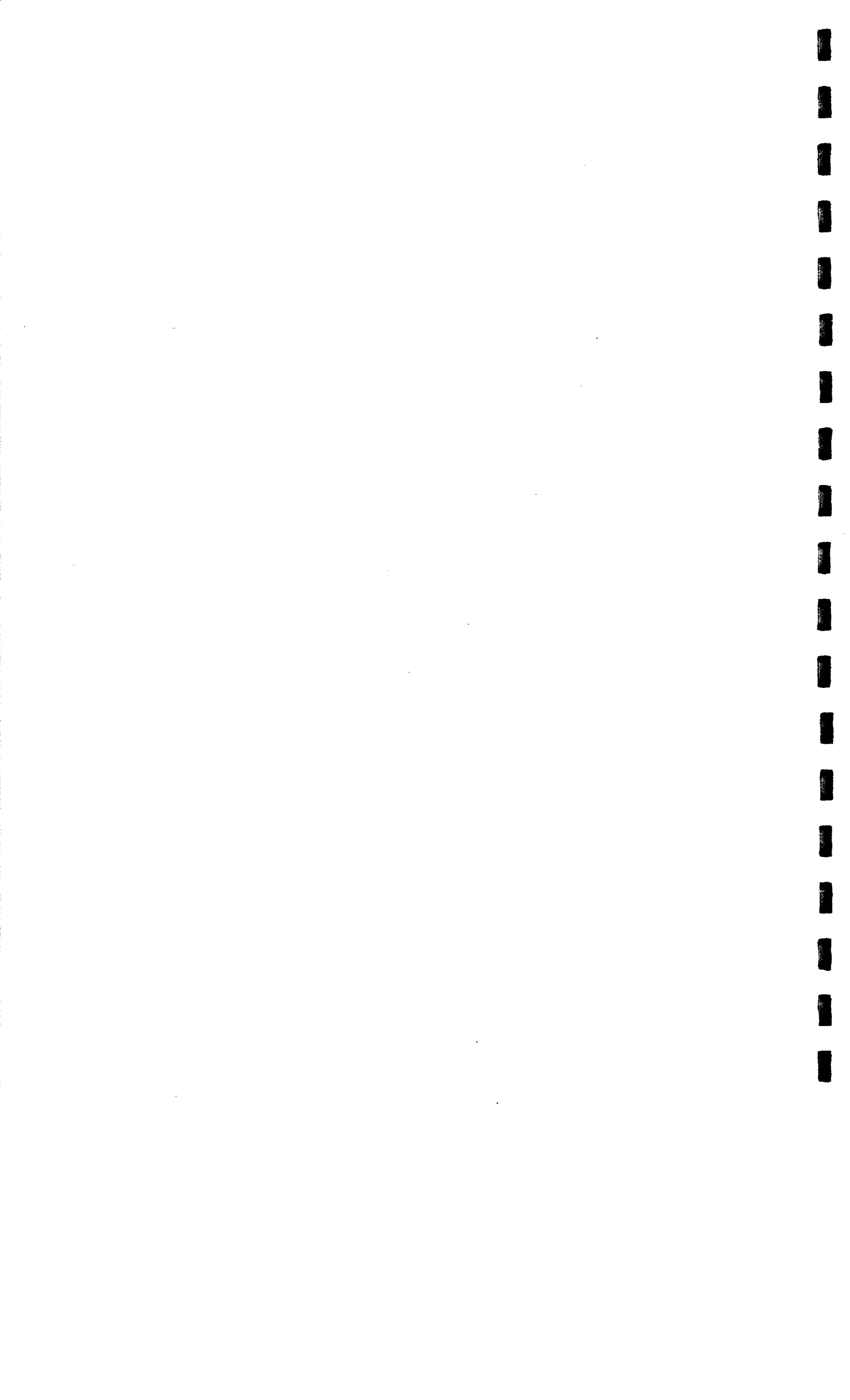
DISCLAIMER

LEGAL NOTICE This report was prepared by the Bureau of Economic Geology as an account of work sponsored by the Gas Research Institute (GRI). Neither GRI, members of GRI, nor any person acting on behalf of either:

- a. Makes any warranty or representation, express or implied, with respect to the accuracy, completeness, or usefulness of the information contained in this report, or that the use of any apparatus, method, or process disclosed in this report may not infringe privately owned rights; or
- b. Assumes any liability with respect to the use of, or for damages resulting from the use of, any information, apparatus, method, or process disclosed in this report.



REPORT DOCUMENTATION PAGE	1. REPORT NO. GRI-86/0161	2.	3. Recipient's Accession No.
4. Title and Subtitle Coordination of Geological and Engineering Research in Support of Gulf Coast Co-Production Program		5. Report Date August 31, 1986 (date published)	
7. Author(s) Malcolm P. R. Light, Mary L. W. Jackson, and Walter B. Ayers, Jr.		6.	
9. Performing Organization Name and Address Bureau of Economic Geology The University of Texas at Austin University Station, Box X Austin, Texas 78713		8. Performing Organization Rept. No.	
12. Sponsoring Organization Name and Address Gas Research Institute 8600 West Bryn Mawr Avenue Chicago, Illinois 60631		10. Project/Task/Work Unit No.	
Project Manager: Scot C. Hathaway		11. Contract(C) or Grant(G) No. (C) 5084-212-0924 (Gas (G) Research Institute)	
		13. Type of Report & Period Covered Annual Report (Aug. 1, 1985-May 31, 1986)	
15. Supplementary Notes		14.	
16. Abstract (Limit: 200 words) Gas fields with co-production potential in the Gulf Coast were selected and evaluated; 150 gas fields were reviewed and 25 were selected, of which Port Acres, Ellis, and Esther fields were evaluated. Reserve estimates are 70 Bcf, 3 to 11 Bcf, and 97 Bcf, respectively. The accuracy of the Frio "A" sandstone reservoir simulation of the Hitchcock N.E. field was improved with a modified depositional model. Bound water, estimated by pyrolysis analyses of the Anahuac and Frio Formation shales, varies from 23 to 29 weight percent. Investigations of the source of gas and condensate in the Frio "A" sandstone indicated that local degassing of adjacent shales apparently added methane to hydrocarbons generated at deeper levels. Diagenetic, hydrocarbon, and geopressure generation zones were related to sediment accumulation and salt dome development, allowing different fluid migration pulses to be differentiated and dated. The effect of several high neutron-capture cross-section trace elements on the neutron log was estimated. Resistivity measurements were made at elevated pressures and temperatures and at intermediate rock wettabilities. A deterministic model was developed for estimating resistivity of the mud filtrate. The authors consulted on logging programs for the Gas Research Institute project.			
17. Document Analysis a. Descriptors Central Texas, East Texas, Louisiana, potential and producing co-production reservoirs, Frio sandstone, Hackberry sandstone, Planulina sandstone			
b. Identifiers/Open-Ended Terms selection and evaluation of co-production reservoirs, hydrothermal model for origin of hydrocarbons and heavy metals, logging research			
c. COSATI Field/Group			
18. Availability Statement Release unlimited		19. Security Class (This Report) unclassified	21. No. of Pages 287
		20. Security Class (This Page) unclassified	22. Price



RESEARCH SUMMARY

Title Coordination of Geological and Engineering Research in Support of Gulf Coast Co-Production Program

Contractor Bureau of Economic Geology and Center for Energy Studies, The University of Texas at Austin
GRI Contract Number: 5084-212-0924

Principal R. J. Finley, D. W. Koppenaar, M. H. Dorfman, and
Investigators H. F. Dunlap

Report August 1985-May 1986
Period Annual Report

Objectives

To select and evaluate gas fields with co-production potential. This involved reexamining favorable test reservoirs listed by Gregory and others (1983) as well as additional reservoirs listed in Dwight's Energydata Co. (1985a,b,c,d,e,f) for Railroad Commission Districts 2, 3, and 4. The Port Acres, Ellis, and Esther fields were evaluated for their co-production potential.

To evaluate the mechanism of secondary gas recovery by co-production in a slightly geopressed watered-out reservoir. This involved additional geologic interpretations of the Hitchcock N. E. field to define the reservoir parameters adequately for reservoir simulation by Dowdle, Fairchild, and Ansell.

To investigate the potential for shale dewatering occurring as a result of fast pressure drawdown during co-production of gas and water.

To investigate the hydrocarbon sources of gas and condensate, i. e., whether they are locally derived or have migrated from deeper levels.

To evaluate the quantitative gas saturation calculations using a variety of well logs run in open hole and cased hole.

To evaluate sanding predictions in wells making high water volumes by compressional and shear velocities from long array digital sonic logs.

To continue the study of short-term variations in mud and mud-filtrate resistivity and their effect upon logging calculations.

To evaluate the pulsed neutron log estimates and changes in gas saturation in the Delee No. 1 and other wells.

To evaluate the effect of certain trace and rare earth elements in formation water or rocks on neutron logs.

Technical
Perspective

Technical coordination and liaison with the Department of Energy in those parts of the geopressured-geothermal project that are of mutual benefit to the Gas Research Institute.

More than 150 gas fields were reviewed; 25 were selected. Port Acres, Ellis, and Esther fields were evaluated. Reserve estimates were similar to estimates made by Eaton Operating Co.

The Hitchcock N.E. field was reviewed with reference to the effect of shale and permeability seals in the Frio "A" sandstone, modifying historical production rates at different well sites.

Shale dewatering was examined in the context of three types of fluid movement: original migration of hydrocarbons into the trap, shale dewatering from burial, and pressure-drawdown dewatering owing to production. Water content of shales adjacent to the Frio "A" sandstone was estimated by geochemical techniques.

The source of the gas and condensate has been investigated by a number of geochemical techniques, but final analyses of rocks and fluids have not yet been completed by the Mineral Studies Laboratory at the Bureau of Economic Geology. Communications were established with Dr. Phillip Randolph of IGT regarding collaborative work on fluid analyses for Hitchcock N.E. and Port Arthur fields. In return for the sampling assistance of IGT, the Mineral Studies Laboratory at the Bureau of Economic Geology has analyzed and characterized and will perform analyses of IGT samples beyond the date stated in the contract proposal. Work has also begun on the brine stability and preservation studies.

The different periods and types of fluid migration that have occurred in the Gulf Coast succession and the different diagenetic, hydrocarbon, and hydrothermal (geopressure) generation zones formed during sediment accumulation were isolated. Compaction and geothermal heating have been modeled with simultaneous structural development of salt domes and salt dome cap rocks.

The accuracy and field applicability of various instruments used to measure mud filtrate resistivity were measured.

A review was made of the techniques for estimating the mud filtrate resistivity that are currently being used by the petroleum industry.

A deterministic model was developed for estimating the Rmf using data from mud engineers' reports.

Analyses were made of data gathered at the GRI Port Arthur Unit 1-6 well.

Results

More than 150 gas fields were reviewed and 25 fields were selected using modified specific selection criteria as outlined by Gregory and others (1983). Further evaluation of these fields is necessary to obtain a new ranking for Gregory's class A, B, and C divisions. A list of the 25 most favorable fields was sent to Eaton Operating Co., who were to approach likely companies to initiate joint ventures in co-production.

Four reservoirs containing dispersed gas were examined for their co-production potential. Reservoirs in Port Acres and Ellis fields produce from the Hackberry Member of the Oligocene Frio Formation, and two reservoirs in Esther field produce from the lower Miocene Planulina Zone. Log-pattern and lithofacies maps, together with stratigraphic position, suggest that the reservoirs are in ancient submarine-fan deposits. Dip-elongate, channel-fill sands are characteristic; reservoir sands pinch out along strike. Growth faults, common in the submarine slope setting, form updip and downdip boundaries, producing combination traps. In Ellis field, co-production accounts for 300 Mcf ($8.5 \times 10^6 \text{ m}^3$) of gas per day. Port Acres field contains the largest remaining reserves, but other technical and economic factors limit co-production there. Recent drilling has extended primary production and delayed co-production in Esther field. The Gas Research Institute requested that further work on the selection and evaluation of potential co-production gas fields be terminated because funds were required for the Port Arthur project.

A fence diagram constructed for the Frio "A" sandstone reservoir in the Hitchcock N.E. field showed five distinct stacked depositional units, each representing a distributary mouth bar sandstone lobe separated by draped shale seals. This data was conveyed to Eaton Operating Co., where it was combined with shale-thickness maps to show the limits of the shale seals. Dowdle, Fairchild, and Ansell have used this information to improve the accuracy of their reservoir simulation of the Hitchcock N. E. field.

The quantity of bound water in Anahuac and Frio Formation shales was estimated by pyrolysis analysis at the Mineral Studies Laboratory, Bureau of Economic Geology. Bound water content varies from 23 to 29 percent by weight, indicating that abundant water is available for shale dewatering at the depth of the Frio "A" sandstone.

Twenty-five samples of formation water from the Delee No. 1 well and possible fluid source rocks (shale, sandstone, carbonate, lignite) were subjected to major- and trace-element analyses at the Mineral Studies Laboratory, Bureau of Economic Geology. These data support a source of the varying iron, manganese from production equipment, and barium from barite-weighting material.

Twenty other samples of formation water from Hitchcock N.E. field and Port Arthur field were also subjected to element analyses by the Mineral Studies Laboratory working in collaboration with the Institute of Gas Technology. Some calibration problems were encountered using the new ICP mass spectrometer for rare earth element analyses of formation waters and rocks, but the instrument has now been modified and rare earth element analyses should be completed within a few months.

A detailed study of the compositions and isotopic nature of fluids, hydrocarbons, and rocks, and the sequence of salt dome and salt dome cap rock formation, has resulted in the isolation of three main periods of fluid flushing in the Gulf Coast Basin. Anhydrites within the salt with high $^{87}\text{Sr}/^{86}\text{Sr}$ ratios suggest early generation of underlying or laterally adjacent fluids rich in radiogenic strontium that were incorporated in the salt during its diapiric rise to the surface. The first major fluid flush occurred less than 25 Ma during major diapirism of the Gulf Coast salt domes. This diapirism removed a large volume of the Louann "mother" salt, caused settling of the Gulf Coast Basin along reactivated growth faults, and produced conduits for the upward migration of fluids derived from Jurassic strata. The brines caused the major conversion of smectite to illite and may have introduced isotopically heavy sulfur into the shallower section. A second fluid flush occurred less than 750,000 to 1 Ma ago and introduced hydrocarbons into the Frio Formation. These late-stage, hydrocarbon-rich, saline hydrothermal fluids migrated up the margins of salt domes and caused the precipitation of several generations of calcite cements. The hydrocarbons were derived from the marine slope shales in the Upper Vicksburg or lower Frio, which have acted as a detachment plane for growth faults in the Frio growth-fault trend. The last fluid flush is younger than 5 Ma and may have begun 35,000 to 130,000 yr ago, whereas it still continues in the upper Frio. The brine was hot (120°C to 180°C , 248°F to 356°F) and saline, contained aromatic hydrocarbons, lead, zinc, and barium, and was derived from about 20,000 ft (6,100 m) in the lower Frio Formation. This deeply derived brine caused the precipitation of Mississippi Valley lead-zinc mineralization in salt dome cap rocks and waterwashed condensates in the upper Frio Formation. The sequence of fluid flushing is consistent with the sequence of mineralization defined by salt dome cap rocks. Fluids present in the lower Frio (deeper than 14,000 ft, 4,270 m) at the Pleasant Bayou test well are highly saline and enriched in iron, manganese, lead, zinc, methane, carbon dioxide, and aromatic hydrocarbons. These lower Frio waters must have migrated into the area recently as they are out of isotopic stability with albite cements that formed less than 5 to 7.5 Ma ago. Isotopic and geochemical stability data suggest that the fluids trapped by geopressure in the lower Frio at the Pleasant Bayou test well are the parent fluids that caused the salt dome cap rock mineralization. The detailed sequence of fluid migration

cap rock mineralization. The detailed sequence of fluid migration defined for the Gulf Coast may allow better estimates to be made of the relative amounts of various fluids introduced into co-production fields using elemental and isotopic fluid identification procedures.

The degree of waterwashing of condensates at any locality is a measure of the transmissibility of the formation and proximity to growth faults where late hot brine migration has occurred. Therefore an areal knowledge of the degree of waterwashing should allow the identification of the major water conduits when this is combined with structural and stratigraphic data. This information is vital in choosing the best locations for production and guard wells during development of a co-production field and could lead to the identification of additional hydrocarbon reservoirs or heavy metal deposits.

Isotopic analyses of gases, condensates, and formation waters suggest that some 50 to 70 percent of the methane and heavy hydrocarbons originated at 20,000 ft, whereas the rest of the methane appears to have been locally derived from the degassing of mature shales. Degassing of mature shales closely interbedded with the Hackberry or Planulina deep marine sandstones could form an additional source of hydrocarbons when large pressure drawdowns are exerted on reservoirs during co-production of gas and water.

The semi-empirical mass balance model (MBM-S) has been applied to mud report data from four Gulf Coast wells that used lignosulfonate muds. Calculated values of mud-filtrate resistivity were too high in the upper several thousand feet and too low in the lower several thousand feet of the wells in question.

Two resistivity meters were judged most suitable for field application because they account for all dissolved ions that contribute to the conductivity of the solution and are fairly simple to use. The sodium ion electrode was judged unsuitable at present for field application because it only accounts for the effects of dissolved NaCl, its use is time consuming, and it is highly sensitive to changes in the environment.

Overton and Lipson's (1958) method of estimating mud-filtrate resistivity when applied to daily measured values of R_m proved to be fairly accurate in most cases in lignosulfonate muds, with a standard error of about 20 percent.

The mass-balance model developed for estimating the resistivity of the mud was more accurate at most depths than log header values of R_{mf} (standard error R_{mf} 31% compared to 61%).

A new correlation of m (cementation exponent) with ϕ (porosity) and k (permeability) was developed. The correlation

should allow estimation of the high-pressure values of m from low-pressure measurements.

Cells were designed for cementation and saturation exponent studies as a function of wettability, pressure, and temperature and resistivity measurement studies as a function of elevated pressure and temperature.

Problems were encountered with the new ICP mass spectrometer at the Mineral Studies Laboratory at the Bureau of Economic Geology in trace and rare earth element studies. The equipment is now being modified. Cadmium forms less than 2 ppm in 23 core samples studied and will not produce a significant effect on the neutron log. The analyses of other trace elements of interest (boron and gadolinium in particular) are still to be done.

Technical Approach

To bring the status of Gregory and others' (1983) class B field up to date, the Bureau of Economic Geology examined all reservoirs within the 134 class B fields. Cumulative production (an indicator of field size), pressure gradient, and number of active wells were used as preliminary ranking criteria during reevaluation. A minimum pressure gradient in the producing zone of greater than 0.25 psi/ft and a minimum bottom-hole shut-in pressure (BHSIP) of 1,000 psi were used as cutoffs so that pressure drawdowns in candidate reservoirs would be high enough to make co-production economically viable. A maximum of 10 active wells per reservoir was another criterion for ranking.

Base maps, a selected number of well logs, and production and reservoir quality data were acquired from Eaton Operating Co., the Texas Railroad Commission, and service companies. This information was used to prepare new cross sections and maps illustrating the stratigraphic characteristics of the Hackberry and Planulina sandstones. Initial gas in place was estimated using initial bottom-hole shut-in pressures and temperatures and the volume of net gas-filled sandstones.

Four cross sections were prepared as a fence diagram and one map to illustrate the stratigraphy and shale breaks of the Frio "A" sandstone. Depositional systems and constituent facies were defined from maps and cross sections and described cores in the Delee No. 1 well.

Bound water was estimated by measuring the percentage of carbon and hydrogen in pyrolyzed shale using an automated CHN analyzer. Elemental analyses of formation waters and rocks are being done by wet chemical, ICP (inductively coupled plasma), and ICP mass spectrometry techniques.

A detailed set of figures showing the simultaneous development of salt domes in the Gulf Coast basin and different diagenetic,

hydrocarbon, and hydrothermal (geopressure) zones was prepared to isolate different periods of fluid flow.

Project
Implications

Results of these projects are an important part of the GRI Co-Production Research Program to locate and evaluate reservoirs where research production tests can be conducted. The best possible geological mapping and definition of reservoir properties are necessary for the reservoir engineering studies designed to enhance gas production. These detailed geochemical studies on the reservoir rock and fluid have also provided improved understanding of the possible sources of the gas and of how the fluids have migrated in the reservoir system.

GRI Project Manager
Scot C. Hathaway



CONTENTS

Evaluation of Favorable Co-production Test Reservoirs.....	1
Geology and Co-production Potential of Submarine-fan Deposits along the Gulf Coast of East Texas and Louisiana.....	5
Introduction.....	5
Hackberry Trend.....	7
Port Acres field.....	9
Introduction.....	9
Production history and structure.....	12
Depositional setting.....	20
Ellis field.....	20
Structure and field history.....	20
Depositional environment and gas occurrence.....	25
Planulina Trend.....	25
Esther field.....	30
Field history, geology, and methodology.....	30
Depositional environment and gas occurrence, 13,700 sand.....	32
Depositional environment and gas occurrence, 14,060 sand.....	37
Reserve Estimates.....	44
Conclusions.....	47
Integrated Hydrothermal Model for the Texas Gulf Coast Basin; Origins of Geopressured Brines and Lead-Zinc, Barium, Uranium, Hydrocarbon, and Cap-rock Deposits.....	49
Introduction.....	49
Diagenetic zone and salt dome model.....	50
Salt dome cap rocks.....	74
Fluid migration in the Oligocene.....	76

Cap-rock formation.....	84
Age of migration events.....	102
Lead-zinc-barite mineralization.....	104
Potential sources of fluids.....	105
Ore carriers.....	108
Late-stage mineralization.....	109
Gulf Coast brines.....	112
Age of mineralization.....	113
Conclusions.....	115
Gas Chromatography, Mass Spectrometry, and Isotopic Analyses of Hydrocarbons from the Hitchcock N.E. Field, Galveston County.....	126
Shale Dewatering during Compaction and Production.....	133
Immediate Research Plans.....	135
Acknowledgments.....	146
References.....	147
Appendices.....	175

FIGURES

1. Hackberry and <u>Planulina</u> trends, Louisiana and Texas.....	6
2. Frio and Hackberry stratigraphy, index fossils, and electric-log marker horizons (A2-A5).....	8
3. Submarine-fan environments and representative log patterns.....	10
4. Structure map, top of the lower Hackberry interval, Port Acres field.....	11
5. Cross section through Port Acres field.....	13
6. Fence diagram, Hackberry lower reservoir, Port Acres field.....	14
7. Structure map on top of Hackberry Main sand, Port Acres field.....	15
8. Spontaneous potential log patterns, Hackberry lower reservoir, Port Acres field.....	16

9. Net-sand distribution in lower Hackberry sequence, Port Acres - Port Arthur area.....	17
10. Net-sand map of lower Hackberry interval, Port Acres field.....	18
11. Net-gas-sand map, Hackberry lower reservoir, Port Acres field.....	19
12. Log-pattern map, Hackberry lower reservoir, Port Acres field.....	21
13. Structure map, top of <u>Nodosaria</u> 3 sand, Ellis field.....	22
14. Fence diagram, <u>Nodosaria</u> 3 interval, Ellis field.....	23
15. Fault plane map, <u>Nodosaria</u> 3 sand, Ellis field.....	24
16. Net-sand map, <u>Nodosaria</u> 3 sand, Ellis field.....	26
17. Log-pattern map, <u>Nodosaria</u> 3 sand, Ellis field.....	27
18. Net-gas-sand map, <u>Nodosaria</u> 3 sand, Ellis field.....	28
19. Structure on top of <u>Cristellaria</u> 5 sand.....	31
20. Structure map on top of 13,700 sand.....	33
21. Cross section B-B'	34
22. Sand isolith map, 13,700 sand.....	35
23. Log-pattern map, 13,700 sand.....	36
24. Net thickness of gas-bearing sand, 13,700 sand.....	38
25. Structure map on top of 14,060 sand.....	40
26. Sand isolith map, 14,060 sand.....	41
27. Log-pattern map for 14,060 sand.....	42
28. Strike section A-A'	43
29. Net thickness of gas-bearing sand, 14,060 sand.....	45
30. Location of Pleasant Bayou geopressured-geothermal test well and Hitchcock N.E. field.....	51
31. Model depicting the addition of radiogenic strontium to sulfates in the primary depositional environment.....	52
32. Model depicting the addition of radiogenic strontium to sulfates within the salt stock.....	54
33. Generalized, probable Triassic lithofacies distribution, Gulf of Mexico basin.....	55

34. Schematic dip section illustrating the offlapping Tertiary stratigraphic sequence of the Texas Gulf Coastal Plain and a west-to-east section across the East Texas Basin.....	56
35. Model depicting the development of diagenetic, geopressed-geothermal and hydrocarbon generation zones and salt dome and salt dome cap-rock formation and mineralization for the coastal basin of the Gulf Coast.....	61
36. Variation of source fluid and diagenetic mineral and ore temperatures through geologic time for Hockley dome.....	62
37. Proportion of illite and smectite in mixed-layer clay versus depth, Pleasant Bayou No. 1 well.....	63
38. Fluid pressure, geothermal, and thermal maturity profiles for the Pleasant Bayou No. 2 test well.....	64
39. Potassium versus chloride for Frio Formation water samples within the Houston delta system.....	66
40. Generation of gases from organic compounds.....	68
41. Schematic cross section of a salt dome showing a fully developed set of cap rock lithotypes.....	79
42. Classification of antithetic and homothetic faults around salt stocks.....	80
43. Stylized stratigraphic dip section across the Texas Gulf Coast.....	82
44. Six-stage sequence showing the development of salt dome cap rocks.....	85
45. $^{87}\text{Sr}/^{86}\text{Sr}$ versus $1/\text{Sr}$ for Hockley anhydrite samples.....	89
46. $\delta^{13}\text{C}$ of calcites versus depth in Oakwood cap rock.....	92
47. Schematic diagram showing the characteristic closed system behavior of the two coexisting phases, CH_4 and CO_2 , during mineral precipitation.....	94
48. $\delta^{18}\text{O}$ of calcites versus depth in Oakwood cap rock.....	98
49. $\delta^{13}\text{C}$ of methane and carbon dioxide showing stability variation with temperature.....	100
50. Burial history diagram for the Hitchcock N.E. field.....	103
51. General paragenesis showing the relationships between basin maturation and cap rock evolution.....	116

52. Mole ratios of Brazoria County waters versus depth and seawater.....	117
53. Chlorine-bromine ratio versus total dissolved solids for wells of the Gulf Coast region of Texas.....	119
54. Mass spectrograms of the aromatic fraction of condensates, Delee No. 1 and Prets No. 1 wells, Hitchcock N.E. field.....	127
55. Structure map on top of the Frio "A" pay zone.....	129
56. Diagrams showing hydrocarbon generation zones versus thermal maturity, percentage C ₂ versus $\delta^{13}\text{C}$ (methane), δD (methane) versus $\delta^{13}\text{C}$ (methane), and $\delta^{13}\text{C}$ (ethane) versus $\delta^{13}\text{C}$ (methane) for gases.....	132
57. Sodium versus chloride in brines from the Houston delta system.....	136
58. Calcium versus chloride in brines from the Houston delta system.....	137
59. Strontium versus chloride in brines from the Houston delta system.....	138
60. Boron versus chloride in brines from the Houston delta system.....	139
61. Magnesium versus chloride in brines from the Houston delta system.....	140
62. Iron versus chloride in brines from the Houston delta system.....	141
63. Manganese versus chloride in brines from the Houston delta system.....	142
64. Lithium versus chloride in brines from the Houston delta system.....	143
65. Bromide versus chloride in brines from the Houston delta system.....	144
66. δD (SMOW) versus depth in brines from the Houston delta system.....	145

Tables

1. Top 25 gas fields by district for districts 2, 3, and 4 ranked by production.....	3
2. Reserve calculations, Port Acres, Ellis, and Esther fields.....	39
3. Geochemical characterization of principal ground-water regimes of the northwestern Gulf Coast Basin.....	59
4. Upper temperature limits for the growth of bacteria.....	96
5. Stable isotope analyses, Delee No. 1 and Prets No. 1 wells.....	131
6. Calculated bound shale water, Delee No. 1 well.....	134

EVALUATION OF FAVORABLE CO-PRODUCTION TEST RESERVOIRS

by Mary L. W. Jackson, assisted by Wendy D'Attilio

Gregory and others (1983) evaluated numerous gas fields to select favorable test reservoirs for co-production. Frio/Vicksburg and Wilcox fields on the Texas Gulf Coast were screened using specific criteria and classified into three categories: (1) class A fields, most favorable for co-production; (2) class B fields, having marginal potential or needing more data for evaluation; and (3) class C fields, those rejected as prospects. Only the Port Arthur field in Jefferson County was ranked as a class A field, and it was evaluated in detail by Gregory and others (1983). However, many class B fields were rejected because of their active status. Periodic reevaluation of class B fields is appropriate, therefore, as field conditions change and wells begin to water out.

To bring the status of class B fields up to date, the Bureau of Economic Geology (BEG) examined all reservoirs within each of the 134 class B fields. Cumulative production (an indicator of field size), pressure gradient, and number of active wells were used as preliminary ranking criteria during reevaluation. A minimum pressure gradient in the producing zone of greater than 0.25 psi/ft and a minimum bottom-hole shut-in pressure (BHSIP) of 1,000 psi were used as cutoffs so that pressure drawdowns in candidate reservoirs would be high enough to make co-production economically viable. A maximum of 10 active wells per reservoir was another criteria for ranking.

For each reservoir, cumulative production was taken from Dwight's Energydata Co. (1985d,e,f) for the inactive wells. To this number was added the cumulative production, by well, of the active wells (Dwight's Energydata Co., 1985a,b,c). The total cumulative production was entered into the computer. After all cumulative

production data for each reservoir were entered, the reservoirs were sorted and the 50 largest reservoirs listed.

In addition to the fields listed by Gregory, all gas reservoirs listed in Dwight's Energydata Co. (1985a,b,c,d,e,f) for Railroad Commission Districts 2, 3, and 4 were screened by BEG. Those with cumulative production above 1×10^{11} Mcf were added to the top 50 from Gregory's list and included in the reevaluation process, making a total of 119 listed reservoirs. The combined list was again ranked according to cumulative production, and the number of active wells was identified. For those fields with more than zero but fewer than 10 active wells, pressure gradient was calculated by dividing the bottom-hole pressure (BHP) by the average depth of the perforated zone. Data were obtained from Dwight's Energydata Co. (1985a,b,c,d,e,f). Reservoirs were eliminated from the list if they had greater than 10 or no active wells or pressure gradients of less than 0.25 psi/ft (including automatically wells with BHSIP less than 1,000 psi). Reservoirs with no BHP data were also eliminated.

The top 25 fields selected in this manner are listed by size in table 1. Further evaluation of these fields is necessary to obtain a new ranking for Gregory's class A, B, and C divisions. Should funding become available for more co-production test sites, important reservoir characteristics such as temperature, permeability, and total number of wells in the reservoir must be obtained for the fields in table 1.

Table 1. Ranked fields with co-production potential.

Rank	Field (County)	Reservoir	Total cumulative production (Mcf)	Average pressure gradient (psi/ft)
1	Clear Lake, W. (Harris)	Frio	$1.23 \cdot 10^{11}$	0.31
2	Anahuac (Chambers)	Anahuac	$1.14 \cdot 10^{11}$	0.35
3	Blanconia (Bee)	4000 Sinton	$1.04 \cdot 10^{11}$	0.31
4	Yorktown (DeWitt)	Wilcox 11,000 Lo.	$4.83 \cdot 10^{10}$	0.26
5	Buck Snag (Colorado)	Frio 3770	$3.68 \cdot 10^{10}$	0.37
6	Fishers Reef (Chambers)	Frio 8200	$2.92 \cdot 10^{10}$	0.41
7	Duncan Slough (Matagorda)	Frio-6	$1.90 \cdot 10^{10}$	0.30
8	Cabeza Creek (Goliad)	Melrose	$1.83 \cdot 10^{10}$	0.33
9	Encinal Channel (Nueces)	FB-C, M-4	$1.75 \cdot 10^{10}$	0.41
10	Laguna Larga (Kleberg)	K-3	$1.46 \cdot 10^{10}$	0.43
11	Clayton (Live Oak)	Massive	$1.30 \cdot 10^{10}$	0.27
12	Umbrella Point (Chambers)	F14	$9.69 \cdot 10^9$	0.44
13	Encinal Channel (Nueces)	FB-A, M-2	$8.92 \cdot 10^9$	0.33
14	Bonnie View (Refugio)	4700	$5.31 \cdot 10^9$	0.39
15	Chapman Ranch (Nueces)	C-16	$5.17 \cdot 10^9$	0.37
16	Cecil Noble (Colorado)	Wilcox 7925	$4.87 \cdot 10^9$	0.41
17	Burnell (Karnes)	Wilcox 7300	$4.07 \cdot 10^9$	0.38

Table 1. (cont.)

Rank	Field (County)	Reservoir	Total cumulative production (Mcf)	Average pressure gradient (psi/ft)
18	Columbus (Colorado)	12-B Wilcox	$4.05 \cdot 10^9$	0.31
19	New Ulm (Colorado)	New Ulm	$3.85 \cdot 10^9$	0.40
20	Collins Lake (Brazoria)	Frio 11,400 FB-B	$3.24 \cdot 10^9$	0.56
21	Wilson Creek (Matagorda)	10,000 sd FB-C	$3.21 \cdot 10^9$	1.00
22	Tidehaven (Matagorda)	10,500	$3.18 \cdot 10^9$	0.38
23	Stedman Island (Nueces)	7300	$3.17 \cdot 10^9$	0.30
24	Mayes, S. (Chambers)	Frio 19	$2.89 \cdot 10^9$	0.52
25	Trull (Matagorda)	Tex.-Miss #2A, N.	$2.65 \cdot 10^9$	0.29

GEOLOGY AND CO-PRODUCTION POTENTIAL OF SUBMARINE-FAN DEPOSITS ALONG THE GULF COAST OF EAST TEXAS AND LOUISIANA

by Mary L. W. Jackson, W. B. Ayers, Jr., and M. P. R. Light

INTRODUCTION

During conventional production from a water-drive gas reservoir, mobile gas is removed from the gas cap. A considerable amount of dispersed gas remains in the water, however, after the field has watered out (Gregory and others, 1984). This dispersed gas can be recovered through co-production (the simultaneous production of gas and water). During co-production, large amounts of water are pumped to the surface, lowering reservoir pressure and causing dispersed gas to expand; the gas then moves to the co-producing well and is produced with the water (Gas Research Institute, undated). If the reservoir has sufficient residual pressure and the pumped water can be disposed of easily, extended production of a field may be economically viable (Gregory and others, 1984). To avoid costly well reentry or drilling of new wells, co-production is best initiated in a watered-out reservoir before the wells have been plugged.

Four reservoirs with co-production potential were selected for detailed study. The reservoirs are located in Port Acres (Texas) and Ellis and Esther (Louisiana) fields (fig. 1). The lower Hackberry and Nodosaria 3 reservoirs, in Port Acres and Ellis fields, respectively, are productive from the Hackberry Member of the Frio Formation, and the two Planulina Zone reservoirs in Esther field are productive from lower Miocene sands. Several factors that determine the suitability of a reservoir for co-production, such as porosity, permeability, and reservoir volume, relate to the geology of the reservoir. Therefore, for each reservoir selected for

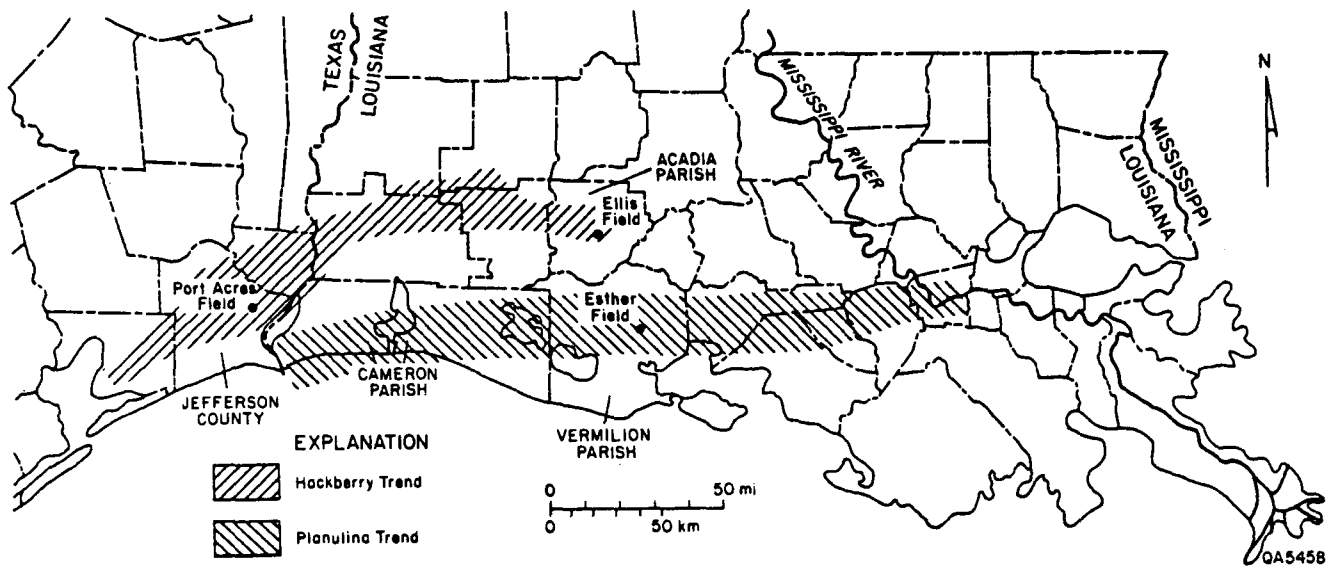


Figure 1. Hackberry and Planulina trends, Louisiana and Texas.

study, all available data were used to interpret the depositional setting of the reservoir sand, the trapping mechanisms, and the volume of the reservoir. Original gas in place and remaining reserves were calculated, and the co-production potential of each field was assessed.

HACKBERRY TREND

The Frio Formation (Oligocene) is a major progradational wedge of dominantly sandy sediment that extends from Texas to Louisiana. Previous workers divided the Frio into three units using log character. In this interpretation the Hackberry Member is laterally equivalent to middle Frio sediments (Ewing and Reed, 1984). The upper boundary of the Hackberry sequence is marked by Marginulina texana, and for the purpose of this paper the lower Hackberry includes the Nodosaria blanpiedi zone, although there is some dispute over the lower boundary of the Hackberry (Le Vie, 1985) (fig. 2).

The Hackberry Member was probably deposited as a submarine-fan complex (Paine, 1968); it is composed mainly of turbidite, or gravity-flow, deposits. The Hackberry Embayment, containing Hackberry submarine fans, extends from southeast Texas eastward to south-central Louisiana (Ewing and Reed, 1984) (fig. 1). The updip limit of Hackberry sediments is the Hartburg flexure, which is more or less coincident with the oldest growth faults in the Frio (Le Vie, 1985). The unit thickens basinward, attaining more than 3,000 ft (900 m) (Paine, 1962). The lower Hackberry is relatively sand rich, with nearly continuous sand sequences up to 800 ft (240 m) thick; the upper Hackberry is almost entirely mud.

Depositional channel-sand axes of the Hackberry trend northwest-southeast in Texas and north-south in Louisiana (Ewing and Reed, 1984). Hackberry reservoir

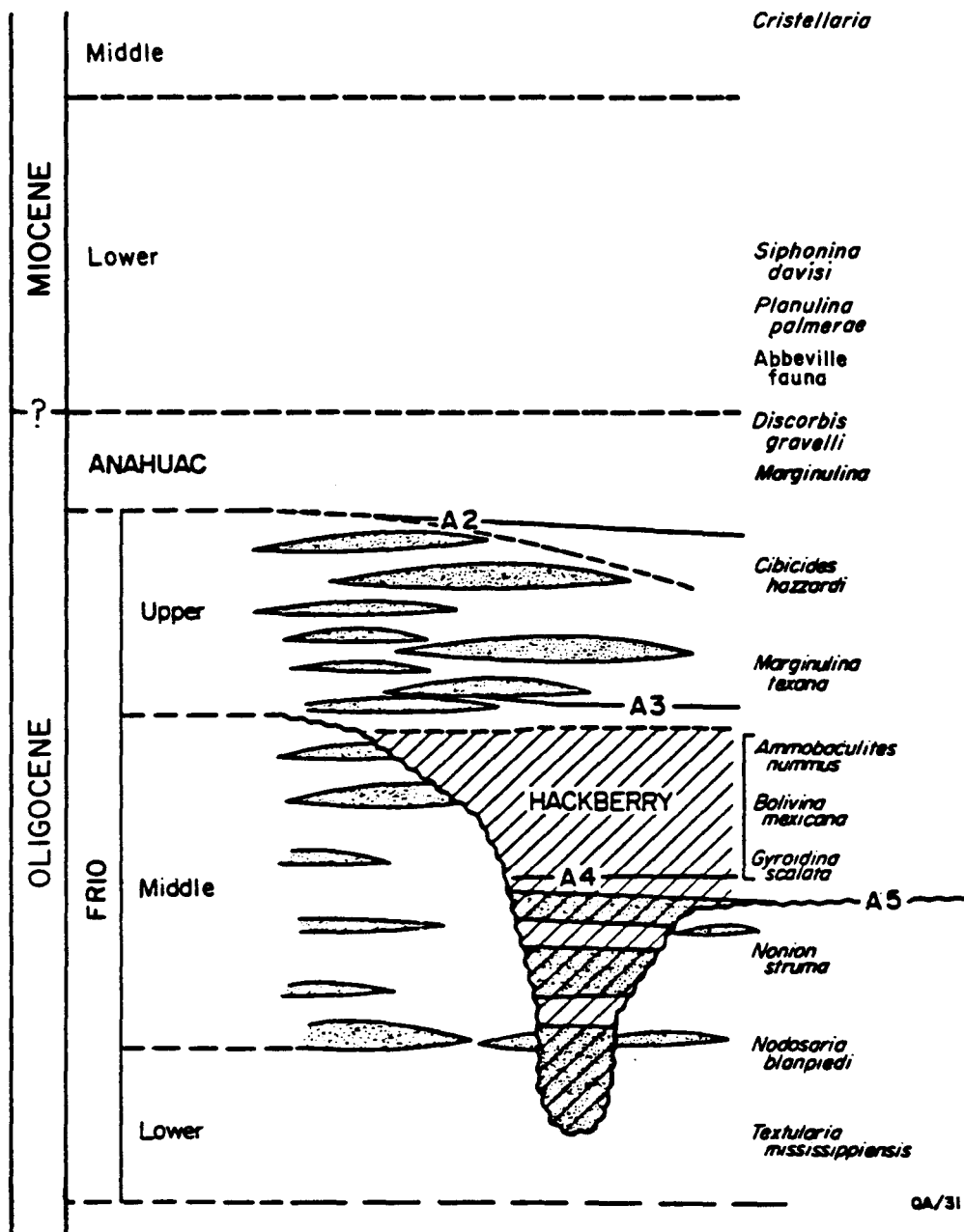


Figure 2. Frio and Hackberry stratigraphy, index fossils, and electric-log marker horizons (A2-A5) (modified from Ewing and Reed, 1984).

sands are highly lenticular and dip elongate; they are an important producing trend in the Gulf Coast (Le Vie, 1985).

A model of submarine-fan sub-environments (Walker, 1979) linked with spontaneous potential log patterns representing the different sub-environments (Ewing and Reed, 1984) (fig. 3) was used to interpret the environments present in the Port Acres and Ellis Hackberry reservoirs.

Port Acres Field

Introduction

Port Acres field is located in east-central Jefferson County, Texas (fig. 1). Previous work on the Hackberry Member in this area of southeast Texas includes a report on the Frio Formation (Reedy, 1949), a study on cores from two wells in Jefferson County (Berg and Powers, 1980), a discussion of geology and early production history of the adjacent Port Acres and Port Arthur fields (Halbouty and Barber, 1961), and most recently a report on depositional systems and structural controls of Hackberry sandstone reservoirs in Jefferson and Orange Counties (Ewing and Reed, 1984).

Marker A4, based on log character and established in the Port Acres - Port Arthur area by Ewing and Reed (1984) (fig. 2), was used in this study as the approximate top of the lower Hackberry Member (fig. 4). Reference to cross sections from Ewing and Reed (1984) aided correlation of the 66 well logs used in the Port Acres field study. Well log identification numbers are shown on figure 4; structure and sand values not shown on figures are listed in appendix A.

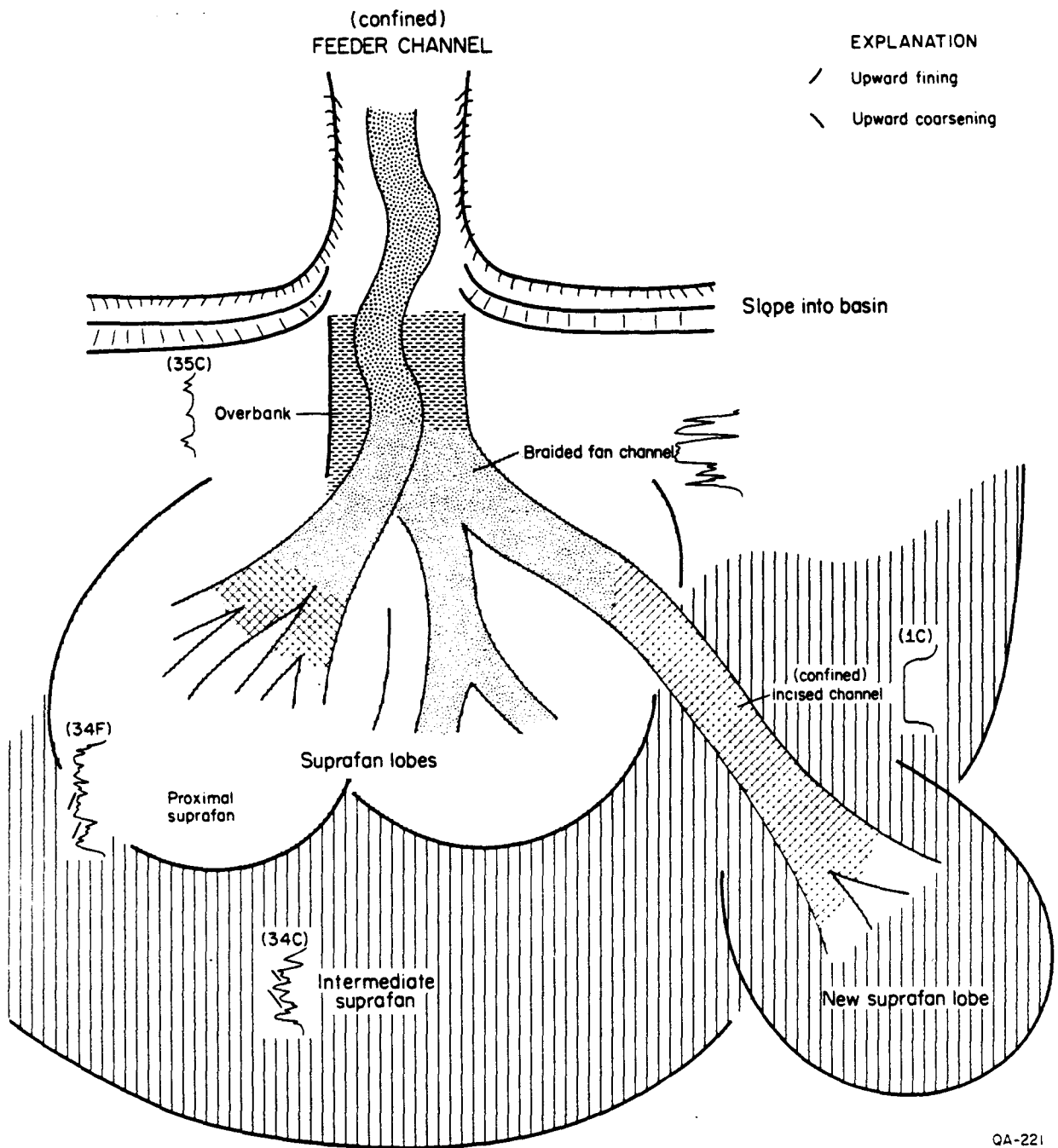


Figure 3. Submarine-fan environments and representative log patterns (from Ewing and Reed, 1984, after Walker, 1979).

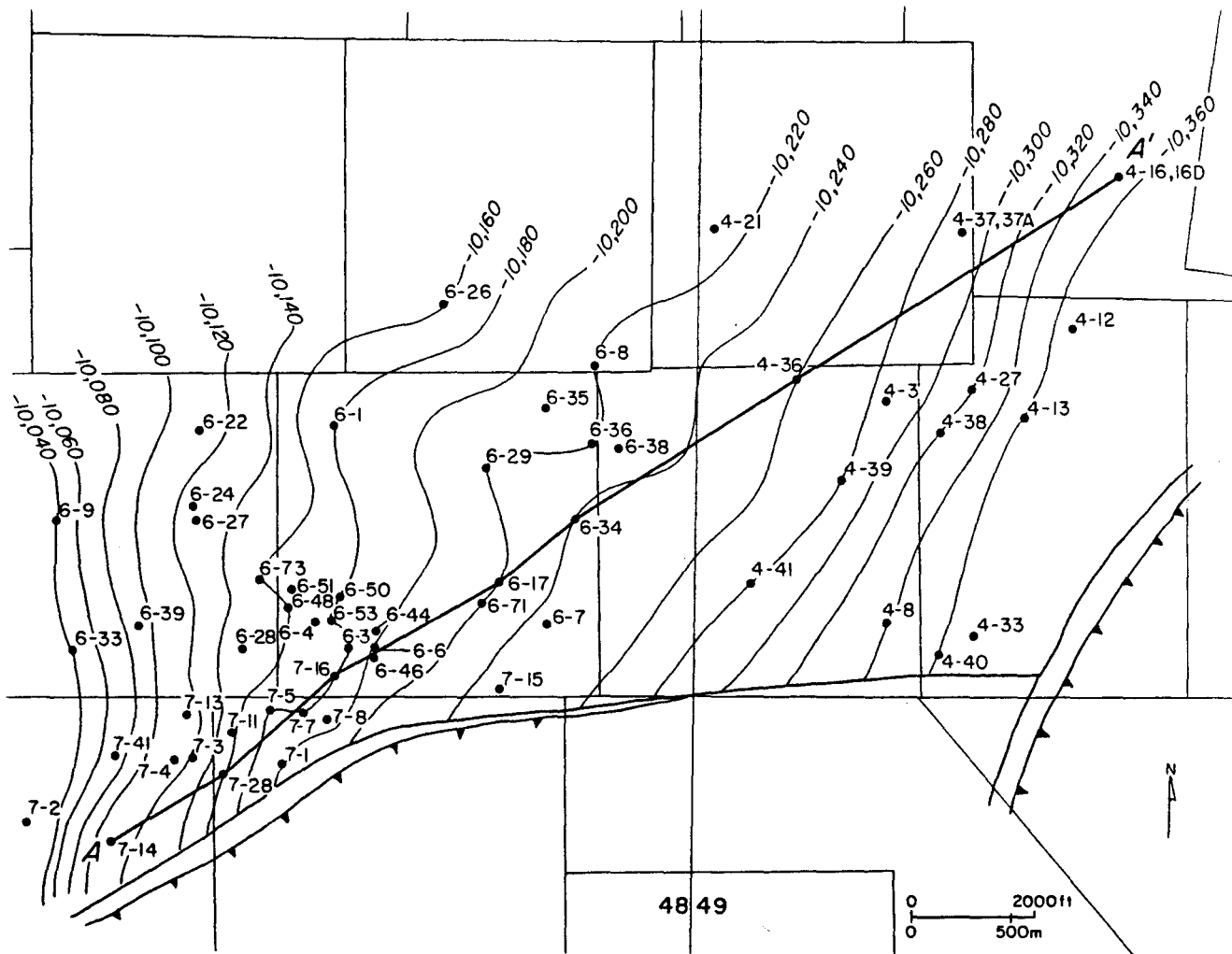


Figure 4. Structure map, top of the lower Hackberry interval (marker A4 on fig. 2), Port Acres field. Wells in the 48- and 49- Tobin grid sections and corresponding structure values are listed in appendix A.

Production history and structure

The productive area of the lower Hackberry reservoir in Port Acres field is about 2,515 acres ($1.0 \times 10^7 \text{ m}^2$). At present, only one well produces gas and condensate from lower Hackberry sands; the field has been "substantially abandoned" since 1978 (Howell and others, 1985). The Hackberry "Main" sand, designated as the 10,500 lower Hackberry reservoir, has produced more than 307 Bcf ($8.7 \times 10^9 \text{ m}^3$) (Dwight's Energydata Co., 1985b,e) since discovery in 1957. The Hackberry 10,450 sand, a stringer sand above the Hackberry Main sand, also has produced gas (fig. 5).

Gas in the reservoir is concentrated in the uppermost 140 ft (43 m) of lower Hackberry sands (figs. 5 and 6). Gas-bearing sands are separated from deeper water-bearing sands by a shale wedge that is 30 ft (9 m) or more thick.

A growth fault with up to 600 ft (180 m) of displacement separates Port Acres field from Port Arthur field to the east. Structure contours on top of the Hackberry Main sand indicate a pronounced anticline developed on the upthrown side of a minor fault; this fault forms a seal on the southern side of the reservoir (fig. 7). Reservoir sands decrease rapidly in thickness to the north and east of the field, and this pinch-out completes the seal on the reservoir (fig. 8).

A sand distribution map of the Port Acres - Port Arthur area defines a canyon axis to the northeast of Port Acres field containing sand thicknesses greater than 600 ft (180 m) (Gregory and others, 1984) (fig. 9). An arm of the canyon-fill sand extends south into Port Acres field and is prominent east of the main fault (fig. 10). However, this area of thicker sands does not contain the most gas. Comparison between figure 7 and figure 11 shows that the western, shallower side of the field, a broad area with 150 to 200 ft (46 to 61 m) of sand thickness, is the

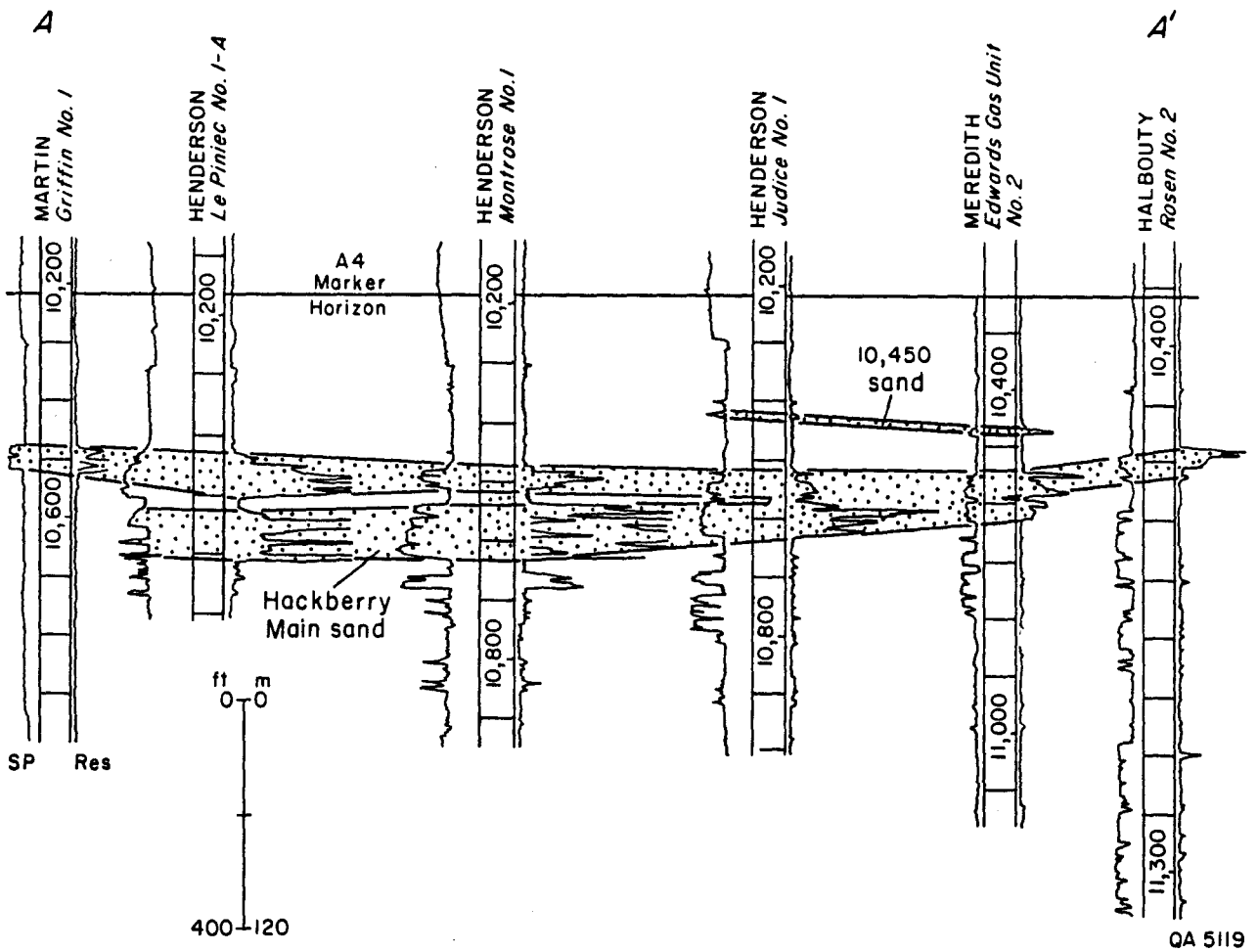


Figure 5. Cross section through Port Acres field; location of section shown on figure 8.

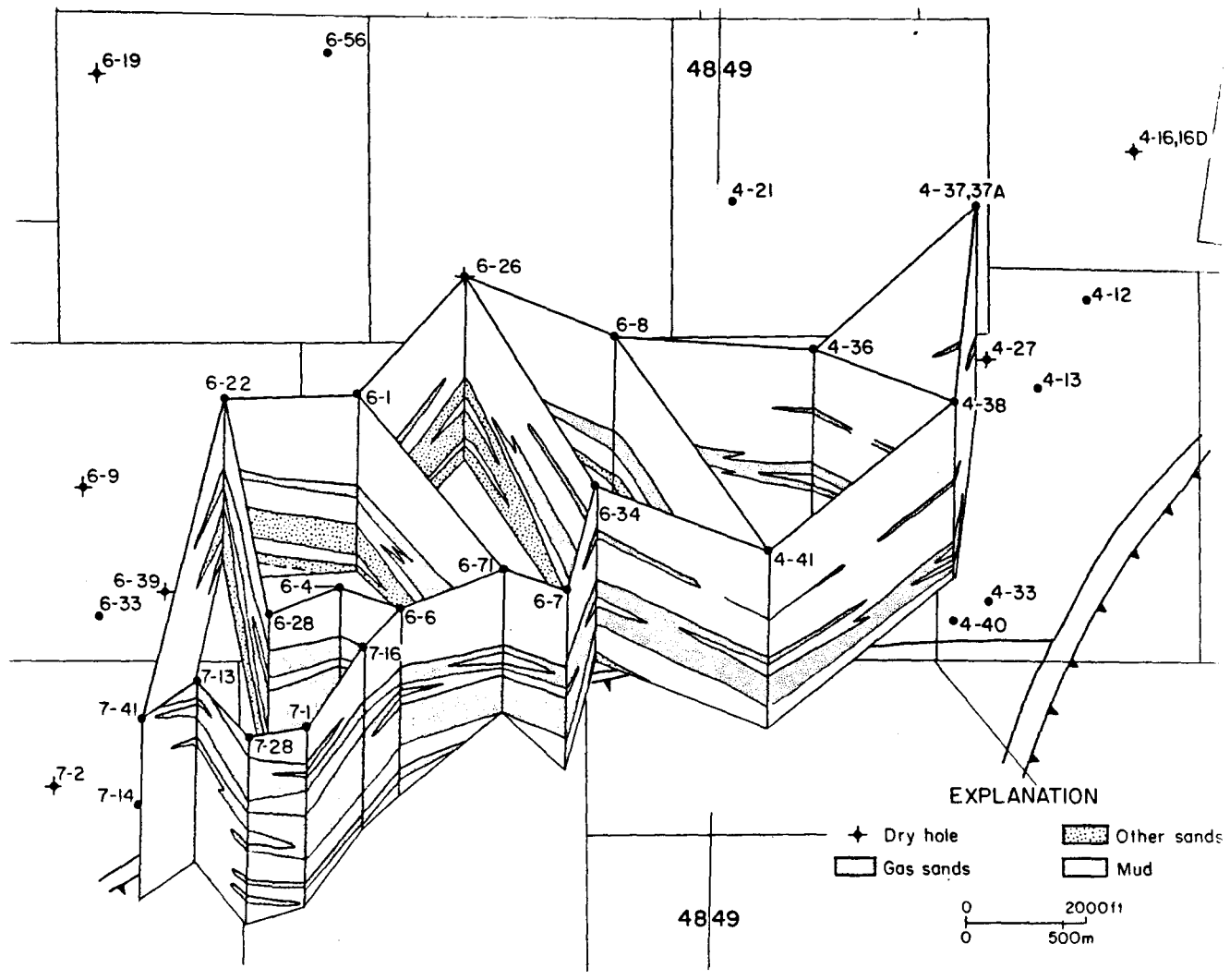


Figure 6. Fence diagram, Hackberry lower reservoir, Port Acres field. Gas sands pinch out rapidly to the west and gradually to the east and north.

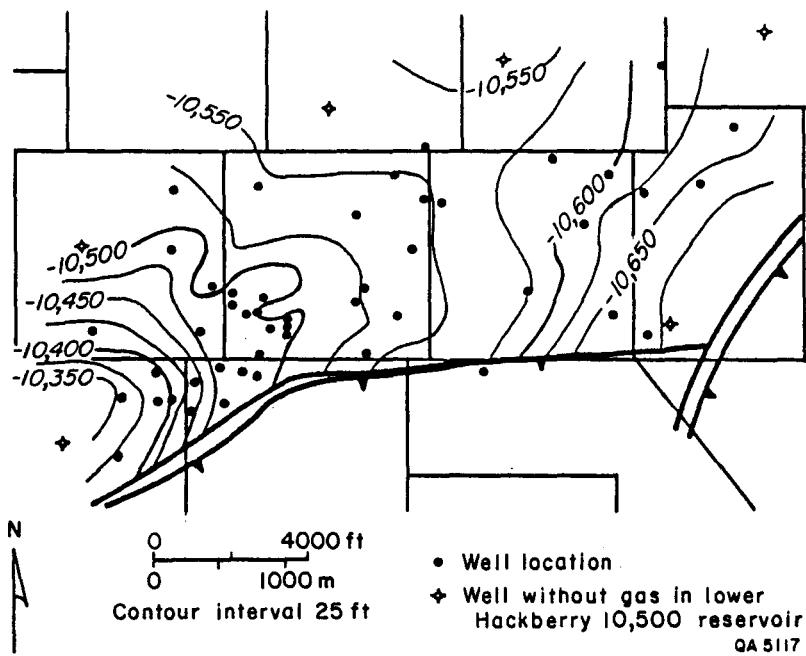


Figure 7. Structure map on top of Hackberry Main sand, Port Acres field. Note broad area in left-center of field.

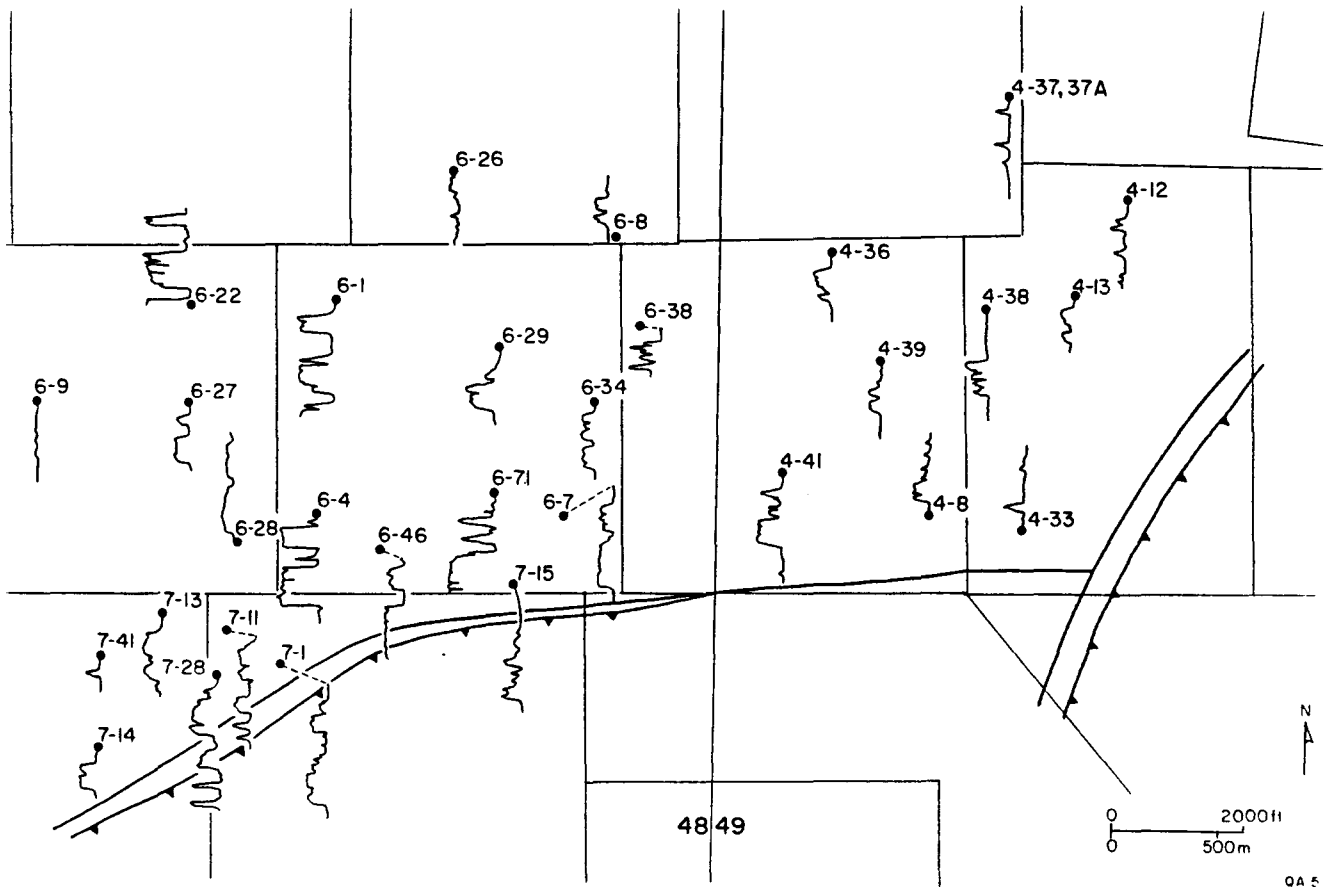


Figure 8. Spontaneous potential log patterns, Hackberry lower reservoir, Port Acres field. Sand pinch-out is evident to the north and east.

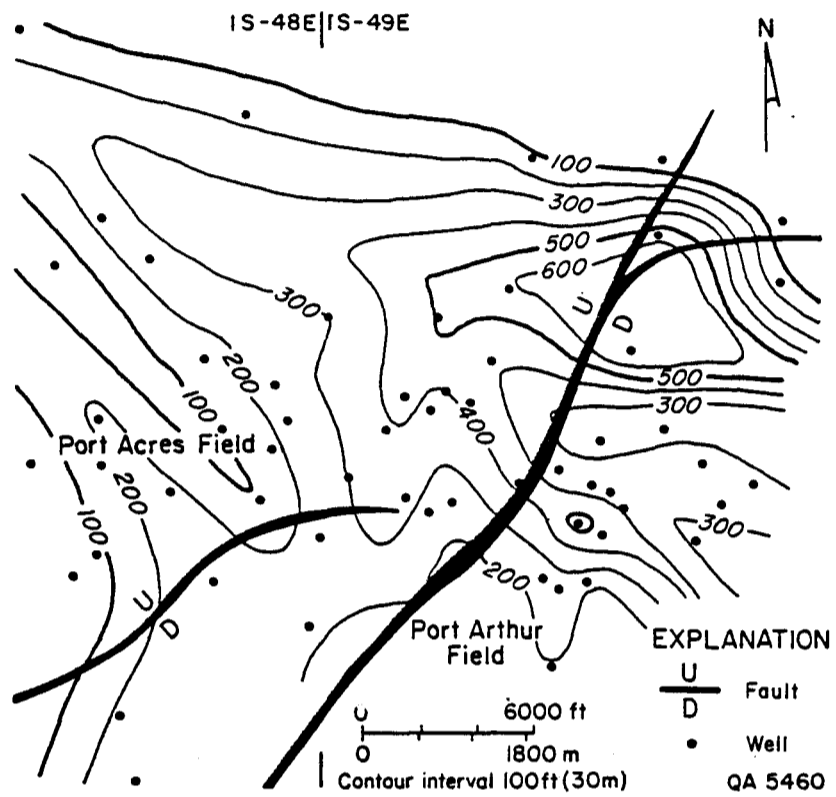


Figure 9. Net-sand distribution in lower Hackberry sequence, Port Acres - Port Arthur area (from Gregory and others, 1984).

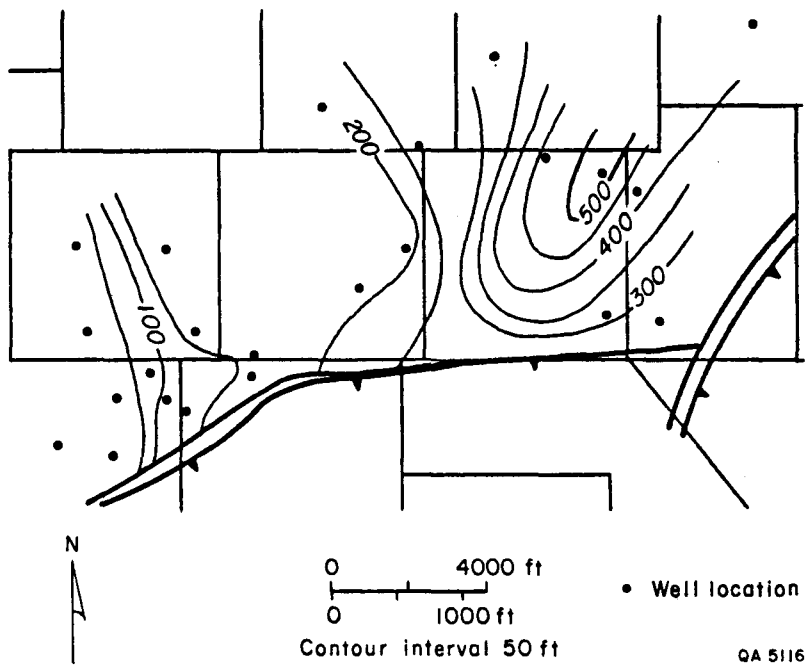


Figure 10. Net-sand map of lower Hackberry interval, Port Acres field. Highest net-sand values lie on the east side of the field.

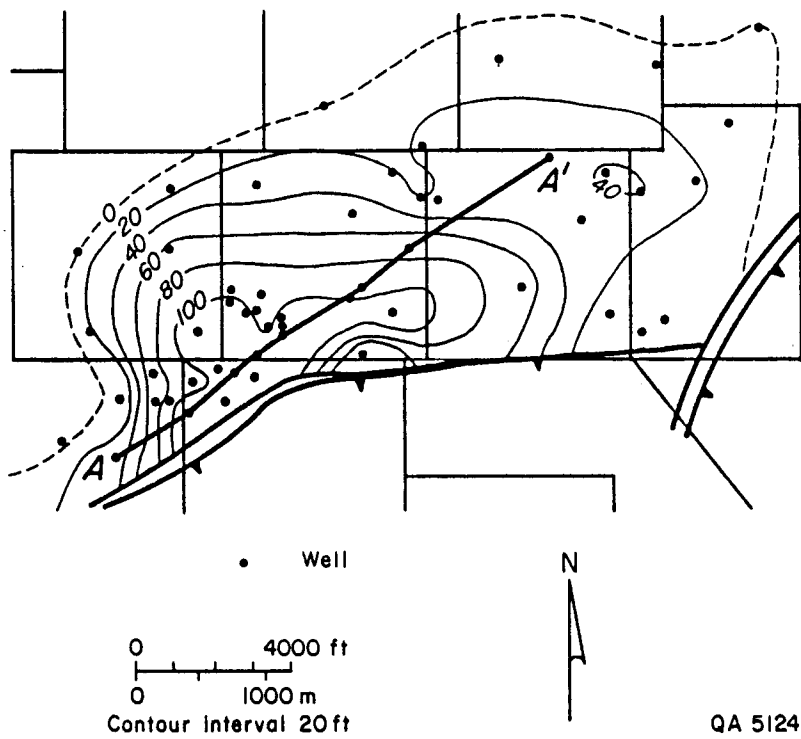


Figure 11. Net-gas-sand map, Hackberry lower reservoir, Port Acres field. High net-gas-sand values coincide with broad area on figure 7.

main gas-bearing area; structural control is more important than sand thickness in the main part of the reservoir. Sand thickness decreases rapidly to the west, where Hackberry sediments are confined by the canyon walls.

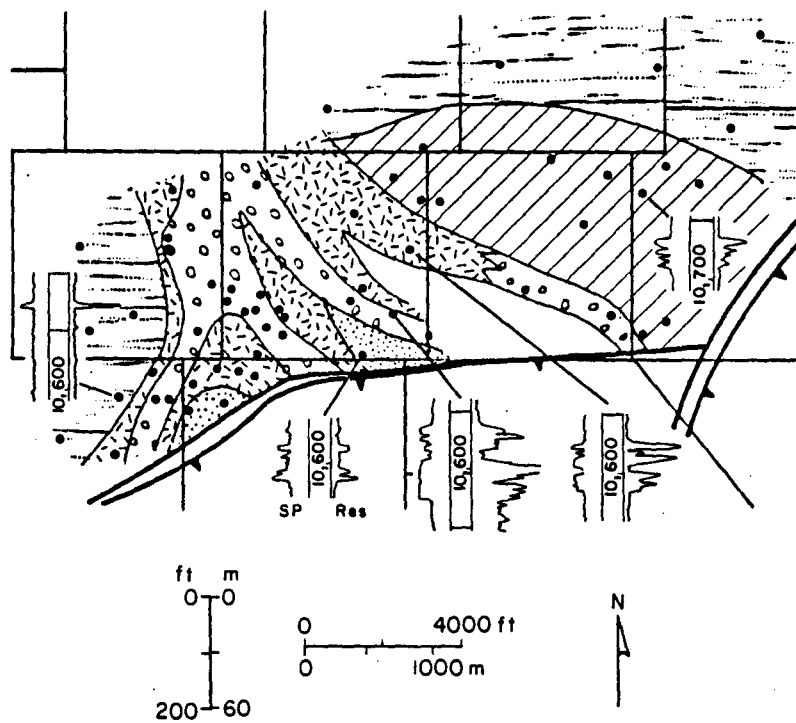
Depositional setting

Dip alignment of Hackberry sands in the Port Acres area is evident (figs. 9 and 10), suggesting deposition in the proximal portion of the submarine-fan system. The log patterns suggest a braided channel system with several incised channel-fill sands (fig. 12). Spontaneous potential (SP) log patterns of the Hackberry Main sand in the central part of the field are blocky, indicating channel-fill sands; patterns on the eastern half of the field show thinner, upward-fining sands, interpreted as intermediate suprafan deposits (figs. 8 and 12). These sands pinch out in the eastern part of the field and to the north, where they interfinger with sand-poor overbank deposits.

Ellis Field

Structure and field history

Ellis field is located in Acadia Parish, Louisiana (fig. 1). Major growth faults bound the field on the northwest and on the south (Paine, 1962; Sun Oil Co., 1963) (fig. 13). The lower Hackberry Nodosaria 3 reservoir sands both pinch out and are faulted downward on the east, sealing them against slope muds. A fault with less than 150 ft (46 m) of displacement crosses the reservoir from northeast to southwest, dividing it into two sections that maintain communication of fluids (Howell and others, 1985) (figs. 14 and 15). The combined productive area of the



EXPLANATION

Submarine-fan facies

- | | |
|---------------------|-----------------------|
| Incised channel | Intermediate suprafan |
| Braided fan channel | Overbank |
| Proximal suprafan | Well |

QA 5115

Figure 12. Log-pattern map, Hackberry lower reservoir, Port Acres field. Channels are interpreted to trend north-south.

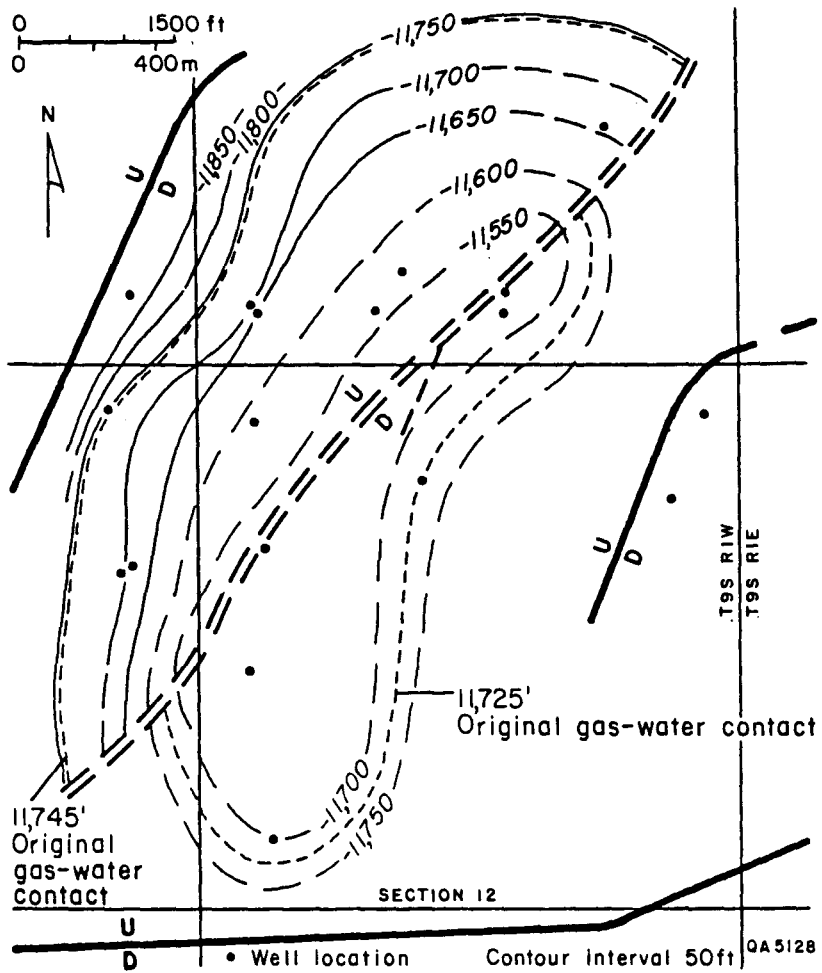


Figure 13. Structure map, top of Nodosaria 3 sand, Ellis field. Fault A divides the field into north and south parts. Well numbers are shown on figure 16; structure values are shown in appendix B.

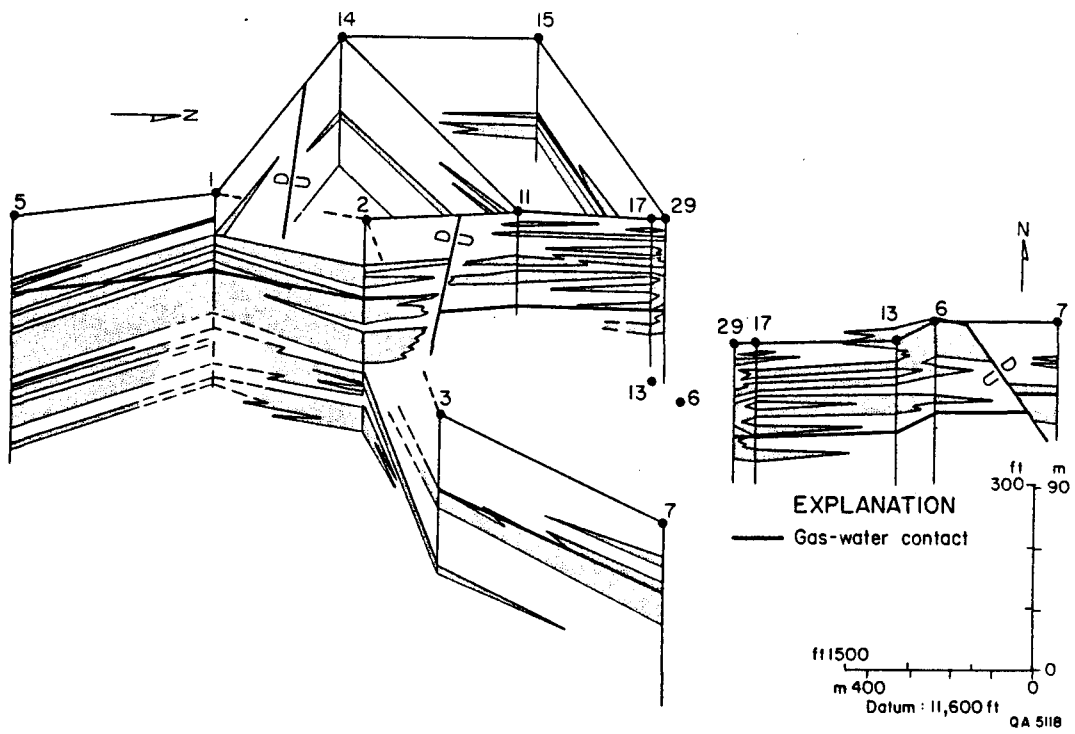


Figure 14. Fence diagram, Nodosaria 3 interval, Ellis field. Thickest sands lie in the southern part of the field.

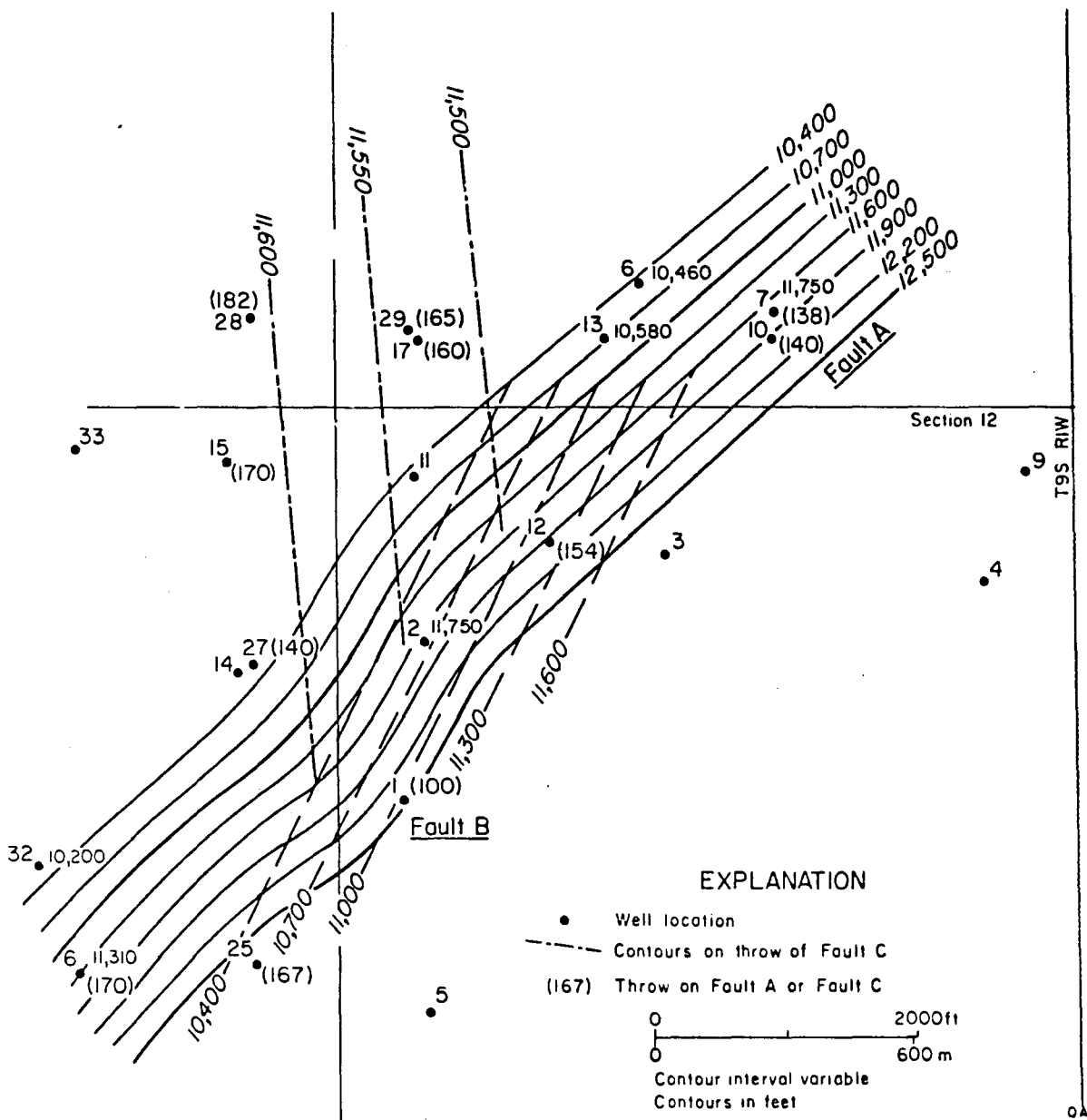


Figure 15. Fault plane map, Nodosaria 3 sand, Ellis field. See figure 13 for location of faults.

reservoir is about 110 acres ($4.4 \times 10^5 \text{ m}^2$). Approximately 45 Bcf ($1.3 \times 10^9 \text{ m}^3$) of gas has been produced since field discovery in 1953 (Dwight's Energydata Co., 1985g). The reservoir was shut in in 1973, but one well was reopened in 1977 and is now co-producing gas and water from the Nodosaria 3 sand in the northern part of the field (Howell and others, 1985). In addition, the Nonion struma and Nodosaria 5 sands, above and below the Nodosaria 3, produce both oil and gas from the Hackberry Member.

Depositional environment and gas occurrence

The regional depositional setting of the Nodosaria 3 sand is difficult to determine because only 17 wells have been drilled in the Nodosaria Zone of Ellis field, and lithofacies maps of nearby areas were unavailable. An inferred submarine-fan channel system generally trends north-south, indicating dip alignment of Hackberry sand bodies similar to that in Port Acres field (figs. 16 and 17). The log-pattern map shows two areas of channel deposits separated by an area of inferred overbank sediments. The northern, gas-rich end of the Nodosaria 3 reservoir coincides with incised channel-fill and braided channel-fill sands (figs. 17 and 18). Similar braided channel-fill sands in the southern part of the field contained much less gas, however, possibly owing to structural control. The original gas-water contacts for the Nodosaria 3 sand are -11,725 ft (-3,574 m) for the southern part of the reservoir and -11,745 ft (-3,580 m) for the northern part.

PLANULINA TREND

The lower Miocene Planulina trend is located basinward of the middle Frio Hackberry trend (figs. 1 and 2). It extends more than 150 mi (240 km) westward

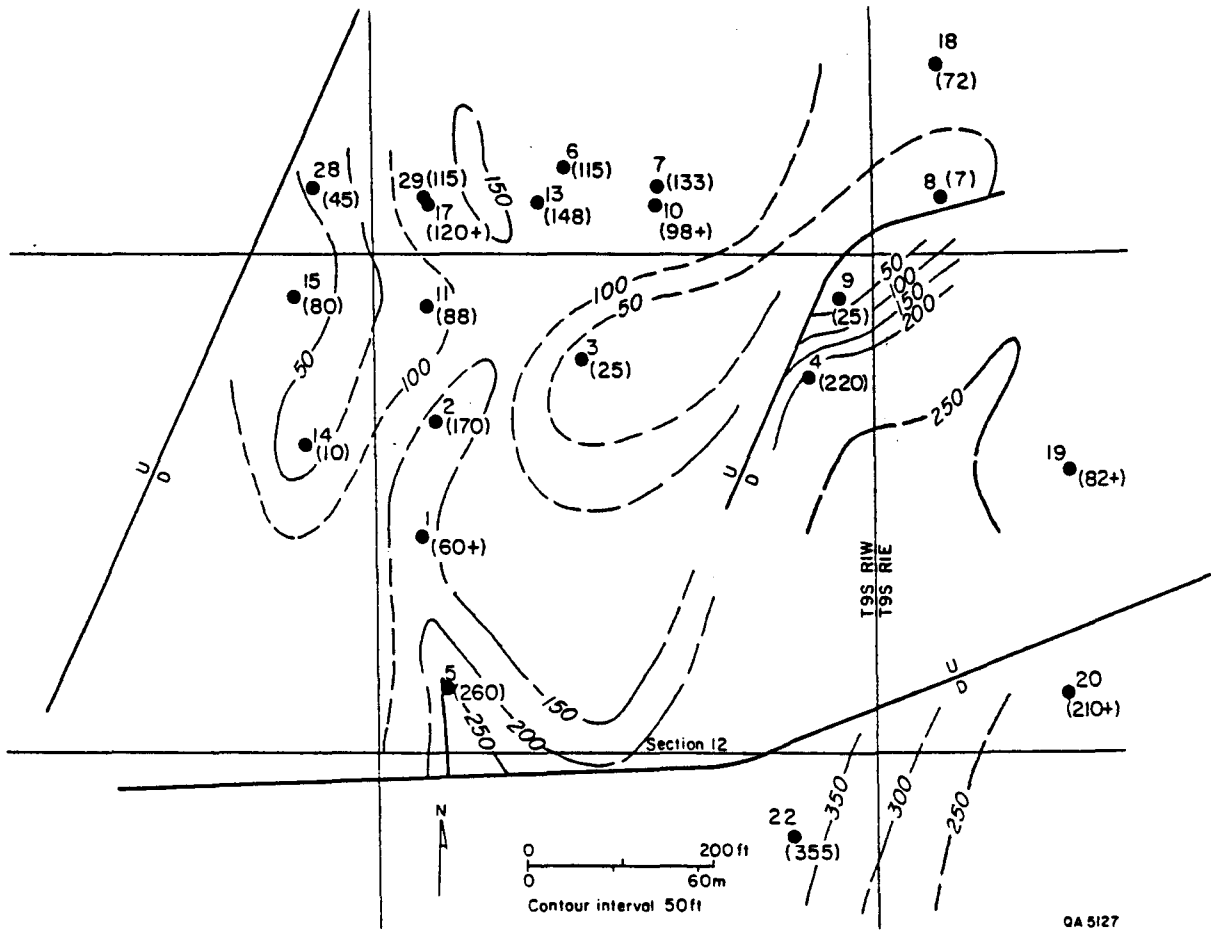


Figure 16. Net-sand map, Nodosaria 3 sand, Ellis field. An area of high sand accumulation follows a north-south trend through the center of the field.

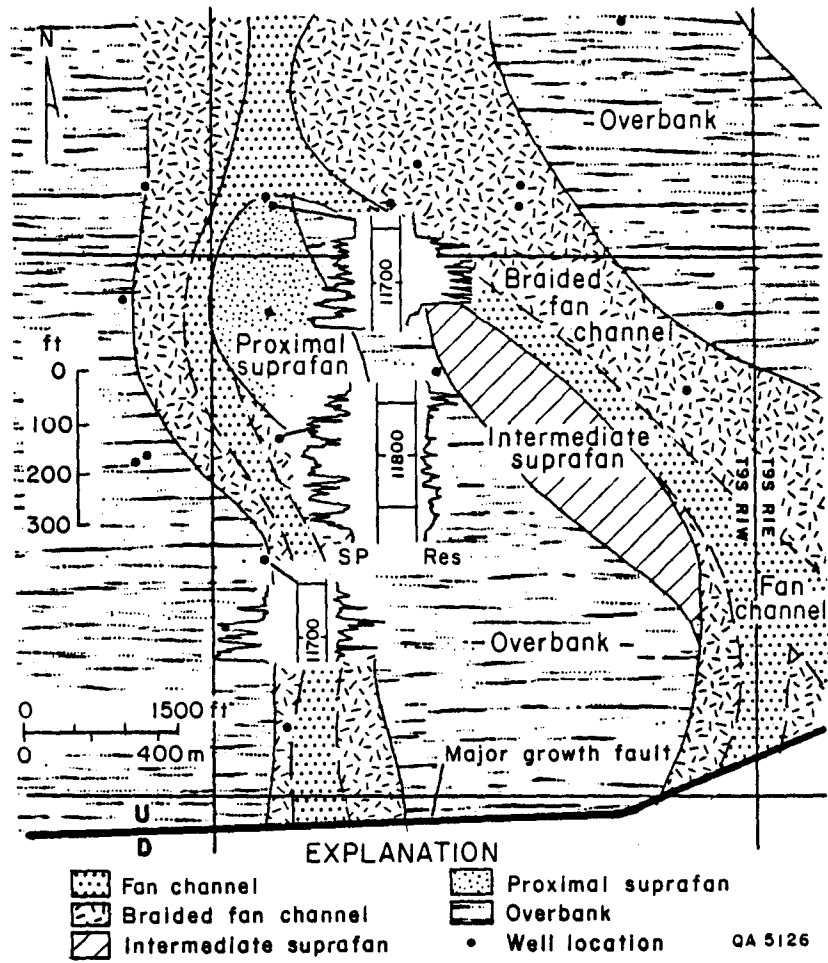


Figure 17. Log-pattern map, Nodosaria 3 sand, Ellis field. Fan channels are interpreted to trend north-south.

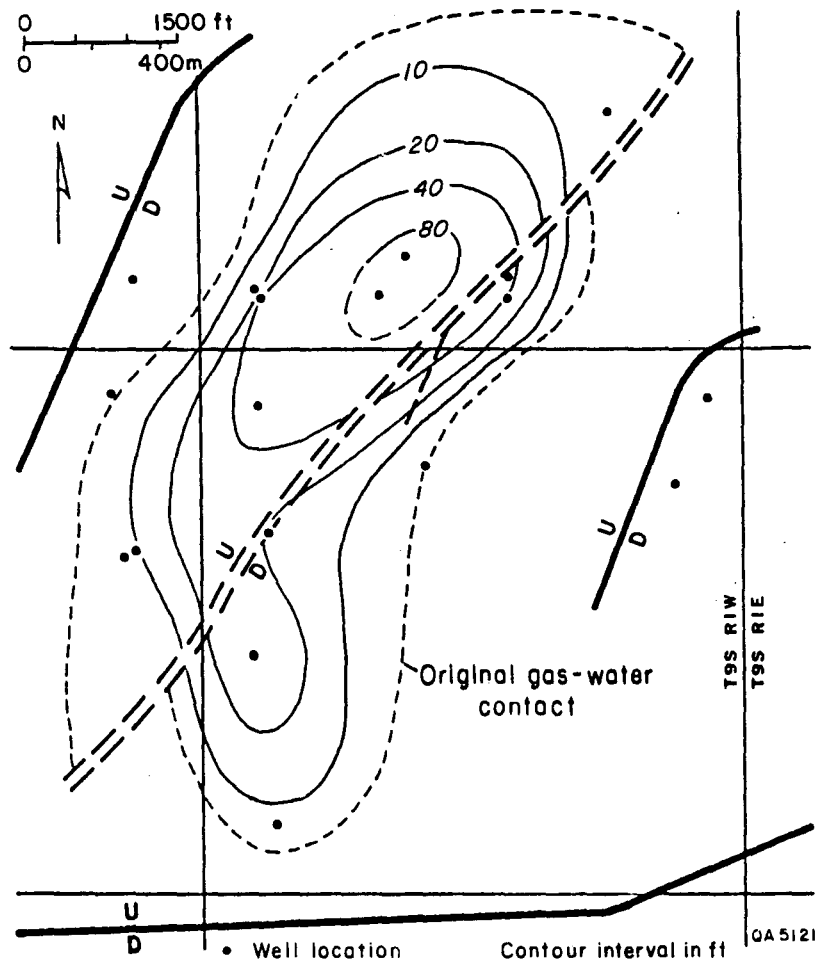


Figure 18. Net-gas-sand map, Nodosaria 3 sand, Ellis field. Thickest gas sands are in the north part of the field, not in the area of thick sand shown in figure 14.

from the Mississippi River to southeast Texas (Goheen, 1959; Sloane, 1971). The Planulina Zone dips about 385 ft/mi (73 m/km) to the south in Vermilion Parish, Louisiana, and the zone thickens southward (Goheen, 1959). The increase in thickness is partly attributable to increased sediment accumulation across growth faults that have vertical displacements as great as 1,000 ft (305 m) (Sloane, 1971; Gotautas and others, 1972). Hydrocarbons in the Planulina trend are found in anticlinal, domal, stratigraphic, and combination traps.

Initial discovery of gas in Planulina sands was made in 1945, in Cameron Parish, Louisiana, at the western end of the trend. Development of the trend was slow for the next 20 years because of failures caused by inadequate drilling techniques and geologic complexity. Improvements in drilling technology and exploration techniques, and a better understanding of the geology, have increased the success ratio and have generated more interest in the trend since the mid-1960's (Sloane, 1971).

The term "Planulina Zone" is informally used by Gulf Coast geologists to specify a lower Miocene wedge of light- to dark-gray marine shale with interbedded sands. The Planulina Zone is recognized by the presence of the intermediate neritic to upper bathyal Planulina palmerae microfaunal assemblage, but contacts are uncertain and correlations are difficult and inconsistent (Goheen, 1959; Limes and Stipe, 1959; Sloane, 1971; Brunhild, 1984).

Efforts to determine the origin of Planulina sands led to suggestions that they were deposited in deltaic distributary channels (Goheen, 1959; Sloane, 1971; Brunhild, 1984), offshore bars (Gotautas and others, 1972; Sonnier, 1978), continental shelf sheet-sand deposits (Goheen, 1959), or submarine fans (Lock, 1982). Because of the complexity of the stratigraphy and structure, clarification of the genesis of these deep-water sands requires an integrated regional study. Nevertheless, the Planulina Zone is part of a major Miocene progradational wedge. Within this wedge, the deep-water Planulina Zone lies basinward of, and below,

shales containing the intermediate neritic Siphonina davisi fauna, which is in turn overlain by a thick regressive sequence of brackish through continental strata (Sloane, 1971; Brunhild, 1984); the Planulina Zone overlies shales containing the upper bathyal Abbeville faunal assemblage. The deep-water origin of the Planulina Zone and its position in the sequence of strata suggest that Planulina strata were deposited on the outer continental shelf to upper slope. From these observations and from the analysis of spontaneous potential well-log patterns, we infer that the Planulina sands were deposited in a setting similar to that of the Hackberry.

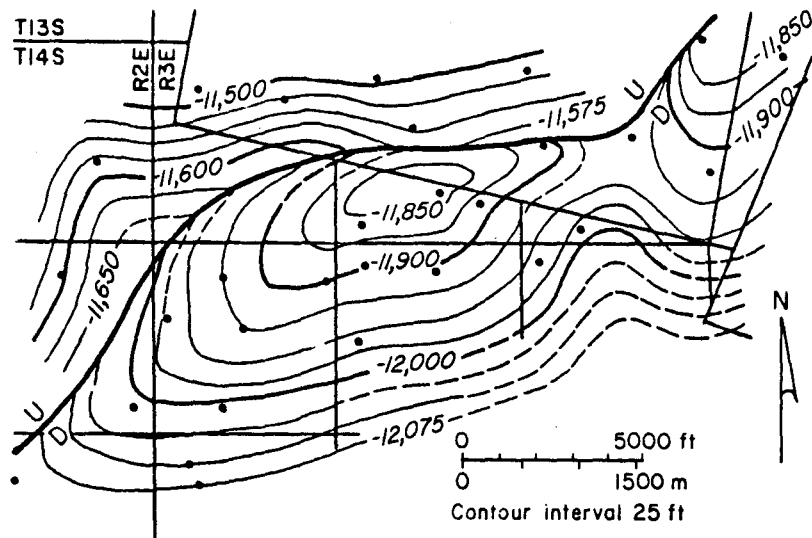
Esther Field

Field history, geology, and methodology

Esther field, located in the Planulina trend in central Vermilion Parish, Louisiana (fig. 1), was discovered in 1977. Since production began in 1978, 41 Bcf ($1.2 \times 10^9 \text{ m}^3$) of gas and 459,900 bbl ($73,080 \text{ m}^3$) of condensate have been produced (Dwight's Energydata Co., 1985g) from two Planulina reservoirs--the 13,700 sand and the 14,060 sand. Recently, the field has been extended to the northeast.

In Esther field, approximately 1,000 ft (305 m) of marine shale with a few interbedded sands separates the 13,700 sand from the overlying paralic and continental strata. Top of geopressure is near the top of the marine shale at about 12,700 ft (3,870 m) (Howell and others, 1985); the Planulina sands are geopressed. The 13,700 sand is separated from the underlying 14,060 sand by 200 to 250 ft (60 to 75 m) of mudstone.

A structure map (fig. 19) was drawn on top of the Cristellaria 5 sand, which is approximately 1,800 ft (550 m) above the 13,700 sand. It is the closest



EXPLANATION

- Well
- $\frac{U}{D}$ Fault

QA 5319

Figure 19. Structure on top of Cristellaria 5 sand. Esther field formed in fault-bounded anticline (fault modified from Harrison, 1981).

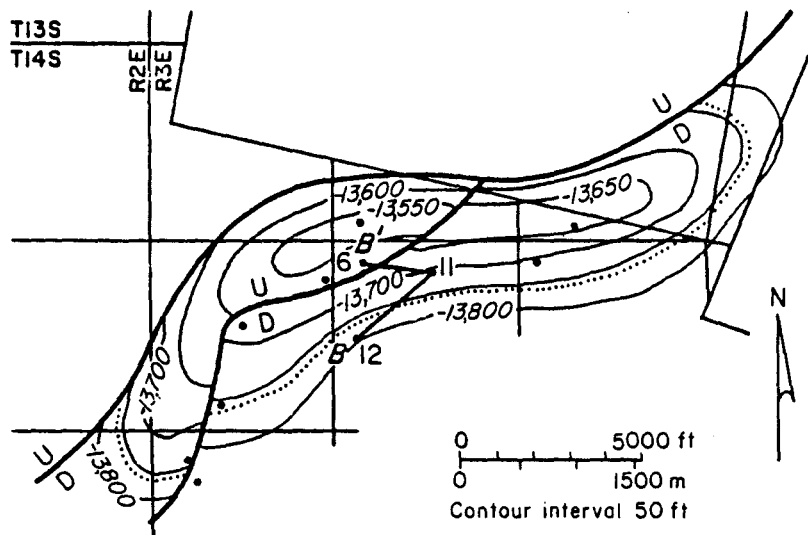
mappable horizon to the Planulina sands. Esther field lies in an anticlinal trap that formed on the south side of a major northeast-trending growth fault that offset the Cristellaria 5 sand by 300 to 400 ft (90 to 120 m).

Interpretations of structure and of sand-body geometry and trends are tentative because few geophysical well logs were available--9 penetrate the 13,700 sand and 8 test the 14,060 sand--and because the wells are located in a line nearly parallel to inferred paleostrike. Lacking regional structural and lithofacies maps, but recognizing the similarities between the Planulina and Hackberry depositional settings, we evaluated Esther field using a submarine-fan depositional model, which is consistent with the interpretation of Lock (1982). Data from geophysical well logs were used to make structure, net-sand, net-gas-sand, and log-pattern maps for the 13,700 and 14,060 reservoirs.

Depositional environment and gas occurrence, 13,700 sand

The structure map on top of the 13,700 sand (fig. 20) and cross section B-B' (fig. 21) demonstrate the fault-bounded anticlinal trap and the gas-water contact. They also show that the field is bisected by a minor nonsealing fault with about 150 ft (45 m) of vertical displacement. If the minor fault is indeed nonsealing, it probably does not bisect the entire field as shown, in view of the offset of the reservoir sands against mudstone (fig. 21).

The net thickness of sands (fig. 22) ranges from 25 to 77 ft (8 to 23 m). Sand thicknesses are about 10 ft (3 m) greater on the downthrown side of the minor fault, suggesting syndepositional fault movement. Dip-elongate (north-south) sand-body trends are inferred from the regional paleoslope and from the Hackberry analog. Spontaneous potential (SP) response for the 13,700 sand (fig. 23) shows inferred braided channel-fill sands (blocky SP log patterns with shale partings) and incised channel-fill sands (blocky SP log pattern with few shale partings) coincident

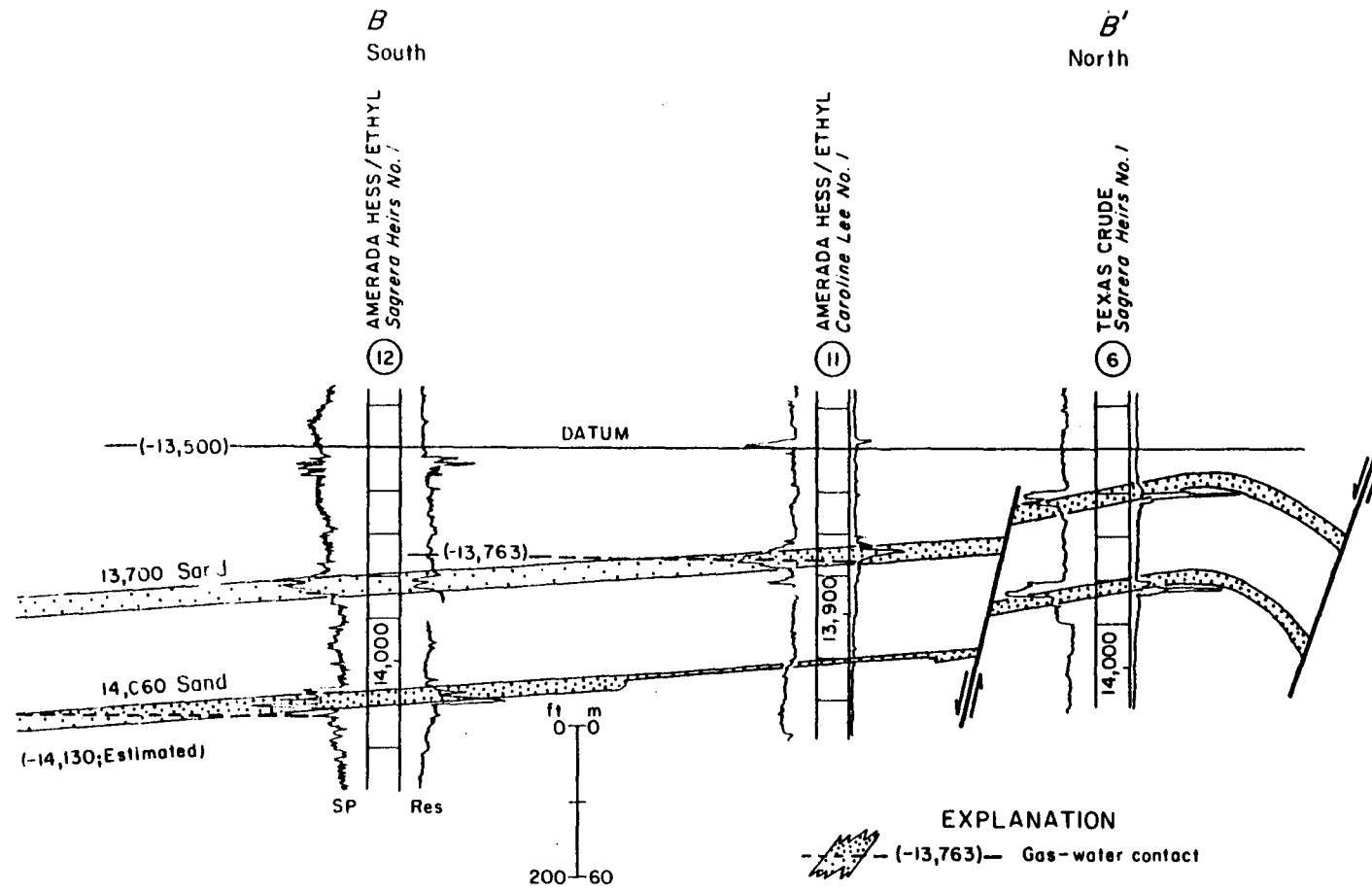


EXPLANATION

- Well
- $\frac{U}{D}$ Fault
- Gas-water contact (-13,763 ft)

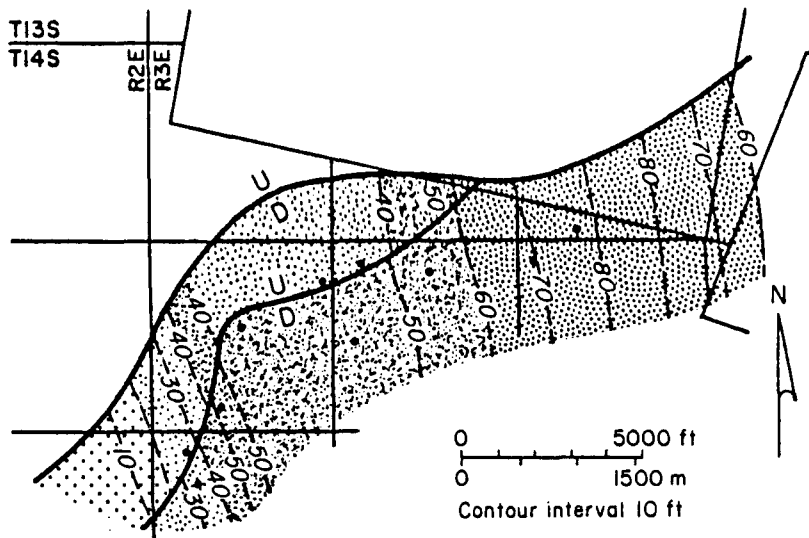
QA 5320

Figure 20. Structure map on top of 13,700 sand. Anticlinal structure crossed by minor fault (faults modified from Harrison, 1981).







QA 5318

Figure 21. Cross section B-B'. Esther field formed in a fault-bounded anticline; minor fault offsets reservoir sands. Location of section shown on figure 20.



EXPLANATION

- | | | |
|---|------------------------|---------------------|
|  | > 60 ft (18.3 m) | |
|  | 40-60 ft (12.2-18.3 m) | • Well |
|  | 20-40 ft (6.1-12.2 m) | $\frac{U}{D}$ Fault |
|  | < 20 ft (6.1 m) | |

QA 5321

Figure 22. Sand isolith map, 13,700 sand. Net-sand thicknesses are greatest on downthrown side of minor fault.

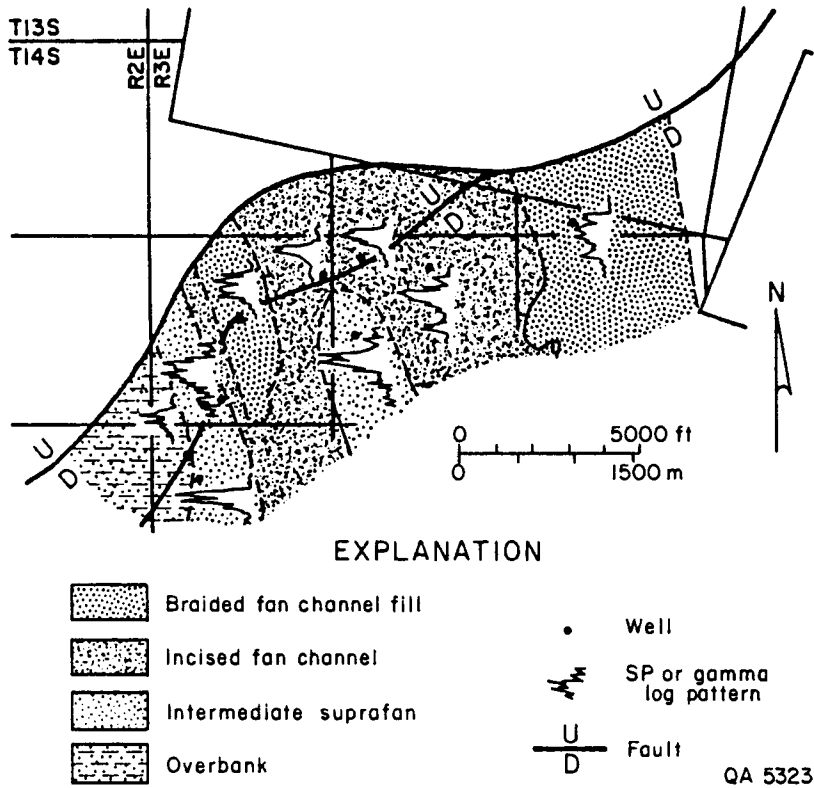


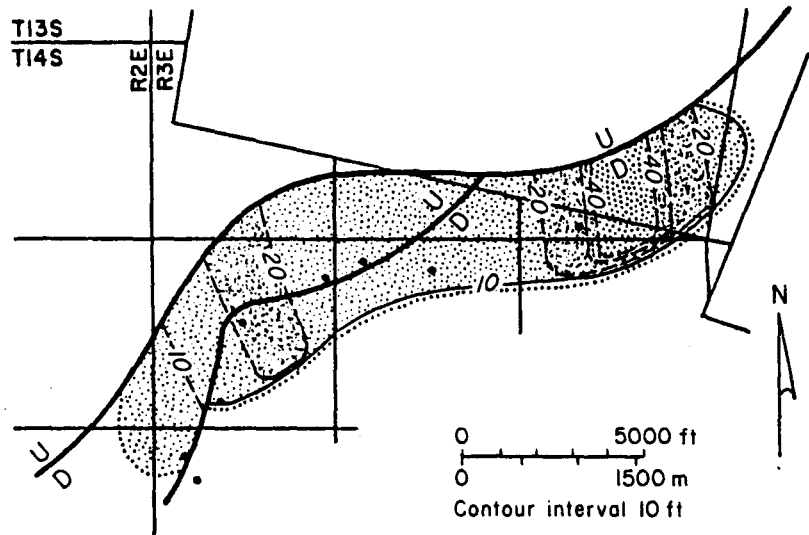
Figure 23. Log-pattern map, 13,700 sand.

with dip-elongate sand-body trends of the lithofacies map (fig. 22, see fig. 23 for well numbers and appendix B for structure and sand values). Two possible channel systems are identified. The larger system encompasses the eastern third of the field; the smaller system lies in the western third of the field (fig. 23). Intermediate suprafan (upward-coarsening log patterns) and overbank (serrate SP log patterns) deposits are marginal to the channel-fill sands.

The net thickness of gas-bearing sand is estimated to range from 6 ft to more than 40 ft (1.8 to 12 m) (fig. 24). High values of net gas sand (fig. 24) coincide with mapped channel axes (fig. 22). The original gas-water contact for the 13,700 sand is at -13,763 ft (-4,195 m) (figs. 21 and 24). The area of the reservoir is 1,420 acres ($5.74 \times 10^6 \text{ m}^2$) and initial gas in place is 71 Bcf ($2.0 \times 10^9 \text{ m}^3$) (table 2).

Depositional environment and gas occurrence, 14,060 sand

The interpretation of the structure map for the 14,060 reservoir (fig. 25) is similar to that for the 13,700 reservoir (see discussion above). However, the lithofacies distributions differ. Net thickness of the 14,060 sand is greatest (63 ft, 19 m) on the west side of the field on the downthrown side of the minor fault (well 15, fig. 26; see fig. 27 for well numbers and appendix C for structure and sand values not on figures). The 14,060 sand is absent in well 14, which is on the upthrown side of the minor fault and less than 1,000 ft (305 m) to the north of well 15. In the center of the field, the 14,060 sand is inferred to be absent owing to pinch-out (figs. 26 and 28). Alternatively, the minor fault may pass south of well 11, thus accounting for the low net-sand value in that well. Inferred braided and incised channel-fill sands on the log-pattern map (fig. 27) coincide with



EXPLANATION




- | | | | |
|---|-----------------------|---------------|-----------------------------------|
|  | > 40 ft (12.2 m) | • | Well |
|  | 20-40 ft (6.1-12.2 m) | $\frac{U}{D}$ | Fault |
|  | < 20 ft (6.1 m) | | Gas-water contact
(-13,763 ft) |
- QA 5322

Figure 24. Net thickness of gas-bearing sand, 13,700 sand; gas-water contact from figure 14.

Table 2. Reserve calculations, Port Acres, Ellis, and Esther fields.

Trend	Hackberry		Planulina	
Field	Port Acres	Ellis	Esther	
Reservoir	Lower Hackberry	Nodosaria 3	13,700 ft	14,060 ft
Initial reservoir temperature (°F)	225	225.2	260	265
Initial reservoir pressure (psia)*	9,015	9,720	11,500	11,700
Gas gravity (air = 1)	0.626	0.7	0.65	0.65
Gas saturation	0.7	0.8	0.65	0.65
Porosity	0.29	0.3	0.25	0.25
Pseudoreduced temperature	1.87	1.91	1.92	1.94
Pseudoreduced pressure	13.46	14.57	17.19	17.49
Compressibility factor, Z	1.33	1.38	1.57	1.53
Gas formation volume factor, Bg (ft ³ /Scf)	350.32	363.51	359.63	372.86
Volume of field (acre-ft)	122,044	12,600	27,782	25,711
Initial gas in place (Bcf)	378	48-56	71	68
Total production (Bcf)**	307.46	45.24	16.35	25.09
Remaining gas in place (Bcf)	70	7-11	54	43

39

* from Howell and others (1985).

** from Dwight's Energydata Co. (1985a,b,c,d,e,f,g).

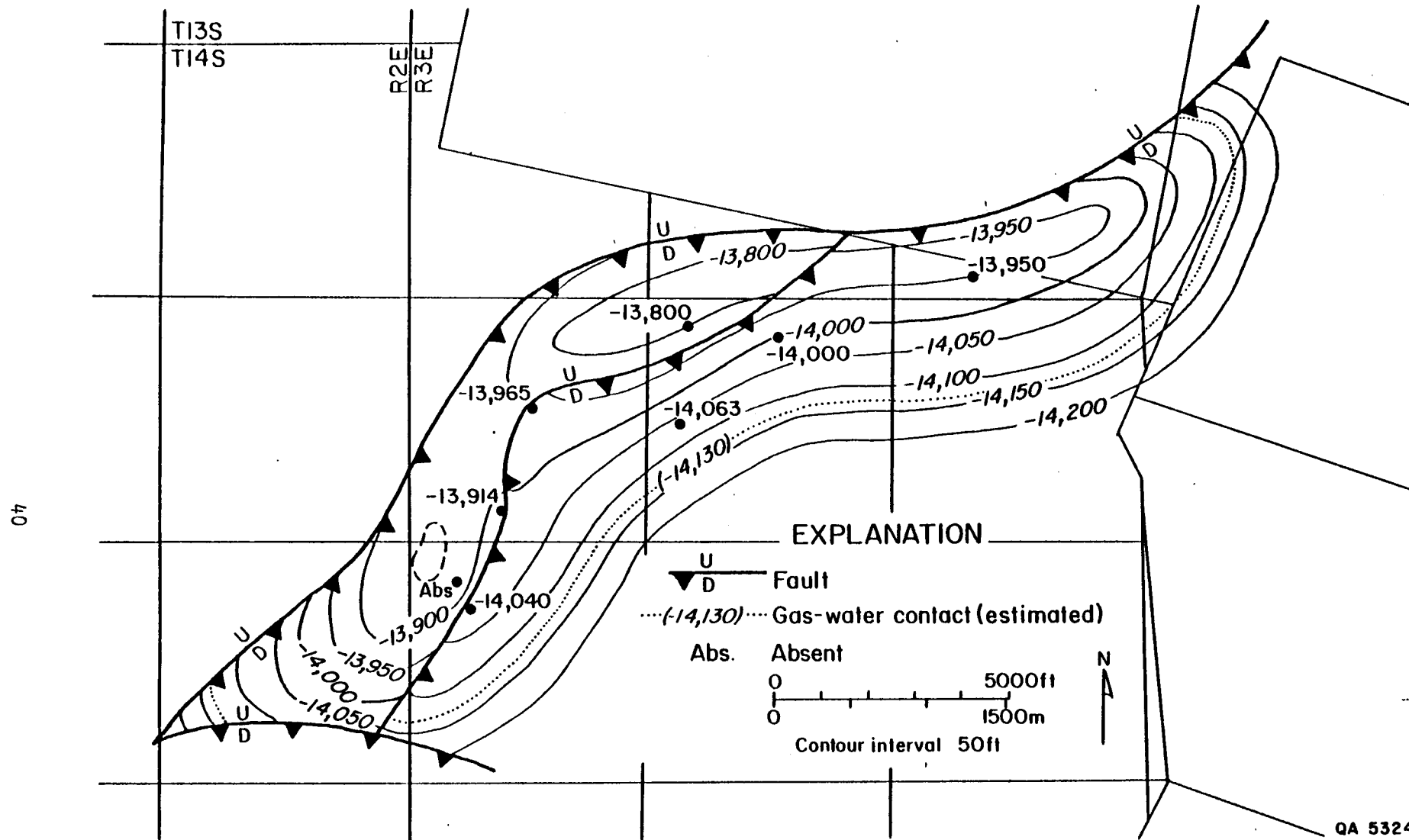


Figure 25. Structure map on top of 14,060 sand showing an anticline bounded on the north by a major growth fault and bisected by a minor fault with less than 150 ft (45 m) vertical displacement. The gas-water contact is estimated (faults modified from Harrison, 1981).

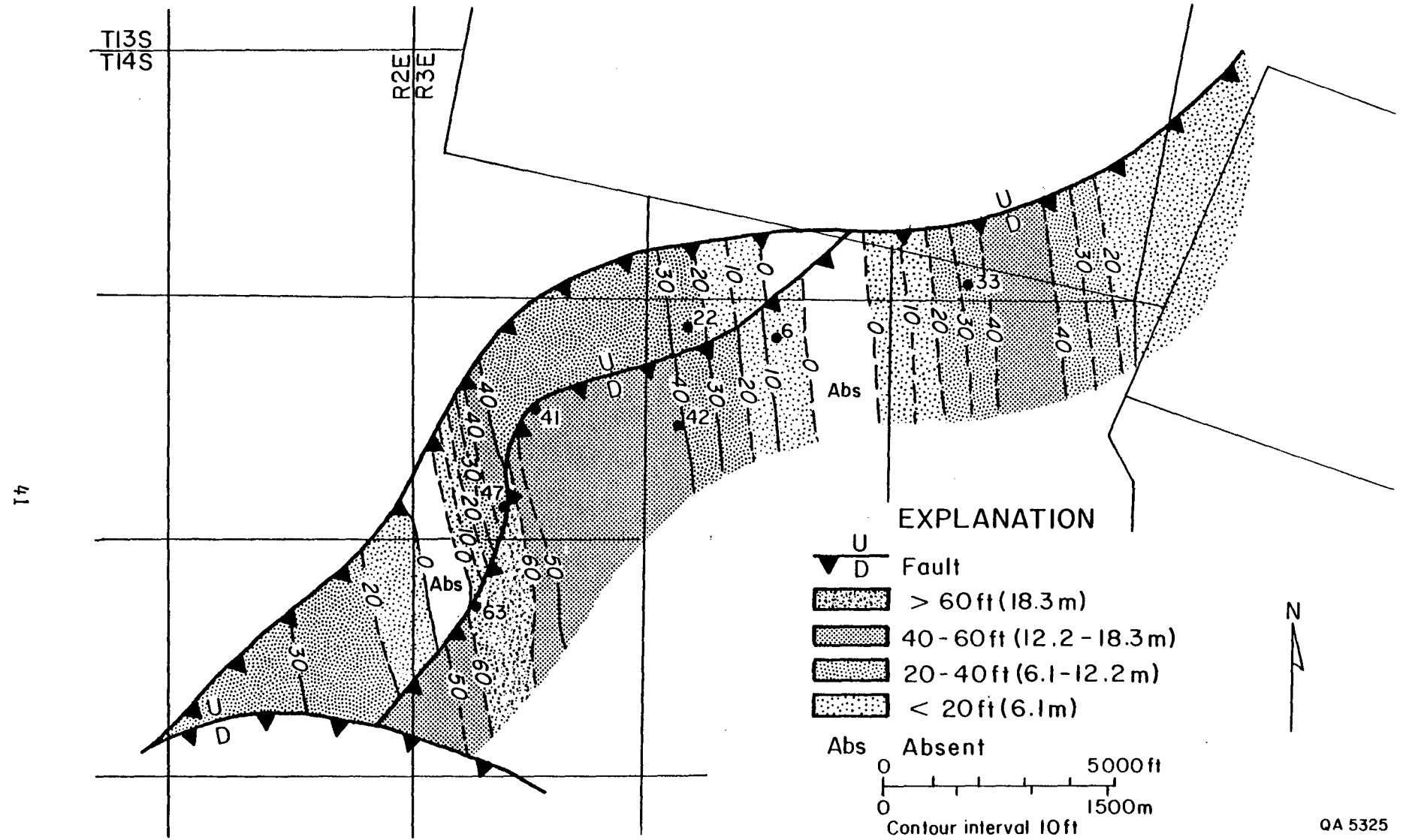


Figure 26. Sand isolith map, 14,060 sand. North-south-trending sand bodies are inferred. Net-sand thicknesses are greatest on the downthrown side of the minor fault.

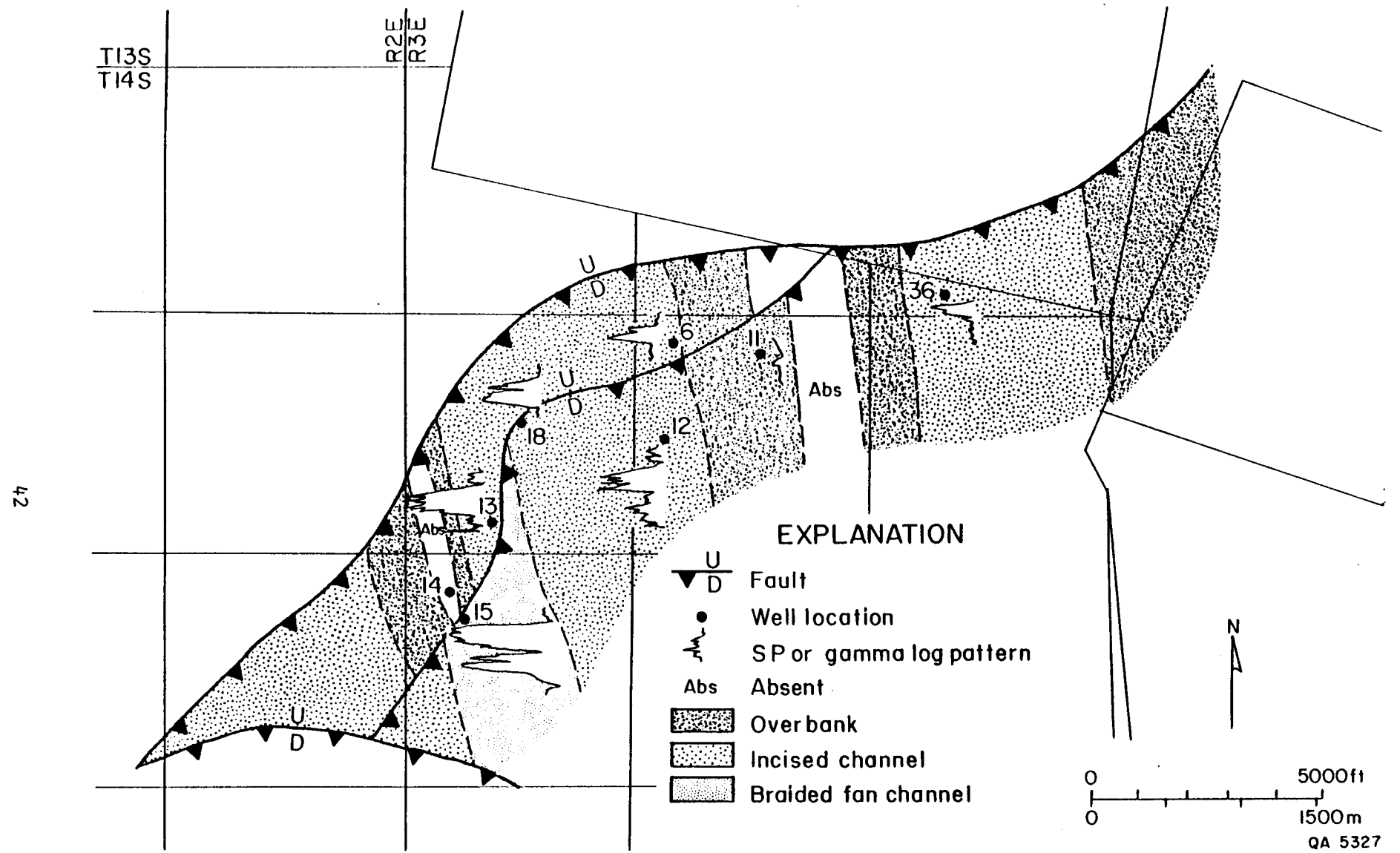


Figure 27. Log-pattern map for 14,060 sand.

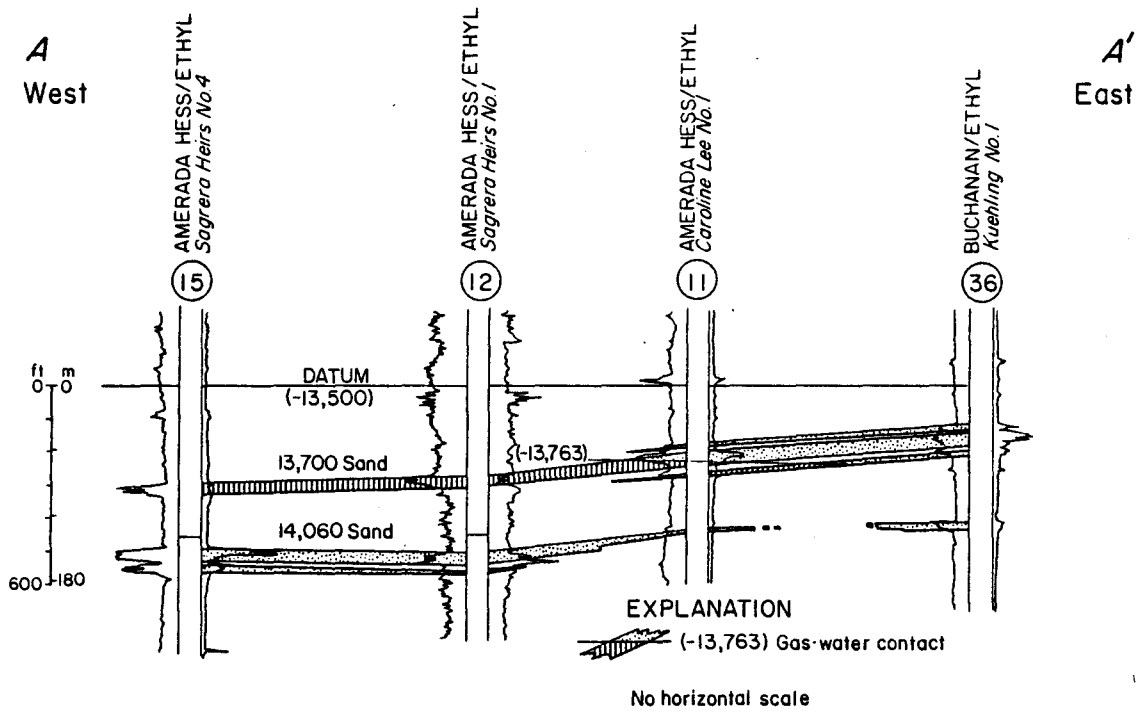


Figure 28. Strike section A-A'. The 14,060 sand is inferred to pinch out on the east side of the field. See figure 25 for location of section.

postulated dip-elongate sand-body trends (fig. 26) and are flanked by overbank deposits.

If the 14,060 sand pinches out in the center of the field as interpreted (fig. 28), two reservoirs exist. The net thickness of gas-bearing sand (fig. 29) is as much as 30 ft (9.1 m), and the area of the reservoirs is 1,963 acres ($7.9 \times 10^6 \text{ m}^2$). The gas-water contact is below the level of the 14,060 sand on all available logs; it is estimated at -14,130 ft (-4,307 m) (figs. 21 and 25). Initial gas in place in the 14,060 sand was 68 Bcf ($1.9 \times 10^9 \text{ m}^3$) (table 2).

RESERVE ESTIMATES

Net-gas-sand maps were planimetered and initial gas in place was calculated for the lower Hackberry, Nodosaria, and Planulina reservoirs. Initial gas reserves were estimated by a volumetric method (Z. S. Lin, personal communication, 1985). This method requires a knowledge of the initial (at discovery) reservoir fluid pressure and temperature, average porosity, gas saturation, volume of gas-saturated formation, and gas gravity (table 2). From these data, first the pseudocritical and pseudoreduced temperatures and pressures, then the compressibility factor for natural gas (Z), and finally the gas formation volume factor (B_g) can be derived (Standing and Katz, 1942; Brown and others, 1948; Carr and others, 1954; Craft and Hawkins, 1959).

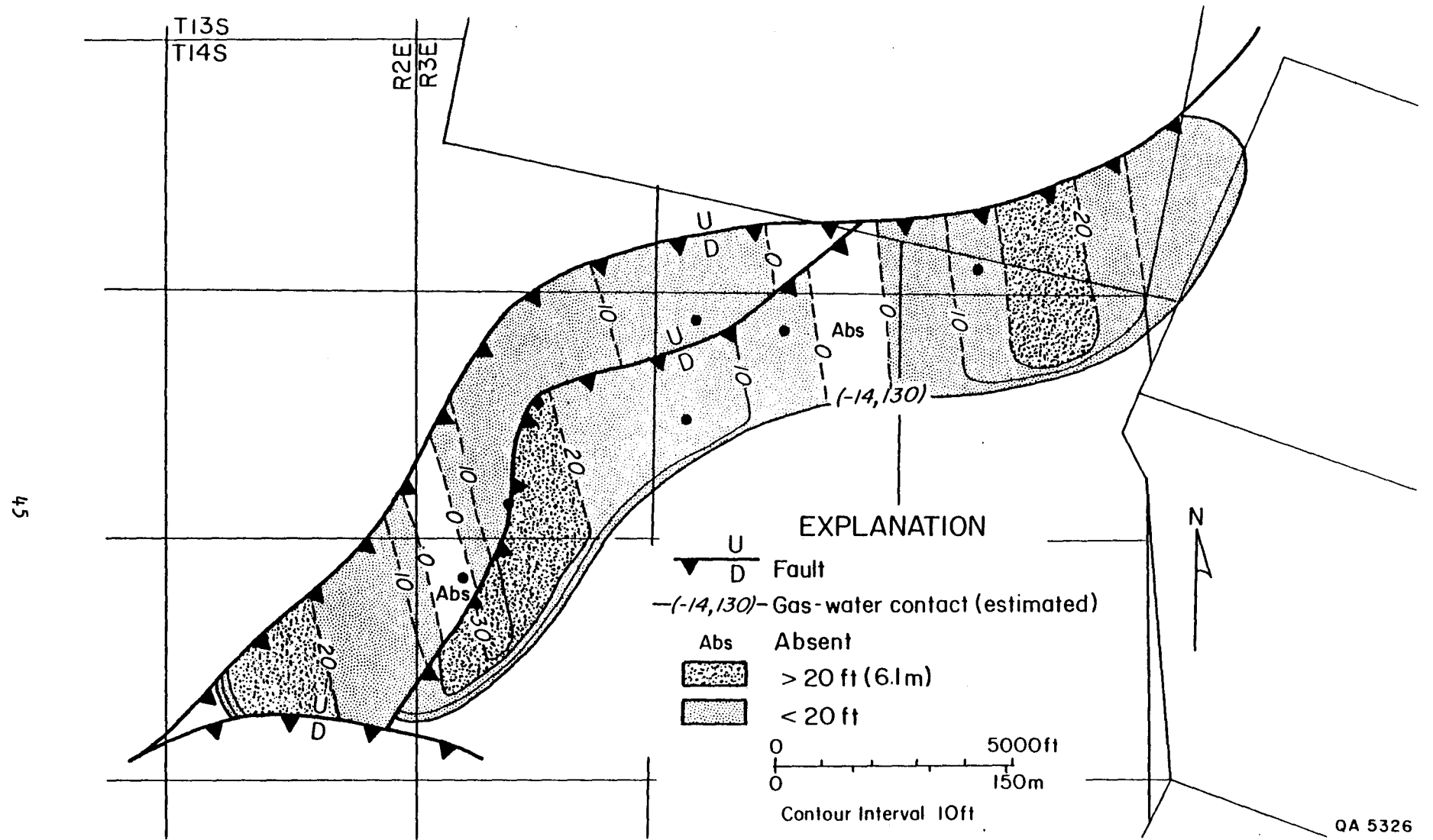


Figure 29. Net thickness of gas-bearing sand, 14,060 sand.

The equation used to estimate the initial gas in place (IGIP) is:

$$\text{IGIP} = (43,560)(A)(h)(\phi)(1-S_w)(B_g) \quad (1)$$

Where A = area of field (acres)

h = effective net-pay thickness (ft)

ϕ = porosity fraction

S_w = water saturation fraction

B_g = gas formation volume factor (ft³/Scf) (Finley and others, 1985).

The remaining natural gas available for co-production (GCP) is estimated by the following equation:

$$\text{GCP} = \text{IGIP} - \text{total production to date (see appendices)} \quad (2)$$

Additional gas may also be produced from solution as a result of the large pressure drawdown sustained during co-production. However, methane solubility is estimated to be 22 Scf (4,900 m³) per bbl of water at Port Acres field; hence, only 110 Mcfd (3.1 x 10⁶ m³/d) of solution gas could be obtained from a well producing methane-saturated formation water at a rate of 5,000 bbl/d (800 m³/d) (Gregory, 1980). This volume of gas, which is insignificant compared to potential free gas production from the three fields, has been disregarded in the reserve estimates.

The initial free gas reserve estimate for Port Acres field is 378 Bcf (1.1 x 10¹⁰ m³), with 71 Bcf (2.0 x 10⁹ m³) of remaining gas in place (table 2). Earlier estimates by Halbouty and Barber (1962) ranged from 400 to 500 Bcf (1.1 to 1.4 x 10¹⁰ m³), whereas Howell and others (1985) indicate a range of 326 to 374 Bcf (0.9 to 1.1 x 10¹⁰ m³) of remaining gas in place. They estimate an additional

recovery of some 9.6 to 28.2 Bcf (2.7 to $7.9 \times 10^8 \text{ m}^3$) using co-production techniques that would require the removal of up to 20 million bbl ($3.0 \times 10^6 \text{ m}^3$) of water (Howell and others, 1985).

The initial free gas reserve estimates for the Nodosaria 3 reservoir (Ellis field) vary from 48 to 56 Bcf (1.3 to $1.6 \times 10^9 \text{ m}^3$), with some 7 to 11 Bcf (2.0 to $3.1 \times 10^8 \text{ m}^3$) of gas currently remaining in place when calculated by Eq. 2 (table 2). Five to 10 Bcf (1.4 to $2.8 \times 10^8 \text{ m}^3$) of remaining gas in place was estimated using p/z data (Z. S. Lin, personal communication, 1985). Howell and others (1985) indicate that a gas production rate of 1,000 Mcfd ($2.8 \times 10^7 \text{ m}^3/\text{d}$) and 3,000 bbl (477 m^3) of water per day can be sustained in Ellis field for 10 years, which gives a total volume of 3.65 Bcf ($1.0 \times 10^8 \text{ m}^3$) of co-produced gas.

Initial gas in place in the Planulina reservoirs (total for the 13,700 and 14,060 sands) is estimated to be 139 Bcf ($3.9 \times 10^9 \text{ m}^3$), with 97 Bcf ($2.7 \times 10^9 \text{ m}^3$) of gas remaining in place (table 2). At least 7 Bcf ($2.0 \times 10^8 \text{ m}^3$) of additional gas can be recovered from Esther field by producing up to 10,000 bbl ($1,589 \text{ m}^3$) of water per day (Howell and others, 1985).

CONCLUSIONS

The submarine-fan depositional setting of Hackberry and Planulina reservoir sands controls several reservoir properties. Gas reservoirs are dip-elongate, channel-fill sands that pinch out laterally into overbank muds. Growth faults, common in the submarine slope environment, bound the fields on one or more sides, producing combination traps. The trapping mechanisms--growth faults and pinch-outs--restrict reservoir size, but they also retard water invasion during pumping, which may allow for increased mobility of dispersed gas.

Of the three co-production fields studied, Port Acres has the largest remaining reserves, but other factors, such as leasehold costs, sand production controls, and

artificial lift requirements (Howell and others, 1985), affect the economic potential of co-production in this reservoir. Eaton Operating Co., Inc. estimates that if 6 wells are used in a co-production project, each well should need to pump only 1,000 bbl/d (159 m³/d) (Howell and others, 1985).

Secondary gas recovery is now underway at Ellis field. A well in the northern part of the field was reactivated in 1977; water production since then has been as high as 2,400 bbl/d (381 m³/d) (Howell and others, 1985). Recently, the well has produced 1,200 bbl (191 m³) of water and 300 Mcf (8.5 x 10⁶ m³) of gas per day, and it is estimated that reduced gas saturation will compensate for declining reservoir pressure to extend co-production through 1996 (Howell and others, 1985).

Some wells in Esther field are watering out and are suited for co-production. Primary production in the Planulina Zone continues, however, and additional wells have recently been completed on the northeast side of the reservoir. Co-production possibilities, therefore, may be reevaluated at a later date.

INTEGRATED HYDROTHERMAL MODEL FOR THE TEXAS GULF COAST BASIN;
ORIGINS OF GEOPRESSURED BRINES AND LEAD-ZINC, BARIUM, URANIUM,
HYDROCARBON, AND CAP-ROCK DEPOSITS

by M. P. R. Light

INTRODUCTION

Land (1984) has outlined the evidence for vertical movement of diagenetic fluids at least several kilometers from Jurassic to Pleistocene formations in the Gulf Coast. This evidence includes the following: (1) discharge at the land surface of Mesozoic-derived brines as "bad water"; (2) emplacement of Mississippi Valley-type lead-zinc mineralization by fluids derived from Mesozoic formations in salt dome cap rocks at or near the land surface; (3) emplacement of uranium in Tertiary aquifers as a result of reduction by ascending reduced sulfur, presumably of Mesozoic origin; (4) emplacement of calcite cement derived from Mesozoic strata in Tertiary sandstones; and (5) presence of fluids in Plio-Pleistocene rocks with chemical signatures that could only have been derived from Mesozoic strata.

The Mesozoic age of the migrating diagenetic fluids is based on the $^{87}\text{Sr}/^{86}\text{Sr}$ of diagenetic minerals, which correspond to those of Jurassic-age seawaters (0.7068-0.7076) (Burke and others, 1982). Strontium isotopes do not fractionate during diagenetic mineral crystallization and are the same as they were in the original connate or seawater.

An integrated hydrothermal model has been devised that describes the sequential formation of salt domes and diagenetic, hydrothermal, and hydrocarbon generation zones as a consequence of the burial of the basinal succession and the Louann "mother" salt beneath an increasingly thick sediment accumulation. Posey

(1986) showed that the primary anhydrites within the Louann salt have variable strontium isotope values that range from Mid-Jurassic seawater ratios (0.7068-0.7076) consistent with an evaporitic origin during the deposition of the Louann salt to anomalously high strontium isotope ratios (0.7092), indicating a high radiogenic strontium content (Posey, 1986). However, only the salt domes within the Houston diapir province of the exterior Gulf Coast Basin and Gyp Hill salt dome in the South Texas diapir province show these anomalously heavy strontium isotope ratios (fig. 30; Posey, 1986). This is an area characterized by a thicker and more deeply buried section of Louann "mother" salt (T. E. Ewing, personal communication, 1985).

Diagenetic Zone and Salt Dome Model

Posey (1986) has proposed several possible scenarios for generating the high strontium-isotope ratio anhydrites present in the salt diapirs within the Houston diapir province. The strontium isotope ratios that are present in these anhydrites could have originated in the primary depositional environment from high $^{87}\text{Sr}/^{86}\text{Sr}$ continental clastics, meteoric waters that traversed continental materials, or hydrothermal waters extracted from distant shale or arkosic (red bed) successions (fig. 31). However, a continental origin for the radiogenic strontium is ruled out, in part, because the strontium isotopic ratios of anhydrites in salt domes in the interior basins, which are closer to the continental source, are lower than those of the Gulf Coast (exterior) Basin and because the salts themselves are marine type rather than continental type (fig. 30; Posey, 1986). Water with high $^{87}\text{Sr}/^{86}\text{Sr}$ could also be extracted from arkosic (red-bed) successions underlying or adjacent to the "mother" salt, but the waters would be required to pass through the salt to transfer the radiogenic strontium to the anhydrites

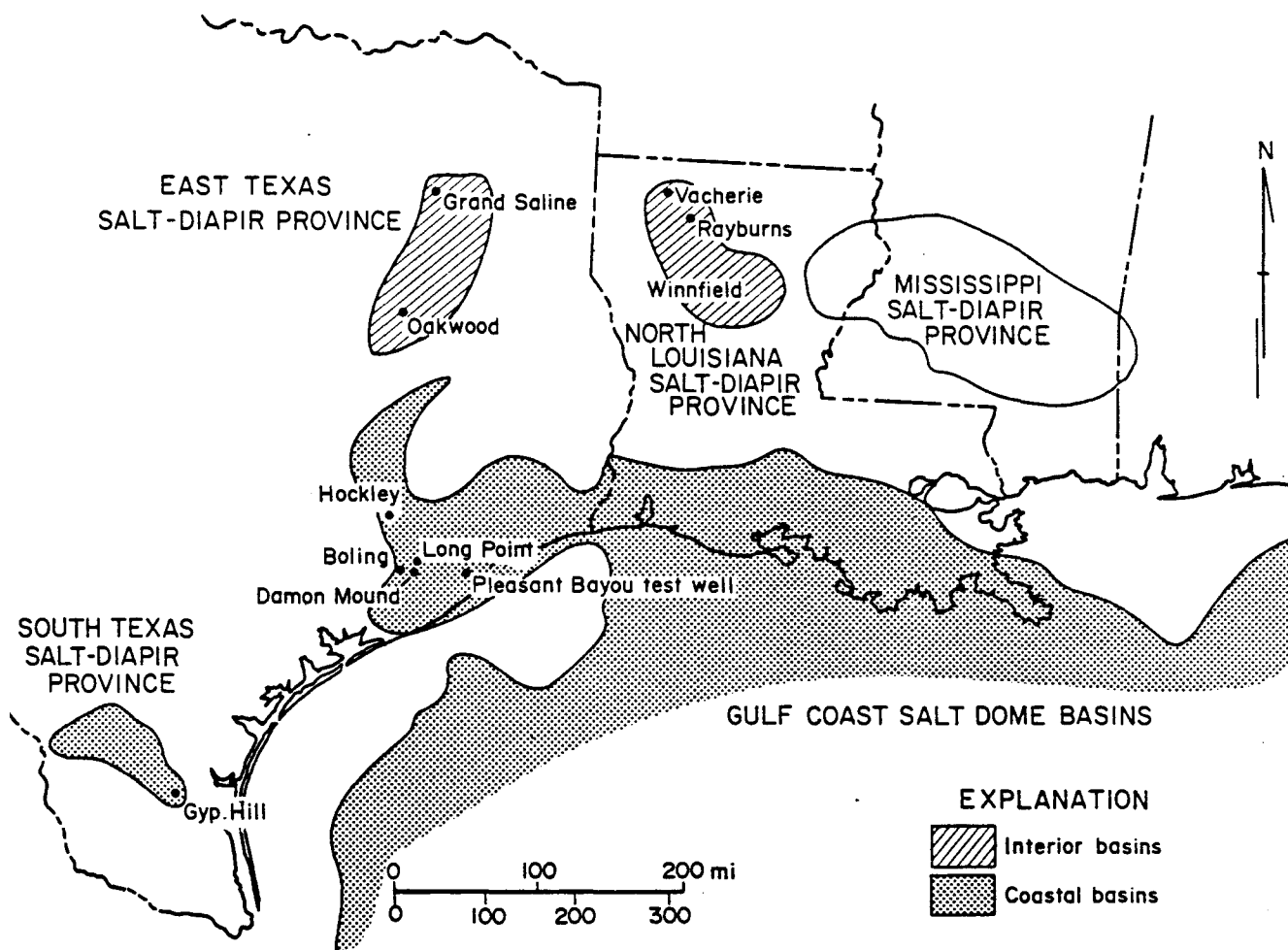


Figure 30. Location of Pleasant Bayou geopressedured-geothermal test well and Hitchcock N.E. field compared with the interior and exterior salt dome basins, after Halbouty, 1979.

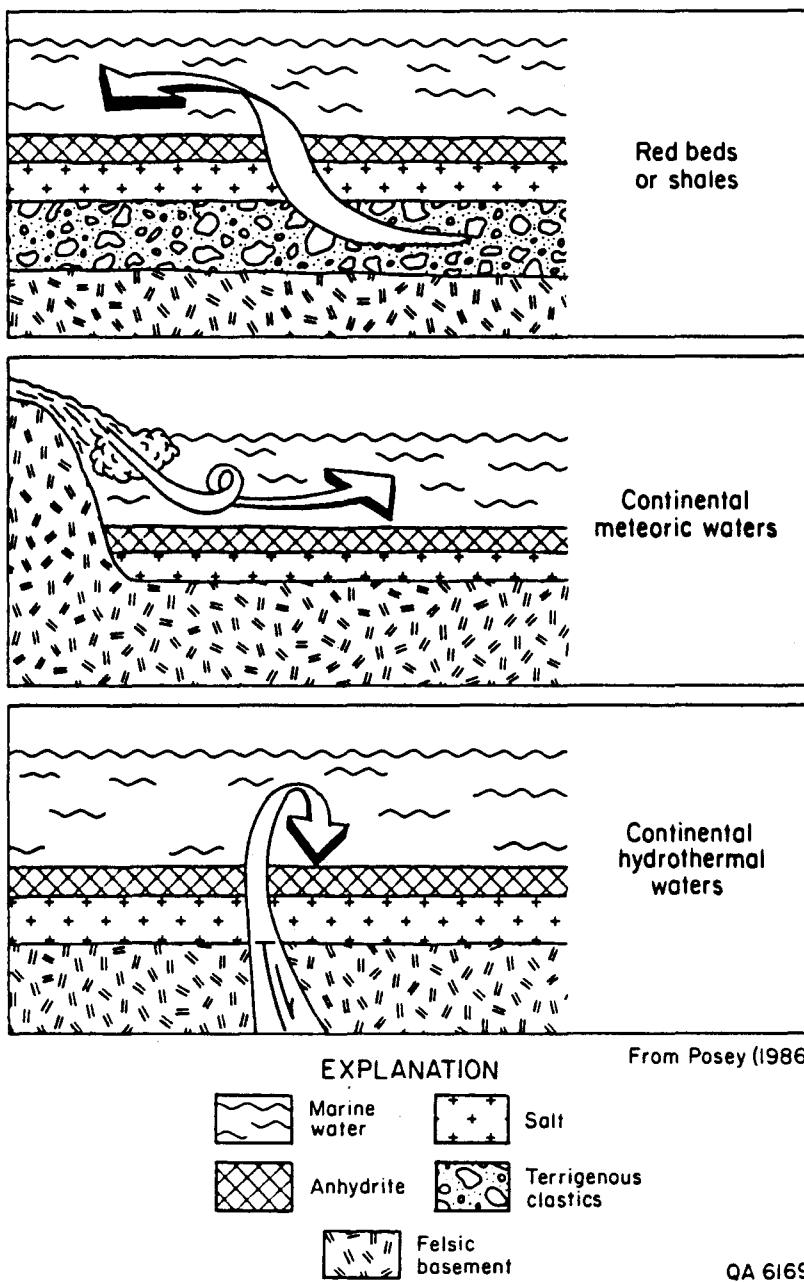
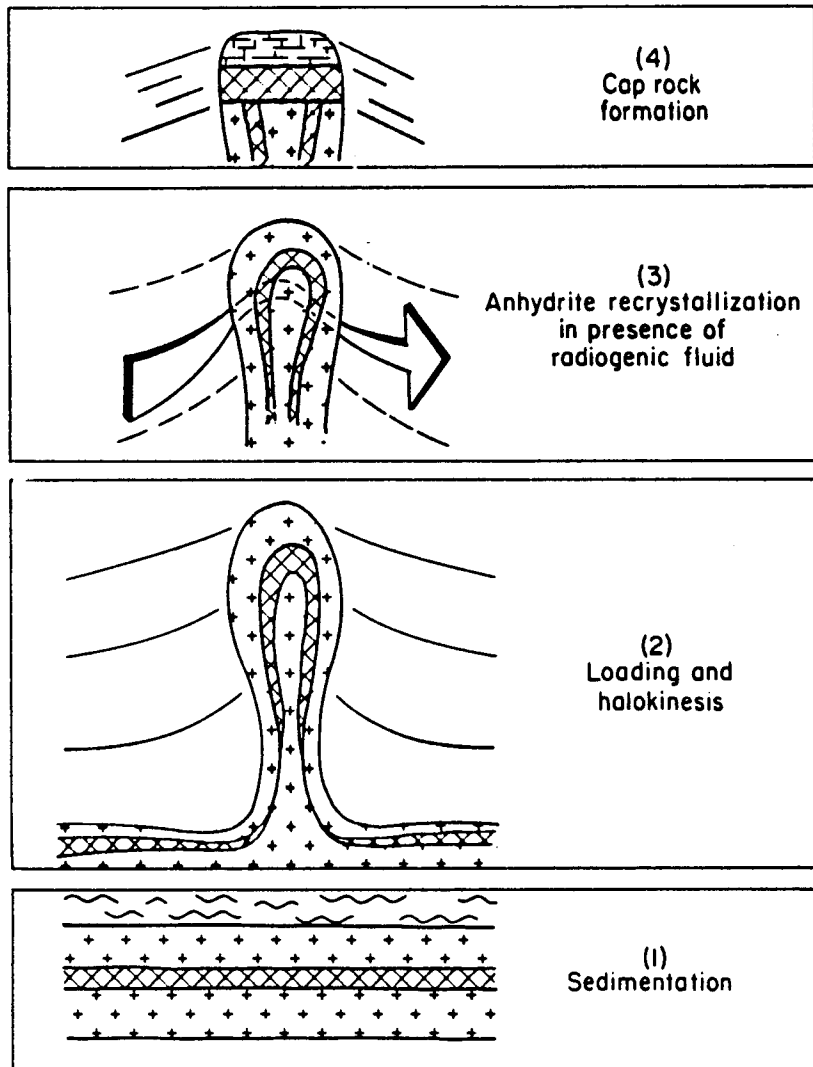


Figure 31. Model depicting the addition of radiogenic strontium to sulfates in the primary depositional environment by waters sourced in underlying terrigenous clastics or continental meteoric or hydrothermal waters. From Posey, 1986.

(fig. 31; Posey, 1986). A third method of generating high strontium isotopic anhydrites in the salt would require the recrystallization of the anhydrites in the presence of a radiogenic strontium-bearing fluid that migrated through the salt domes during halokinesis but prior to cap-rock formation (Posey, 1986). Such a mechanism would require fluid conduits to be present through the salt and the dissipation within it of the high $^{87}\text{Sr}/^{86}\text{Sr}$ waters that would result in the recrystallization of the anhydrites (fig. 32).

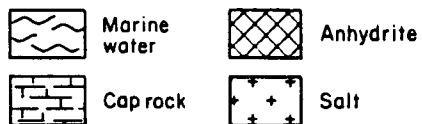
A new model has been devised that takes into account the sequence of fluid generation, diagenesis, and salt dome formation which results from sediment accumulation and subsequent burial of the Louann "mother" salt layer. In this model the introduction of heavy radiogenic strontium-rich fluids into the salt is a direct consequence of the burial and geopressing of the underlying arkosic Eagle Mills and Werner Formations. During the Early Triassic to Middle Jurassic the arkosic Eagle Mills and overlying Werner anhydrite formations were deposited as the initial synrift deposits in the Gulf Coast Basin (fig. 33) (Murray, 1966), and thicknesses as much as 4,600 ft (1,400 m) have been penetrated (Flawn and others, 1961). Sediments in the Gulf Coast basin are from 30,000 ft to 50,000 ft (9 to 15 km) thick in the vicinity of the Texas shoreline (Martin, 1978; Gregory and others, 1979).

The older Eagle Mills and Late Paleozoic rock sequence is sharply onlapped and isolated by the Werner Anhydrite and Louann "mother" salt, but the salt eventually laps out updip against it in a landward direction (fig. 34) (Todd and Mitchum, 1977). The Louann salt is estimated to have had an original bedded thickness of about 5,000 ft (1,500 m) and unconformably overlies Paleozoics and Eagle Mills (Andrews, 1960). The Louann is probably the source or "mother" bed for all the piercement domes of the four sub-basins that now exist within the Gulf Coast Basin (Andrews, 1960). The Louann salt is onlapped by the Late to Middle Jurassic Norphlet and Upper Jurassic, carbonate-rich Smackover, Buckner,



EXPLANATION

From Posey (1986)



QA 6166

Figure 32. Model depicting the addition of radiogenic strontium to sulfates within the salt stock at some time after deposition by waters derived from clastic rocks adjacent to the diapir. From Posey, 1986.

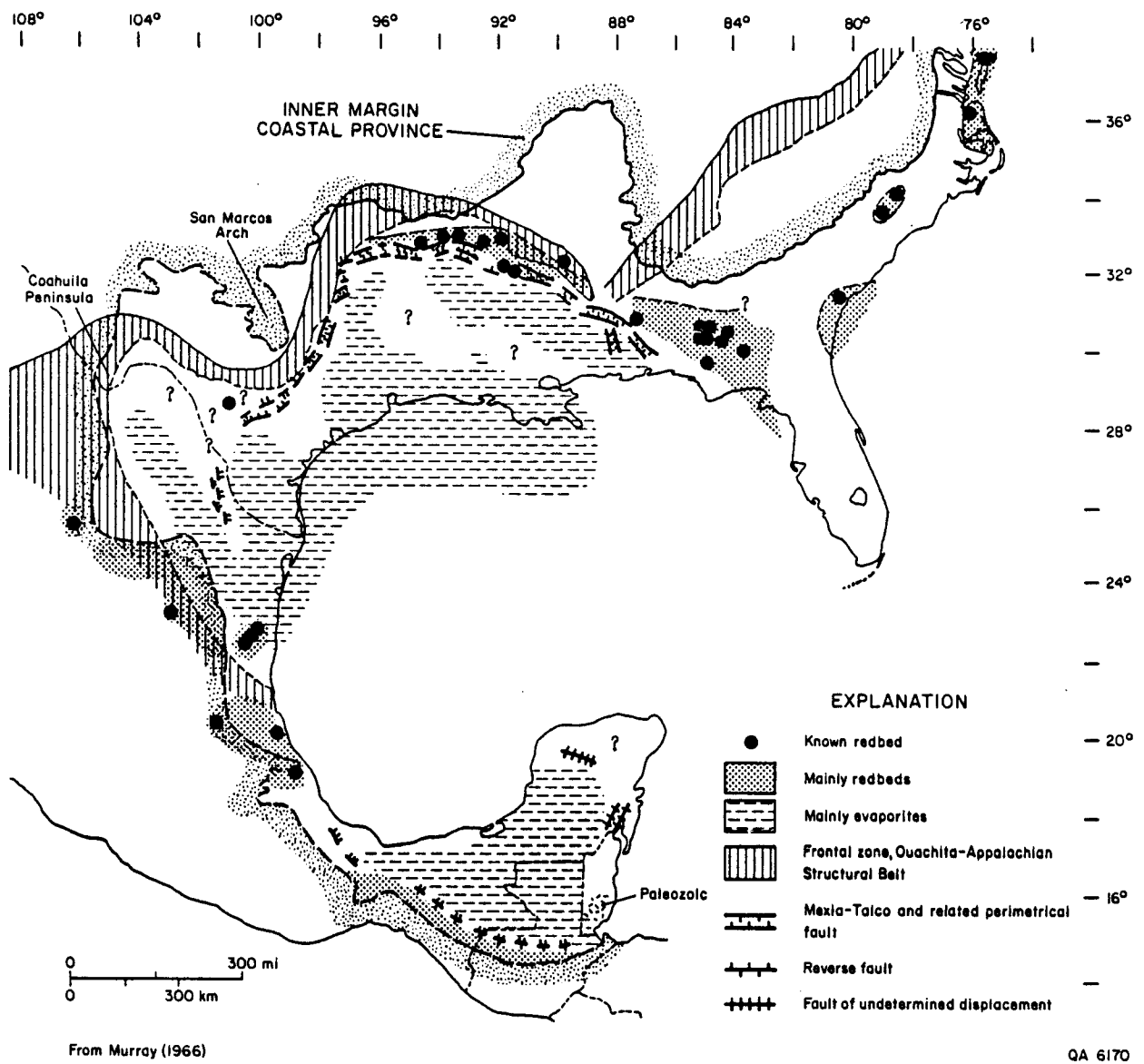


Figure 33. Generalized, probable Triassic lithofacies distribution, Gulf of Mexico basin. From Murray, 1966.

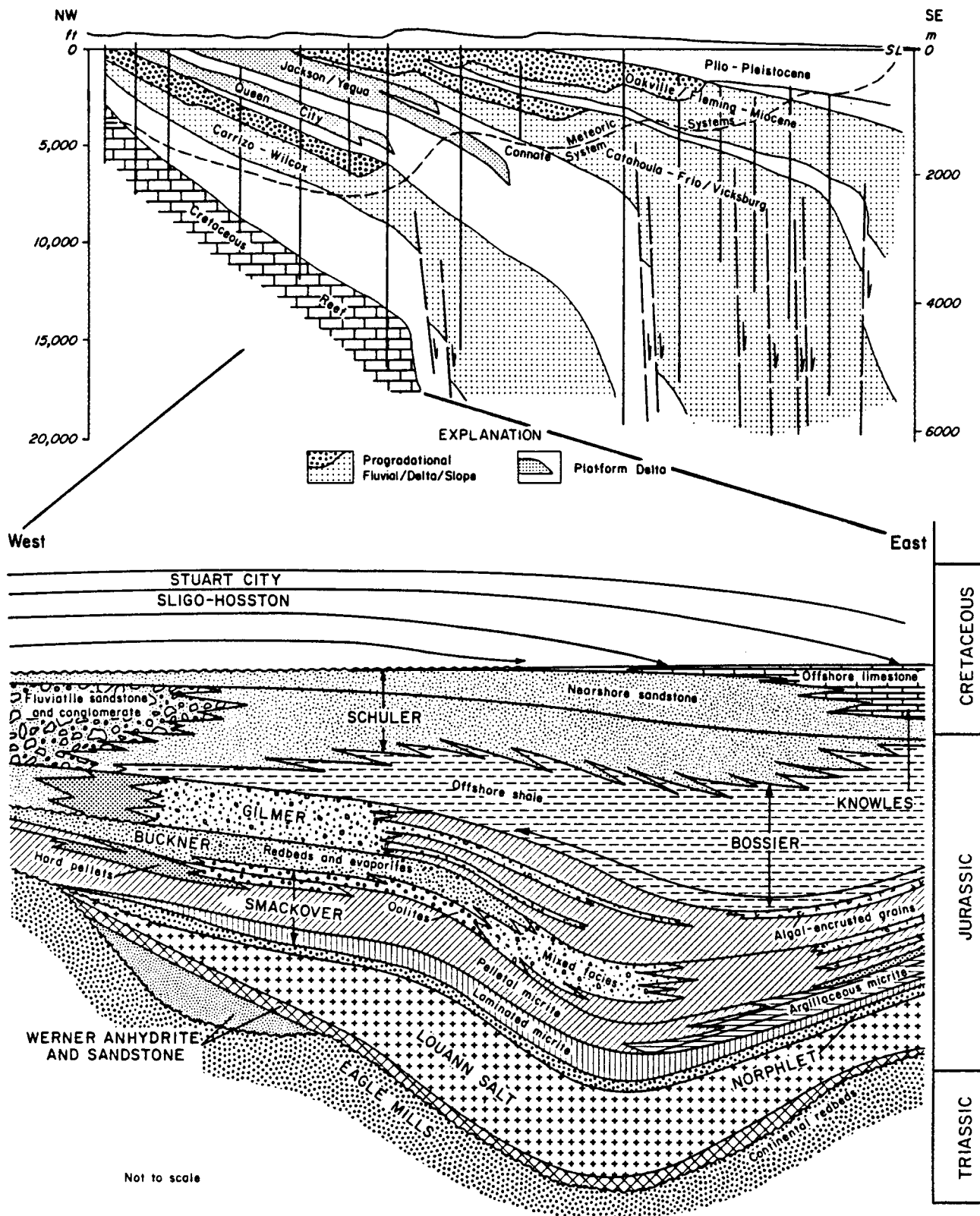


Figure 34. Schematic dip section illustrating the offlapping Tertiary stratigraphic sequence of the Texas Gulf Coastal Plain (from Galloway and others, 1982) and a west-to-east section across the East Texas Basin showing formational units within each sequence (from Todd and Mitchum, 1977).

Gilmer sequence (fig. 34) (Todd and Mitchum, 1977). The Norphlet Formation, which overlies the Louann salt, represents a thin interval of red and pink sandstone and siltstone (Todd and Mitchum, 1977), similar to the underlying Eagle Mills Formation (fig. 34). The Werner Anhydrite, thought to represent a marginal equivalent of the Louann salt, consists of horizontal laminated to cross-laminated anhydrite and locally coarse sandstone and conglomerate (fig. 34; Todd and Mitchum, 1977). The Werner Anhydrite are underlain by the Werner Red-Bed Member made up of red clays and sands, some conglomeratic up to 100 ft thick (30.5 m) (Hazard and others, 1945). The Louann-Werner evaporite sequence is dated as Middle Jurassic by Kirkland and Gerhard (1971) and Watkins and others, (1976).

The Eagle Mills Formation is a red-bed section of shale, siltstone, sandstone, and conglomerate, and intrusive igneous sills and dikes are common (Todd and Mitchum, 1977). Basaltic intrusives suggest that the Eagle Mills is largely Late Triassic (Baldwin and Adams, 1971), while plant macrofossils indicate that it could be as young as Early Jurassic at its top (Scott and others, 1961; Todd and Mitchum, 1977).

Sulfates (gypsum or anhydrite) that precipitated within the Louann salt during Middle Jurassic times had $^{87}\text{Sr}/^{86}\text{Sr}$ ratios consistent with Middle Jurassic seawater (0.7068-0.7076; Posey, 1986). The strontium isotope ratios of the evaporitic anhydrites in the interior basins are much lower than the isotopic ratios of anhydrites present within the Houston Diapir province and the South Texas diapir province (Posey, 1986; fig. 30). The presence of dolomites in stable equilibrium with anhydrites suggests that halite, dolomite, and anhydrite all probably formed at near-surface conditions (Posey, 1986).

Galloway (1982) has defined three regions in the Texas Gulf Coast sedimentary prism: (1) a meteoric regime that extends down to 5,000 ft (1,500 m), (2) an Elysian (compactional) regime from 8,000 to 12,000 ft (2,500 to

3,700 m), and (3) a deeply buried Abyssal (thermobaric) regime at greater depths (Table 3). In the Abyssal regime the fluid pressures approach lithostatic pressure, gas generation and clay dehydration accelerates, and microfractures develop (Bogomolov and others, 1978).

In the meteoric regime, waters are commonly fresh to brackish in the Gulf Coast and mixed calcium-sodium-bicarbonate-chloride types (Galloway, 1982). The trace and heavy-metal content of the meteoric water (Cu, Zn, Pb, and Ni) is low (less than 0.1 to 0.01 mg/L) whereas iron is less than 0.1 to 1 mg/L, and total dissolved solids are between 100 and 10,000 mg/L (Galloway, 1982). Although the U_3O_8 content of the meteoric fluids is less than 0.1 mg/L, it is some 10,000 times that of the Abyssal regime fluids (Galloway, 1982).

The fluids in the compactional Elysian regime have been modified into sodium chloride brines of the marine connate type similar to the Abyssal regime fluids with measured pH values between 6 and 8 (White, 1965; Kharaka and others, 1977). The rocks here are dominantly reduced, containing iron sulfides or dispersed organic material or both, whereas the hydrogen sulfide content of the fluids is low (less than 10 mg/L; Galloway, 1982). The heavy-metal content (Cu, Zn, Pb, and Ni) of fluids in the Elysian regime is generally less than 1 mg/L. Uranium has not been detected (Galloway, 1982). Liquid petroleum is generated in this interval, and the produced gases (methane, heavier fractions, and distillate) commonly contain 0.1 to 1 mole percent of carbon dioxide (Galloway, 1982), much less than the carbon dioxide content of Abyssal waters (\pm 10 percent in the Lower Frio at the Pleasant Bayou well; Morton, 1981).

Hot thermobaric waters are generated between 8,000 and 20,000 ft (2,500 m to 6,000 m, Abyssal regime) and are moderately to highly saline (10,000 to 200,000 mg/L; Gustavson and Kreitler, 1977) with the greatest values in those parts of the Gulf Coast characterized by salt diapirism (Galloway, 1982). Light

Table 3. Geochemical characterization of principal ground-water regimes of the northwestern Gulf Coast Basin, from Galloway, 1982.

	<i>Abyssal</i>			
	<i>Meteoric</i>	<i>Elisian</i>	<i>Terrigenous</i>	<i>Carbonate</i>
Depth range (generalized)	0-2,000 ft; 5,000+ max 0-600 m; 1,500+ max	2,000-12,000 ft ± 600-3,600 m ±	<12,000 ft ± <3,600 m ±	<20,000 ft <6,000 m
TDS	10 ² -10 ⁴	10 ⁴ -10 ⁵	10 ⁴ -10 ⁵	10 ³
Ca	10-10 ³	10 ² -10 ⁴	10 ² -10 ⁴	10 ⁴
HCO ₃	10 ² -10 ³	10 ²	10 ² -10 ³	n.d.
SiO ₂	10-10 ²	10-10 ²	10-10 ²	n.d.
Fe	10 ⁻¹ to <10 ⁰	≤10	10 ⁻¹ -10	10 ³ -10 ⁴
Heavy metals (Cu, Zn, Pb, Ni)	<10 ⁻¹	<10 ⁰	<10 ⁻¹ -10	10-10 ² + (Zn; Pb)
Se, Mo, As	<10 ⁻²	≤10 ⁻²	<10 ⁻²	n.d.
U ₃ O ₈	≤10 ⁻¹	n.d.	≤10 ⁻⁵	n.d.
SO ₄	10-10 ³	<10 ⁰ -10 ²	10 ⁰ -10 ²	10-10 ²
H ₂ S, HS ⁻	≤10	<10	<10 ⁻² mol % in gases; ≤10 ⁰	10 ⁻² to 10 ⁻¹ mol % + in gases
Eh	+500 to -200 mV	Reducing	Reducing	Reducing
pH	6.8 - 8.2	5.5 - 7.5	4 - 6.5	n.d.

Data compiled from analyses in White (1965), Gustavson and Kreitler (1977), Kharaka and others (1977), Dorfman and Fisher (1980), and Prezbindowski (in preparation).

hydrocarbons (principally methane), hydrogen sulfide, and carbon dioxide are generated from organic materials at the temperatures characteristic of the abyssal zone (Galloway, 1982). Isotopically light methane and isotopically heavy carbon dioxide are generated from the decarboxylation of acetic acid between 80°C and 200°C (176°F and 392°F) (Kharaka and others, 1985). Thermal gas predominates between 170°C and 180°C (338°F to 356°F) (Dozy, 1970; Karstev and others, 1971).

The meteoric regime represents the type of environment that existed during the initial stages of burial of the Eagle Mills, Werner, and overlying Louann "mother" salt prior to a temperature increase from about 70°F to 176°F (21°C to 80°C) (fig. 35a and 36).

Smectite undergoes transformation to the ordered mixed-layer 20 percent smectite/80 percent illite as temperature and pressure increase owing to burial (Burst, 1969; Boles and Franks, 1979). Although this transformation is partly controlled by temperature (Loucks and others, 1981), other factors must also play a role. In the Pleasant Bayou geopressured-geothermal test well this transformation occurs in the upper Frio Formation (fig. 37; Freed, 1979) at about 11,500 ft or 119°C to 123°C (246°F to 253°F). This is 25°C to 30°C (45°F to 54°F) higher than in Hidalgo County in South Texas (Loucks and others, 1981). The smectite-illite transformation occurs near the uppermost major marine sandstone unit in the Frio, the uppermost appearance of geopressure in the sandstones, and the upper limit of anomalously high vitrinite reflectance (fig. 38).

The amount of water lost by dehydration during the smectite-illite transition represents 10-15 percent of the compacted bulk volume of the argillaceous sediments (Mooney and others, 1952; Burst, 1969). This period of apparent clay dehydration coincides with a maturity level of 0.5 percent R_o (Foscolos and others, 1976; Powell and others, 1978). The transformation of smectite to illite is

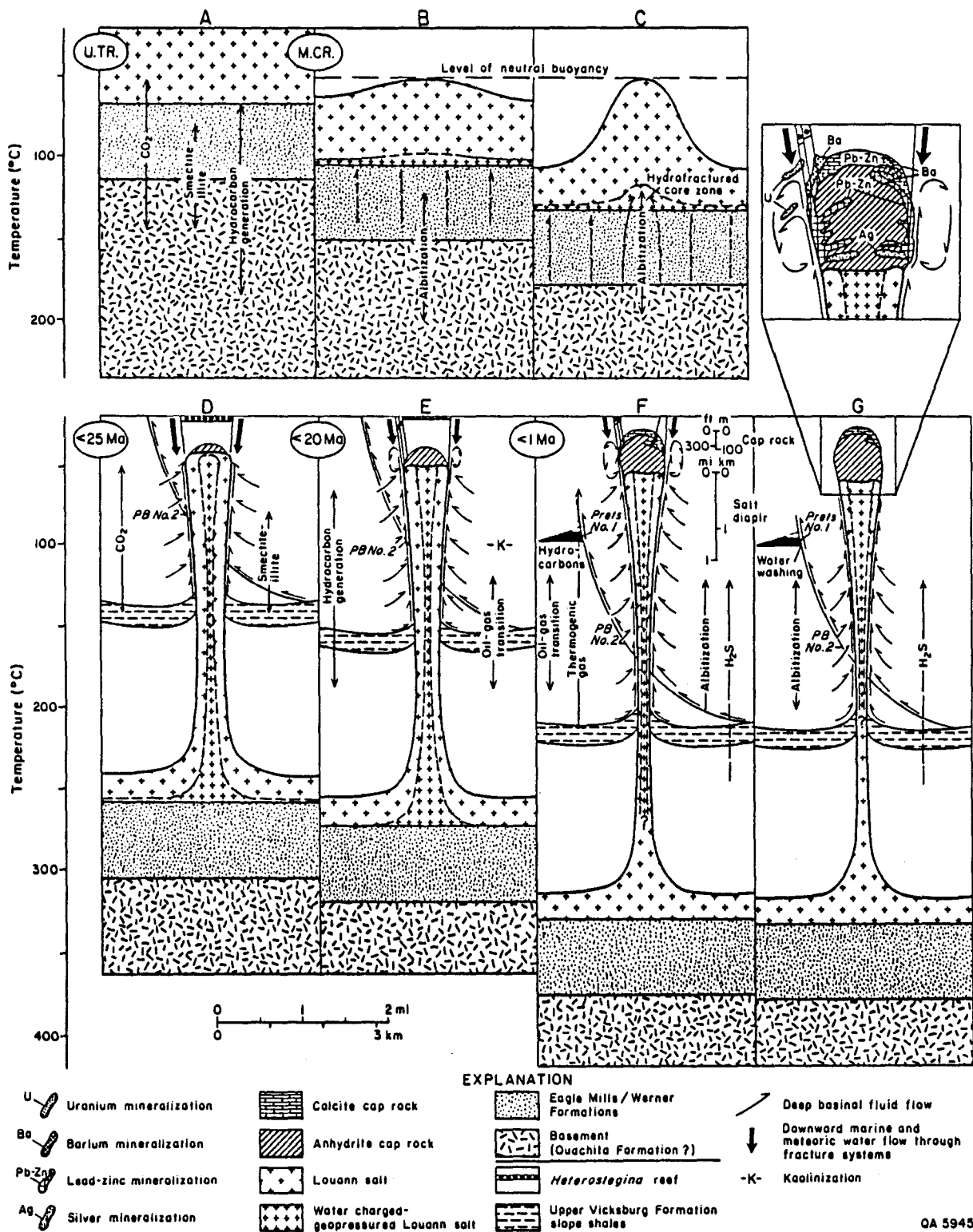


Figure 35. Model depicting the development of diagenetic, geopressured-geothermal, and hydrocarbon generation zones and salt dome and salt dome cap rock formation and mineralization for the coastal basin of the Gulf Coast. Diapiric model from Woitdt, 1978. Cap rock model from Price and others, 1983. Diagenetic temperatures from Loucks and others, 1981. Hydrocarbon generation temperatures from Hunt, 1979, and Kharaka and others, 1985.

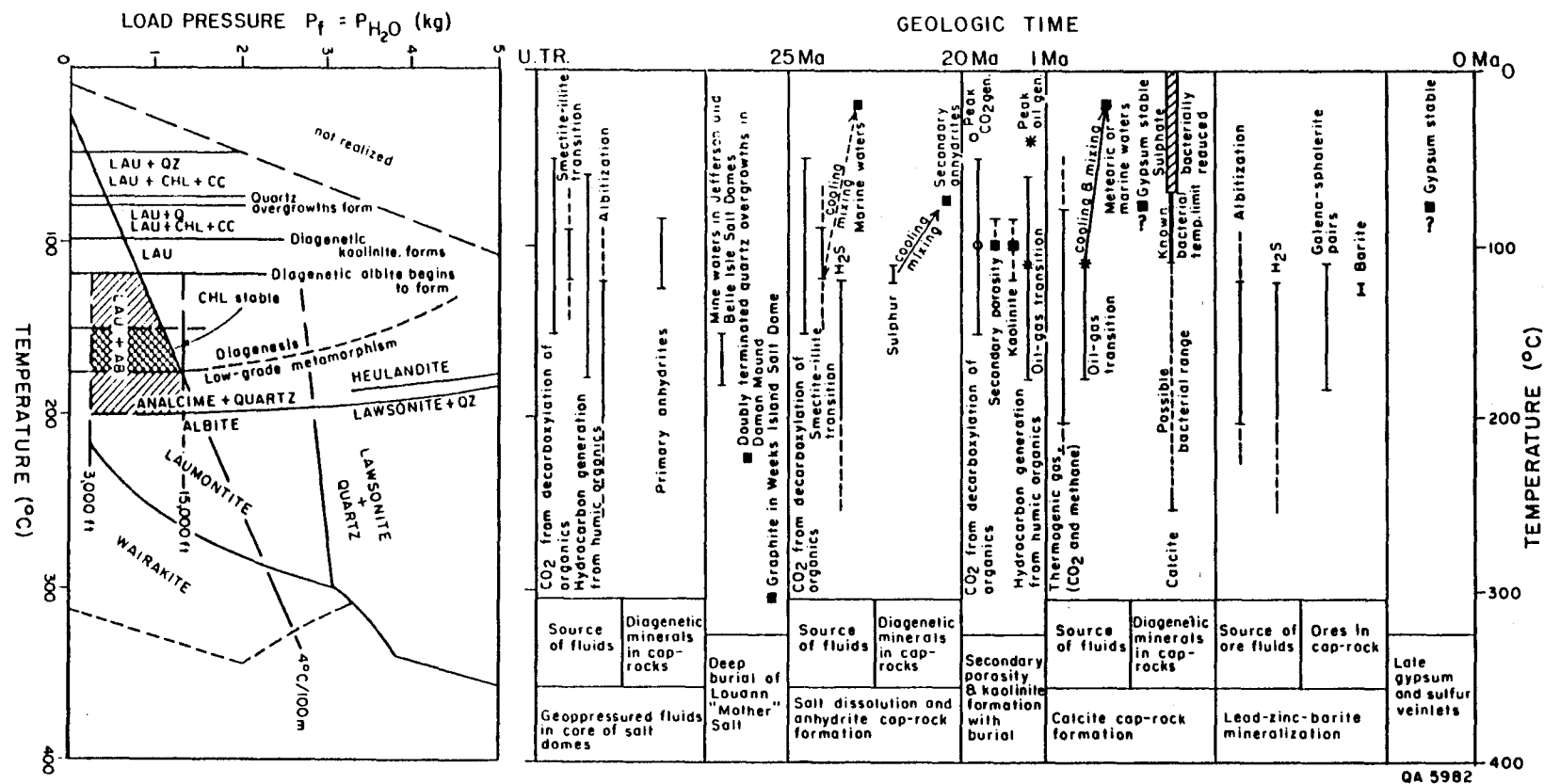


Figure 36. Variation of source fluid and diagenetic mineral and ore temperatures through geologic time for Hockley dome compared with the pressure-temperature stability field for laumontite, albite, and chlorite. Fluid inclusion and mineral stability data from Price and others, 1983; Kreitler and Dutton, 1983; Kaiser and Richmann, 1981; Loucks and others, 1981; Weaver, 1980; Knauth and others, 1980; Winkler, 1976; Liou, 1970, 1971; and Hay, 1966. Hydrocarbon generation temperatures from Kharaka and others, 1985; and Hunt, 1979. Bacterial limits from Brock, 1985.

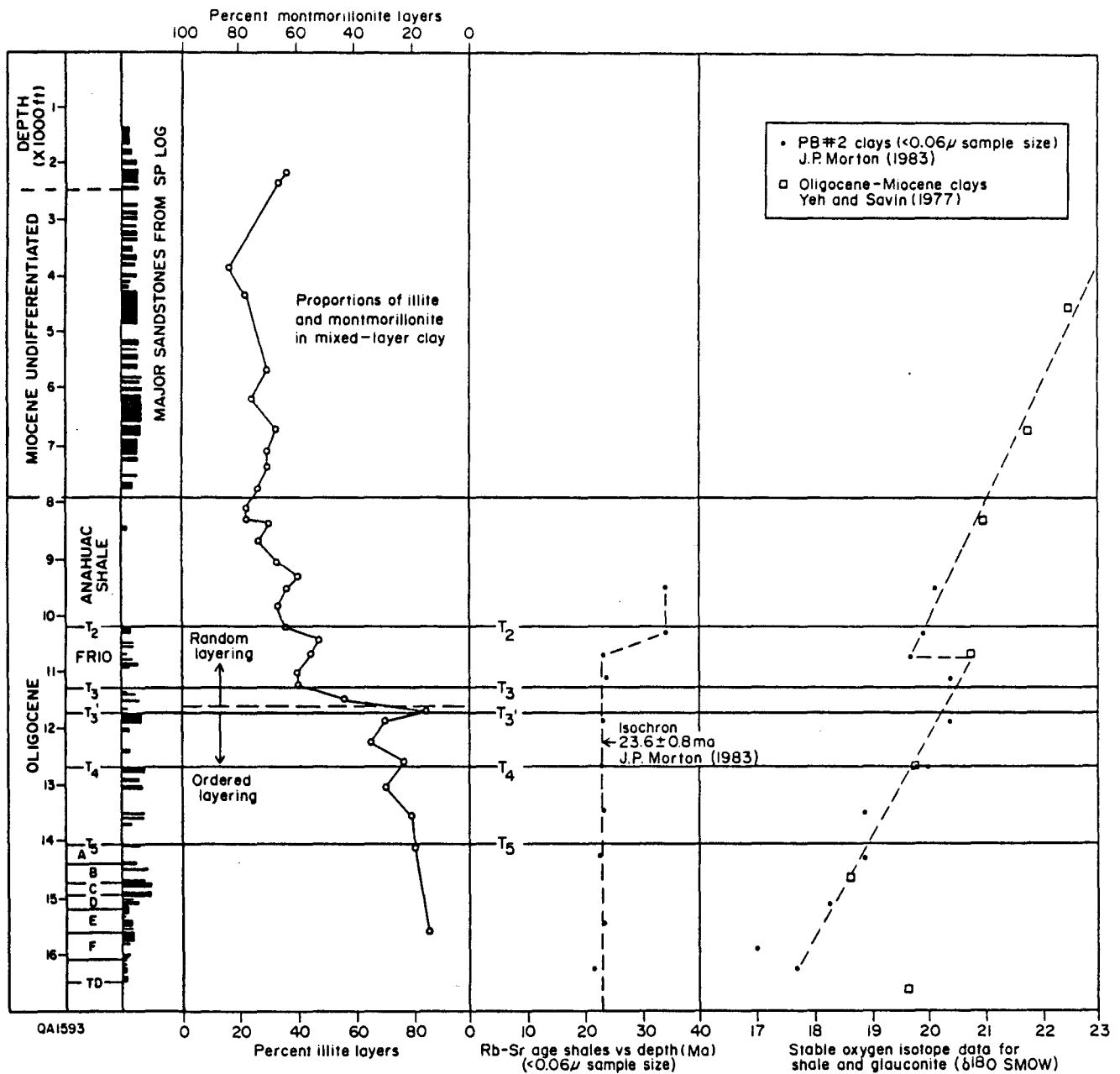
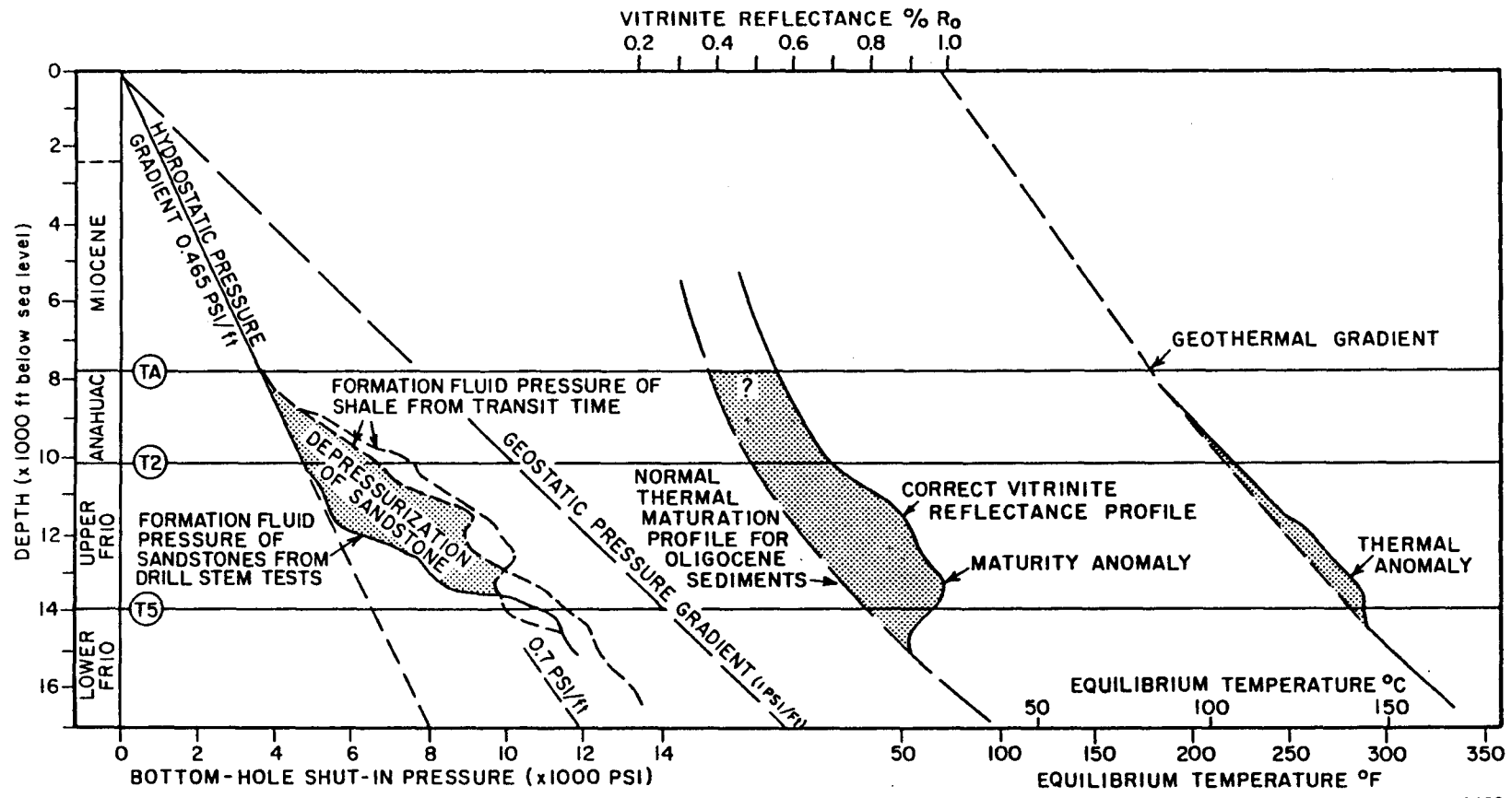


Figure 37. Proportion of illite and smectite in mixed-layer clays versus depth, Pleasant Bayou No. 1 well (Freed, 1979); apparent Rb-Sr age of clays <math><0.06 \mu\text{m}</math> in diameter versus depth in the test well (J. P. Morton, 1983); and oxygen isotope values for shale and glauconite versus depth in the test well (Yeh and Savin, 1977; J. P. Morton, 1983). From Ewing and others, 1983.

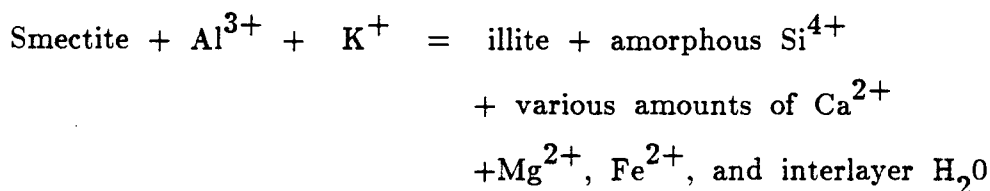


QA 4402

Figure 38. Fluid pressure, geothermal, and thermal maturity profiles for the Pleasant Bayou No. 2 test well. From Light and D'Attilio, in press.

potentially important if water and ions released by this reaction migrate into the sandstones, where they may affect diagenesis (Loucks and others, 1981).

Boles and Franks (1979) have shown that smectite-illite reactions with aluminum as an immobile component release significantly more cations (silica release increases more than five times) than do reactions in which aluminum is considered a mobile component (Loucks and others, 1981). The transformation reaction is outlined below:



(Hower and others, 1976)

During the normal conversion of smectite to illite in shale bodies the potassium content of associated brines is depleted (fig. 39; Collins, 1975). Clay minerals readily adsorb potassium, and in illite it is incorporated in the crystal structure in such a manner that it cannot be removed by ion-exchange reactions (Lyon and Buckman, 1960). Rubidium, which has a similar ionic radius to potassium, has a greater tendency to be absorbed by clays than does potassium and is removed much more readily from solution than is lithium (Collins, 1975). Potassium, rubidium, and cesium ions are large enough to replace interstitial water molecules between clay layers, whereas lithium, barium, and magnesium are easily adsorbed onto clays (Collins, 1975).

Strontium behaves geochemically in a similar way to calcium, as it has the same charge and a similar ionic radius (Ahrens, 1965a,b). During the conversion of smectite to illite, water, calcium, common strontium, and radiogenic strontium derived from rubidium interstitial in the clay layers will be released.

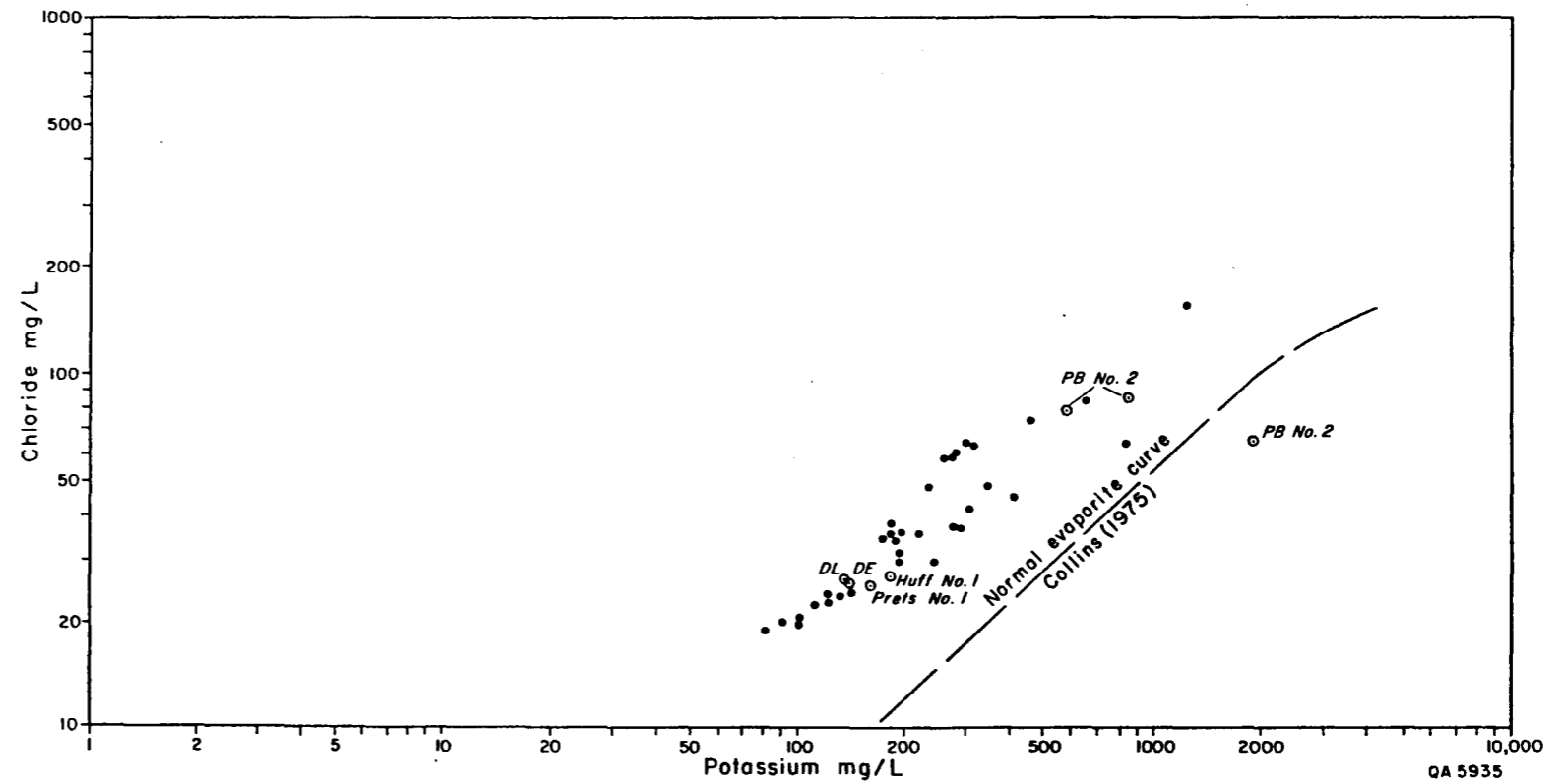
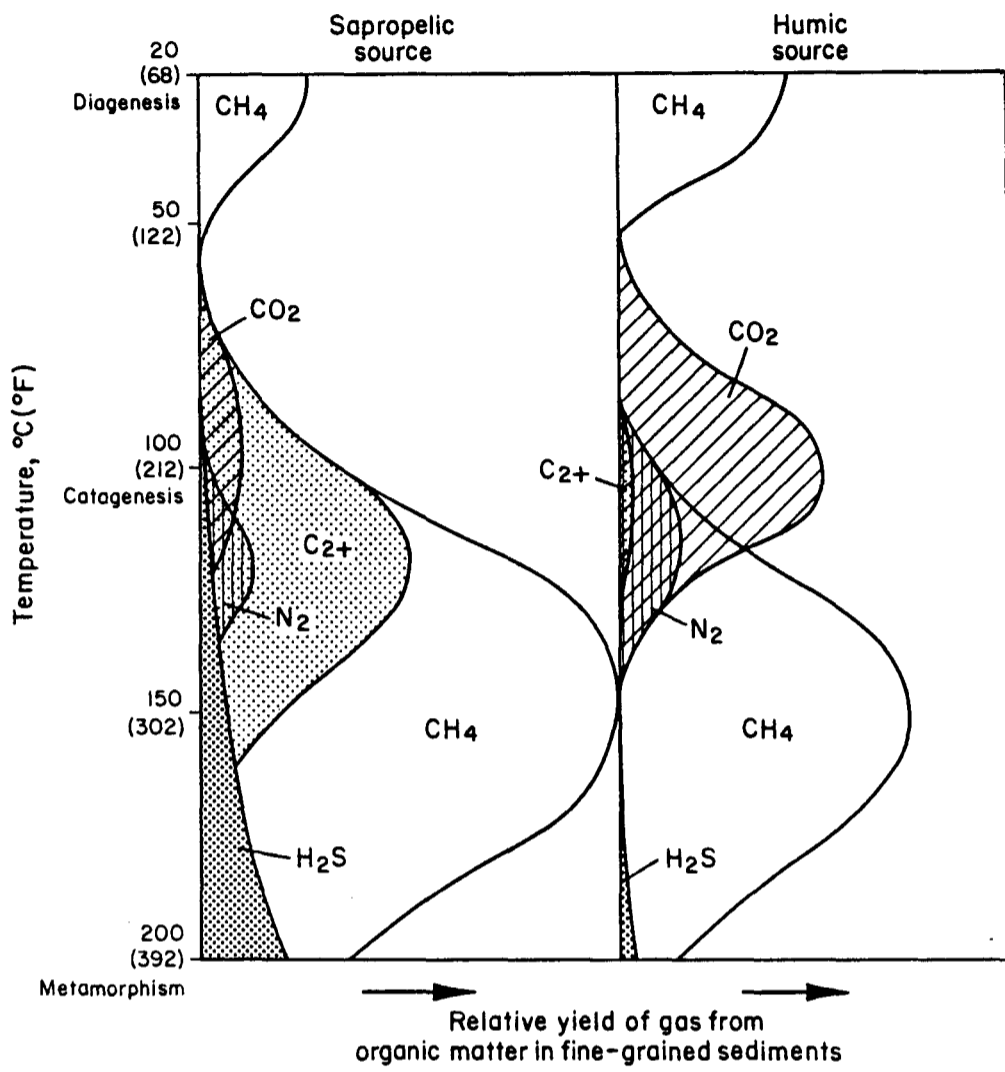


Figure 39. Potassium versus chloride for Frio Formation water samples within the Houston delta system, indicating an increase in potassium content with salinity and depth.

The arkosic Eagle Mills and Werner Formations entered the smectite-illite transition zone when temperatures exceeded 80°C (176°F), and this resulted in the generation of relatively fresh waters from the conversion of smectite to illite (Powers, 1967; Burst, 1969; Loucks and others, 1981). Waters developed below the Louann salt were probably enriched in radiogenic strontium. Relatively fresh shale waters generated in the Eagle Mills and Werner Anhydrite Formations would probably be trapped by, and collect below, the impermeable Louann "mother" salt, where salt dissolution may have proceeded in the undersaturated fluids (fig. 35b). This region would become aquathermally pressured from the continuous temperature increase with progressive increase in depth of burial (Palciauskas and Domenico, 1980).

The Eagle Mills and Werner Anhydrites entered the compactional Elysian regime when they were buried to depths greater than 2,000 to 5,000 ft (600 to 1,500 m) (fig. 35a, Galloway, 1982). Continued burial of the Eagle Mills and Werner Formations below the 50°C to 110°C (122°F to 230°F) isotherm (fig. 35b and 36) will result in the generation of carbon dioxide and subsequently of hydrocarbons in rocks with sufficient organic matter (Hunt, 1979). In addition, Kharaka and others (1985) showed that isotopically light methane and isotopically heavy carbon dioxide can be generated by the decarboxylation of acetic acid between about 80°C and 200°C (176°F and 392°F) over this depth range, which will result in a further increase in geopressure.

The peak of carbon dioxide generation during the maturation of organic matter occurs at 100°C (212°F), some 20°C (36°F) cooler than the peak of oil generation in humic rocks. Hence, initial fluids will have high carbon dioxide contents prior to formation of free hydrocarbons (fig. 40; Hunt, 1979). The generation of carbon dioxide would acidify the fluids and result in the generation



From Hunt (1979)

QA 6171

Figure 40. Generation of gases from organic compounds. From Hunt, 1979.

of secondary porosity by the dissolution of early diagenetic calcites (Selley, 1979). Secondary porosity formation in the Andrau ("C") sandstone in the lower Frio Formation at the Pleasant Bayou geopressured-geothermal well is dated by burial history methods as first starting some 19.5 Ma ago but reaching a peak between 14 Ma and 7.5 Ma ago. This period of carbon dioxide generation postdates the 23.6 Ma smectite-illite transition event at the same level (J. P. Morton, 1983a) and predates hydrocarbon migration into the sandstones in the Hitchcock N.E. field, consistent with Hunt's (1979) temperature model. Upward migration of the acidic carbon-dioxide-bearing fluids through shallower Cretaceous and Tertiary carbonate sequences could result in carbonate being taken into solution and its precipitation at shallower levels in salt dome cap rocks.

When the Eagle Mills and Werner Anhydrite Formations had been buried sufficiently, they entered the zone of albitization of feldspars at temperatures in excess of 120°C (248°F) (Loucks and others, 1981). The albitization of potassium feldspars and in part plagioclases (Deer and others, 1969) is a major process through which calcium and radiogenic strontium are released to the fluids. The fluids may also have been saturated with magnesium as well as calcium released from the shale dewatering at this time, because dolomite appears to have remained stable (Posey, 1986).

Price and others (1983), from fluid inclusion work, indicate that the temperature range of primary anhydrite crystallization in salt domes ranges from 85°C to 124°C (185°F to 255°F). This temperature range encompasses the smectite-illite transition zone (Loucks and others, 1981), the hydrocarbon generation zone from humic source rocks (Hunt, 1979), and part of the feldspar albitization zone (Loucks and others, 1981), indicating that this is the region where the fluids were generated, leading to the recrystallization of isotopically heavy anhydrites present in the salt dome cap rocks. The formation temperature

has increased more than 45°C (81°F), compared with surface temperatures in this interval (80°C to 125°C, 176°F to 257°F), and this coupled with the shale water, carbon dioxide, methane, and heavy hydrocarbon generation would soon lead to high geopressuring, microfracturing, and dilation of the Eagle Mills and Werner Formations as well as the zone of irregular dissolution at the base of the Louann "mother" salt (figs. 35b and 35c).

Extensive microfractured zones develop in rocks when the cumulative fluid pressure exceeds the minimum principal stress and the enhanced pore volume can accommodate the volumetric expansion of the heated water, providing pressure relief (Palciauskas and Domenico, 1980). For sedimentary rocks containing progressively heated pore fluids, microfracturing and dilatancy have been observed when the ratio of the pore fluid pressure to the geostatic pressure exceeds 0.8 (Handin and others, 1963; Palciauskas and Domenico, 1980), assuming that the Louann "mother" salt acted as a permeability seal in the area. This result is probably correct for sandstone, limestone, siltstone, and shale, as it is not controlled by the rheology of the rocks (Palciauskas and Domenico, 1980).

Dilatancy appears to occur within a temperature range of 125°C to 200°C (257°F to 392°F), assuming a surface temperature of 20°C (70°F) and a normal geothermal gradient of 30°C/km (1.6°F/100 ft; Palciauskas and Domenico, 1980). The time that dilatancy occurs is therefore consistent with the peak of oil generation (Hunt, 1979) and major albitization of the feldspars (Loucks and others, 1981). Furthermore, the fluid volume increase that results from the transformation of smectite to illite (Powers, 1967; Burst, 1969) acts in much the same way as the thermally expanded fluid and can contribute to the initiation of dilatancy (Palciauskas and Domenico, 1980).

If a geothermal gradient of $25^{\circ}\text{C}/\text{km}$ ($1.37^{\circ}\text{F}/100\text{ ft}$) is assumed for the sedimentary succession, dilatancy occurs at a depth in excess of 4,000 m (13,123 ft) (Palciauskas and Domenico, 1980). The initiation of dilatancy is independent of the rate of burial, and for a given geothermal gradient and depth to the dilatancy zone there is a wide range of maturation possibilities prior to microfracture development (Palciauskas and Domenico, 1980).

Jackson and Seni (1983) have shown that the initial salt pillow formation in the Louann salt was initiated in mid-Cretaceous by the deposition of thick mid-Cretaceous limestones, which then began to slide down the basin slope on a detachment plane within the Louann salt, buckling the underlying formations. The formation of salt pillows or ridges at this time may have confined the geopressured fluids below the core of the salt-centered structures (fig. 35c). Fluids within the Eagle Mills-Werner sequence may have become isolated below the Louann "mother" salt during initial salt dome movement, so that fluid pressures rose to the point where widespread dilation of the Eagle Mills-Werner and the base of salt occurred. The base of the salt would probably have already developed an erratic dissolution zone when shale waters collected below it (fig. 35c).

During major diapirism of the salt, the zone of fluids would be progressively drawn into the center of the salt ridge or dome as it formed, consistent with the fact that core zones of salt domes contain older rocks (Jackson and Seni, 1983). Anhydrites with Jurassic $^{87}\text{Sr}/^{86}\text{Sr}$ ratios then recrystallized in the presence of the geopressured fluids, which contained abundant radiogenic strontium derived from albitization reactions and the smectite-illite transition. The recrystallization of the primary anhydrites may have occurred simultaneously with salt dome movement, and varying amounts of radiogenic strontium incorporated in the newly formed mineral grains have resulted in the variable but high $^{87}\text{Sr}/^{86}\text{Sr}$ isotope ratios found in them.

Furthermore, inclusions in rock salt at Winnfield Dome consist largely of carbon dioxide, water, and smaller amounts of heavier hydrocarbons under pressures ranging from 7,350 to 14,700 psi (500 to 1,000 bars at 0°C) and have caused blowouts during salt mining (Hoy and others, 1962). These pressures correspond to depths of 14,000 to 21,000 ft (4,300 m to 6,400 m) using a normal hydrostatic and a geopressure gradient of 0.7 psi/ft for the Gulf Coast. The estimated depth range for salt recrystallization indicates that the geopressed fluid inclusions were probably derived from beneath or adjacent to the salt, in the shale dewatering, carbon dioxide, and hydrocarbon generation zones. Similar inclusions occur in the Oakwood Dome but appear to have been trapped between 1,750 ft and 2,500 ft (213 m and 765 m) (Dix and Jackson, 1982).

Though methane is the dominant constituent in abyssal zone brines, carbon dioxide averages several mole percent in fluids in limestone or sandstone reservoirs (Galloway, 1982). In the Pleasant Bayou geopressed-geothermal test well the carbon dioxide content of fluids in the lower Frio exceeds 10 percent, and the fluids are saturated in methane (Morton, 1981).

Buried organic matter begins to generate hydrogen sulfide when temperatures exceed 120°C (250°F), and generation reaches a peak at 170°C (338°F) (fig. 40; Hunt, 1979; Galloway, 1982). The waters are also reducing relative to iron because of the presence of sulfide and the common occurrence of pyrite in host sand-shale sediments that have removed most of the hydrogen sulfide from solution (Galloway, 1978). High concentrations of water-soluble hydrogen sulfide is therefore confined primarily to carbonate reservoirs where it is enriched in ³⁴S, as is typical of deep thermal sulfide (Galloway, 1978; Goldhaber and others, 1979). It is important to note that the temperature of initial hydrogen sulfide generation in organic matter (120°C, 250°F; Hunt, 1979) is the same as the temperature of initiation of albitization reactions in feldspars (Loucks

and others, 1981) that releases metals (Pb, Zn; Möller, 1983), suggesting a close relationship between fluids generated at this depth and lead-zinc deposits in salt dome cap rocks. Abyssal regime fluids contain high contents (0.1 to 10 mg/L) of heavy metals (Cu, Zn, Pb, Ni, and Fe), which can reach 10 to 100 mg/L in carbonate rocks, but the uranium content is low (0-10 mg/L) (Galloway, 1978). These fluids are thus probably not the source of the enriched uranium found in uranium mineralization fronts (Galloway, 1982).

Geochemical evidence indicates that salt domes ("mother" salt, pillows or diapirs) have been buried to considerable depths before reaching their present positions (Kreitler and Dutton, 1983). Graphite has been found in salt at the Weeks Island salt dome (Louisiana), indicating high temperatures (300°C, 570°F) and deep initial burial (fig. 36) (Weaver, 1980). Isotope data from mine water at Weeks Island, Jefferson Island, and Belle Isle salt domes (Louisiana) suggest that these waters are formation waters introduced at temperatures of 150°C to 180°C (300°F to 360°F) or depths of 3 to 4 km (2 to 2.5 mi; fig. 36; Knauth and others, 1980; Kreitler and Dutton, 1983). Price and others (1983) showed that doubly terminated quartz crystals within the cap rocks at Damon Mound (Gulf Coast Basin) contain fluid inclusions that crystallized at temperatures of about 240°C (464°F). They suggest that the doubly terminated quartz crystallized within the salt at depths of about 22,000 ft (6.7 km). Geopressured fluids trapped below the Louann "mother" salt would become saturated in silica, and continued burial of the "mother" salt through the zone of albitization at temperatures in excess of 200°C (392°F) would allow these fluids to be drawn into the core zone of the salt diapirs and thus rise to the surface. Increasing acidity of the deep abyssal brines due to organic acid and carbon dioxide generation between 80°C and 200°C (176°F and 392°F) (Kharaka and others, 1985) would lead to precipitation of the silica and its incorporation in the salt

(figs. 35d and 36). There is therefore clear evidence that thermobaric fluids from the Abyssal regime (Galloway, 1982) have been introduced into salt domes when they were buried to considerable depths (3 to 6.7 km; 10,000 to 22,000 ft) and that some of the anhydrite appears to have recrystallized under metamorphic conditions of high temperatures and pressures in a deep saline environment during salt dome uplift (Goldman, 1952; Kreitler and Dutton, 1983; Price and others, 1983). This data is consistent with the introduction of hot geopressured saline fluids into the core zone of a rising salt diapir. This would mobilize the core and cause it to rise more buoyantly, resulting in folding and dissipation of geopressured brines and recrystallization of the anhydrites under high temperature and pressure conditions (fig. 35d).

Cretaceous forereef slope and basinal carbonate and shale units form the stratigraphic foundation of the clastic Tertiary sequence below 20,000 ft (6,000 m)(fig. 34) (Galloway, 1982). Fluids in abyssal terrigenous formations are acid with pH values varying from 4 to 6.5 (Galloway, 1978). Therefore the upward migration of such fluids through carbonate formations would lead to deep carbonate dissolution and transfer of carbonate to shallower levels where it could precipitate as pore occluding cements, diagenetic seals, or salt dome calcite cap rocks.

Salt Dome Cap Rocks

Gose and others (1985) dated the anhydrite cap rock of the Winnfield dome in the North Louisiana Basin as Late Jurassic (160 Ma) using paleomagnetic data. This age is consistent with the Late Jurassic - Early Cretaceous rapid salt diapirism in the interior basins of the Gulf Coast (Seni and Jackson, 1983). Major widespread diapirism of salt domes in the coastal basins (fig. 30) was

initiated in the Tertiary by the deposition of Wilcox (fig. 34) and subsequent thick fluvio-deltaic sequences that quickly loaded the basinal sequence and caused a large buoyancy differential, the external driving mechanism for salt dome diapirism (figs. 35c and 35d) (Jackson and Seni, 1983).

A quickly rising salt diapir would draw geopressured brines into its core zone, causing the salt-hosted anhydrites to recrystallize. Core zones of salt domes are found to rise faster than the peripheries and early recumbent folds, developed in salt pillows and ridges by basal irregularities and flow drag, become refolded by subvertical curtain folds within the diapir (Jackson and Seni, 1983). When diapirs approach the surface, the low-density sediments less than 3,000 ft (1,000 m) deep act as a parachute break, and the salt bodies tend to bulge out, overfold, and incorporate underlying material in them (fig. 35d) (Jackson and Seni, 1983). Both the complex folding within the salt during major diapirism and the mixing at the surface would dissipate the radiogenic-rich geopressured brines throughout the salt such that anhydrites within the diapir would be able to assimilate varying amounts of radiogenic strontium during their recrystallization.

Initially the core zones of salt domes would be more buoyant than the rims as they would contain hot, low-density geopressured brines. This buoyancy differential could result in the formation of a convection system within the salt that would further increase the rate of uplift of the core zone and mixing and dissipation of the geopressured fluids throughout the salt. Added water would aid diapirism by permitting intergranular dislocation gliding or creep owing to the addition of intergranular fluids. Salt layers could be undergoing cyclic convection in regions with a thermal gradient as low as 30°C/km (1.64°F/100 ft) (Jackson and Talbot, 1986). The low viscosity required for convection to occur requires strain rates on the order of 10^{-11} sec.⁻¹ in dry rock salt even at several hundreds of degrees centigrade (Jackson and Talbot, 1986). However, similar high

rates have been recorded in damp salt and simple thermal convection is possible in nature in water-softened salt (Jackson and Talbot, 1986).

Kreitler and Dutton (1983) suggest from isotope data that the anhydrite cap rock at Oakwood dome formed by salt dissolution in a high-temperature (50° to 100°C , 122°F to 212°F), deep saline environment. However, this anhydrite has been deformed and recrystallized into a moderately well developed granoblastic texture implying "metamorphic" conditions of higher temperatures and pressures (Kreitler and Dutton, 1983). Similar recrystallization textures occur in Vacherie and Sulfur domes and have been attributed to pressure during domal uplift (Goldman, 1952). Anhydrite fractures at low confining pressures and temperatures but deforms by recrystallization at high temperatures (Müller and Siemes, 1974).

Fluid Migration in the Oligocene

Clauer (1976) has shown that the clay fractions of shales (< 2 microns) should generate isochrons clearly indicative of strontium isotope homogenization that will date the time of deposition, diagenesis, or burial metamorphism (Cahen and others, 1984). However, these isochrons most likely record diagenetic or burial metamorphic events (Cahen and others, 1984).

Using rubidium-strontium isotope data, J. P. Morton (1983) documented an isochron in samples from a clay fraction less than 0.06 millimicrons in diameter below 10,500 ft (3,200 m) (Upper Frio Formation) in the Pleasant Bayou geopressured-geothermal test well (fig. 37). This isochron is 23.6 ± 0.8 Ma (Oligocene-Miocene transition) with an initial ratio of 0.7088 ± 0.0004 , approximating that of Middle to Late Miocene seawater (fig. 37; J. P. Morton, 1983; Ewing and others, 1984). Shales above 10,500 ft (3,200 m) give an older

age (34 Ma) than the deeper shales, indicating that they record depositional or crystallization ages (J. P. Morton, 1983). The date of 23.6 Ma is stratigraphically equivalent to the T2-Mid Anahuac Formation interval some 500 to 2,000 ft (152 to 610 m) shallower, and the shallowest shale sample (10,500 ft, 3,200 m) falling on this isochron corresponds to a break in the linear trend of the oxygen isotope ratios for clay minerals in the area (fig. 37; J. P. Morton, 1983; Ewing and others, 1984).

J. P. Morton (1983) interprets the 23.6 Ma date as the age of the smectite-illite transition and suggests that at this time, the Frio, which had been rapidly depressed, was invaded by deeply derived fluids containing potassium, generated during feldspar dissolution, that converted smectite to illite. This conversion occurred between 65° and 75°C (149°F and 166°F) (estimated from oxygen isotope data, J. P. Morton, 1983), some 25° to 50°C (45° to 90°F) hotter than the ambient temperature of the sediments that were buried at much shallower depths (500 to 2,000 ft, 152 to 610 m) at that time. Evidently the sediments below 10,500 ft (3,200 m) in the Pleasant Bayou test well have been flushed by hot fluids 23.6 Ma ago (J. P. Morton, 1983).

There is evidence for widespread salt dome diapirism in the Gulf Coast Basin prior to the Oligocene-Miocene transition (Mid-Anahuac, 22 to 24.8 Ma ago, T. E. Ewing, personal communication, 1985). Seismic evidence indicates that major diapirism was initiated in the Hockley Dome - Katy field area about 60 Ma ago (lower Wilcox), whereas it terminated about 45 Ma ago (Yegua Formation) (P. E. Price, personal communication, 1985).

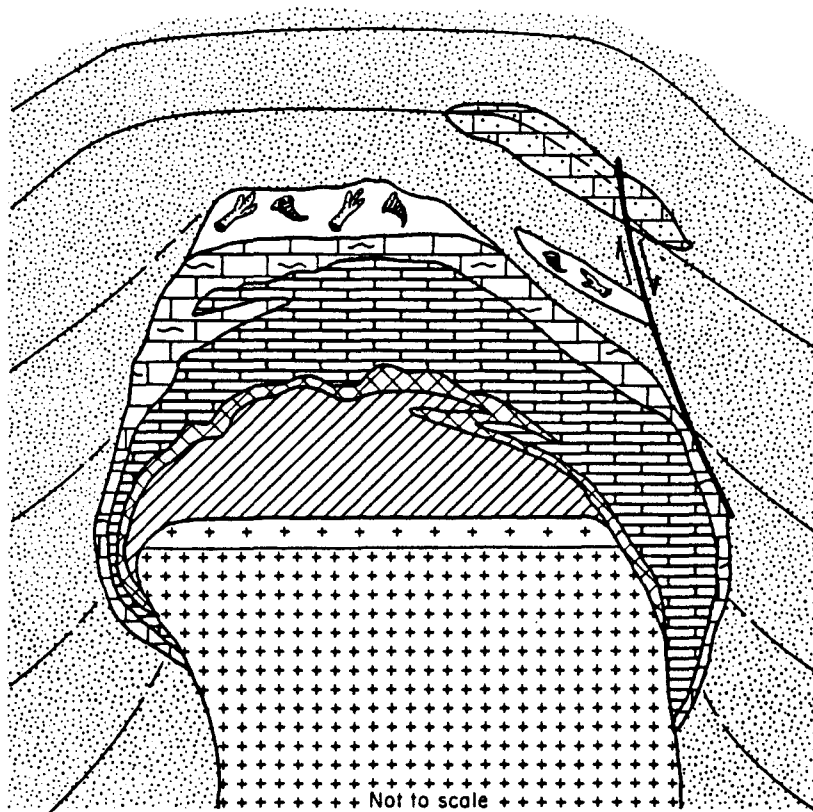
Damon Mound and surrounding Gulf Coast salt domes appear to have prominent highs on the Gulf of Mexico shelf during the Oligocene as they are covered by Heterostegina reefs (Collins, 1985), whereas the rest of the shelf area consists of Heterostegina Zone shales (Frost and Schafersman, 1979). The

Heterostegina Zone represents the greatest extent of Late Oligocene transgression (Frost and Schafersman, 1979). Rezak (1985) used the interlaminated Porites, corals, and muds in the Heterostegina Zone as evidence for periodic diapirism of Damon Mound in Late Oligocene times, though there are other stratigraphic explanations for this layering.

The age of the Heterostegina reef on Damon Mound (Mid-Anahuac, 22 to 24.8 Ma, T. E. Ewing, personal communication, 1984) corresponds closely to the 23.8 Ma age found for the smectite-illite transition (J. P. Morton, 1983), which suggests that the widespread diapirism represented by the Heterostegina reefs and the diagenesis of the Gulf Coast shales might be related. This limestone reef represents a perched marine false cap rock in the nomenclature devised by Posey (1986) (fig. 41) and has probably formed before or simultaneously with the upper part of the underlying true calcite cap rocks.

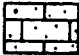







Seni and Jackson (1984) showed that the major rapid diapirism of the salt domes in the Gulf Coast Basin was initiated in the Tertiary by the deposition of the Wilcox and subsequent thick fluvio-deltaic sequences that quickly loaded the basinal sediments. By the end of the Oligocene the salt diapirs had reached the surface and entered the post-diapir stage of development (Seni and Jackson, 1984; Collins, 1985): At this stage the domes stay near the surface despite continued regional subsidence and deposition (fig. 35d) (Seni and Jackson, 1984).

Intrusion of diapirs can result in the formation of several types of crestal, flank, and tangential faults that can be subdivided into homothetic and antithetic types (fig. 42; Cloos, 1928; Dennis and Kelley, 1980; Jackson and Seni, 1984). The homothetic crestal faults provide unequivocal evidence of the rise of the salt plug relative to the surrounding strata (Jackson and Seni, 1984). On dome flanks homothetic faults are likely to form in strata that dipped toward the dome



From Posey (1986)

EXPLANATION

	Perched false calcite cap rock		Gypsum (transitional) cap rock
	Marine false calcite cap rock		Anhydrite cap rock
	Detritus-bearing false calcite cap rock		Salt dissolution zone
	True calcite cap rock		Salt stock

QA 6167

Figure 41. Schematic cross section of a salt dome showing a fully developed set of cap rock lithotypes. From Posey, 1986.

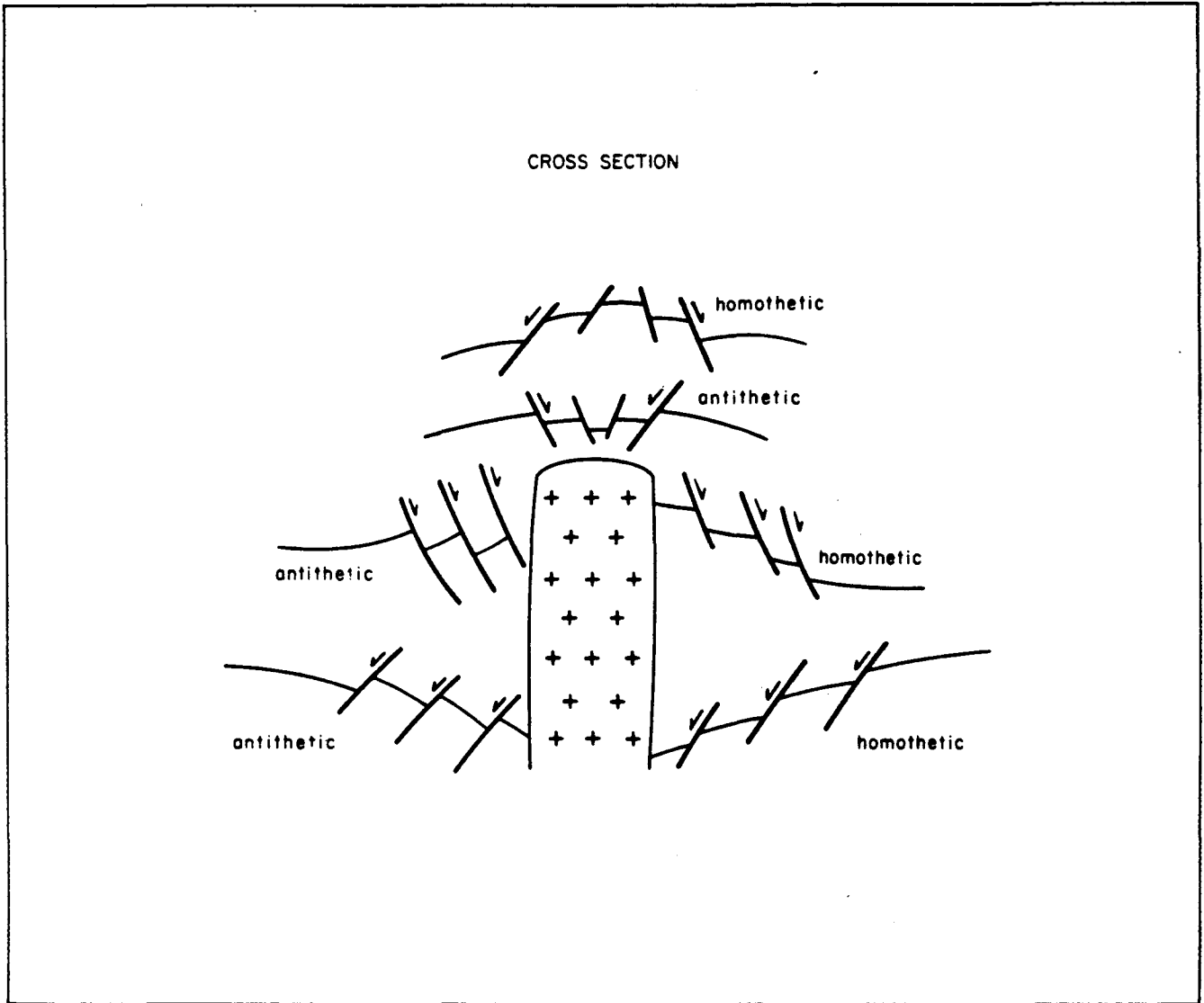


Figure 42. Classification of antithetic and homothetic faults around salt stocks, from Cloos, 1928, Dennis and Kelley, 1980, and Jackson and Seni, 1984.

during diapiric growth and pillow subsidence (Jackson and Seni, 1984). The Frio growth-fault system, which dips seawards into the Houston diapir province, therefore represents a homothetic fault system that would be reactivated by rapid diapiric uplift of the Gulf Coast Basin diapirs during regional settling of the basin into the void produced by the extruded "mother" salt (figs. 3d through 3g). The rapid diapiric uplift of salt domes would not only produce radial and tangential fracture systems around salt domes, which would allow the upward migration of deeply derived hot brines, but also inclined growth fault channels, which would channel these brines away landward and updip from the rising salt stocks (figs. 35d through 35g and 43).

There is a clear correspondence between evidence that Gulf Coast Basin diapirs had reached the surface (*Heterostegina* Zone limestones, Frost and Schafersman, 1979) and a major period of conversion of smectite to illite by waters at elevated temperatures (J. P. Morton, 1983). This suggests that prior to development of the Oligocene-Miocene boundary there was a period of rapid uplift of the Houston diapir province salt stocks and concomitant removal of the "mother" salt that culminated in the salt stocks puncturing the Anahuac shelf and being capped by *Heterostegina* reef facies at the end of the Oligocene (fig. 35d). Removal of the salt would have resulted in the subsidence and reactivation of the Frio growth-fault system at this time and could also be related to major subsidence of the Gulf Coast Basin, which resulted in the Late Oligocene transgression (Frost and Schafersman, 1979). Formation of fracture conduits would allow deeply sourced saline brines to migrate up around salt diapirs and away from them along growth faults through the Frio Formation sandstones and shales, where they subsequently reset the Rb-Sr age of the shales to 23.8 Ma (J. P. Morton, 1983) (fig. 35d). The driving mechanism for a period of major diapirism in the Oligocene in the Gulf Coast Basin may have been the

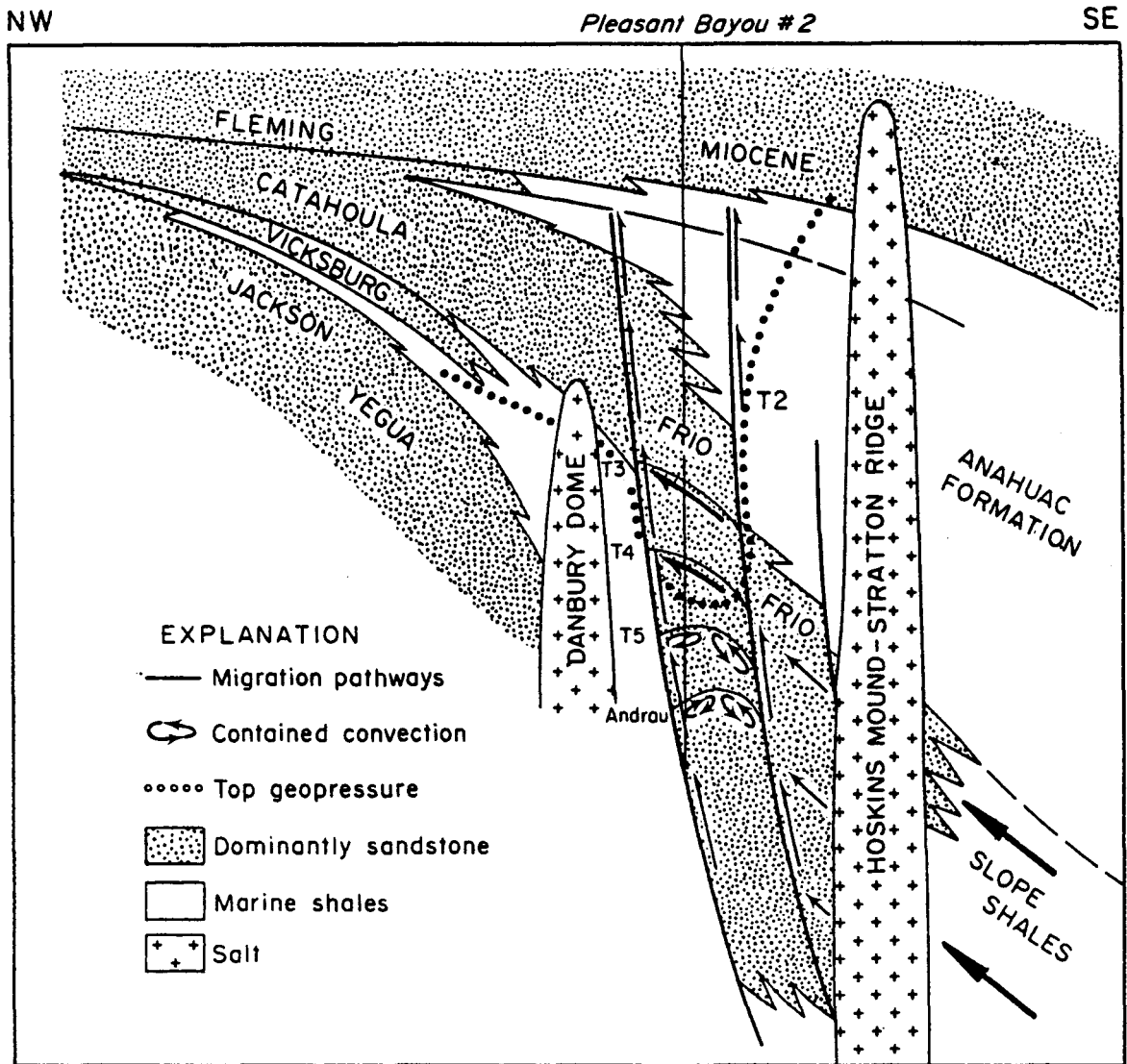


Figure 43. Stylized stratigraphic dip section across the Texas Gulf Coast showing the relative position of the GCO/DOE Pleasant Bayou geopressured-geothermal test wells. From Light and D'Attilio, in press.

deposition of the thick fluviodeltaic Frio Formation (Houston and Norias delta systems; Galloway, 1982), which loaded the "mother" salt, whereas the removal of a large part of the "mother" salt by diapirism resulted in subsidence and the major Anahuac transgression.

Galloway (1982) has described the sequence of sulfide mineralization associated with uranium deposits at Ray Point in the Wilcox fault zone. At Ray Point early (pre-uranium ore) pyrite pseudomorphing iron titanium oxide is rimmed successively by marcasite and then by authigenic smectite. Pyrite in the epigenetic sulfide and resulfidized altered zone has isotopically heavy sulfur isotopes between +10 and +28 ppt whereas the marcasite is isotopically light ($\delta^{34}\text{S}$ averages about -55 ppt), consistent with a bacterial or inorganic reduction of groundwater sulfate (Goldhaber and others, 1979; Galloway, 1982). Sulfides associated with uranium in the Hockley dome also have sulfur isotope ratios of +26 to +30 (Kyle and Price, 1985), indicating a deep source at temperatures similar to the Ray Point values demonstrated by Goldhaber and others (1979). Hockley sulfides have a sulfur isotopic composition similar to H_2S from South Texas gas fields, suggesting that externally reduced sulfur might have migrated to the structural trap provided by the salt diapir (Busche and others, 1982; Kyle and Price, 1985). The isotopically heavy sulfur isotopes imply that the sulfide bearing waters were generated near the base of the Gulf Coast sequence in this area (Land, 1984).

The isotopically heavy nature of the early pyrite at the Ray Point uranium deposit and the fact that it predates biogenic marcasite and diagenetic smectite suggests that in this environment it may have been derived from an early upward migration of deeply derived sulfur-bearing brines. Waters with $\text{Ca}^{2+}/\text{Fe}^{2+}$ ratio of less than 10,000 form ferroan-calcite, and to form calcite virtual absence of ferrous iron is required (Kaiser and Richmann, 1981). The presence of diagenetic calcite cement predating the smectite-illite transition

supports the early sulfur-bearing brine hypothesis, as calcite is stable in sulfide waters (Kaiser and Richmann, 1981).

Roll-front uranium mineralization at the Felder uranium deposit, Live Oak County, Texas, gives a well-defined $^{207}\text{Pb}/^{204}\text{Pb}$ - $^{235}\text{U}/^{204}\text{Pb}$ isochron age of 5.07 ± 0.15 Ma (Ludwig and others, 1982). At this deposit, ore-stage marcasites have light $\delta^{34}\text{S}$ sulfur, values while post-ore pyrites have heavy $\delta^{34}\text{S}$ sulfur, indicating a late (less than 5 Ma old) resulfidization by deeply derived H_2S . The uranium deposits are concentrated in or near faults of the Oakwood fault zone, which along with other faults in the area control location of oil and leakage of sour gas (Klohn and Pickens, 1970; Eargle and others, 1975). The $\delta^{34}\text{S}$ sulfur values of the late iron sulfide minerals in the Felder deposit are similar to those defined for sour gas from the underlying Edwards limestone of Cretaceous age, a possible source for the sulfur (Ludwig and others, 1982). Heavy sulfide present in uranium deposits at Hockley dome postdates diapirism and may therefore be a sequential variation in $\delta^{34}\text{S}$ from relatively shallow, light sulfur to deeper, heavier sulfur (Posey, 1986).

Cap-Rock Formation

Murray (1966) modeled salt dome cap rock formation (fig. 44). He stated that when a salt diapir reaches the surface it is truncated, folds are developed, and a solution table forms with the salt undergoing dissolution by undersaturated fluids, resulting in the accumulation of residual anhydrite. These fluids were, however, saturated in iron, calcium, and magnesium, as pyrrhotite rims euhedral anhydrite (Ulrich and others, 1984), and euhedral-zoned dolomite was stable (Posey, 1986), but the fluids were undersaturated in sodium and chloride as salt continued to be dissolved. The high iron, calcium, and magnesium content of the

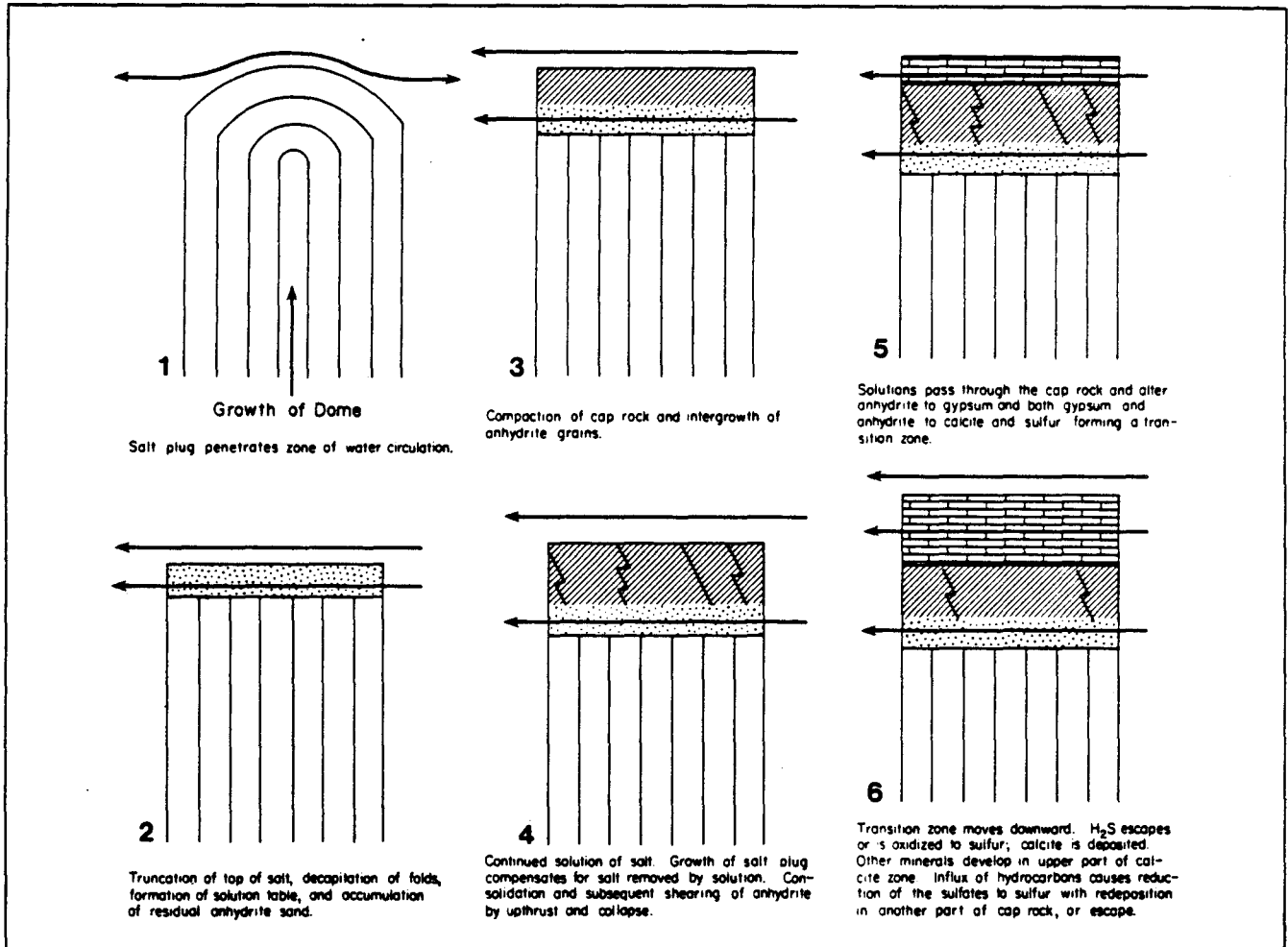


Figure 44. Six-stage sequence showing the development of salt dome cap rocks. Modified by Kyle and Price, 1985, after Murray, 1966.

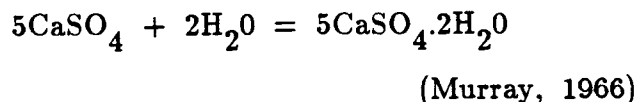
fluids suggests that they were derived from the smectite-illite transition zone (fig. 35d) over the temperature range 80°C to 123°C (176° to 253°F) (Hower and others, 1976; Loucks and others, 1981). The transformation of smectite to illite releases silica and various amounts of calcium, magnesium, iron, and water (Hower and others, 1976). Fracture conduits that developed above and around the margins of the salt domes during diapiric movement would allow the moderately deeply derived fluids passage to the surface, where they would mix with downward-percolating meteoric or marine waters and form the initial salt dissolution table (fig. 35d).

S. J. Seni (personal communication, 1985) showed that there are two distinct periods of sulfur crystallization in the salt dome cap rocks. Anhydrite cap rock crystals are rimmed and pseudomorphed by early lead-zinc sulfides and sulfur and contain remnant anhydrite (P. E. Price and S. J. Seni, personal communications, 1986). The early sulfides and sulfur predate calcite cap rock formation. The early sulfur may have formed at the high sulfur formation temperatures recorded by Price and others (1983) from mineral inclusion studies (110°C to 120°C , 230°F to 248°F) (fig. 36). The temperature range for sulfur formation (85°C to 124°C , 185°F to 255°F) is similar to that for primary (salt hosted) anhydrites but is too high for the formation of secondary anhydrites or calcite cap rocks (less than $\pm 70^{\circ}\text{C}$, 158°F), which S.J. Seni (personal communication, 1985) showed was predated by the early sulfur. This early sulfur may have originated from oxidation by mixing of deeply sourced, hydrogen-sulfide-bearing, hot, acid, reducing brines (abyssal regime H_2S , 120°C to 170°C , 250°F to 338°F formation temperature; Hunt, 1979; Galloway, 1982) with oxidizing alkaline meteoric fluids (Galloway, 1982) in a convective flow system (Workman and Hanor, 1985) formed on the fractured flanks of salt dome cap rocks (fig. 35e to 35g). The deeply derived hydrogen sulfide will be isotopically

enriched in $\delta^{34}\text{S}$ and may have resulted in the formation of early isotopically heavy pyrite in uranium deposits at this time. These highly pressured abyssal brines probably migrated up fracture zones developed along the salt dome margins by diapiric movement (Price and others, 1983) after the more shallowly derived illite-smectite brines, mixed with meteoric or marine waters, became undersaturated with salt and formed the salt dissolution table. Initial introduction of some heavy-metal sulfides into salt dome cap rocks indicates that some of the fluids originated from albitization in the abyssal zone. Salt dissolution at depth could theoretically occur around these salt domes as a result of upwelling deep fluids but in many places may have been prevented by a clay wall that commonly mantles salt stocks at depth (Murray, 1966), whereas the fluids would soon become saturated and unable to take further salt into solution at the progressively lower temperatures and pressures of the rocks with which they came in contact. However, addition of relatively fresh water at various levels from shale dewatering reactions could lead to additional salt dissolution as the fluids moved progressively up structure. Some thinning of salt domes thought to result from structural movement at depth could result from dissolution by this mechanism.

Inclusion studies on gypsum that has replaced anhydrite indicate that gypsum formed at temperatures of 76°C to 78°C (169°F to 172°F) in the salt dome cap rocks (fig. 36) (Price and others, 1983). However, Holland and Malinin (1979) state that gypsum is probably unstable above 75°C (167°F), which suggests that these inclusions may have been stretched during preparation (H. H. Posey, personal communication, 1986). This gypsum may have formed from the

hydration of the anhydrite at a transition zone that moves progressively downward during continuous salt dissolution (fig. 41; Posey, 1986):



Price and others (1983) showed that secondary anhydrites crystallized at temperatures of about 69°C (156°F) when the fluids became saturated with anhydrite from primary anhydrite dissolution and replacement by sulfur (fig. 36). These secondary anhydrites cement primary anhydrites. Cap rock anhydrites appear to have exchanged strontium with the fluid on cap rock formation, as they have lower concentrations than most salt-hosted anhydrites (Posey, 1986) except at Sulfur Dome where they are higher (Walker, 1974). Posey (1986) plotted the $^{87}\text{Sr}/^{86}\text{Sr}$ ratio of anhydrites in the salt and salt dome cap rocks against the reciprocal of the strontium content (fig. 45). The strontium isotope data from anhydrites within the salt are variable but lie on a straight line, suggesting that they are the result of the mixing of two components, one with a low $^{87}\text{Sr}/^{86}\text{Sr}$ ratio (0.7071 or less, probably Jurassic, evaporitic sourced material, Posey, 1986) and one with a high $^{87}\text{Sr}/^{86}\text{Sr}$ ratio (0.7094 [Posey, 1986], heavy radiogenic strontium sourced from albitization processes and/or transition of smectite to illite). The cap rock strontium isotope data can be included within a triangular area having a low 1/Sr or high ppm Sr side represented by the salt-included anhydrites and a high 1/Sr or low ppm Sr vertex ($^{87}\text{Sr}/^{86}\text{Sr}$ ratio = 0.7081, Posey, 1986) characteristic of Early Miocene marine carbonates (Posey, 1986). Some points fall out of the triangular area, but these represented specimens may contain gypsum and therefore may not have the composition of pure anhydrite. If the positions of these additional points are taken into account, the vertex of the triangle that includes cap rock data moves

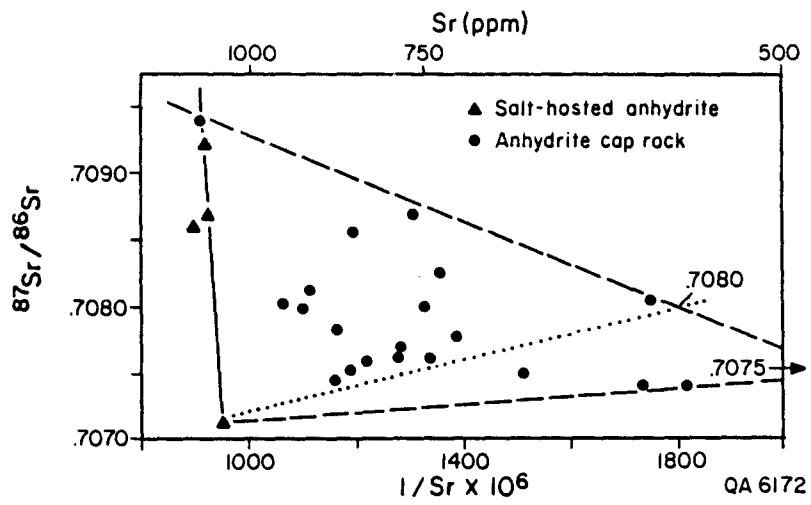


Figure 45. $^{87}\text{Sr}/^{86}\text{Sr}$ versus $1/\text{Sr}$ for Hockley anhydrite samples, from Posey, 1986.

to higher $1/\text{Sr}$ values and corresponds to a $^{87}\text{Sr}/^{86}\text{Sr}$ ratio of 0.70752 ppt characteristic of late Cretaceous marine carbonates (Posey, 1986). This suggests that the primary anhydrites recrystallized either in the presence of water of deep origin, with a Late Cretaceous marine carbonate component that migrated up the flanks of the salt dome, or in the presence of Early Miocene marine waters that migrated down the flanks of the cap rock after the salt dome had punctured the shelf. Although this relationship may be fortuitous the isotope data suggest that an Early Miocene age for the marine fluids is most likely and the salt domes must therefore have been close to or have punctured the sea bed at that time to have produced peripheral open fracture systems down which marine waters could have leaked into the salt dissolution zone and anhydrite cap rock area. These fluids would mix with deep basinal brines, reset the age of the recrystallizing anhydrites, and produce the variable $^{87}\text{Sr}/^{86}\text{Sr}$ ratios found in the cap rock anhydrites.

There appears to be a continuous temperature drop from the early high temperature sulfides and sulfur (110°C to 120°C , 230°F to 248°F ; Price and others, 1983) that replaced the primary anhydrites (S.J. Seni, personal communication, 1986) and gypsum after anhydrites (76°C to 78°C , 169°F to 172°F ; Price and others, 1983) to temperatures of less than 70°C (158°F) (Price and others, 1983) for the crystallization of secondary anhydrites and biogenic formation of calcite caprocks (fig. 36; Murray, 1966). Gypsum, however, is only stable at temperatures less than 75°C (167°F) (Holland and Malinin, 1979), which casts doubt on the inclusion temperature obtained for it by Price and others (1983). This temperature fall could simply be a result of the mixing of increasing quantities of cool early Miocene seawaters with hot deeply sourced brines in the salt dissolution zone and anhydrite cap rock area. The early Miocene age for the salt domes deforming the shelf at the time the *Heterostegina*

reefs formed (Rezak, 1985) is consistent with the smectite-illite transition in the Pleasant Bayou geopressured-geothermal test well (J. P. Morton, 1983), also believed to be a consequence of the same process.

During salt dome cap rock formation, hydrocarbon-bearing saline brines pass through the cap rock and alter the anhydrite to calcite and hydrogen sulfide in the presence of hydrocarbons and bacteria at a transition zone (figs. 35f and 44; Murray, 1966) that moves progressively downward (Posey, 1986). Initially formed calcites are dark, full of pyrite and residual materials, and cement early anhydrites or replace euhedral dolomite rhombohedrons (Kreitler and Dutton, 1983; Posey, 1986). These calcites are granular, sucrosic, and probably crystallized quickly from concentrated saline solutions (Posey, 1986). Later, void-filling calcites are larger light-colored crystals that probably crystallized from more dilute solutions (Posey, 1986). Some sphalerite occurs interleaved in the void filling calcites (P. E. Price, personal communication, 1986), indicating continued, though minor, addition of fluid components derived from albitization in the abyssal zone.

In the Oakwood dome, Kreitler and Dutton (1983) indicate that the carbon isotope data of calcites in the calcite cap rocks show three trends (fig. 46): (1) the calcites are isotopically depleted in $\delta^{13}\text{C}$ (relative to PDB), typical of calcite cap rock that has originated from the oxidation of hydrocarbon and the reduction of anhydrite; (2) both the light and dark calcites become depleted in $\delta^{13}\text{C}$ with depth ($\delta^{13}\text{C}$ varies from -9 to -11 ppt PDB), suggesting that they are related in origin (fig. 46). A similar, sometimes more poorly developed, trend is visible in other calcite cap rocks including at least Hockley and Winnfield (Posey, 1986); and (3) the dark (early) calcites are generally more depleted in $\delta^{13}\text{C}$ than the light calcites at the same depth. For any single dark-light calcite

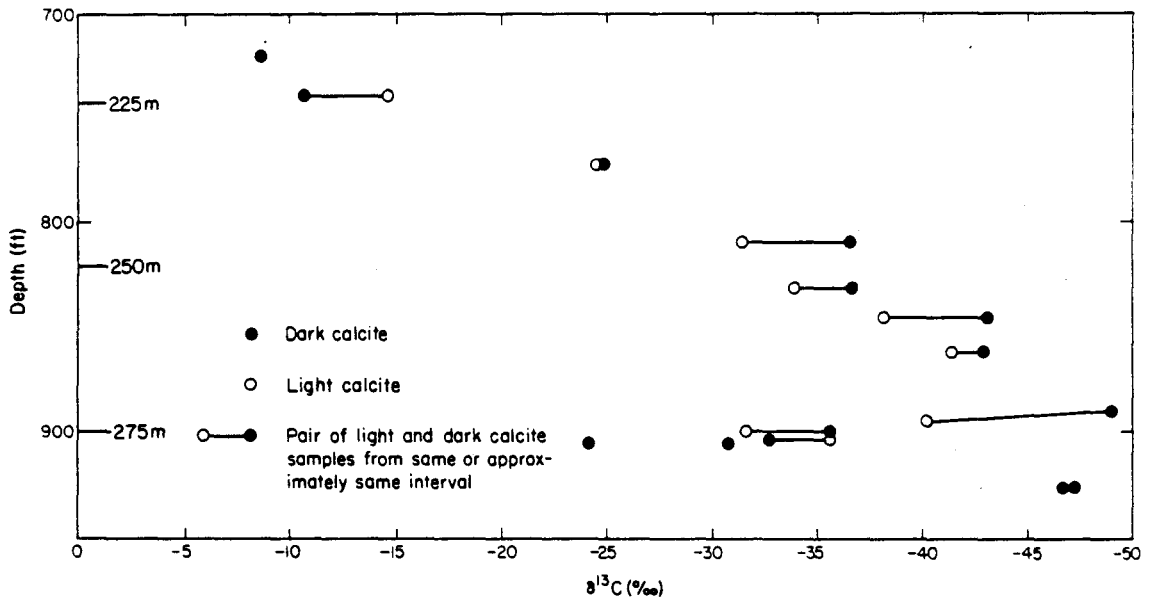


Figure 46. $\delta^{13}\text{C}$ (relative to PDB standard) of calcites versus depth in Oakwood cap rock. From Kreitler and Dutton, 1983.

couplet in a closed system that crystallized from a single fluid, the early crystallizing calcites would preferentially accept the heavy ^{13}C component, increasing the concentration of the light ^{12}C in the residual fluid (fig. 47; Posey, 1986). The later, light colored calcites should therefore be isotopically lighter (fig. 47; Posey, 1986). Furthermore, assuming a single reservoir of fluid in which the reactions are occurring, the residual fluid will become more and more depleted in ^{13}C , with increased formation of dark-light components (Kreitler and Dutton, 1983) with increasing time and depth as the calcite cap rock stratigraphy is time reversed (Posey, 1986). This is the most likely explanation for the depletion trend found in the carbon isotope ratios of the calcite cap rocks with depth in the Oakwood Dome (Kreitler and Dutton, 1983). P. E. Price (personal communication, 1986) found similar dark-light and carbon-isotope depth trends at the Winnfield Dome. However, Posey (1986) found that although the $\delta^{13}\text{C}$ becomes lighter with depth at Hockley Dome, the light-dark pairs are isotopically reversed compared with the Oakwood and Winnfield domes. In the Hockley Dome the dark-light calcite pairs appear to have formed from two carbon reservoirs rather than one. In some cap rocks, however, there are at least three generations of dark and light calcites, crosscut by pale crystalline calcite veins, introducing uncertainty into the interpretation of the isotopic data (H. H. Posey, personal communication, 1986).

Kreitler and Dutton (1983) showed that the solutions that caused the precipitation of the dark calcites were saline. These calcites contain clay and pyrrhotite and the solutions from which they crystallized must have been enriched in iron. The solutions that precipitated the light calcites had lower salinities and resulted in the precipitation of dolomite and celestite.

Posey (1986) indicates that, in general, the marine false cap rocks (Heterostegina Zone on Damon Mound) have $\delta^{13}\text{C}$ between +2.5 and -2.5 ppt,

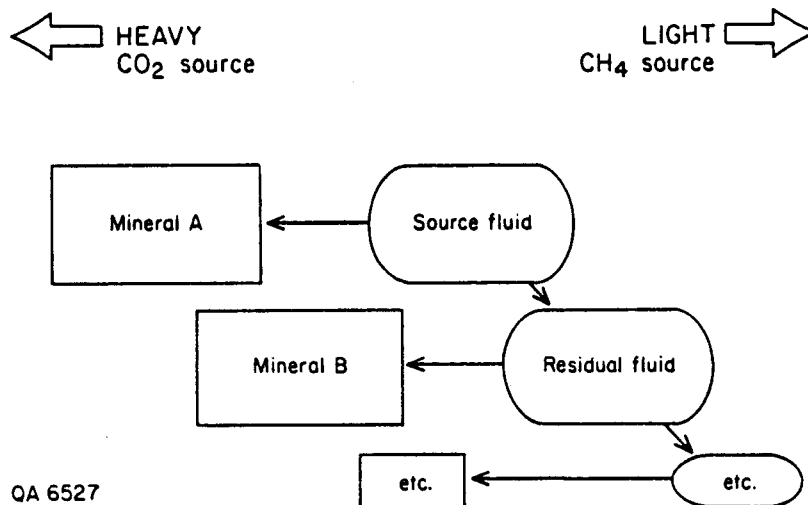


Figure 47. Schematic diagram showing the characteristic closed system behavior of the two coexisting phases, CH₄ and CO₂, during mineral precipitation. From Posey, 1986.

whereas the underlying detritus-bearing carbonate false cap rocks are even more depleted (-5 to -25 ppt) and the true calcite cap rocks are the most depleted, reaching -50 ppt. Since the Heterostegina-coral zone formed under marine conditions at the Oligocene-Miocene boundary, it suggests that the more depleted marine, detritus-bearing false cap rocks and true calcite cap rocks have crystallized under a separate fluid system.

Kreitler and Dutton (1983) state that the depleted $\delta^{18}\text{O}$ values for the calcites from the Oakwood cap rock suggest a high temperature (greater than 100°C , 212°F) precipitation, which contradicts previous temperature estimates and appears to be unrealistically high. Though bacterial remains in the calcite support a biological origin for calcite precipitation, the average maximum temperature for oil biodegradation and the survival of bacteria was assumed to be about 66°C to 70°C (150°F to 160°F) (Phillipi, 1977; Kreitler and Dutton, 1983) (fig. 36). However, recent work has shown that above 60°C (140°F) only bacteria exist, but that the upper temperature limit for bacteria is between 110°C and 250°C (230°F and 482°F) when peptide and phosphodiester bonds and amino acids are destroyed (Brock, 1985). Two species of Pyrodictium that are anaerobic and use H_2 and S° can grow at temperatures as high as 110°C (230°F) (Brock, 1985). In addition, some of these thermophilic bacteria that grow at temperatures above 55°C to 100°C (131°F to 212°F) are also acidophilic and exist in water with a pH between 1 and 4 (table 4; Brock, 1985). There is thus a great diversity of bacteria living in boiling water, including sulfur-producing bacteria, hydrogen-oxidizing bacteria, and elemental sulfur-respiring bacteria (Brock, 1985).

Calcites within the Oakwood dome with $\delta^{18}\text{O}$ values of -11 ppt are only stable with formation waters at temperatures greater than 135°C (275°F) in the Texas Gulf Coast (fig. 48; Kreitler and Dutton, 1983), suggesting that the

Table 4. Upper temperature limits for growth of bacteria.

Group	Approximate upper temperature (°C)
Prokaryotic microorganisms	
Chemolithotropic bacteria	>100°
Heterotrophic bacteria	>100°

Species and genera of thermophilic bacteria discovered in recent years (25).

Archaeobacteria

- Aerobic acidophiles, autotrophs
- Sulfolobus acidocaldarius* type species
- Sulfolobus brierleyi*
- Sulfolobus solfataricus*

Grow at 70° to 90°C (optimum, 75° to 85°C); pH to 4; use organic compounds and S° as energy source; use O₂ or Fe³⁺ as electron acceptor

Thermoproteales

- Thermoproteus tenax*
- Desulfurococcus mobilis*
- Desulfurococcus mucosus*
- Thermophilum pendens*
- Thermococcus celer*

Grow at 70° to 85°C (optimum, 85°C); anaerobic; acidophilic to neutrophilic; use organic compounds as energy sources; use S° as electron acceptor

Pyrodictium

- Pyrodictium brockii*
- Pyrodictium occultum*

Grow at 85° to 110°C (optimum, 105°C); anaerobic; use H₂ and S°; autotrophic

From Brock, 1985

formation waters that formed the calcite cap rocks at the Oakwood dome were derived from the zone of albitization of feldspars in the temperature range of 120°C to 200°C (248°F to 392°F) (Loucks and others, 1981). Early, dark-light pairs with $\delta^{18}\text{O}$ values of about -9 ppt would form at the shallowest levels in the time-reversed stratigraphy in fluids that had cooled to about 115°C (239°F) by mixing with shallower waters. The late, lower calcite cap rocks with $\delta^{18}\text{O}$ values of ± 11 ppt (fig. 46; Kreitler and Dutton, 1983) would form at average fluid temperatures of about 135°C (275°F) during the terminal dark-light calcite cap-rock crystallization. The temperature range for the formation of calcite cap rocks at Oakwood dome lies within the probable upper limit for bacteria (110°C to 200°C [230°F to 392°F]; Brock, 1985). Hence, the period of calcite cap rock formation can be considered to result from the influx of one major flush of progressively hotter (greater than 115°C, 239°F) saline brine, derived from the albitization and hydrocarbon-generation zones, that then cooled as it mixed with meteoric or marine waters in the vicinity of the cap rocks during the successive formation of the increasingly depleted dark-light calcite pairs (fig. 35f). Light hydrocarbons, formed in the oil-gas transition zone, migrated up growth-fault systems and became trapped in the Frio Formation at this time (fig. 35f). At the Hockley Dome the $\delta^{18}\text{O}$ of the late calcites are lighter than the early cap rock calcites, suggesting that an increased component of light $\delta^{18}\text{O}$ waters was mixed with the progressively cooled, deep saline brines during the formation of the light calcites in each dark-light couplet (Posey, 1986). Strontium isotopes also support mixing, as they show no consistent dark-light trend and have extremely wide variation (Posey, 1986).

The major flush of fluids causing calcite cap rock formation appears to have been generated at temperatures at or above the peak of methane generation from humic organics (Hunt, 1979), which is consistent with the introduction into

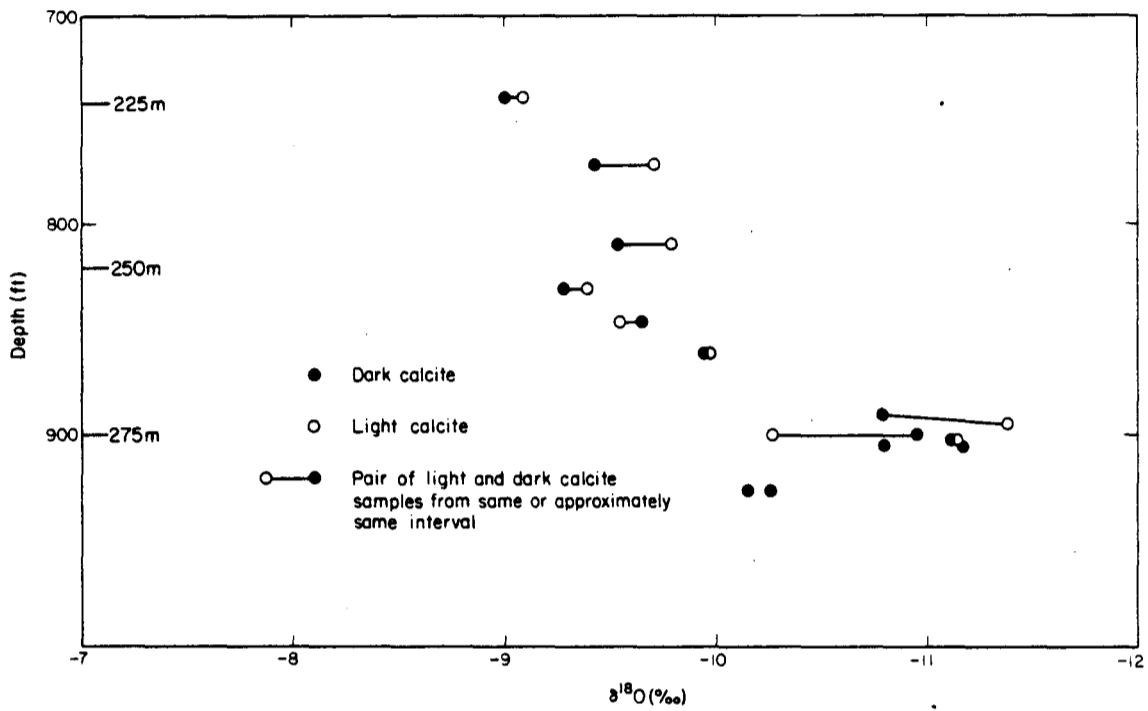


Figure 48. $\delta^{18}\text{O}$ (relative to PDB standard) of calcites versus depth in Oakwood cap rock. From Kreitler and Dutton, 1983.

the cap rocks of isotopically light methane dissolved in these brines (fig. 49; Fritz and Fontes, 1980). Hence, both the $\delta^{13}\text{C}$ and $\delta^{18}\text{O}$ data suggest that the cap rocks were subjected to a single or several major upward pulses of deep saline waters at temperatures above 115°C (239°F) followed by a period of cooling and isotopic depletion of the $\delta^{13}\text{C}$ and $\delta^{18}\text{O}$ in the waters from cooling, mixing, and mineral crystallization effects. The 115°C (239°F) temperature of the initial fluid is consistent with the temperatures of formation of sulfur from anhydrite (110°C to 120°C , 230°F to 248°F) prior to calcite cap rock formation, galena-sphalerite (110°C to 180°C , 230°F to 356°F), and barite (120°C to 127°C , 248°F to 261°F) (figs. 35e and 36) (Price and others, 1983; Kyle and Price, 1985).

Variations in the content of magnesium in the formation fluids are believed to have resulted in changes in the calcite crystal shape and opacity (Posey, 1986). Scalenohedral crystals probably formed in Mg-rich saline fluids whereas blocky crystals formed in Mg-poorer (high meteoric component ?), less-saline fluids (Folk and Land, 1975). Meteoric waters generally contain less than 5 ppm Mg whereas seawater may have in excess of 1,000 ppm Mg (Mason, 1966). Repetitive changes in the types and opacity of calcite crystals represent changes in degrees of mixing of saline and meteoric fluids of deep origin.

The early dark and light calcites are commonly brecciated and cemented by late pale calcite veins (Kreitler and Dutton, 1983; Posey, 1986). This brecciation may be due to a volume loss in the transition of anhydrite to calcite in the calcite cap rock (Posey, 1986). Kreitler and Dutton (1983) show that, assuming a closed system with a 1 to 1 molecular conversion of anhydrite to calcite, 1 cm^3 of anhydrite will form 0.79 cm^3 of calcite. This volume loss can explain the deformation features observed in the calcite section (both in the deeper brecciated sections and the shallower, less deformed subhorizontal layered

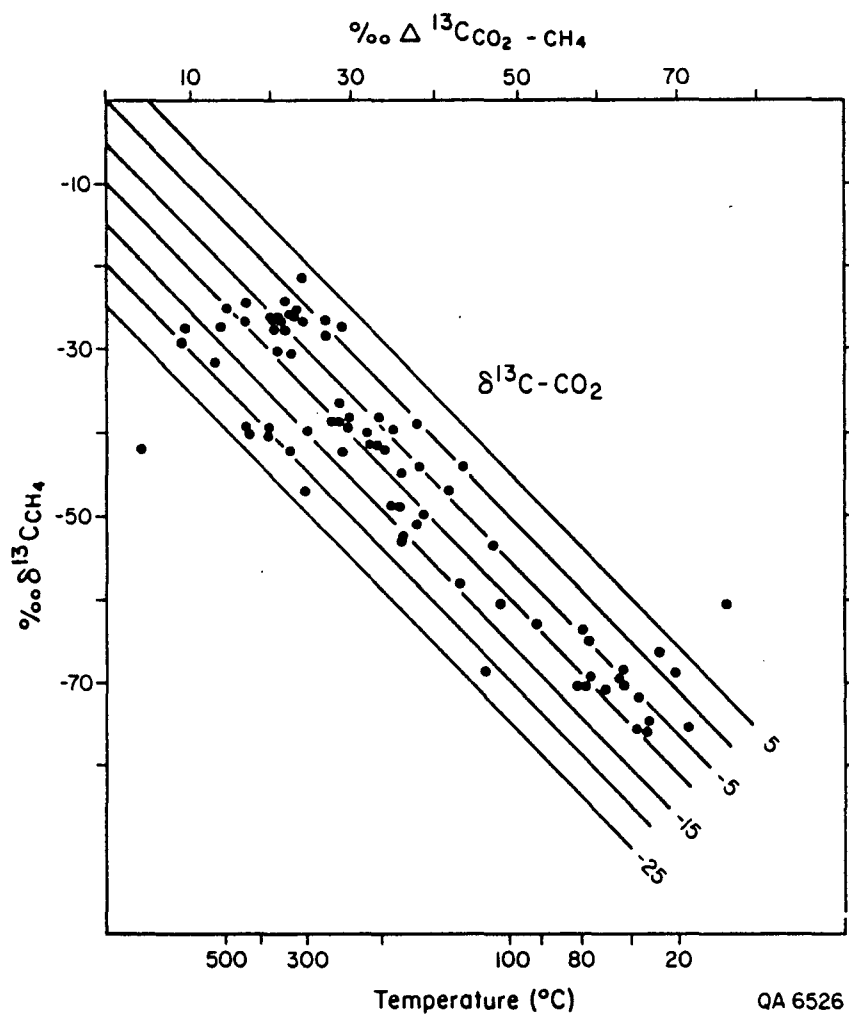


Figure 49. $\delta^{13}\text{C}$ of methane and carbon dioxide showing stability variation with temperature. From Fritz and Fontes, 1980.

dark and light calcite (Kreitler and Dutton, 1983). They argued that deformation in the calcite section is not related to solution of the salt because there is no evidence of deformation in the anhydrite zone. Dix and Jackson (1982) showed that the contact between the rock salt and the anhydrite cap rock may be either an abrupt transition (Oakwood, Tatum, and Vacherie Domes; Teas, 1931; Goldman, 1933; Eargle, 1962; Nance and others, 1979) or a cavity that may exceed 2 ft (0.6 m) in depth (Gyp Hill, Winnfield, Jefferson Island, and Lake Washington Domes; O'Donnell, 1935; Hoy and others, 1962; Dutton and Kreitler, 1980). In areas where the salt dissolution zone is widely developed, block settling of the relatively heavy (specific gravity 2.89 to 2.98) plastic anhydrite downward into the cavity could result in stresses being imposed on the relatively brittle calcite cap rock with its consequent fracturing and brecciation. If the rate of settling of the anhydrite was relatively slow, few deformation structures may have developed.

The layered early-dark, late-light calcite pairs appear to have formed consecutively in a time-reversed stratigraphy (Posey, 1986). A void probably formed at the base of the calcite cap rock from the anhydrite-calcite volume decrease (Kreitler and Dutton, 1983) or block settling of the anhydrite. Saline fluids of deep origin could enter the peripheries of this dissolution zone and alter the top of the anhydrite to calcite by biogenic activity in the presence of hydrocarbons. This continued until all the hydrocarbons were used up or channels were choked off or diverted away from the cap rock (Posey, 1986). Finally, clear calcite would precipitate from less saline residual fluids as a void fill (Posey, 1986). As the early, dark calcites would tend to lose strontium to the fluid and produce an insoluble residue at the dark-light contact (Posey, 1986), dissolution of the early dark calcites has not occurred.

Reactivation of the diapiric movement of the salt stocks owing to the progressive dissolution of salt at the salt dissolution zone, which will result in buoyancy differential, can produce peripheral fracture zones and conduits for the upward movement of brines of deep origin.

Age of Migration Events

Porosity is frequently occluded below gas-water contacts by diagenetic reactions in formation waters, whereas it is preserved above gas-water contacts by the gas phase (Selley, 1979). Such reactions have not affected the overall permeability distribution in the Frio "A" sandstones in the Delee No. 1 well, Hitchcock N.E. field. Furthermore, the formation of kaolinite must have preceded the introduction of hydrocarbons into the trap as kaolinite is abundant both above and below the gas-water contact.

Diagenetic kaolinite may initially form at 80°C (176°F) (R. Guillemette, personal communication, 1986). However, in the acidic brines (estimated in situ pH, 4 to 6) present in the Frio Formation (Brazoria County), isotopic analyses show that kaolinite began to replace plagioclase at about 100°C (212°F) (Kaiser and Richmann, 1981; Loucks and others, 1981). The pore-filling kaolinite postdates quartz overgrowths and much of the leaching and is stable at 100°C (212°F) under geopressured conditions, whereas plagioclase is stable under hydro pressured conditions at this temperature (Kaiser and Richmann, 1981). At the Delee No. 1 well the Frio "A" sandstone is slightly geopressured and is at a temperature of 102°C (215°F), suggesting that kaolinite formation is a recent event, whereas the well appears to show normal thermal maturity consistent with not being subjected to long periods of flushing by hot migrating fluids (Light and D'Attilio, in press). Burial history data (fig. 50) combined with initial

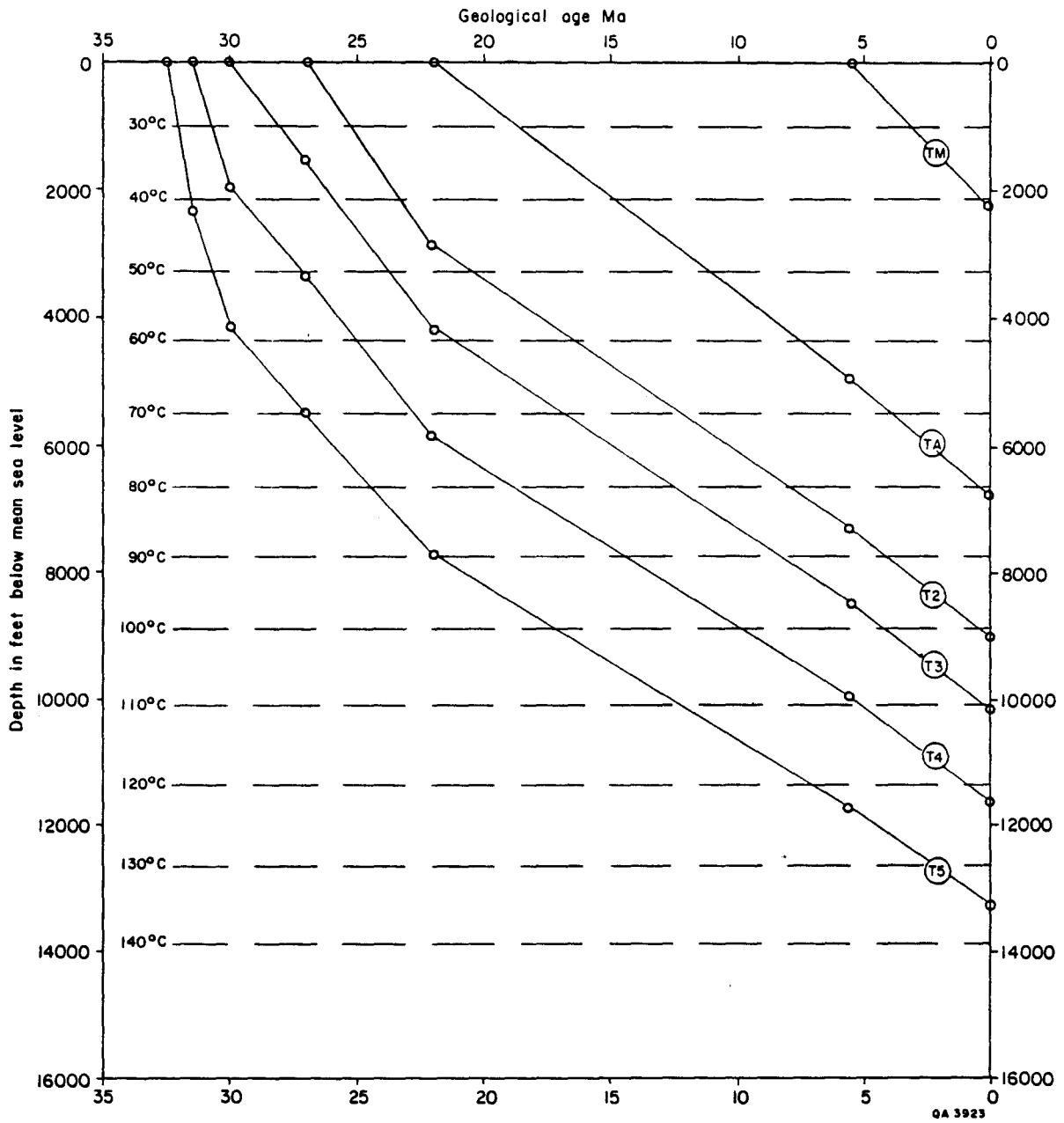


Figure 50. Burial history diagram for the Hitchcock N.E. field. From Light and D'Attilio, in press.

formation temperatures (80°C to 100°C , 176°F to 212°F) indicate that major kaolinite crystallization occurred between 7.5 Ma and 1 Ma at the level of the Frio "A" sandstone, suggesting that the introduction of hydrocarbons was an even more recent event (<1 Ma ago).

Lead-Zinc-Barite Mineralization

Price and others (1983) showed that calcite cap rock formation was succeeded by the formation of crosscutting Mississippi Valley-type lead-zinc and barite deposits along the margins of salt domes (fig. 35g). Mineral stability studies indicate a temperature of crystallization of 110°C to 180°C (230°F to 356°F) for the sulfur minerals, whereas the metalliferous brines appear to have leaked up the margins of the salt stocks (Price and others, 1983). These fluids would therefore need to have originated from either the smectite-illite transition zone or the zone of albitization or both (80°C to 200°C) in the Abyssal regime (Galloway, 1982; Price and others, 1983; Posey, 1986).

In most Mississippi Valley-type ore deposits the elemental abundances generally decrease from iron to zinc and barium, whereas lead is the least abundant (H. H. Posey, personal communication, 1985). The major exception is southeast Missouri where iron and lead are dominant over zinc. Barite, if related at all, forms separately from the lead deposits and is more abundant than zinc (H. H. Posey, personal communication, 1985). Although in salt dome cap rocks barium tends to be more abundant than zinc or lead, the paragenetic sequence is early iron sulfides followed by lead-zinc sulfides and finally barium sulfates in the more oxidized parts of the deposits (Price and others, 1983).

Although the paragenesis of sulfides present in salt dome cap rocks vary and are repetitive, in general they begin with early pyrrhotite that is present in the Anhydrite cap rocks and that preceded the main period of lead-zinc formation (Ulrich and others, 1984). The later sulfides and sulfates include rare acanthite, marcasite, pyrite, high-iron sphalerite, sphalerite and galena, repeated marcasite and sphalerite, marcasite and late-stage barites that rarely rim pyrrhotite (Price and others, 1983; Ulrich and others, 1984; Price and Kyle, in press). The major sulfide zones appear to crosscut the boundaries between false cap rocks, true calcite cap rocks, and anhydrite cap rocks as well as the transition zone, indicating that most of the ore mineralization is a more recent event (Posey, 1986).

Potential Sources of Fluids

Land (1984) presented evidence that the Mississippi Valley-type lead-zinc mineralization of salt dome cap rocks in the Texas Gulf Coast was a result of fluids derived from the Mesozoic, particularly Jurassic carbonate source rocks. However, dissolution and albitization of feldspars (Milliken and others, 1981) and other water rock interactions (smectite-illite transition) could account for the release of metals to the formation fluids (Möller, 1983; Price and others, 1983; Thornton and Seyfried, 1985).

Zinc, which tends to be concentrated in limestones, has an ionic radius and geochemistry similar to Mg^{+2} , Co^{+2} , Fe^{+2} , and Mn^{+2} (Collins, 1975). Acidic brines of deep origin, with a high CO_2 content (Morton, 1981), could extract zinc from Jurassic and Cretaceous carbonates (Land, 1984).

The stable oxidation state of lead in an igneous environment is Pb^{+2} (Ahrens, 1965b). The radius of the Pb^{+2} ion is large (1.33 Å), and this ion can replace both Ca^{+2} (radius 1.06 Å) in plagioclase and K^+ (1.33 Å) in potash

feldspar (Ahrens, 1965b). The replacement of potassium by lead is greater than of calcium⁺² (Ahrens, 1965a), hence the breakdown or albitization of potassium feldspars should release abundant lead. When feldspars decompose during the formation of a fluid the rare earth elements are released with other trace elements such as lead and zinc (Möller, 1983). The rare earth element pattern will be given over to the fluid. Such a solution may form lead-zinc mineralization in favorable geochemical traps and a high europium anomaly within these minerals (for example, galena) will document derivation of the lead from feldspar (Graf, 1977; Möller, 1983). Heyl and others, 1974) showed that the isotopic composition of lead in Mississippi Valley-type ores indicates a derivation from sandstones or basement.

The lead-zinc ratios (3 to 8) of fluids produced by experimental clay-rich marine shale reactions at 200°C and 300°C (482°F to 572°F) (Thornton and Seyfried, 1985) are within those of salt dome cap rocks and Mississippi Valley lead-zinc deposits (H. H. Posey, personal communication, 1985). The magnesium and iron content of formation fluids present in the Gulf Coast fluids (Kharaka, 1977) can be produced by marine shale reactions in the 200°C to 300°C (392°F to 572°F) range under oxidizing or reducing conditions (Thornton and Seyfried, 1985). However this temperature range is high for normal Mississippi Valley ore fluid temperatures (Cathles and Smith, 1983). Although these are marine shales, Thornton and Seyfried (1985) compared the fluid data and mineralogical assemblages to those of the Gulf Coast. They stated that the observed differences are due to a higher degree of reaction in the geologic environment and increased stability of illite and chlorite in geologic fluids. Their data suggest that copper-bearing solutions accompanied by lead and zinc may evolve in sedimentary basins characterized by oxidizing conditions, whereas zinc and lead will predominate in a more reducing environment (Thornton and Seyfried, 1985). Reducing conditions exist in the Abyssal zone in the Gulf Coast (table 3; Galloway, 1982). The lack

of copper mineralization in salt dome cap rocks (P. E. Price and H. H. Posey, personal communications, 1986) implies that shale reactions may have occurred under reducing conditions to have formed the mineralizing fluids.

There is a worldwide association of porphyry copper-molybdenum mineralization, calc-alkaline volcanism, and convergent plate boundaries (Sillitoe, 1972; Barnes, 1979). Oceanic basalts, or lower crustal amphibolites, contain sufficient copper to ultimately yield a porphyry copper deposit provided the metal is concentrated by hydrothermal processes at shallow crustal levels (Barnes, 1979).

Volcanic-arc rocks of the Sierra Madre Occidental in Mexico contain normal amounts of copper whereas volcanic rocks from the Trans-Pecos area have lesser amounts (J. G. Price, personal communication, 1986). The Vicksburg Formation undoubtedly contains a major component of volcanic material derived from the easily eroded ash flow tuffs in the Trans-Pecos area (W.E. Galloway, personal communication, 1985). Volcanic material derived from the Sierra Madre Occidental in Mexico (J. G. Price, personal communication, 1986) is also abundant in the Frio and updip Catahoula Formations in the form of smectite and kaolinite and in the underlying Jackson and Yegua Formations (W. E. Galloway, personal communication, 1985). Volcanically derived material should therefore act as an effective source for copper in the Frio Formation.

Measured zinc and copper concentrations in upper Frio sandstones are less than 21 mg/L and 4 mg/L whereas upper Frio shales contain up to 95 mg/L and 18 mg/L, respectively (D. W. Koppenaar, personal communication, 1986). For comparison, oceanic basalt can contain about 90 mg/L copper (Barnes, 1979). Formation waters within the upper Frio contain up to 0.15 mg/L copper, 0.092 mg/L zinc, and less than 0.62 mg/L lead (Randolph, 1985). As the

zinc-to-copper ratio in the formation waters is 0.6 whereas it is 5 in the enclosing upper Frio sandstones and shales, it is likely that the waters are derived from deeper Frio or underlying formations. Furthermore, the high zinc and copper contents in the upper Frio shales imply that zinc and copper should have been released to the fluids by the alteration of smectite to illite as the formation lies within the smectite-illite transition zone but above the albitization zone (Light and D'Attilio, in press). Formation waters in the lower Frio at the Pleasant Bayou well have higher lead and zinc concentrations (Pb, 0.43-1.1 mg/L; Zn, 1.5-1.6 mg/L; Kharaka and others, 1980) consistent with this interpretation. The lower Frio lies within the zone of albitization (Loucks and others, 1981), suggesting that this process and not the transition of smectite to illite is the main source of the lead and zinc in the waters.

Ore Carriers

In hydrothermal solutions, ferrous iron is dominant over ferric iron except in abnormal, highly oxidizing environments (Barnes, 1979). The iron content of the solution is strongly affected by pH and Eh, and high concentrations of iron are only possible in acid-reduced fluids (Mason, 1966; Thornton and Seyfried, 1985). At Mississippi Valley ore-fluid temperatures (80°C to 200°C , 176°F to 392°F ; Cathles and Smith, 1983), ferrous chloride and bisulfide complexes are ineffective metal carriers (Seward, 1977), and some form of organic and ammine complex is required to carry the quantity of iron observed (Barnes, 1979). This is consistent with deriving initial cap rock formation fluids, which were saturated in iron (Ulrich and others, 1984), from the smectite-illite transition zone (80°C

to 123°C, 176°F to 253°F) where organic material was maturing (Hunt, 1979) and organic complexes could form.

The dominant complex for zinc in hydrothermal solution is $ZnCl_2$ (Barnes, 1974). Lead also forms chloride complexes that become more stable with increasing temperature (Helgeson, 1969; Smith and Martell, 1976; Giordano, 1978). Lead sulfide complexes are not sufficiently stable to form low-temperature hydrothermal ore deposits (Hamman and Anderson, 1978; Barnes, 1979). The dominant aqueous copper complex is cuprous chloride at all temperatures in more reduced environments (Snellgrove and Barnes, 1974; Crerar and Barnes, 1976). Copper bisulfide complexes do, however, become relatively more important in weakly acid solutions below 250°C (482°F). Seward (1976) showed that the chloride complexes of silver are strong, whereas bisulfides become stable in near neutral solutions. Chloride complexes in hot, acid, reducing brines would therefore appear to be the dominant carriers of zinc, lead, and silver during Gulf Coast salt dome cap rock mineralization.

The transition from early organic complexes required to transfer iron to later chloride complexes required to transfer lead and zinc is consistent with the change in source of the fluids through time, from a shallower generation zone, dominated by smectite-illite transition and hydrocarbon generation, to a deeper zone of feldspar albitization where very saline brines occur (figs. 35d through 35g).

Late-Stage Mineralization

Barite, which forms the late-stage mineralization event in salt dome cap rocks (figs. 35g and 36) and may locally replace early pyrrhotite crystals, has a

heavy strontium isotopic ratio, suggesting that the fluid it crystallized from contained radiogenic strontium derived at depth from either albitization or dissolution of feldspars or shale dewatering (Posey, 1986). Fluid inclusions within the barite indicate temperatures of 120°C to 127°C (248°F to 261°F), suggesting that the fluids were derived from the albitization zone, whereas H₂S having relatively heavy sulfur (Goldhaber and others, 1979) is generated in shaly sediments at these temperatures (Hunt, 1979).

The barite that contains isotopically heavy strontium also contains extremely heavy sulfur (Kyle and Price, 1985; Posey, 1986). This heavy sulfur may result from partial sulfate reduction in which light sulfur isotopes are fractionated into the reduced phase (pyrite and sulfides) such that the residual fluid becomes isotopically heavier, as the sulfur is too heavy to have been simply sourced at high temperatures (Kyle and Price, 1985; Posey, 1986). At Moss Bluff dome, hydrogen sulfide with a $\delta^{34}\text{S}$ of -15 ppt coexists with dissolved sulfate with a $\delta^{34}\text{S}$ of +40 ppt (Feeley and Kulp, 1957), supporting this contention (Kyle and Price, 1985).

The salinity of the fluid inclusions within the barite varies from 3 to 12 percent NaCl equivalent (91,000 to 307,000 mg/L) within the range of deep geothermal brines in the Houston delta system. Fluid inclusions within the salt at the salt-cap rock interface in the Oakwood dome are formed of fluids that formed the last dissolution event (Kreitler and Dutton, 1983) during anhydrite cap rock formation. The $\delta^{18}\text{O}$ value of +5.4 ppt SMOW indicates a deep-basin origin for these waters, and the enriched $\delta^{18}\text{O}$ value is typical for saline formation waters in the Gulf Coast Basin (Kharaka and others, 1977) and is significantly different from continental meteoric water in the region (Kreitler and Dutton, 1983). Furthermore, the $\delta^2\text{H}$ of the fluid inclusions in the Oakwood salt is depleted (-69.2 ppt SMOW), suggesting a deep methane source. This depletion

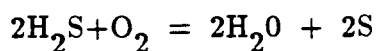
may result from clay dewatering and increased isotope exchange between formation waters and depleted methane formed at high temperatures from decarboxylation of acetic acid (Kharaka and others, 1985).

Although lithium, barium, and magnesium are easily adsorbed onto clays (Collins, 1975), it seems likely that barium with calcium and strontium are derived from the albitization or dissolution of K-feldspars. Destruction of K-feldspars and micas during diagenesis would release barium (Barnes, 1979).

Barite shows increasing solubilities at high pressures and salinities (Barnes, 1979). The barium-rich brines have probably been derived from the deepest and most saline source, consistent with the barite having formed the final mineralization event. The solubility of barite also increases with temperature up to 150°C (286°F), at salinities above 0.2 mole (77,300 mg/L Cl). Hence barite will precipitate from simple cooling (Barnes, 1979), pressure decrease, or mixing of basinal brines with less saline surface waters. The barium-rich geothermal brines would also precipitate out barite when they came in contact with sulfate-rich fluids in the anhydrite cap rock zone, as high concentrations of barium are only possible at low sulfate contents (Collins, 1975). This is the most plausible mechanism for barite precipitation in salt dome cap rocks.

Thus both the initial dissolution of the salt domes during anhydrite cap rock formation and the final formation of barite suggest a major component of deep, hot brines in cap rock fluids.

The most recent major mineral event in salt dome cap rocks is the formation of late-stage gypsum after anhydrite (Posey, 1986) and crosscutting sulfur dikes. These may have formed from the reaction of oxygen-rich ground waters with hot, H₂S bearing brines as shown in the following equation.



(Davis and Kirkland, 1979)

Gulf Coast Brines

Iron, zinc, and lead contents of Gulf Coast oil field brines and cap rock deposits are comparable (Kyle and Price, in press). Produced reservoir fluids in the Gulf Coast are enriched in calcium, strontium, barium, and fluorine and depleted in sodium, potassium, magnesium, and sulfate relative to seawater (Hanor, 1979). Iron, manganese, lead, and zinc concentrations in fluids in the Andrau sandstone at the Pleasant Bayou geopressured-geothermal test well are higher than in adjacent oil and gas fields (Kharaka and others, 1980). Kharaka and others (1980) showed that the chlorine-bromine ratios of fluids trapped in the lower Frio Formation (Andrau sandstone) at the Pleasant Bayou test well indicate that they have a component derived from salt dissolution. These data suggest that the fluids trapped in the lower Frio by high geopressure are the parent fluids of those that caused the salt dome cap rock mineralization.

The geochemistry of strontium (ionic radius 1.18 Å) is fairly closely related to that of calcium as they have similar ionic radii and ionic bonds with other ions, in contrast to the preferential replacement of potassium by lead (Ahrens, 1965b). However, strontium may also replace K⁺ because the radii of these two cations do not differ greatly (Ahrens, 1965). Up to 100 ppm of strontium occurs in K-feldspar and up to 500 ppm in plagioclase (Ahrens, 1965b). High concentrations of calcium, strontium, and barium are only possible at relatively low sulfate levels and these three elements as well as iron and traces of other metals frequently occur in encrustations on oil field pipes (Collins, 1975).

Formation waters from the lower Frio Formation in the Pleasant Bayou well have sulfate contents of some 5.4 to 21 mg/L, and the strontium varies from 867 to 1020 mg/L (Kharaka and others, 1980). Fluids developed in marine shales, reacted at 200°C and 300°C (482°F and 572°F), and contain 146 to 2,743 mg/L sulfate and 0.8 to 9.3 mg/L strontium (Thornton and Seyfried, 1985), even though similar concentrations of strontium are present in these and Gulf Coast shales. Evidently high-temperature clay reactions produce two orders too much sulfate and two orders too little strontium to have been the source of the strontium in the geopressed brines. The calcium content is also too high in the lower Frio waters at Pleasant Bayou (Kharaka and others, 1980) to have been derived from high-temperature clay reactions and is a consequence of albitization of feldspars (Morton and others, 1983a). Albitization of K-feldspars and plagioclases at temperatures greater than 120°C (248°F) (Loucks and others, 1981) is probably also the source of the strontium and barium in the Gulf Coast brines.

Age of Mineralization

The lower Frio waters in the Pleasant Bayou test well must have migrated recently because they are out of isotopic equilibrium with the diagenetic albite cements (Light and D'Attilio, in press). Burial history data tells us that the albite cements began to form 5 to 7.5 million years ago (Light and D'Attilio, in press) at temperatures greater than 120°C (248°F) (Loucks and others, 1981). Sulfur of deep origin (H₂S) has been introduced into roll-front uranium deposits before and after the uranium mineralization at 5 Ma (Galloway, 1982; Ludwig and others, 1982), probably by basinal brines.

The burial history model is based on the assumption that the rate of burial remained relatively uniform, that there was no significant uplift or erosion

involved, and that the paleogeothermal gradient can be estimated for the region. Galloway and others (1982) have estimated the thermal maturity of sediments at the beginning and end of the Oligocene using a uniform present geothermal gradient, and the estimated vitrinite reflectance values (R_o) are comparable with the measured values. A similar correlation was found between estimates of the maturity of the highly geopressed lower Frio Formation using measured vitrinite reflectance values (R_o), the present geothermal gradient at the Pleasant Bayou test wells, and Dow's (1978) average thermal maturity profile for Gulf Coast sediments (Light and others, 1984). Evidently we can assume that the present geothermal gradient combined with the measured rate of burial is an accurate estimate of the average thermal maturity of the lower Frio Formation since the Oligocene.

At Damon Mound, warped late Pleistocene sediments, probable correlatives of the Beaumont Formation, are thought to have accumulated during the Wisconsin interstadial (34,000 yr B.P.) (Jenkins, 1979) or the last major Pleistocene highstand of about 80,000 to 130,000 yr B.P. (Bernard and Le Blanc, 1965; Collins, 1985). Eighty feet (24 m) of uplift is recorded in the Pleistocene Beaumont strata at Damon Mound, indicating an uplift rate of about 2 ft (0.6 m)/1,000 yr (Beaumont Formation, 34,000 yr old) or 0.6 ft (0.19 m)/1,000 yr (Beaumont Formation, 130,000 yr old) (Collins, 1985). These high recent uplift rates measured at Damon Mound are in contrast to the 0.25 ft (0.8 m)/1,000 yr since the Oligocene (Collins, 1985) and could result in the reactivation of faults peripheral to the diapirs and major growth faults in the Gulf Coast Basin by additional removal of the "mother" salt basal layer. Such activity would reactivate conduits for fluid flow and allow upward migration of lead-zinc bearing basinal brines generated in the Abyssal zone that would precipitate as the late crosscutting ore bodies in the salt dome cap rocks (fig. 35g). An anomaly present in the geothermal profile in the upper Frio

Formation at the Pleasant Bayou test well suggests that hot updip basinal brine migration still continues at this level (fig. 38; Light and D'Attilio, in press).

The main period of sulfide and barite mineralization appears to postdate most of the true calcite cap rock formation but precedes late gypsum and crosscutting sulfur veinlet formation (fig. 51; Posey, 1986).

CONCLUSIONS

Present fluids in the lower Frio Formation below 14,000 ft (4,270 m) at the Pleasant Bayou geopressured-geothermal test well (Brazoria County, Texas) are highly saline and enriched in iron, manganese, lead, and zinc (Kharaka and others, 1980). These formation waters contain 29 standard cubic feet of gas per barrel of water of which 85.5 volume percent is methane and 10.5 volume percent is carbon dioxide (Morton, 1981). Morton and others (1983a) showed the vertical variation of salinity with depth at the Chocolate Bayou and Alta Loma fields close to the Pleasant Bayou test well. In the Chocolate Bayou field the salinities increase with depth below 12,000 ft (3,660 m) whereas the reverse is seen in data from the Alta Loma field (Morton and others, 1983a). However, the calcium-sodium ratio in both fields increases with increasing depth below 10,000 ft (3,048 m) and becomes constant at greater depths (fig. 52; Morton and others, 1983a). Increases in the fluid content of calcium, decrease in sodium-calcium and magnesium-calcium ratios, and increase in the potassium-sodium ratio with depth can be related to albitization that occurs below the 200°F to 250°F (93°C to 121°C) isotherm (figs. 35f, 35g, 36, and 52) (Loucks and others, 1981; Milliken and others, 1981).

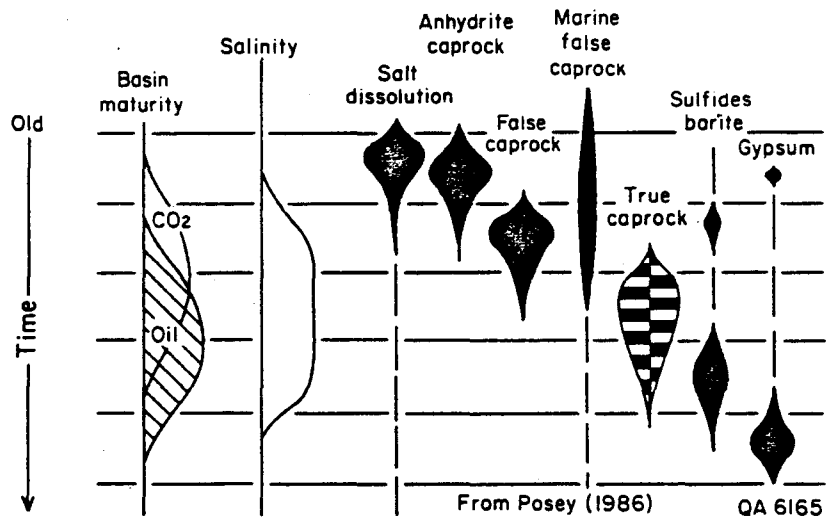


Figure 51. General paragenesis showing the relationships between basin maturation and cap rock evolution. From Posey, 1986.

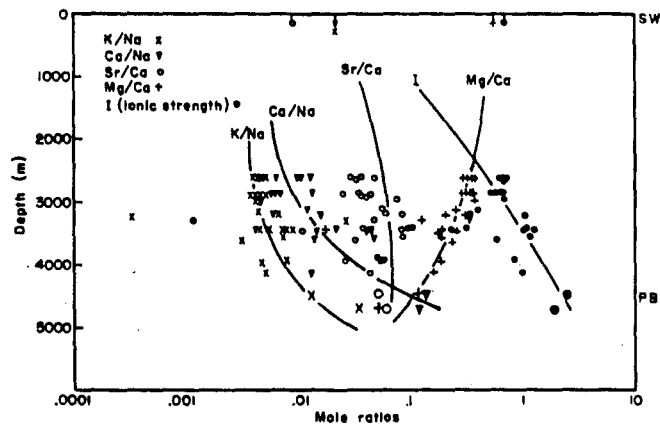


Figure 52. Mole ratios of Brazoria County waters versus depth and seawater. From Kaiser and Richmann, 1981.

Salinities are much higher in formation waters in the Pleasant Bayou test well (131,320 mg/L; Morton, 1981) than in waters from adjacent oil and gas fields, probably resulting from the dissolution of evaporites (Kharaka and others, 1980). Furthermore, fluids in this well are depleted in bromine compared with chlorine, which further supports this conclusion (Kharaka and others, 1980). In general, Tertiary sediments are found to be depleted in bromide compared with the normal evaporation line, whereas Cretaceous and Jurassic sediments are enriched in bromide (Collins, 1975).

The high chloride-bromide ratios of the fluids in Pleasant Bayou indicate that they are partly derived from salt dissolution (fig.53; Light and others, 1984). These data suggest that the fluids in the lower Frio Formation trapped by the geopressure in the Pleasant Bayou well are the parent fluids of those causing the salt dome cap rock mineralization. Such fluids could initially dissolve salt at temperatures greater than 70°C (158°F), resulting in anhydrite cap rock formation and producing calcite cap rocks at lower but then increasing temperatures. During a final fluid flush, lead-zinc minerals with heavy sulfur isotopes crystallized owing to changes in the composition of the upward fluid column as it was progressively derived from deeper and hotter zones.

Ewing (1986) indicated that the Frio style of growth faulting consists of several major, sinuous, moderately listric faults, possibly flattening into a regional detachment at 20,000 to 25,000 ft (6,100 to 7,600 m). There is substantial mobilized shale in diapirs and ridges, although the influence of salt tectonics is surprisingly small (Ewing, 1986).

Hoskins Mound and Stratton Ridge lie southeast and south of the Pleasant Bayou - Chocolate Bayou fault block and intersect the major growth-fault system forming the southeastern margin of the Chocolate Bayou oil and gas field (Light and others, 1984). The upper Frio sandstones appear to have formed a migration

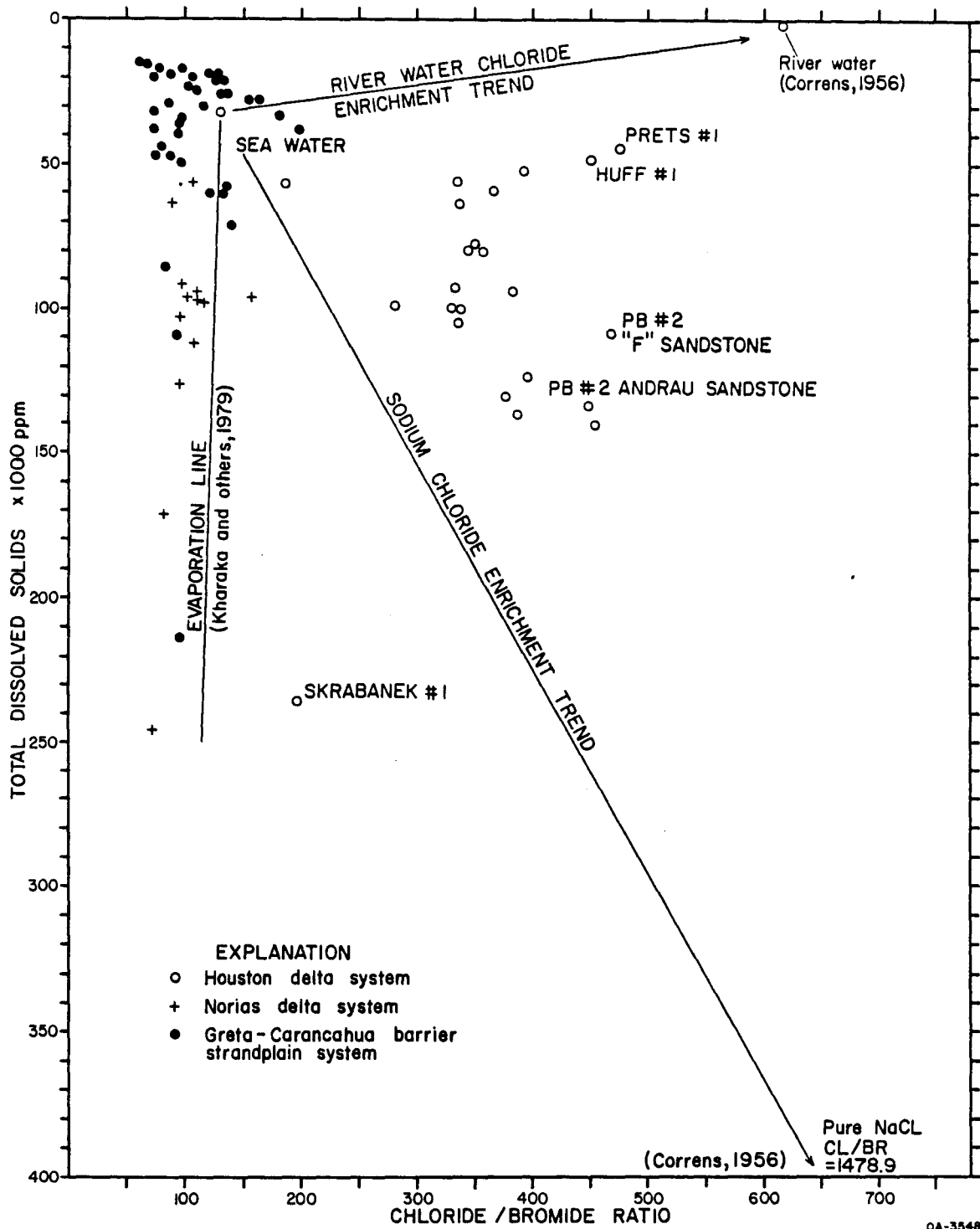


Figure 53. Chlorine-bromine ratio versus total dissolved solids for wells of the Gulf Coast region of Texas.

pathway up and out of the basin for hydrocarbons now trapped in the Chocolate Bayou field (Morton, 1983b). This migration was partially driven by a horizontal pressure gradient that exists between the Pleasant Bayou - Chocolate Bayou fault block and more seaward fault blocks (Light and others, 1984).

Marked changes in salinity and chemical composition over short lateral distances suggest that fluids have migrated out of the basin along faults and discontinuities (Morton, 1983b). As the major growth faults sole out into the lower Frio or Vicksburg slope shales between 20,000 and 25,000 ft (6,100 to 7,600 m) (Ewing and others, 1984), both the marine source for the hydrocarbons (gas and oil) and the migration pathways (growth faults) are present at this level. In addition, abundant generation of gas and hydrocarbons in the slope shales probably contributed to the formation of high geopressures, rock failure, and the "base Frio" growth-fault detachment plane at these levels (20,000 to 25,000 ft, 6,100 to 7,600 m). Furthermore, deep dissolution of the Stratton Ridge and Hoskins Mound salt domes by hot basinal fluids migrating along these growth faults could produce the high chlorine-to-bromine ratios of the Pleasant Bayou brines (Kharaka and others, 1980). Evidently dewatering of the lower Frio or Vicksburg slope shales has occurred between 20,000 and 25,000 ft (6,100 to 7,600 m) assisted by the generation of methane and carbon dioxide by the decarboxylation of organic acids (Kharaka and others, 1985). The salinity of these brines has been enhanced by the dissolution of salt as the fluid migrated past deep salt zones (Light and others, 1984). Fast migration of the hot brines through the upper Frio sandstones raised the ambient temperature of these rocks.

Cathles and Smith (1983) showed that Mississippi Valley-type mineral deposits may form as the result of episodic compactive expulsion of basin brines. If dewatering occurs in a cycle as fluid pressure builds up to lithostatic pressures

and is then released, up to 50 dewatering pulses may occur every million years as strata subside to 3,000 to 5,000 m (9,850 to 16,400 ft) (Cathles and Smith, 1983). At these depths temperature is in the range of Mississippi Valley-type mineralization (80°C to 200°C, 176°F to 392°F) but commonly 100°C to 150°C (212°F to 302°F) (Anderson and Macqueen, 1982; Cathles and Smith, 1983).

Mississippi Valley lead-zinc deposits occur primarily in carbonates but also in some sandstone hosts (Ohle, 1952; Beales and Onasick, 1970) and are associated with pinch-outs that surround domal structures, basin growth faults, and nearshore reefs (Cathles and Smith, 1983). Mississippi Valley-type lead and zinc mineralization is present in salt dome cap rocks that lie at or near the land surface in Texas (Price and others, 1983; Land, 1984). Furthermore, the concentrations of iron, manganese, lead, and zinc from the lower Frio waters in the Pleasant Bayou geopressed-geothermal test well in Brazoria County are higher than those of most waters from geopressed zones and from adjacent oil and gas fields (Kharaka and others, 1980; Morton, 1981). The lower Frio sandstones are highly geopressed (>0.7 psi/ft, 15.83 kPa/m) so that updip hot basinal flow was retarded and the thermal maturity remained relatively unchanged (Light and others, 1984). Hence these sandstones contain fluids that most closely represent the composition of the migrating basinal fluids that introduced the hydrocarbons and lead-zinc mineralization into the overlying rocks.

Lead isotope data from galena in the Hockley Dome cap rocks yield a young age and lie within the field of Cenozoic pelagic sediments and Holocene metalliferous saline brines (Doe and Zartman, 1979; Price and others, 1983). Furthermore, sulfur isotopes between apparently co-precipitated sphalerite and galena pairs yield an approximate equilibrium temperature between 113°C and 180°C (234°F and 356°F) similar to the temperatures suggested for the source of

the saline brines in the Pleasant Bayou well (Price and others, 1983; Kyle and Price, 1985). Saline inclusions occur in doubly terminated quartz crystals extracted from the mineralized zone (Price and others, 1983). Salinity within these inclusions is 34 weight percent NaCl, and the quartz crystals appear to have grown authigenically within the Louann salt at depths of about 22,000 ft (6,700 m) (Price and others, 1983).

The metallic sulfides appear to have been derived from similar depths as were the saline brines at the Pleasant Bayou well (Light and others, 1984). Formation of the cap rock and metal sulfide deposition resulted from the leakage of relatively hot, saline metalliferous formation waters along the margins of the rising salt diapir when it was within 5,000 ft (1,500 m) of the surface (Price and others, 1983).

In general within the salt dome cap rocks, the strontium isotopes become more enriched and the carbon depleted radially outward and downward, suggesting a deep peripheral source for the heavy $^{87}\text{Sr}/^{86}\text{Sr}$ and light carbon (Posey, 1986). This is consistent with a source from the zone of smectite-illite transition, hydrocarbon generation, and feldspar albitization (80°C to 200°C , 176°F to 392°F interval).

The lead isotope data support the broad distribution of recently evolved metalliferous fluids and recent sulfide deposition derived from Gulf Coast formation fluids (Price and others, 1983). The lead-zinc ratio of 3:1 also supports a derivation of the metals from a basin of the character of the Gulf Coast Basin (Sangster, 1983).

Hydrocarbons have been observed bleeding from freshly cut sections of massive sulfides at Hockley dome and may result from primary capture during the precipitation of the mineralization or later introduction into the porous mineralization zone (Price and others, 1983). However, Kreitler and Dutton (1983) showed that the calcite cap rock in the Oakwood dome results from the

oxidation of hydrocarbons and concomitant reduction of anhydrite to form calcite and the reduced sulfur species, and most of the cap rock formation precedes sulfide deposition (Price and others, 1983). Hence hydrocarbon introduction must have largely preceded or occurred contemporaneously with sulfide formation and was a very late event.

Data from salt domes therefore support the idea of early periods of deep basinal brine migration and a late, hot ($>100^{\circ}\text{C}$, 212°F), saline-, hydrocarbon-, and most metalliferous-bearing brine migration through the Gulf Coast Tertiary sequence (fig. 35g). The late saline, hydrocarbon, and most metalliferous brines originated at depths of 20,000 to 25,000 ft (6,906 to 7,600 m) within the lower Frio or Vicksburg marine slope shales, which acted as a detachment plane for the Frio growth faulting (Ewing, 1986). Initial fluid migration was updip along the growth faults and then through the upper Frio sandstones (T2 to T5 interval) that formed continuous conduits to surface formations.

There appear to have been at least three major periods of fluid migration that have affected formations and salt dome cap rocks in the Gulf Coast Basin. An early period around 23.6 Ma was probably related to major diapirism of the salt domes and resulted in the initial transformation of smectite to illite (J. P. Morton, 1983) and may have introduced early anhydrite-rimming sulfides and sulfur into salt dome cap rocks and isotopically heavy sulfur into pre-ore sulfides related to 5-Ma uranium deposits (Ludwig and others, 1982). These fluids were at temperatures in excess of 120°C (248°F) but cooled to about 70°C (158°F) by mixing with late Oligocene marine waters near the surface in fracture zones surrounding and within salt dome cap rocks that had begun to form from salt dissolution.

A second flush of deep basinal fluids resulted in the introduction of gas and condensates into the upper Frio Formation after major kaolinization of the sandstones had occurred less than 7.5 to 1 Ma ago but may have been preceded by the introduction of heavier hydrocarbons less than 20 Ma ago. These fluids were at temperatures greater than 100°C (212°F) when they reached the anhydrite cap rocks and resulted in the progressive downward formation of the true calcite cap rocks. The progressively hotter fluids appear to have cooled by mixing with meteoric or marine waters and must have become alkaline for calcite to have been stable.

The last fluid flush introduced "Mississippi Valley" lead-zinc and barite deposits that crosscut the calcite cap rocks and therefore postdate the less than 7.5 to 1 Ma fluid migration event. Uranium deposits precipitated at or near salt dome rims whereas oils in the upper Frio Formation were waterwashed by the deeply sourced hot, aromatic-rich brines (fig. 35g). Albite isotopic stability data and isotopically heavy post-ore sulfides in 5-Ma-old uranium deposits (Ludwig and others, 1982) also indicate that this last period of fluid migration occurred less than 5 to 7.5 Ma ago. Geothermal data at Pleasant Bayou No. 2 suggest that updip migration of hot brines is still active in the upper Frio (Light and D'Attilio, in press). Rapid uplift of Damon Mound since 130,000 to 34,000 years ago (Collins, 1985) suggests that faults may have been activated recently in the Gulf Coast Basin and formed conduits for the upward migration of fluids still active in the upper Frio Formation (Light and D'Attilio, in press).

The sequence of fluid migration is consistent with studies on salt dome cap rocks (fig. 51; Posey, 1986) and suggests that true calcite cap rocks may be from more than 20 Ma to less than 1 Ma old. Such a hypothesis could be tested by Rb-Sr and K-Ar age determinations of shales present in the dark calcite layers (Posey, 1986). In addition, magnetostratigraphic dating of the mud

and coral layers in the Heterostegina reef on Damon Mound and strontium isotope dating of the Porites coral layers could give evidence for the periodicity of diapiric uplift. A detailed knowledge of the rates of diapiric uplift of salt stocks is important to basic research as well as from the safety considerations of giant hydrocarbon storage facilities that are housed in these salt bodies along the Gulf Coast. The detailed sequence of fluid migration that has been unraveled for the Gulf Coast succession may allow better estimates to be made of the relative amounts of fluids introduced by original migration, sediment compaction and co-production pressure-drawdown shale dewatering. Large pressure drawdowns could also reactivate the upward migration of gas-saturated brines, introducing additional reserves into largely depleted reservoirs. Changes in the lead, zinc, and copper contents of reservoir fluids can be used to define the amounts of basinal brines added by this mechanism.

GAS CHROMATOGRAPHY, MASS SPECTROMETRY, AND ISOTOPIC
ANALYSES OF HYDROCARBONS FROM THE HITCHCOCK N.E. FIELD,
GALVESTON COUNTY

by Malcolm P. R. Light

Saturate and aromatic hydrocarbons in condensate samples from the Prets and Delee No. 1 wells, Hitchcock N. E. field, Galveston County, Texas, have been analyzed by gas chromatography and mass spectrometry by Geochem Laboratories Inc. and the results are shown in fig. 54 and appendix 2. However, this data has not been completely interpreted and a more detailed report will be submitted later. Both the Prets and Delee No. 1 condensate samples were collected at the primary separators, but gas was recombined with the Prets No. 1 sample to reproduce the reservoir conditions (Foh and Osif, 1985). Though the two samples were not identical, the presence of gas in the Prets No. 1 sample could not produce the differences observed between the mass spectrometry analyses of these two condensates (P. K. Mukhopadhyay, personal communication, 1986). A provisional interpretation based on these analyses is included in this report because it has relevance to the migration model outlined prior to this section.

Comparison of the aromatic mass fragmentograms from the Prets and Delee No. 1 wells clearly indicates a loss of the low molecular weight aromatics as well as a reduction in methylnaphthalene, C2-alkylnaphthalene isomers, and phenantrene because of waterwashing. Normal paraffins appear unaffected by biodegradation probably because brine temperature was above 212°F (100°C). Also, steranes at the two wells do not show any significant differences, whereas the hopanes at C-10 have been demethylated in Prets No. 1 condensates.

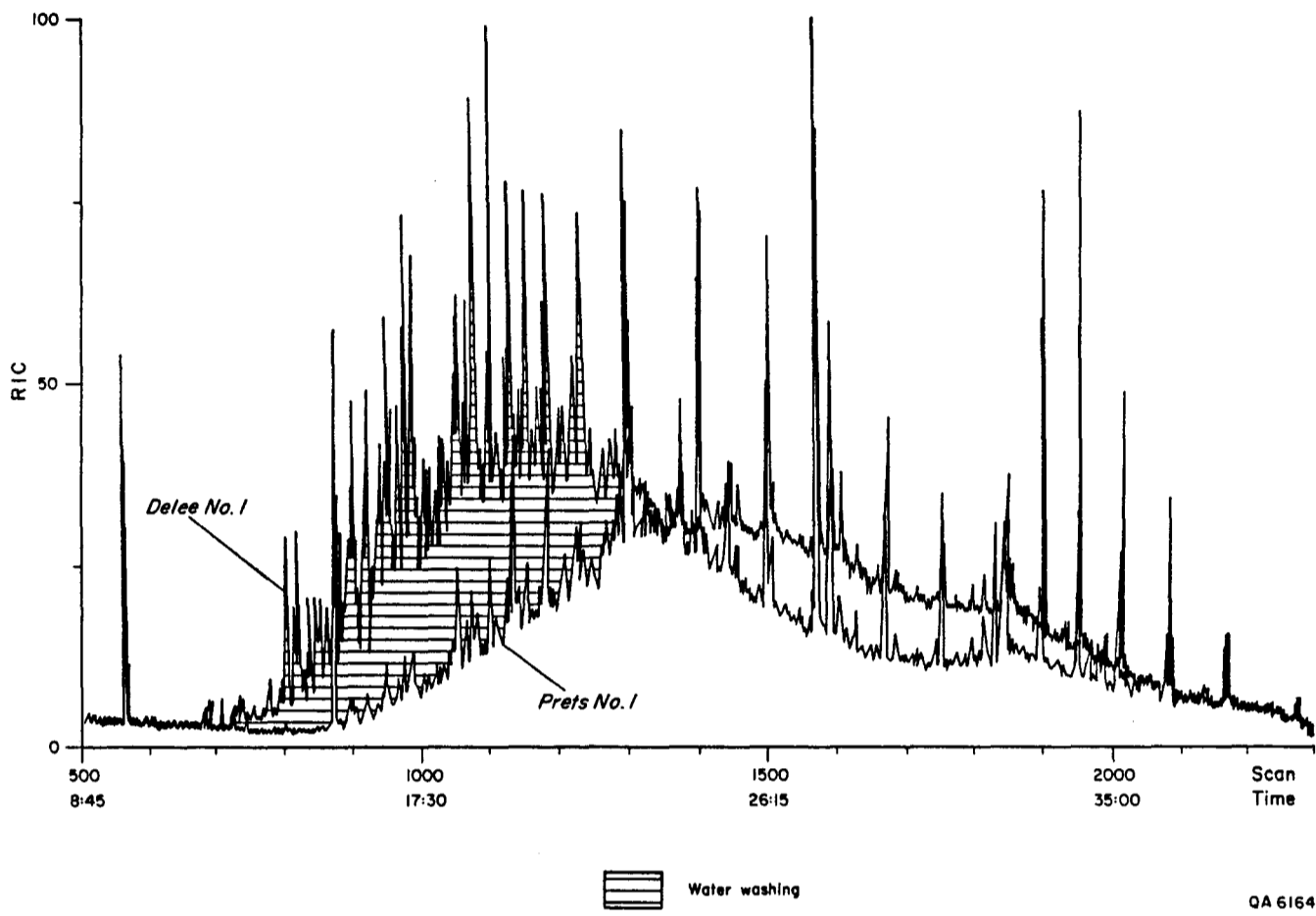


Figure 54. Mass spectrograms of the aromatic fraction of condensates, Delee No. 1 and Prets No. 1 wells, Hitchcock N.E. field.

Toluene shows an anomalously large increase in the waterwashed Prets No. 1 condensate, which suggests that waterwashing resulted from contact of hot, aromatic-rich, upward-migrating basinal brines with trapped hydrocarbons. High solubility of toluene in hydrocarbons and low solubility of toluene in brines may explain this phenomenon. Basinal brines tested during the geopressured-geothermal program contain abundant aromatic hydrocarbons, and isotopic data indicate that they formed at high temperatures at a depth of about 20,000 ft (6,100 m).

That the process of waterwashing postdated migration of hydrocarbons into the reservoir is demonstrated by the observation that condensates have isotopic and geochemical characteristics denoting a marine source, whereas organics of adjacent shales are of terrestrial origin. High-temperature waterwashing with no biodegradation is a newly defined process that has relevance to hydrocarbon reservoirs in the Gulf Coast, where large scale migration of hot basinal brines has occurred.

The Prets No. 1 well is close to the crest of the Hitchcock N.E. structure as well as splay faults that radiate off from the major growth fault on the southeast margin of the field (fig. 55). As the condensates are waterwashed at this location but not at the Delee No. 1 well, which lies on the northwest flank and downdip, it suggests that the major upward migration pathway for the toluene-rich basinal brines was up along growth faults. Such fluid migration could be initiated at the present time when large pressure drawdowns are imposed on the Hitchcock N.E. field during co-production.

The degree of waterwashing of condensates at any locality is a measure of the transmissibility of the formation in that area and its proximity to growth faults. Therefore, an area-wide knowledge of the degree of waterwashing of the condensates in the Hitchcock N.E. field should allow the identification of the

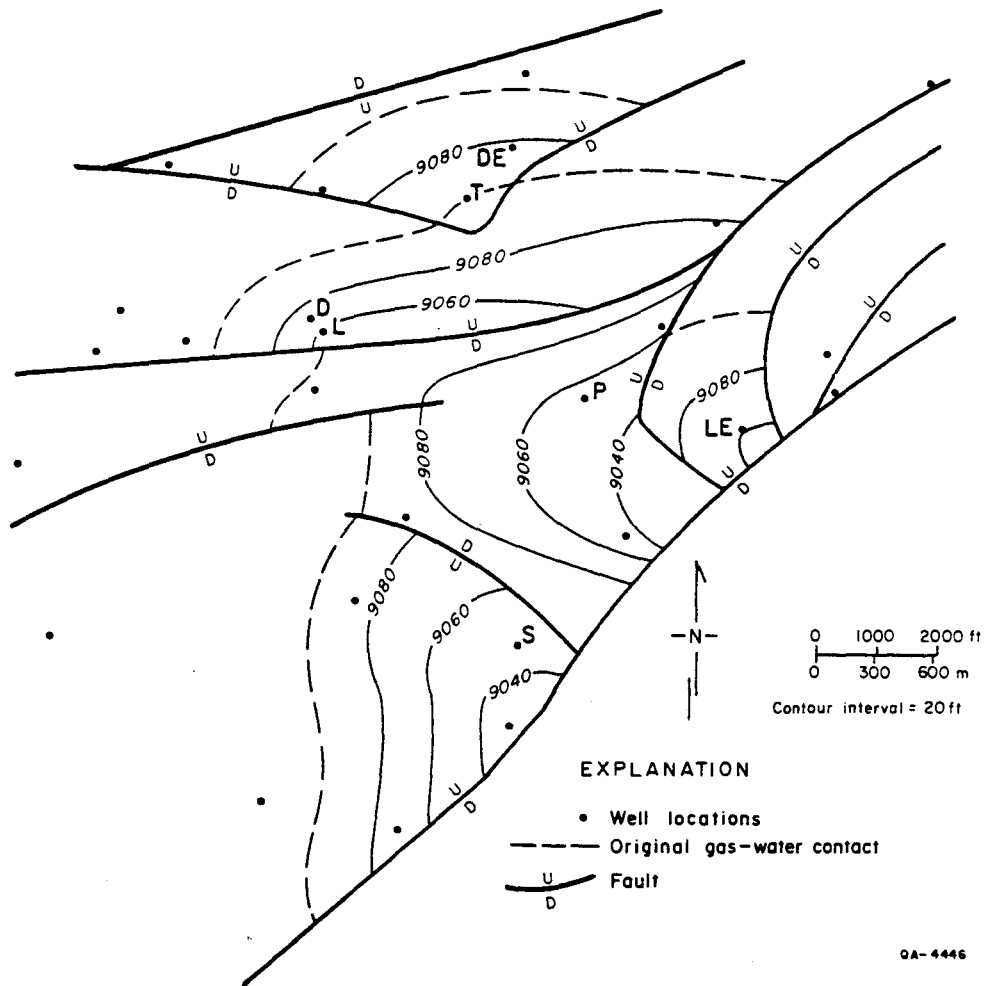


Figure 55. Structure map on top of the Frio "A" pay zone. Lettered oil well locations are Phillips No. 1 Delaney (DE), Thompson (T), Louise (L), Prets (P), Sundstrom (S), Secondary Gas Recovery No. Delee (D), and Cockrell No. 1 Lowell Lemm (LE).

major water conduits when this is combined with structural and stratigraphic data. This information will be vital in choosing the best locations for production and guard wells during development of a co-production field.

Isotopic analyses of gases, oils, and formation waters from the Delee and Prets No. 1 wells were conducted by Coastal Science Labs (table 5). This data falls within the field of Tertiary migrated gas when plotted on Schoell's (1983) crossplots of $\delta^{13}\text{C}$ (methane) versus percentage C₂₊, $\delta^{13}\text{C}$ (ethane), and δD (methane) and suggests that the gases were derived from a thermal maturity (vitrinite reflectance) of some 1.2% R_o (fig. 56). This is consistent with the condensates having formed high temperatures in the oil-gas transition zone (fig. 56). At this thermal maturity, methane forms with a $\delta^{13}\text{C}$ isotopic ratio of about -40 ppt (Schoell, 1983). Therefore, the measured $\delta^{13}\text{C}$ of the methane (-43 to -44 ppt) at the Prets and Delee No. 1 wells is probably due to mixing of 30 to 50 percent of locally derived methane with $\delta^{13}\text{C}$ values of -50 to -60 ppt (Schoel, 1983) at a thermal maturity of about 0.5% R_o with the deep methane.

Table 5. Stable isotope analyses, Delee No. 1 and Prets No. 1 wells.

	<u>S.G.R. Delee #1</u> <u>$\delta^{13}\text{C}_{\text{PDB}}$</u>	<u>Prets #1</u> <u>$\delta^{13}\text{C}_{\text{PDB}}$</u>
<u>Gas</u>		
CH ₄	-42.6, -42.8	-44.0, -44.1
C ₂ H ₆	-27.5, -27.5	-27.5
C ₃ H ₈	-18.0, -18.2	-17.5, -17.7
C ₄ H ₁₀	-32.0	-32.1
CO ₂	-5.4, -5.2	-5.7, -5.5
<u>Condensate</u>		
whole	-26.9, -26.9	N.R.
saturate	-27.2, -27.2	-27.4, -27.5
aromatic	-26.8, -26.8	-26.6, -26.6
polar	-26.6, -26.7	-26.6, N.R.
<u>Formation water</u>		
	<u>$\delta^{18}\text{O}_{\text{SMOW}}$</u>	
	+3.8, +3.9	+4.1, +4.1

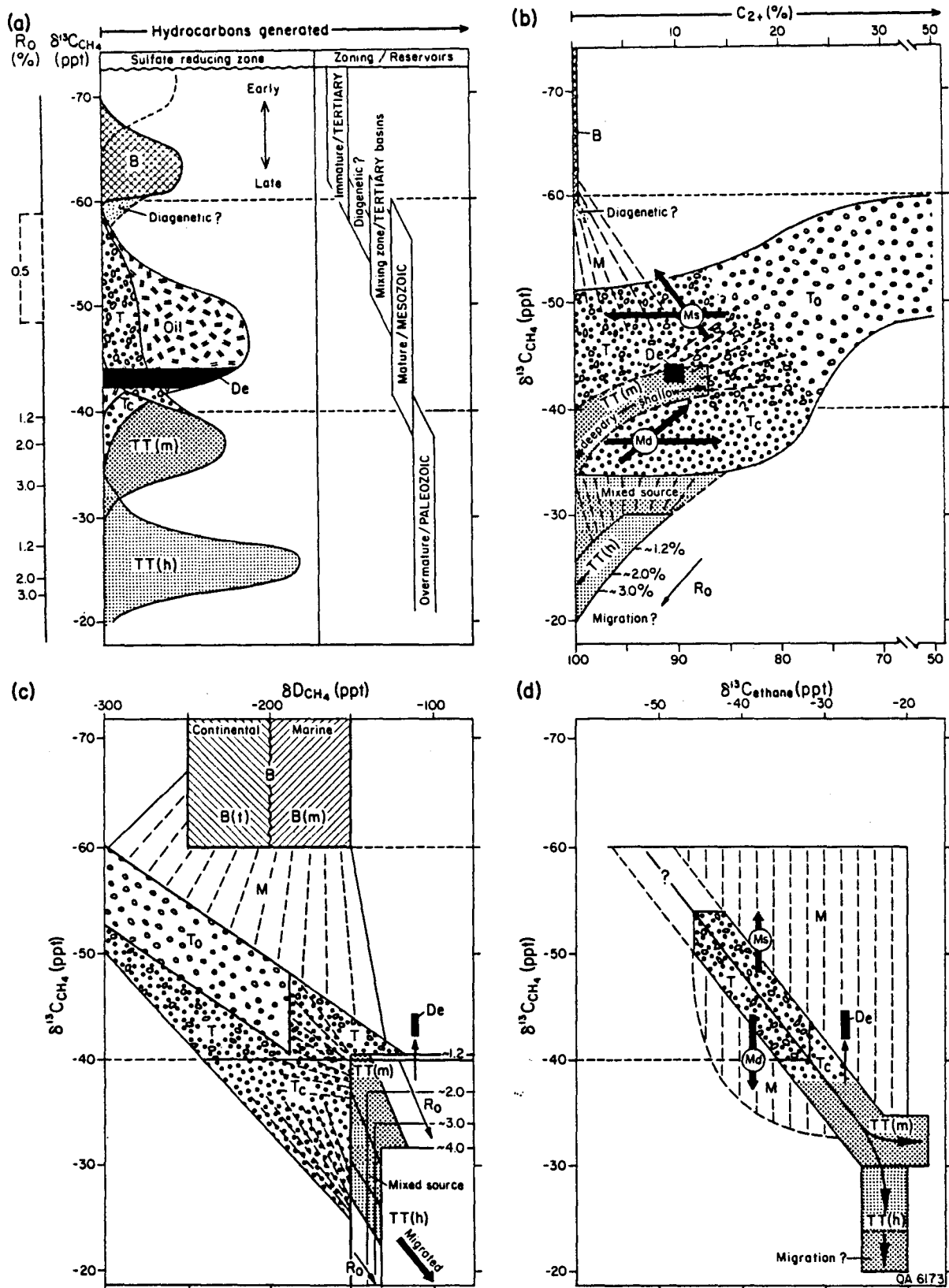


Figure 56. Diagrams showing (a) hydrocarbon generation zones versus thermal maturity (R_o), (b) percentage C_{2+} versus $\delta^{13}C$ (methane), (c) δD (methane) versus $\delta^{13}C$ (methane), and (d) $\delta^{13}C$ (ethane) versus $\delta^{13}C$ (methane) for gases, from Schoel, 1983.

SHALE DEWATERING DURING COMPACTION AND PRODUCTION

by Malcolm P. R. Light and David W. Koppenaal

Areas of variable indurated sandstone containing mottled kaolinite zones developed in the Frio "A" sandstone adjacent to thin shale units in the Delee No. 1 core and probably result from the effects of fluids emitted from the shales during compaction (Light and D'Attilio, 1985). These shales appear to have a constant illite-smectite composition. Slight reductions in the salinity during production at the Prets No. 1 well may be evidence for contemporaneous dewatering of the shales (Light and D'Attilio, 1985). The Anahuac and Frio shales adjacent to the Frio "A" sandstone in the Hitchcock N. E. field have been analyzed for their content of carbon and hydrogen from which the amount of bound water present in the shale can be estimated (table 6). Bound water appears to vary between 23 and 29 percent by weight, indicating that there is abundant water that could be released by shale dewatering. Normally, 10 to 15 percent of the compacted bulk weight of shales is lost as water during the conversion of smectite to illite (Burst, 1969). The concentration of major, trace, and rare earth elements in formation waters and possible source rocks from the Hitchcock N. E. field area are being measured by the Mineral Studies Laboratory at the Bureau of Economic Geology. These data will be used to distinguish between local shale dewatering as a source of the fluids and more deeply derived brines. Only major and trace elements have been analyzed so far (appendix 1), but it is hoped that the ICP mass spectrometer will soon be able to accurately measure the concentrations of the rare earth elements in formation waters and rocks. The variation of elemental abundance, compounds, and isotopes has been

Table 6. Calculated bound shale water, Delee No. 1 well.

Sample Preparation/Treatment

Samples were shatterboxed for 2½ minutes and dried at 105°C for 1 hour.

Sample Analysis Method

<u>Constituent</u>	<u>Technique</u>
%C	Automated C, H, N Analyzer
%H	

RESULTS

<u>MSL ID#/LOC ID#</u>	<u>%C</u>	<u>%H</u>	<u>Calculated bound - H₂O, %</u>
85-1091/9068'	0.58	5.68	25.6
85-1092/9077.2'	0.61	6.44	29.0
85-1093/9099.6'	0.48	5.16	23.2
85-1094/9102.3'	0.80	6.40	28.8
85-1095/9180.4-9182'	0.84	6.04	27.2

Analyst:

Cynthia Mahan

plotted against depth and chlorine content for wells in Brazoria and Galveston Counties (figs. 39, 57 through 66). Most of the elements show a rough linear distribution with depth, with values from the Hitchcock N.E. field tending to plot on the opposite end of the trend compared with those from the Pleasant Bayou geopressured-geothermal test wells. However, the iron content shows a large variation (0.1 to more than 20 mg/L), and fluid sampled early in the production of the Delee No. 1 well had 100 times more iron in it than fluid sampled later (fig. 62). The manganese also shows a marked decrease between these two samples (fig. 63), whereas other major elements remain unchanged (figs. 59 through 61 and 64). This suggests that the well was cleaning up and that the iron and manganese were probably derived from rusted production equipment. The bromide also shows a slight decrease (fig. 65).

IMMEDIATE RESEARCH PLANS

The major part of the effort of the Bureau of Economic Geology will be to carry out a detailed reevaluation of the stratigraphic architecture of the Hackberry reservoirs in the Port Arthur field. Future research in the Port Arthur field will be split into two project subareas: (1) Hackberry reservoir production geology and (2) geological constraints on disposal-well location. These studies will build on the foundations laid by investigations of Gregory and others (1984). Hackberry reservoir analysis will focus on the internal architecture of the composite deep-water sandstone bodies and the potential for reservoir compartmentalization. These data will be integrated with completion and production histories so that untapped reservoir compartments may be defined.

Produced water is to be injected into shallow Miocene sandstones. Our primary function in this area is to determine those sands most capable of

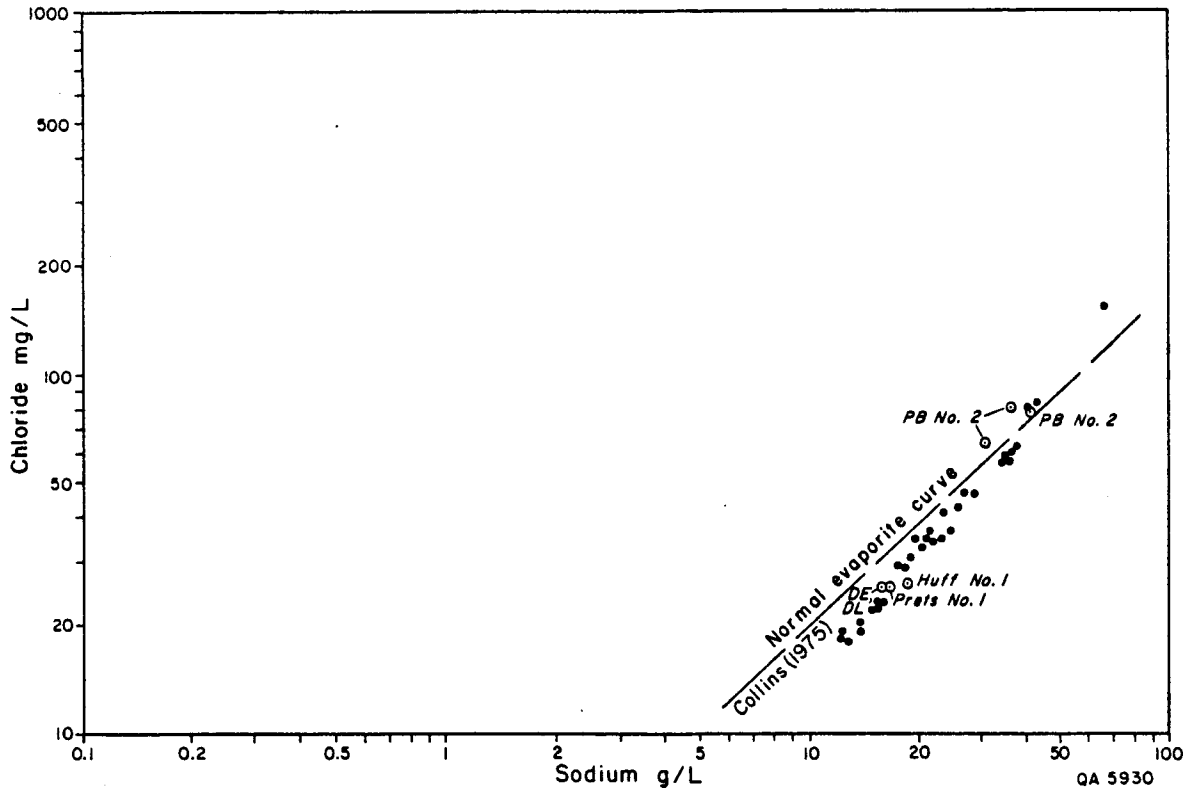
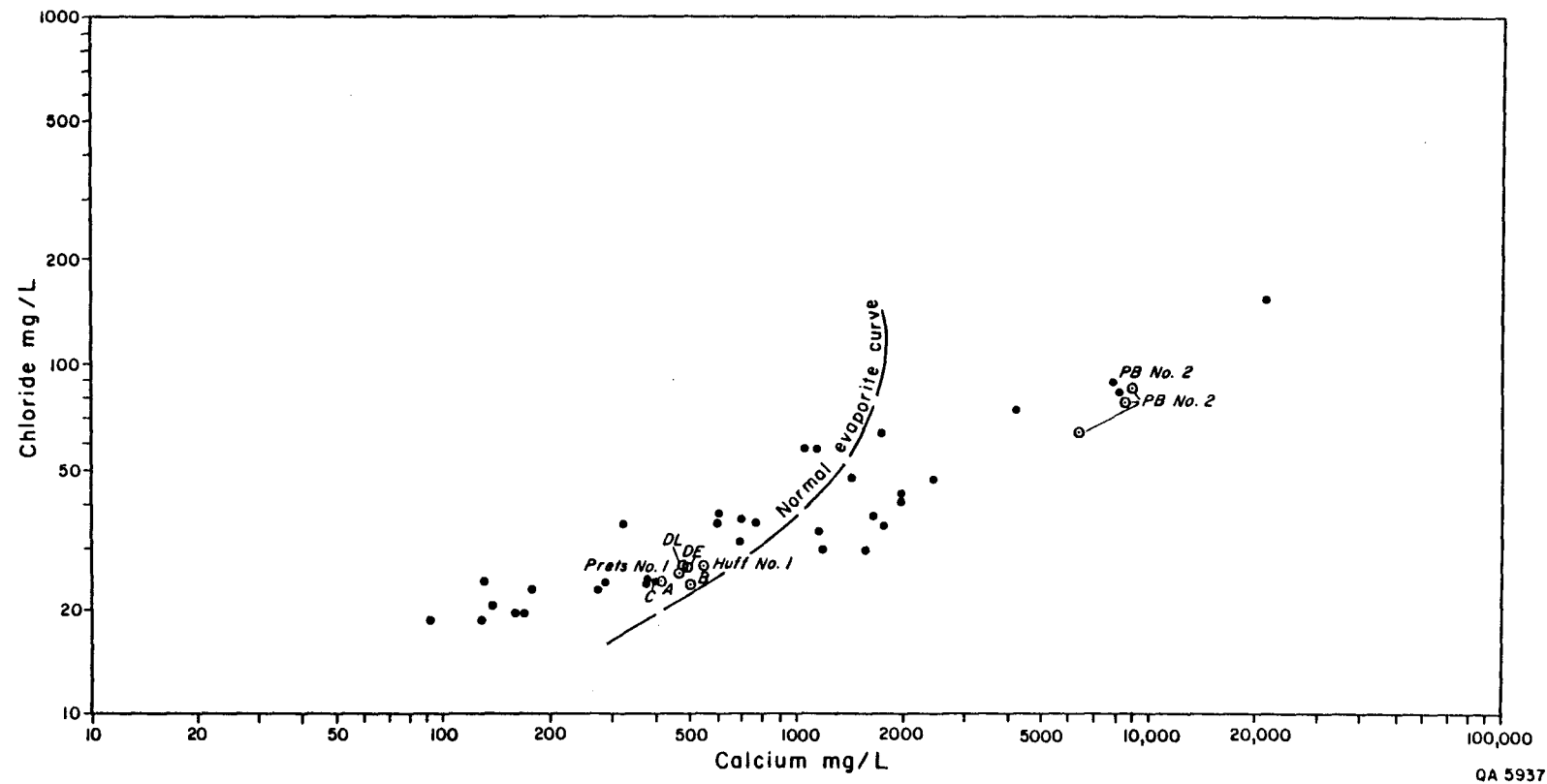


Figure 57. Sodium versus chloride in brines from the Houston delta system. DE and DL are initial and later formation water samples from the Delee No. 1 well.



QA 5937

Figure 58. Calcium versus chloride in brines from the Houston delta system. DE and DL are initial and later formation water samples from the Delee No. 1 well.

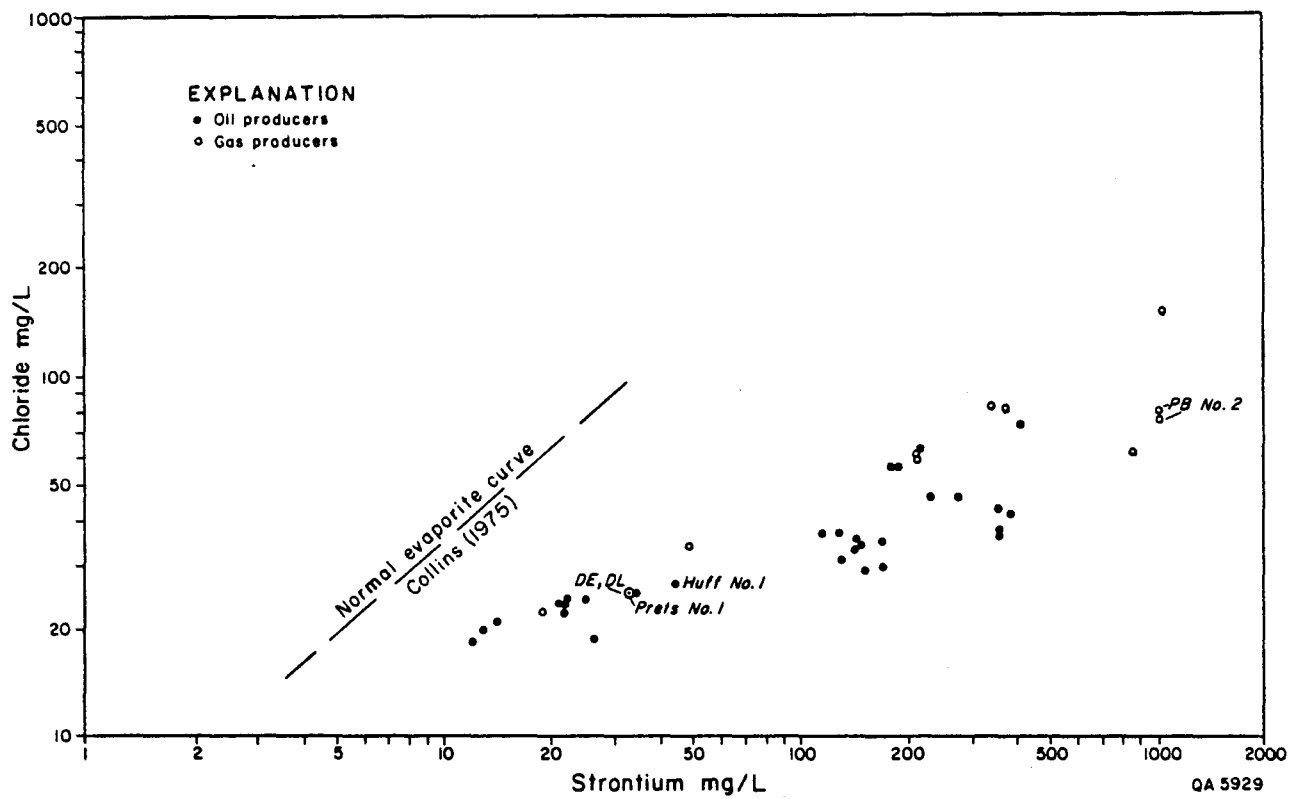


Figure 59. Strontium versus chloride in brines from the Houston delta system. DE and DL are initial and later formation water samples from the Delee No. 1 well.

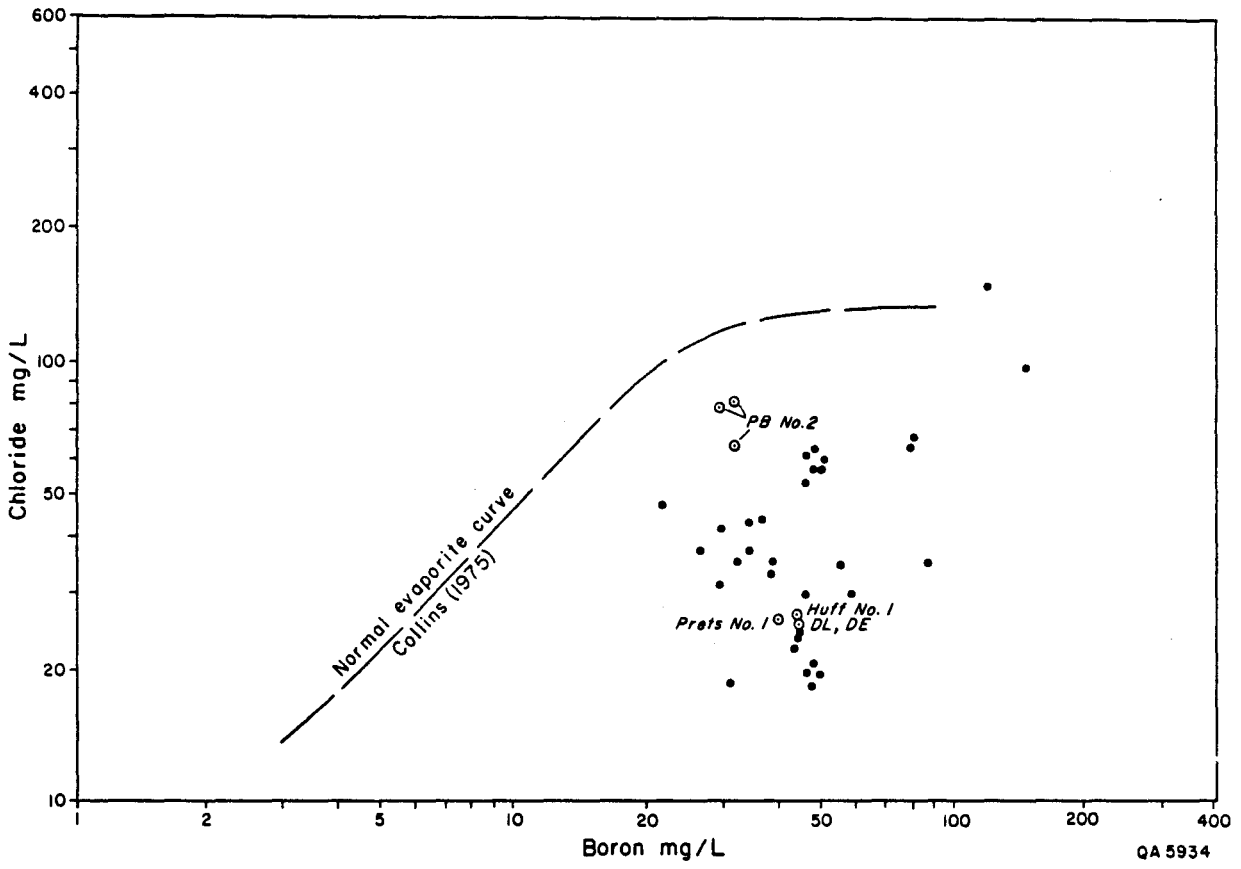


Figure 60. Boron versus chloride in brines from the Houston delta system. DE and DL are initial and later formation water samples from the Delee No. 1 well.

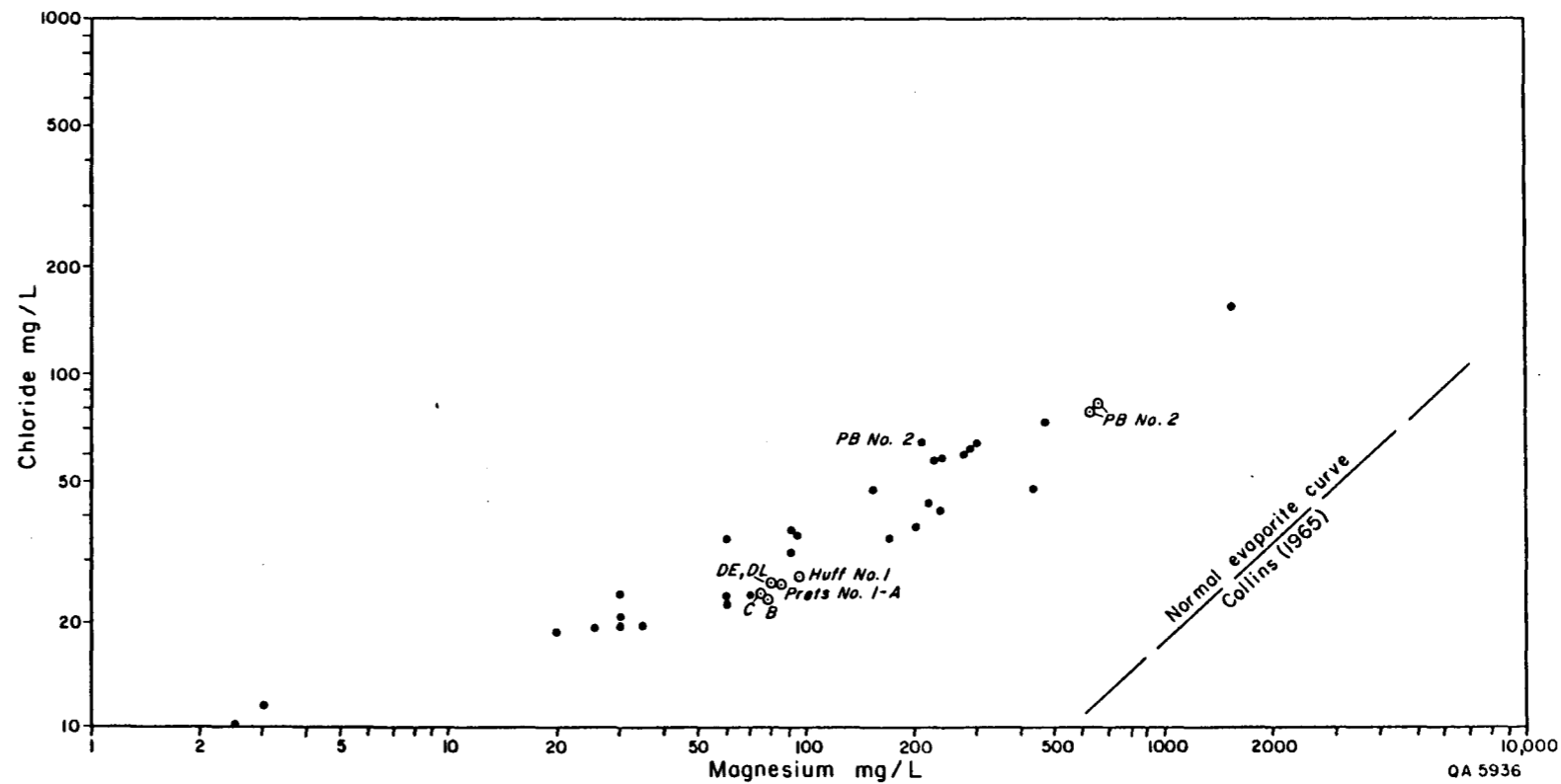


Figure 61. Magnesium versus chloride in brines from the Houston delta system. DE and DL are initial and later formation water samples from the Delee No. 1 well.

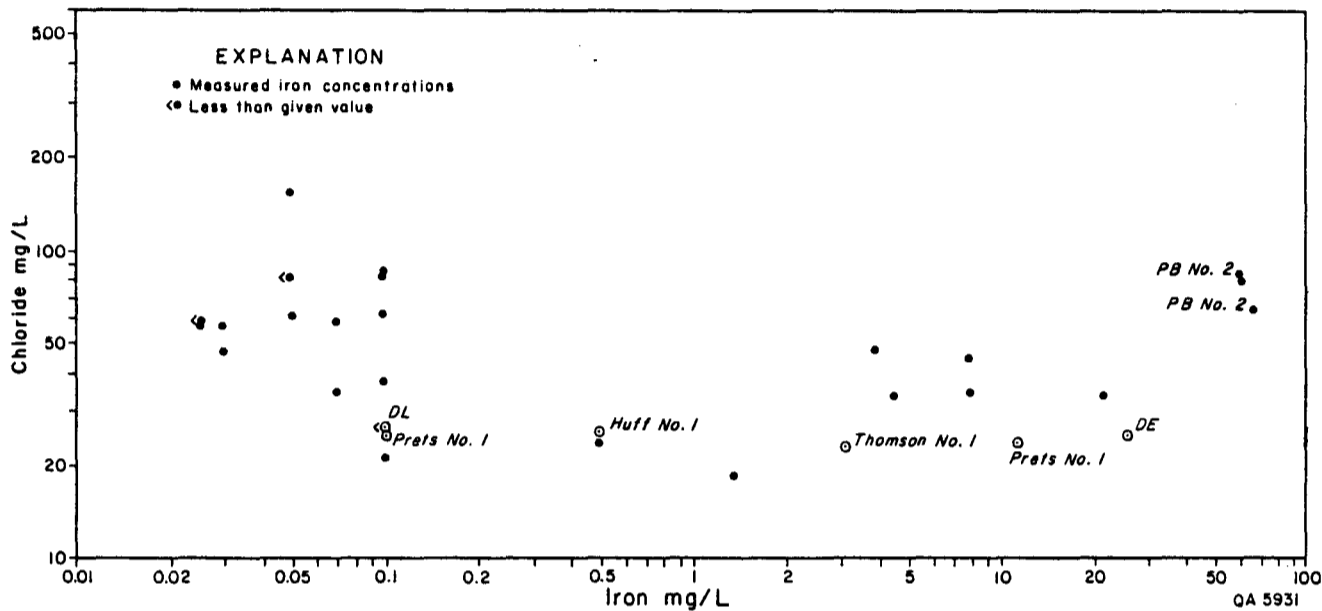


Figure 62. Iron versus chloride in brines from the Houston delta system. DE and DL are initial and later formation water samples from the Delee No. 1 well.

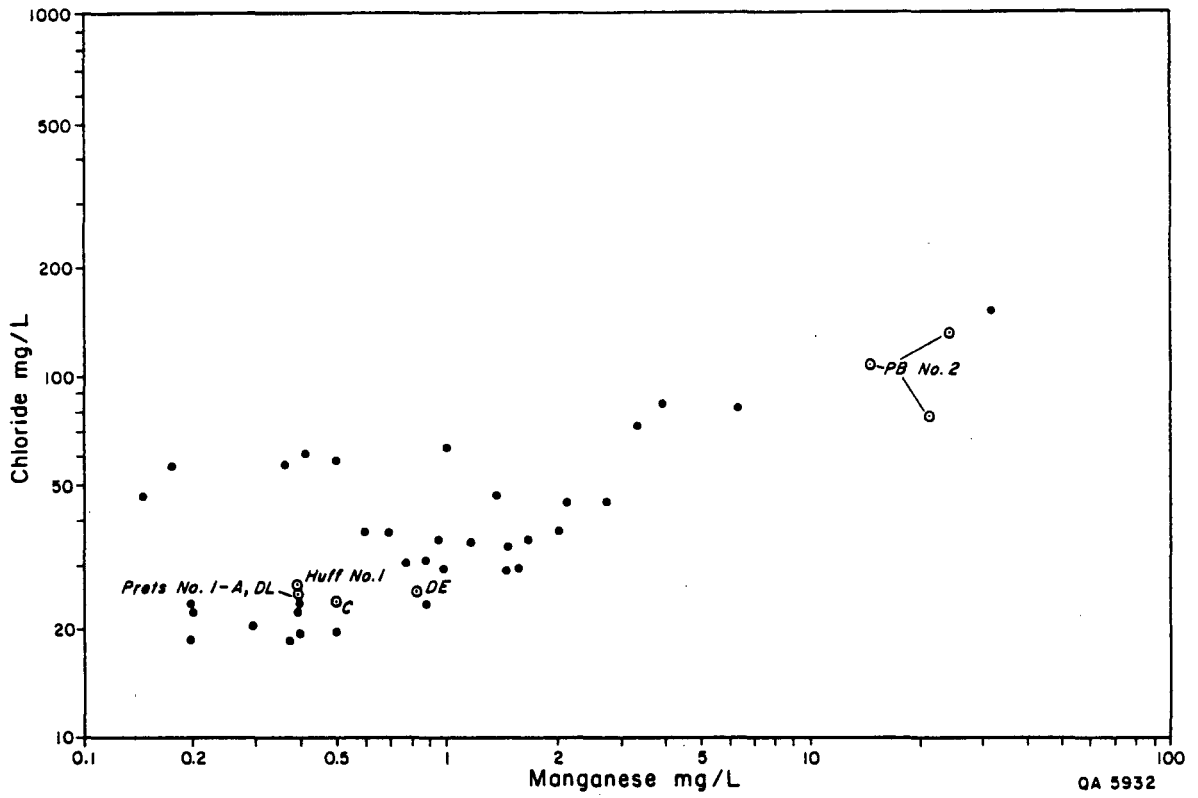


Figure 63. Manganese versus chloride in brines from the Houston delta system. DE and DL are initial and later formation water samples from the Delee No. 1 well.

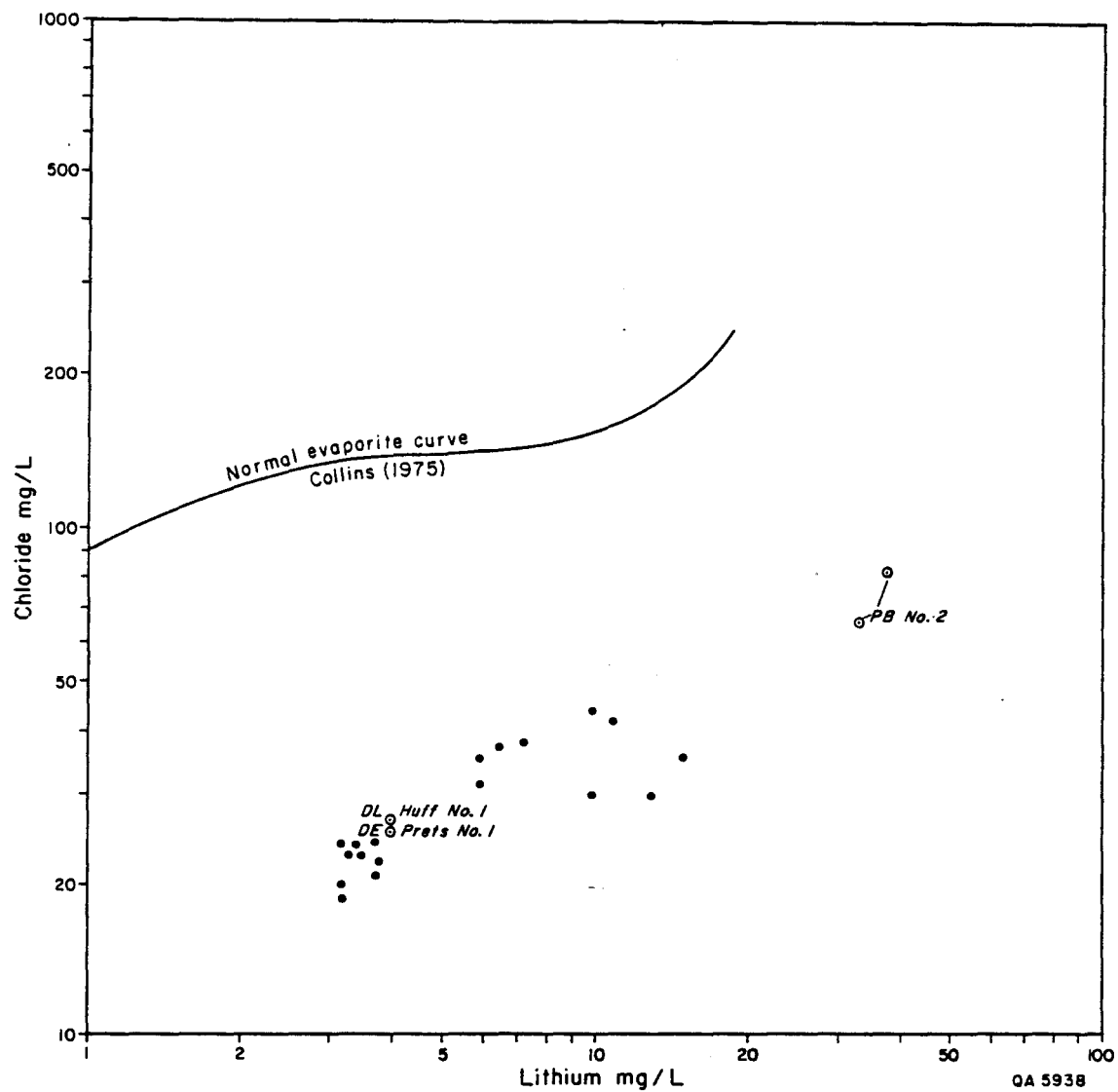


Figure 64. Lithium versus chloride in brines from the Houston delta system. DE and DL are initial and later formation water samples from the Delee No. 1 well.

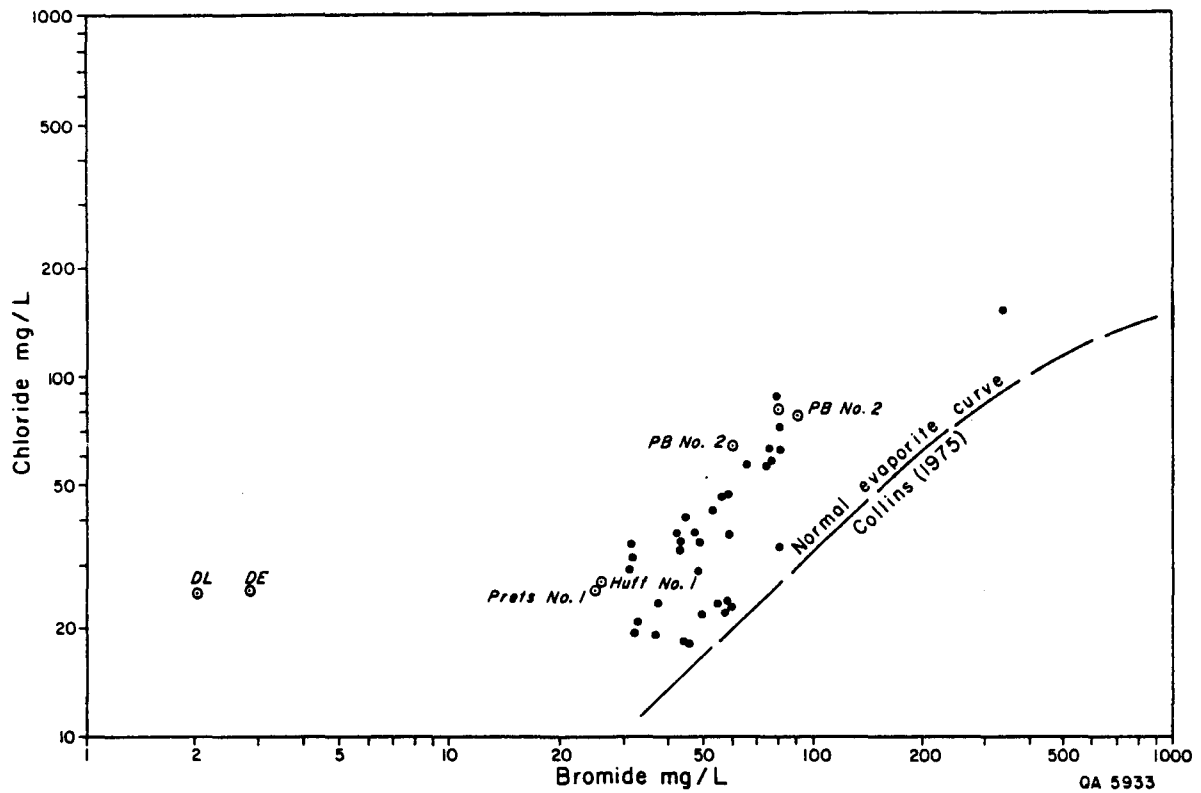


Figure 65. Bromide versus chloride in brines from the Houston delta system. DE and DL are initial and later formation water samples from the Delee No. 1 well.

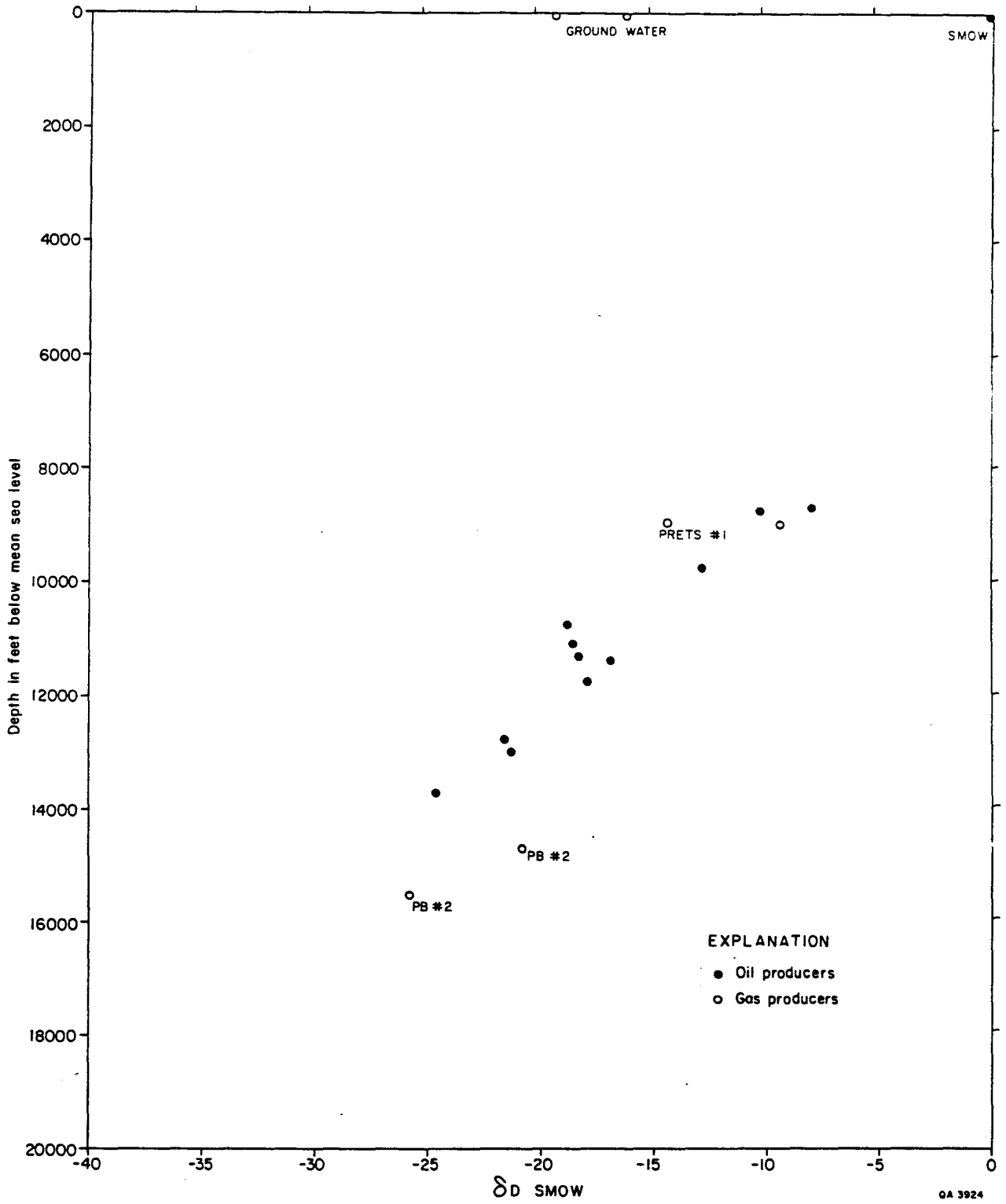


Figure 66. δD (SMOW) versus depth in brines from the Houston delta system.

receiving and dispersing injected water over a sustained period. The approach will be to map sand distribution and to examine lateral and vertical permeability trends from logs and sidewall cores in several potential receptor aquifers. Finally, disposal-well locations and perforation levels will be recommended to the field operators.

Active work on the Hitchcock N. E. field has been terminated, but fluid- and rock-elemental analyses of samples "in house" will be completed and interpreted. In addition, the Mineral Studies Laboratory at the Bureau of Economic Geology will perform analyses of IGT samples beyond that stated in the contract proposal. A detailed interpretation of the gas chromatography, mass spectrometry, and isotope analyses of gases and hydrocarbons from Hitchcock N.E. field and the Pleasant Bayou test well is nearing completion.

ACKNOWLEDGMENTS

Funding for this research was provided by the Gas Research Institute under contract no. 5084-212-0924.

We wish to thank H. H. Posey, E. C. Collins, W. E. Galloway, P. K. Mukhopadhyay, and J. G. Price for valuable discussions. We gratefully acknowledge assistance given by L. L. Anderson, K. P. Peterson, and W. A. Parisi of Eaton Industries of Houston, Inc. ICP and ICP mass spectrometer analyses were done at the Mineral Studies Laboratory by Steven W. Tweedy under the direction of David W. Koppenaar. The manuscript was reviewed by R. J. Finley and word processed by Dorothy C. Johnson under the direction of Lucille C. Harrell. Illustrations were drafted by J. L. Lardon, J. T. Ames, and T. Burke under the direction of Richard L. Dillon. This report was edited by Diane Callis Hall and assembled by Margaret L. Evans.

REFERENCES

- Ahrens, L. H., 1965a, Distribution of the elements in our planet: New York, McGraw-Hill, 110 p.
- _____ 1965b, The comparative geochemistry of potassium, rubidium, calcium, argon, strontium, uranium, thorium and lead in Hamilton, I. E., ed., Applied geochronology: New York, Academic Press, 267 p.
- Anderson, G. M., and MacQueen, R. U., 1982, Ore deposits models-6. Mississippi Valley lead-zinc deposits: Geoscience Canada, v. 9, p. 108-117.
- Andrews, D. I., 1960, The Louann salt and its relationship to Gulf Coast salt domes: Gulf Coast Association of Geological Societies Transactions, v. 10, p. 215-240.
- Baldwin, O. D., and Adams, J. A. S., 1971, K10/Ar10 ages of alkalic igneous rocks of the Balcones fault trend of Texas: Texas Journal of Science, v. 22, nos. 2 and 3, p. 223-231.
- Barnes, H. L., 1979, Geochemistry of hydrothermal ore deposits: New York, John Wiley, 798 p.
- Beales, F. W., and Onasick, E. P., 1970, The stratigraphic habit of Mississippi Valley-type ore bodies: Institute of Mining and Metallurgy Transactions, v. 79, sec. B, p. B145-B154.

- Berg, R. R., and Powers, B. K., 1980, Morphology of turbidite-channel reservoirs, lower Hackberry (Oligocene), southeast Texas: Gulf Coast Association of Geological Societies Transactions, v. 30, p. 41-48.
- Bernard, H. A., and LeBlanc, R. J., Resume of the Quaternary geology of the northwestern Gulf of Mexico province, in Wright, H. E., and Frey, D. G., eds., The Quaternary of the United States: Princeton University Press, p. 137-185.
- Bogomolov, Y. G., Kudelsky, A. V., and Lapshin, N. N., 1978, Hydrogeology of large sedimentary basins, in Hydrogeology of great sedimentary basins: International Association of Hydrological Sciences Publication No. 120, p. 117-122.
- Boles, J. R., and Franks, S. G., 1979, Clay diagenesis in Wilcox sandstones of southwest Texas, implications of smectite diagenesis on sandstone cementation: Journal of Sedimentary Petrology, v. 49, no. 1, p. 55-70.
- Brock, T. D., 1985, Life at high temperatures: Science, v. 230, p. 132-138.
- Brown, G. G., Katz, D. L., Oberfell, G. B., and Alden, R. C., 1948, Natural gasoline and volatile hydrocarbons: Natural Gasoline Association of America, Tulsa, 44 p.
- Brunhild, S. R., 1984, Depositional and structural reconstruction of Southwest Louisiana Oligo-Miocene strata: a temporal-spatial approach: Gulf Coast Association of Geological Societies Transactions, v. 34, p. 9-31.

- Burke, W. H., Denison, R. E., Hetherington, E. A., Koepnick, R. B., Nelson, H. F., and Otto, J. B., 1982, Variation of seawater $^{87}\text{Sr}/^{86}\text{Sr}$ throughout Phanerozoic time: *Geology*, v. 10, p. 516-519.
- Burst, J. F., 1969, Diagenesis of Gulf Coast clayey sediments and its possible relation to petroleum migration: *American Association of Petroleum Geologists Bulletin*, v. 53, p. 73-93.
- Busche, F. D., Reynolds, R. L., and Goldhaber, M. B., 1982, Fault leaked H_2S and the origin of South Texas uranium deposits: implications of sulfur isotopic studies: Society of Mining Engineers of AIME annual meeting, Dallas, Texas, 13 p.
- Cahen, L., Snelling, N. J., Delhal, J., and Vail, J. R., 1984, The geochronology and evolution of Africa: Oxford, Clarendon Press, 512 p.
- Carr, N. L., Kobayashi, R., and Burrows, D. B., 1954, Viscosity of hydrocarbon gases under pressure: *American Institute of Mining Engineers Transactions*, v. 201, p. 264-270.
- Cathles, L. M., and Smith, A. T., 1983, Thermal constraints on the formation of Mississippi Valley-type lead-zinc deposits and their implications for episodic basin dewatering and deposit genesis: *Economic Geology*, v. 78, p. 983-1002.
- Clauer, N., 1976, *Geochimie isotopique du strontium des milieux sedimentaires. Application a la geochronologie de la couverture de craton ouest-africain: Mem. Sci. Geol., University Louis Pasteur, Strasbourg, no. 45.*

Cloos, H., 1928, Über antithetische Bewegungen: Geologische Rundschau, v. 19, no. 3, p. 249-251.

Collins, A. G., 1975, Geochemistry of oil field waters: New York, Elsevier, 496 p.

Collins, E. C., 1985, A review of the geology and Plio-Pleistocene deformations at Damon Mound salt dome, Texas, in Seni, S. J., and others, Phase III, Examination of Texas salt domes as potential sites for permanent storage of toxic chemical waste: The University of Texas at Austin, Bureau of Economic Geology, report prepared for the Texas Water Commission under interagency contract no. IAC(84-85)-2203, p. 275-305.

Correns, C. W., 1956, The geochemistry of the Halogens, in Ahrens, L. H., and others, eds., Physics and chemistry of the Earth: New York, Pergamon, p. 181-233.

Craft, B. C., and Hawkins, M. F., 1959, Applied petroleum reservoir engineering: Englewood Cliffs, New Jersey, Prentice-Hall, 437 p.

Crerar, D. A., and Barnes, H. L., 1976, Ore solution chemistry V, Solubilities of chalcopyrite and chalcocite assemblages in hydrothermal solution at 200°C and 350°C: Economic Geologist, v. 71, p. 772-794.

Davis, J. B., and Kirkland, D. W., 1979, Bioepigenetic sulfur deposits: Economic Geologist, v. 74, no. 2, p. 462-468.

- Dennis, J. G., and Kelley, V. C., 1980, Antithetic and homothetic faults: *Geologische Rundschau*, v. 69, no. 1, p. 186-193.
- Deer, W. A., Howie, R. A., and Zussman, J., 1969, An introduction to the rock-forming minerals: London, Longmans, 528 p.
- Dix, R. O., and Jackson, M. P. A., 1982, Lithology, microstructures, fluid inclusions, and geochemistry of rock salt and of the cap-rock contact in Oakwood Dome, East Texas: significance for nuclear waste storage: The University of Texas at Austin, Bureau of Economic Geology Report of Investigations No. 120, 59 p.
- Doe, B. R., and Zartman, R. E., 1979, Plumbotectonics, the Phanerozoic, in Barnes, H. L., ed., *Geochemistry of hydrothermal ore deposits*: New York, John Wiley, p. 22-70.
- Dorfman, M. H., and Fisher, W. L., eds., 1980, *Proceedings, Fourth United States Gulf Coast Geopressured Geothermal Energy Conference*, volume 1: The University of Texas at Austin, Center for Energy Studies, 514 p.
- Dow, W. G., 1978, Petroleum source beds on continental slopes and rises: *American Association of Petroleum Geologists Bulletin*, v. 62, p. 1584-1606.
- Dozy, J. J., 1970, A geological model for the genesis of lead-zinc ores of the Mississippi Valley, U.S.A.: *Institute of Mining and Metallurgy Transactions*, section B, v. 79, Bulletin 765, p. 163-172.

Dutton, S. P., and Kreitler, C. W., 1980, Cap rock formation and diagenesis, Gyp Hill salt dome, South Texas: Gulf Coast Association of Geological Societies Transactions, v. 30, p. 333-339.

Dwight's Energydata Co., 1985a, Natural gas well production histories, active wells, Railroad Commission of Texas District 2: Richardson, Texas, 780 p.

_____ 1985b, Natural gas well production histories, active wells, Railroad Commission of Texas District 3: Richardson, Texas, 860 p.

_____ 1985c, Natural gas well production histories, active wells, Railroad Commission of Texas District 4: Richardson, Texas, 1868 p.

_____ 1985d, Natural gas well production histories, inactive wells, Railroad Commission of Texas District 2: Richardson, Texas, 947 p.

_____ 1985e, Natural gas well production histories, inactive wells, Railroad Commission of Texas District 3: Richardson, Texas, 923 p.

_____ 1985f, Natural gas well production histories, inactive wells, Railroad Commission of Texas District 4: Richardson, Texas, 1329 p.

_____ 1985g, Natural gas well production histories, active inactive wells, Lafayette District no. 12, Louisiana: Richardson, Texas, v. 3, 3312 p.

Eargle, D. H., 1962, Geology of a core hole WP-1, Tatum Dome, Lamar County, Mississippi: U.S. Geological Survey Open-File Report 474-278, 50 p.

Eargle, D. H., Dickinson, K. A., and Davis, B. O., 1975, South Texas uranium deposits: American Association of Petroleum Geologists Bulletin, v. 59, p. 766-799.

Ewing, T. E., 1986, Section I. Regional fault compartment geometries of the Wilcox and Frio growth-fault trends, Texas Gulf Coast, in Ewing, T. E., and others, Consolidation of geologic studies of geopressed geothermal resources of Texas: The University of Texas at Austin, Bureau of Economic Geology, report prepared for the U.S. Department of Energy under contract no. DE-AC08-79ET27111, 97 p.

Ewing, T. E., Light, M. P. R., and Tyler, N., 1984, Section IV. Integrated geologic study of the Pleasant Bayou - Chocolate Bayou area, Brazoria County, Texas - first report, in Ewing, T. E., and others, Consolidation of geologic studies of geopressed geothermal resources of Texas: The University of Texas at Austin, Bureau of Economic Geology, report prepared for the U.S. Department of Energy under contract no. DE-AC08-79ET27111, p. 90-142.

Ewing, T. E., and Reed, R. S., 1984, Depositional systems and structural controls of Hackberry sandstone reservoirs in southeast Texas: The University of Texas at Austin, Bureau of Economic Geology Geological Circular No. 84-7, 48 p.

Feely, H. W., and Kulp, J. L., 1957, Origin of Gulf Coast salt-dome sulphur deposits: American Association of Petroleum Geologists Bulletin, v. 41, p. 1802-1853.

Finley, R. J., Dutton, S. P., Lin, Z. S., and Saucier, A. E., 1985, The Travis Peak (Hosston) Formation: geologic framework, core studies, and engineering field analysis: topical report prepared for Gas Research Institute under contract no. 5082-211-0708, The University of Texas at Austin, Bureau of Economic Geology, 233 p.

Flawn, P. T., Goldstein, A., Jr., King, P. B., and Weaver, C. E., 1961, The Ouachita System: University of Texas, Austin, Bureau of Economic Geology Bulletin No. 6120, 401 p.

Foh, S. E., and Osif, T. L., 1985, Field and laboratory support for the co-production program: Institute of Gas Technology, Chicago, annual report prepared for the Gas Research Institute under contract no. 5084-212-0971, 55p. plus appendices.

Folk, R. L., and Land, L. S., 1975, Mg/Ca ratio and salinity; two controls over crystallization of dolomite: American Association of Petroleum Geologists Bulletin, v. 59, p. 60-68.

Foscolos, A. E., Powell, T. G., and Gunter, P. R., 1976, The use of clay minerals, inorganic and organic geochemical indicators for evaluating the degree of diagenesis and oil generating potential of the shales: *Geochemica and Cosmochimica Acta*, v. 40, p. 953-960.

Freed, R. L., 1979, Shale mineralogy of the No. 1 Pleasant Bayou geothermal test well: a progress report, in Proceedings, Fourth Conference on Geopressured-Geothermal Energy: The University of Texas at Austin, p. 153-167.

Fritz, P., and Fontes, J. C., 1980, Handbook of environmental isotope geochemistry: Elsevier Scientific Publishing Co., New York, 545 p.

Frost, S. H., and Schafersman, S. D., 1979, Upper Oligocene coral reef on the Anahuac Formation in Damon Mound, Texas: Houston Geological Society Guidebook, p. 26-44.

Galloway, W. E., 1978, Uranium mineralization in a coastal-plain fluvial aquifer system; Catahoula Formation, Texas, in Nash, J. T., ed., Uranium geology in resource evaluation and exploration: Economic Geologist, v. 73, no. 8, p. 1655-1676.

_____ 1982, Epigenetic zonation and fluid flow history of uranium-bearing fluvial aquifer systems, South Texas Uranium Province: The University of Texas at Austin, Bureau of Economic Geology Report of Investigations No. 119, 31 p.

Galloway, W. E., Hobday, D. K., and Magara, K., 1982b, Frio Formation of the Texas Gulf Coast Basin - depositional systems, structural framework, and hydrocarbon origin, migration, distribution, and exploration potential: The University of Texas at Austin, Bureau of Economic Geology Report of Investigations No. 122, 78 p.

Gas Research Institute, undated, Co-production of natural gas and water: program information brochure, 19 p.

Giordano, T. H., 1978, Dissolution and precipitation of lead sulfide in hydrothermal solutions, and the point defect chemistry of galena: Pennsylvania State University, Department of Geological Sciences, Ph.D. dissertation, 167 p.

Goheen, H. C., 1959, Sedimentation and structure of the Planulina-Abbeville trend, South Louisiana: Gulf Coast Association of Geological Societies Transactions, v. 9, p. 91-103.

Goldhaber, M. B., Reynolds, R. L., Rye, R. O., and Grauch, R. I., 1979, Petrology and isotope geochemistry of calcite in a South Texas roll-type uranium deposit: U.S Geological Survey Open-File Report 79-828, 21 p.

Goldman, M. I., 1933, Origin of anhydrite cap rock of American salt domes: U.S. Geological Survey Professional Paper 175-D, p. 83-114.

_____ 1952, Deformation, metamorphism, and mineralization in gypsum-anhydrite cap rock, Sulphur salt dome, Louisiana: Geological Society of America Memoir 50, 169 p.

Gose, W. A., Kyle, J. R., and Ulrich, M. R., 1985, Preliminary paleomagnetic investigation of the Winnfield salt dome cap rock, Louisiana, in Ewing, T. E., ed., Transactions of the 35th Annual Meeting, Gulf Coast Association of Geological Societies, v. 35, p. 97-106.

Gotautas, V. A., Gordon, G. E., Johnson, J., and Lee, C., 1972, Southwest Lake Arthur field, Cameron Parish, Louisiana, in King, R. E., ed., Stratigraphic oil and gas fields: American Association of Petroleum Geologists Memoir 16, p. 389-398.

Graf, J. L., Jr., 1977, Rare earth elements as hydrothermal tracers during the formation of massive sulphide deposits in volcanic rocks: *Economic Geologist*, v. 74, no. 4, p. 527-548.

Gregory, A. R., 1980, Pressure, temperature, and salinity plots: The University of Texas at Austin, Bureau of Economic Geology Open-File Report GRIM FW211-035, unpaginated.

Gregory, A. R., Dodge, M. A., and Posey, J. S., 1979, Progress report on evaluation of entrained methane in deep reservoirs, Texas Gulf Coast, in Dorfman, M. H., and Fisher, W. L., eds., Proceedings, Fourth Congress on Geopressured Geothermal Energy: The University of Texas at Austin, v. 1, p. 414-510.

Gregory, A. R., Lin, Z. S., Reed, R. S., Morton, R. A., and Ewing, T. E., 1983, Exploration and production program for locating and producing prospective aquifers containing solution gas and free gas--Texas Gulf Coast: The University of Texas at Austin, Bureau of Economic Geology, final report prepared for the Gas Research Institute under contract no. 5080-321-0398, 197 p.

_____ 1984, Enhanced gas recovery from watered-out reservoirs--Port Arthur field, Jefferson County, Texas: The University of Texas at Austin, Bureau of Economic Geology Report of Investigations No. 142, 58 p.

Gustavson, T. C., and Kreitler, C. W., 1977, Geothermal resources of the Texas Gulf Coast - environmental concerns arising from the production and disposal of geothermal waters, in Campbell, M. D., ed., Geology of alternate energy resources in the south-central United States: Houston, Texas, Houston Geological Society, p. 297-335.

Halbouty, M. T., 1979, Salt domes, Gulf Region, United States and Mexico (2d ed.), Houston, Gulf Publishing Company, 561 p.

Halbouty, M. T., and Barber, T. D., 1961, Port Acres and Port Arthur fields, Jefferson County, Texas: Gulf Coast Association of Geological Societies Transactions, v. 11, p. 225-234.

_____ 1962, Port Acres and Port Arthur fields, Jefferson County, Texas, in Denham, R. L., ed., Typical oil and gas fields of southeast Texas: Houston Geological Society, p. 169-173.

Hamman, R. J., and Anderson, G. M., 1978, Solubility of galena in sulfur-rich NaCl solutions: Economic Geologist, v. 73, p. 96-100.

Handin, J., Hager, R. V., Friedman, M., Feather, J. N., 1963, Experimental deformation of sedimentary rocks under confining pressure: pore pressure tests: American Association of Petroleum Geologists Bulletin, v. 47, p. 717-755.

- Hanor, J. S., 1979, The sedimentary genesis of hydrothermal fluids, in Barnes, L. H., ed., *Geochemistry of hydrothermal ore deposits*: New York, John Wiley, p. 137-168.
- Harrison, F. W., 1981, Esther field, structure on 13,700' sand: Louisiana Department of Conservation, Docket No. 81-616, Exhibit No. 5.
- Hay, R. L., 1966, *Zeolites and zeolitic reactions in sedimentary rocks*: Geological Society of America Special Paper No. 85, 130 p.
- Hazzard, R. T., Spooner, W. C., and Blanpied, B. W., 1945, Notes on the stratigraphy of the formations which underlie the Smackover Limestone in south Arkansas, northeast Texas and north Louisiana: *Shreveport Geological Society report*, v. 2, p. 483-503.
- Helgeson, H. C., 1969, Thermodynamics of hydrothermal systems at elevated temperatures and pressures: *American Journal of Science*, v. 267, p. 729-804.
- Heyl, A. V., Landis, G. P., and Zartman, R. E., 1974, Isotopic evidence for the origin of Mississippi Valley-type mineral deposits: a review: *Economic Geologist*, v. 69, p. 992-1006.
- Holland, H. D., and Malinin, S. D., 1979, Solubility and occurrence of non-ore deposits, in Barnes, H. L., *Geochemistry of hydrothermal ore deposits*: New York, John Wiley, p. 461-508.

Howell, R. W., Peterson, K. P., Anderson, L. L., and Parisi, W. A., 1985, Co-production of gas and water: The University of Texas at Austin, Bureau of Economic Geology, annual report prepared for Gas Research Institute under contract no. 5084-212-0981, The University of Texas at Austin, Bureau of Economic Geology, 63 p.

Hower, J., Eslinger, E. V., Hower, M. E., and Perry, E. A., 1976, Mechanism of burial metamorphism of argillaceous sediment, 1. Mineralogical and chemical evidence: Geological Society of America Bulletin, v. 87, no. 5, p. 725-737.

Hoy, R. B., Foose, R. M., and O'Neill, B. J., Jr., 1962, Structure of Winnfield salt dome, Winn Parish, Louisiana: American Association of Petroleum Geologists Bulletin, v. 46, no. 8, p. 1444-1459.

Hunt, J. M., 1979, Petroleum geochemistry and geology: San Francisco, W. H. Freeman and Company, 617 p.

International Oil Scouts Association, 1966, International oil and gas development review 1965: v. 36, part 2, p. 428.

Jackson, M. P. A., and Seni, S. J., 1983, Geometry and evolution of salt structures in a marginal rift basin of the Gulf of Mexico, East Texas: Geology, v.11, p. 131-135.

_____ 1984, Atlas of salt domes in the East Texas Basin: The University of Texas at Austin, Bureau of Economic Geology Report of Investigations No. 140, 102 p.

- Jackson, M. P. A., and Talbot, C. J., 1986, External shapes, strain rates, and dynamics of salt structures: Geological Society of America Bulletin, v. 97, p. 305-323.
- Jenkins, J. T., Jr., 1979, Geology and paleontology of the upper clastic interval at Damon Mound, in Damon Mound, Texas: Houston Geological Society Guidebook, p. 45-62.
- Kaiser, W. R., and Richmann, D. L., 1981, Predicting diagenetic history and reservoir quality in the Frio Formation of Brazoria County, Texas, and Pleasant Bayou test wells, in Proceedings, Fifth Conference on Geopressured Geothermal Energy: The University of Texas at Austin, p. 67-74.
- Karstev, A., and others, 1971, The principal state in the formation of petroleum: Eighth World Petroleum Congress, Proceedings: Moscow, v. 2, p. 3-10.
- Kharaka, Y. K., Callender, E., and Carothers, W. W., 1977, Geochemistry of geopressured geothermal waters of the northern Gulf of Mexico basin, 1, Brazoria and Galveston Counties, Texas, in Paquet, H., and Tardy, Y., eds., Proceedings of the Second International Symposium on Water-Rock Interaction. Section II: Strasbourg, France, Université Louis Pasteur, p. 32-41.
- Kharaka, Y. K., Carothers, W. W., and Law, L. M., 1985, Origin of gaseous hydrocarbons in geopressured geothermal waters (abs.): Sixth U.S. Gulf Coast Geopressured Geothermal Energy Conference: The University of Texas at Austin, p. 16.

- Kharaka, Y. K., Lico, M. S., Wright, V. A., and Carothers, W. W., 1980, Geochemistry of formation waters from Pleasant Bayou No. 2 well and adjacent areas in coastal Texas, in Dorfman, M. H., and Fisher, W. L., eds., Proceedings, Fourth U.S. Gulf Coast Geopressured Geothermal Energy Conference, v. 1: The University of Texas at Austin, Center for Energy Studies, p. 168-199.
- Kirkland, D. W., and Gerhard, J. E., 1971, Jurassic salt, central Gulf of Mexico, and its temporal relation to circum-Gulf evaporites: American Association of Petroleum Geologists Bulletin, v. 55, no. 5, p. 680-686.
- Klohn, M. L., and Pickens, W. R., 1970, Geology of the Felder uranium deposit, Live Oak county, Texas: Society of Mining Engineers of the Association of Independent Mining Engineers, reprint 70-I-38, 19 p.
- Knauth, L. P., Kumar, M. B., and Martinez, J. D., 1980, Isotope geochemistry of water in Gulf Coast salt domes: Journal of Geophysical Research, v. 85, no. B9, p. 4863-4871.
- Kreitler, C. W., and Dutton, S. P., 1983, Origin and diagenesis of cap rock, Gyp Hill and Oakwood salt domes, Texas: The University of Texas Bureau of Economic Geology Report of Investigations No. 131, 58 p.
- Kyle, J. R., and Price, P. E., 1985, Mineralogical investigation of sulphide concentrations in the Hockley salt dome cap rock, Texas, in Park, W. C., and others, eds., Applied mineralogy: Metallurgical Society of AIME, p. 1065-1082.

_____ in press, Metallic sulphide deposits in salt dome cap rocks, Gulf Coast, U.S.A.; genetic relationships among ore deposits, metalliferous formation waters, and hydrocarbon reservoirs: Transactions of the Institute of Mining and Metallurgy, Section B. Applied Earth Sciences.

Land, L. S., 1984, Evidence for vertical movement of diagenetic fluids, Texas Gulf Coast (abs.): American Association of Petroleum Geologists Annual Convention, Book of Abstracts, unpaginated.

Le Vie, D. S., Jr., 1985, Interdomal sediment ponding: a new lower Hackberry play?: Gulf Coast Association of Geological Societies Transactions, v. 35, p. 171-178.

_____ in press, Section III. Integrated geologic study of the Hitchcock N.E. field (Galveston County) and the Pleasant Bayou - Chocolate Bayou area, Brazoria County, Texas, in Light, M. P. R., and Ewing, T. E., Consolidation of geologic studies of geopressured geothermal resources in Texas: The University of Texas at Austin, Bureau of Economic Geology, report prepared for the U.S. Department of Energy under contract no. DE-AC08-79ET27111-12.

Light, M. P. R., and D'Attilio, W., 1985, Structure, facies, and internal properties of the Frio "A" reservoir, Hitchcock N. E. field, Galveston County, Texas, in Finley, R. J., and others, Coordination of geological and engineering research in support of Gulf Coast co-production program: The University of Texas at Austin, Bureau of Economic Geology, report prepared for the Gas Research Institute under contract no. 5084-212-0924, p. 1-51.

Light, M. P. R., Ewing, T. E., and Tyler, N., 1984, Section II. Thermal history and hydrocarbon anomalies in the Frio Formation, Brazoria County, Texas--an indicator of fluid flow and geopressure history, in Ewing, T. E., and others, Consolidation of geologic studies of geopressed geothermal resources in Texas: The University of Texas at Austin, Bureau of Economic Geology, report prepared for the U.S. Department of Energy under contract no. DE-AC08-79ET27111.

Limes, L. L., and Stipe, J. C., 1959, Occurrence of Miocene oil in South Louisiana: Gulf Coast Association of Geological Societies Transactions, v. 9, p. 77-90.

Liou, J. G., 1970, Synthesis and stability relation of wairakite $\text{CaAl}_2\text{Si}_4\text{O}_{12}\cdot 2\text{H}_2\text{O}$: Contributions to Mineralogy and Petrology, v. 27, no. 4, p. 259-282.

_____ 1971, P-T stabilities of laumontite, wairakite, lawsonite and related minerals in the system $\text{CaAl}_2\text{Si}_2\text{O}_8\text{-SiO}_2\text{-H}_2\text{O}$: Journal of Petrology, v. 12, p. 379-411.

Lock, B. E., 1982, Towards a better understanding of Gulf Coast Miocene deep water sediments: Gulf Coast Association of Geological Societies Transactions, v. 32, p. 283-288.

Loucks, R. G., Richmann, D. L., and Milliken, K. L., 1981, Factors controlling porosity and permeability in geopressed Frio sandstone reservoirs, General Crude Oil, Department of Energy Pleasant Bayou test wells, Brazoria

County, Texas, in Proceedings, Fourth Congress on Geopressured Geothermal Energy: The University of Texas at Austin, v. 1, p. 46-82.

Ludwig, K. R., Goldhaber, M. B., Reynolds, R. L., Simmons, K. R., 1982, Uranium-lead isochron age and preliminary sulfur isotope systematics of the felder uranium deposit, south Texas: *Economic Geology*, v. 77, p. 557-563.

Lyon, T. L., and Buckman, H. D., 1960, *The nature and properties of soils*: New York, Macmillan, 567 p.

Martin, R. G., 1978, Northern and eastern Gulf of Mexico continental margin: stratigraphic and structural framework: *American Association of Petroleum Geologists Studies in Geology* 7, p. 21-42.

Mason, B., 1966, *Principles of geochemistry*: New York, John Wiley, 329 p.

Milliken, K. L., Land, L. S., and Loucks, R. G., 1981, History of burial diagenesis determined from isotopic geochemistry, Frio Formation, Brazoria County, Texas: *American Association of Petroleum Geologists Bulletin*, v. 65, p. 1397-1413.

Möller, P., 1983, Lanthanoids as a geochemical probe and problems in Lanthanoid geochemistry. Distribution and behavior of Lanthanoids in non-magmatic phases, in Sinha, S. P., ed., *Systematics and the properties of Lanthanides*: Dordrecht, D. Reidel, 648 p.

Mooney, R. W., Keenan, A. G., and Wood, L. A., 1952, Adsorption of water vapor by montmorillonite. 1. Heat of desorption and application of BET theory: *Journal of the American Chemical Society*, v. 74, p. 1367-1371.

Morton, J. P., 1983, Age of clay diagenesis in the Oligocene Frio Formation, Texas Gulf Coast: The University of Texas at Austin, Ph.D. dissertation, 33 p.

Morton, R. A., 1981, Pleasant Bayou No. 2--a review of rationale, ongoing research and preliminary test results: *Proceedings, Fifth Conference on Geopressed Geothermal Energy: The University of Texas at Austin*, p. 55-57.

_____ 1983, Site reviews, in Minutes from DOE/Industry Geopressed Geothermal Resource Development Program Working Group Meeting, Houston, Texas: prepared for the U.S. Department of Energy, p. 71-82.

Morton, R. A., Ewing, T. E., and Tyler, N., 1983a, Continuity and internal properties of Gulf Coast sandstones and their implications for geopressed fluid production: The University of Texas at Austin, Bureau of Economic Geology Report of Investigations No. 132, 70 p.

Morton, R. A., Han, J. H., and Posey, J. S., 1983b, Variations in chemical compositions of Tertiary formation waters, Texas Gulf Coast, in Morton, R. A., Ewing, T. E., Kaiser, W. R., and Finley, R. J., Consolidation of geologic studies of geopressed geothermal resources in Texas: The

University of Texas at Austin, Bureau of Economic Geology, report prepared for the U. S., Department of Energy under contract no. DE-AC08-79ET27111, p. 83-136.

Müller, P., and Siemes, H., 1974, Festigkeit, Verformbarkeit und Gefügeregelung von anhydrit - experimentelle Stauchverformung unter Manteldrücken bis 5 Kbar bei Temperaturen bis 300°C: *Tectonophysics*, v. 23, p. 105-127.

Murray, G. E., 1966, Salt structures of Gulf of Mexico Basin - a review: *American Association of Petroleum Geologists Bulletin*, v. 50, no. 3, p. 439-478.

Nance, D., Rovik, J., and Wilcox, R. E., 1979, Lithology of the Vacherie salt dome core: Louisiana State University, Institute for Environmental Studies, 343 p.

O'Donnell, L., 1935, Jefferson Island salt dome, Iberia Parish, Louisiana: *American Association of Petroleum Geologists Bulletin*, v. 19, no. 11, p. 1602-1644.

Ohle, E. L., 1952, Geology of the Hayden Creek lead mine, southeast Missouri: *Mining Engineering*, p. 477-483.

Overton, H. L., and Lipson, L. B., 1958, Correlation of electrical properties of drilling fluids with solids content: *Petroleum Transactions of the American Institute of Mechanical Engineers*, v. 213, p. 333-336.

Paine, W. R., 1962, Geology of Acadia and Jefferson Davis Parishes: State of Louisiana Department of Conservation, Louisiana Geological Survey Geological Bulletin No. 36, 277 p.

_____ 1968, Stratigraphy and sedimentation of subsurface Hackberry wedge and associated beds of southwestern Louisiana: American Association of Petroleum Geologists Bulletin, v. 52, no. 2, p. 322-342.

Palciauskas, V. V., and Domenico, P. A., 1980, Microfracture development in compacting sediments: relation to hydrocarbon maturation kinetics: American Association of Petroleum Geologists Bulletin, v. 64, no. 6, p. 927-937.

Phillipi, G. T., 1977, On the depth, time, and mechanism of origin of the heavy to medium-gravity naphthenic crude oils: *Geochimica et Cosmochimica Acta*, v. 41, p. 33-52.

Posey, H. H., 1986, Regional characteristics of strontium, carbon and oxygen isotopes in salt dome cap rocks of the western Gulf Coast: The University of North Carolina at Chapel Hill, Ph.D. dissertation, 239 p.

Powell, T. G., Foscolos, A. E., Gunther, P. R., and Snowdon, L. R., 1978, Diagenesis of organic matter and fine clay minerals: a comparative study: *Geochemica et Cosmochimica Acta*, v. 42, p. 1181-1197.

Powers, M. C., 1967, Fluid release mechanisms in compacting marine mudrocks and their importance in oil exploration: American Association of Petroleum Geologists Bulletin, v. 51, p. 1240-1254.

- Prezbindowski, D. R., in preparation, Carbonate rock-water diagenesis, Lower Cretaceous, Stuart City Trend, South Texas: The University of Texas at Austin, Ph.D. dissertation.
- Price, P. E., and Kyle, J. R., in press, Genesis of salt dome hosted metallic sulphide deposits: the role of hydrocarbons and related fluids: Denver Region Exploration Geologists Society.
- Price, P. E., Kyle, J. R., and Wessel, G. R., 1983, Salt dome related lead-zinc deposits, in Kisvarsanyi, G., and others, eds., International Conference on Mississippi Valley Type Lead-Zinc Deposits: Proceedings Volume, p. 558-577.
- Randolph, P. L., 1985, Preliminary N. E. Hitchcock well and reservoir data, April 1, 1985: Unpublished Institute of Gas Technology Report, 158 p.
- Reedy, F., Jr., 1949, Stratigraphy of Frio Formation, Orange and Jefferson Counties, Texas: American Association of Petroleum Geologists Bulletin, v. 33, no. 11, p. 1830-1858.
- Rezak, R., 1985, Local carbonate production on a terrigenous shelf: Gulf Coast Association of Geological Societies Transactions, v. 35, p. 477-484.
- Sangster, D. F., 1983, Mississippi Valley type lead-zinc deposits: a geological melange, in Kisvarsanyi, G., and others, eds., Proceedings of the International Conference on Mississippi Valley type lead-zinc deposits: Rolla, University of Missouri, p. 558-571.

Schoell, M., 1983, Genetic characterization of natural gases: The American Association of Petroleum Geologists Bulletin, v. 67, no. 12, p. 2225-2238.

Scott, K. R., Hayes, W. E., and Fietz, R. P., 1961, Geology of the Eagle Mills Formation: Gulf Coast Association of Geological Society Transactions, v. 11, p. 1-14.

Selley, R. C., 1979, Concepts and methods of subsurface facies analysis, sessions 7, 8, 9, Diagenetic controls of porosity: Short course, Johannesburg, South Africa, 10 p.

Seni, J. J., and Jackson, M. P. A., 1983, Evolution of salt structures, East Texas diapir province, Part 2: pattern and rates of halokinesis: American Association of Petroleum Geologists Bulletin, v. 67, p. 1245-1274.

_____ 1984, Sedimentary record of Cretaceous and Tertiary salt movement, East Texas Basin: times, rates and volumes of salt flow and their implications for nuclear waste isolation and petroleum exploration: The University of Texas at Austin, Bureau of Economic Geology Report of Investigations No. 139, 89 p.

Seward, T. M., 1976, The stability of chloride complexes of silver in hydrothermal solutions up to 350°C: Geochimica et Cosmochimica Acta, v. 40, p. 1329-1341.

- _____ 1977, Solubility of coexisting pyrite and pyrrhotite in the system NaHS-H₂S-NaCl-H₂O at elevated temperature and pressure, in Hodder, A. P. W., ed., Geochemistry 1977: New Zealand Department of Science and Industrial Research Bulletin, 218 p.
- Sillitoe, R. H., 1972, A plate tectonic model for the origin of porphyry copper deposits: Economic Geologist, v. 76, p. 184-197.
- Sloane, B. J., 1971, Recent developments in the Miocene Planulina gas trend of South Louisiana: Gulf Coast Association of Geological Societies Transactions, v. 21, p. 199-210.
- Smith, R. M., and Martell, A. E., 1976, Critical stability constants. Volume 4: Inorganic complexes: New York, Plenum Press, 257 p.
- Snellgrove, R. A., and Barnes, H. L., 1974, Low temperature solid phases and aqueous species in the copper sulfide system (abs.): Transactions of the American Geophysical Union, v. 55, p. 484.
- Sonnier, Marc, 1978, Chalkley field, Cameron Parish: Gulf Coast Association of Geological Societies Transactions, v. 28, p. 581-588.
- Standing, M. B., and Katz, D. L., 1942, Density of natural gases: American Institute of Mining Engineers Transactions, v. 146, p. 140-149.
- Sun Oil Co., 1963, Structural top, Nonion struma A sand: Louisiana Department of Conservation, Docket no. 63-411, Exhibit no. 2.

Teas, L. P., 1931, Hockley salt shaft, Harris County, Texas: American Association of Petroleum Geologists Bulletin, v. 15, no. 4, p. 465-469.

Thornton, E. C., and Seyfried, W. E., Jr., 1985, Sediment-sea-water interaction at 200 and 300°C, 500 bars pressure: the role of sediment composition in diagenesis and low-grade metamorphism of marine clay: Geological Society of America Bulletin, v. 96, p. 1287-1295.

Todd, R. G., and Mitchum, R. M., 1977, Seismic stratigraphy and global changes of sea level, part 8: identification of Upper Triassic, Jurassic, and Lower Cretaceous seismic sequences in Gulf of Mexico and offshore West Africa, in Payton, C. E., ed., Seismic stratigraphy--applications to hydrocarbon exploration: American Association of Petroleum Geologists Memoir 26, p. 145-163.

Ulrich, M. R., Kyle, J. R., and Price, P. E., 1984, Metallic sulfide deposits in the Winnfield salt dome, Louisiana: evidence for episodic introduction of metalliferous brines during cap rock formation, in White, B. R., ed., Gulf Coast Association of Geological Societies Transactions, p. 435-442.

Walker, R. G., 1974, Facies models 8, turbidites and associated coarse clastic deposits, in Walker, R. G., ed., Facies models: Geological Association of Canada, Geoscience Canada Reprint Series 1, p. 91-103.

Watkins, J. S., Worzel, J. L., and Ladd, J. W., 1976, Deep seismic reflection investigation of occurrence of salt in Gulf of Mexico: Texas University Marine Science Institute, Contribution No. 84, 35 p.

- Weaver, C. E., 1980, Graphite in Gulf Coast salt: U.S. Department of Energy, ONWI No. E512-0010, 3 p.
- White, D. E., 1965, Saline waters of sedimentary rocks, in Young, A., and Galley, J. E., eds., Fluids in subsurface environments: American Association of Petroleum Geologists Memoir 4, p. 342-366.
- Winkler, H. G. F., 1976, Petrogenesis of metamorphic rocks (4th ed.): New York, Springer-Verlag, 334 p.
- Woidt, W.-D., 1978, Finite element calculations applied to salt dome analysis: Tectonophysics, v. 50, p. 369-386.
- Workman, A. L., and Hanor, J. S., 1985, Evidence for large-scale vertical migration of dissolved fatty acids in Louisiana oil field brines: Iberia field, south-central Louisiana: Gulf Coast Association of Geological Societies Transactions, v. 35, p. 293-300.
- Yeh, H. W., and Savin, S. M., 1977, The mechanism of burial metamorphism of argillaceous sediments: 3. Oxygen isotopic evidence: Geological Society of America Bulletin, v. 88, p. 1321-1330.



Appendix 1

Appendix A. (cont.)

Well no.	Original operator and well name	Well status	Total depth	Perforated interval(s) [§]	Production period (1st production to date plugged) [§]	Gas production (Mcf) [§]	Condensate produced after 1/1/66 (bbls)* [§]	Structure top lower Hackberry interval	Structure top Hackberry Main sand	Net sand lower Hackberry interval	Net gas sand
48-6-53	Henderson #1 Sassine	P and A	10,690	10,545-10,568	3/59-5/77	14,954,377	65,516	10,180	10,500	--	110
48-6-71	Pace and Allen #1 Sassine	P and A	10,642	10,585-10,595	2/60-4/67	936,734	623	--	10,523	--	80+
48-6-73	Pinnacle #2-A Doornbos	P and A	10,548	10,403-10,535	--	--	--	10,160	10,520	--	--
48-7-01	Barnes #1 Burks	P and A	10,750	10,551-10,594	2/60-3/74	2,101,921	34,542	10,200	10,485	--	126
48-7-02	Owen #2 Norris-Sassine	Dry hole	10,950	--	--	--	--	9,960	--	0	0
48-7-03	Hill #1 Courts-Simoneaux-Nations	P and A	10,800	10,406-10,464	2/60-7/77	4,139,846	42,891	10,120	10,400	104+	84
48-7-04	Gray #1 Arceneaux	P and A	10,535	10,409-10,447	2/60-9/80	4,135,210	58,340	--	10,380	81	78
48-7-05	Martin #1 Delcambre	P and A	10,800	10,542-10,562	3/60-6/76	1,165,725	4,108	10,180	10,486	--	113
48-7-07	Dillon #1 Romero	P and A	10,758	10,545-10,580	1/60-2/72	2,422,955	40,732	10,180	10,485	--	128
48-7-08	Draper Goodale #1 Giesen	P and A	10,665	10,496-10,512	10/61-6/72	1,041,570	15,521	--	10,492	135+	125
48-7-11	Gray #1 Hunter & Purgan	P and A	10,700	10,531-10,536	3/60-2/75	10,349,766	21,391	--	10,434	--	85
48-7-13	Martin #1 Snell	P and A	10,890	10,440-10,458	1/60-6/78	12,992,389	176,353	10,112	10,387	--	81
48-7-14	Martin #1 Griffin	P and A	10,881	10,380-10,413	2/60-5/72	4,120,278	--	10,110	10,380	35	37
48-7-15	Halbouty and Pan Am #7 Rosen	P and A	10,700	10,570-10,578	7/65-1/68	1,163,442	3,282	10,250	10,540	--	43
48-7-16	Henderson #1 Montrose	P and A	10,949	10,548-10,575	4/59-9/77	15,591,647	198,822	10,180	10,480	153	140
48-7-28	Henderson #1-A Piniec	P and A	10,700	10,460-10,545	12/59-5/72	10,627,258	139,162	10,160	10,445	115	118
48-7-37	Halbouty and Pan Am #3 Rosen	P and A	11,403	10,662-10,685	9/58-8/60	643,035	--				
48-7-41	Barnes #1 Wynn	P and A	10,750	10,349-10,359	2/60-2/73	727,386	--	10,070	10,352	9	9
48-7-69	Owens #1 Sassine	P and A	10,940	10,589-10,591	4/62-10/62	6,267	--				
49-4-03	Halbouty and Pan Am #1 Rosen	P and A	11,461	10,696-10,704	12/57-2/69	11,663,049	17,958	10,285	10,604	520	44
49-4-08	Meredith #1 Edwards-Shelby Unit	P and A	11,494	10,665-10,671, 10,674-10,678	4/58-6/72	3,076,933	--	10,340	10,673	335	3
49-4-12	Halbouty #1 Am. Natl. Insurance	P and A	11,002	10,630-10,635, 10,694-10,704	1/58-5/64	3,980,663	--	10,370	10,640	--	4
49-4-13	Pan Am. #1 Gilbert Fee	P and A	10,800	10,671-10,682	12/58-6/67	6,332,413	--	10,360	--	--	24
49-4-16	Halbouty #2 Am. Natl. Insurance	Dry hole	11,400	--	--	--	--	--	--	--	--
49-4-16d	Meredith et al. #1 Am. Natl. Ins.	Dry hole	13,888	--	--	--	--	10,350	--	440	0
49-4-21	Halbouty #1-A Rosen	P and A	11,400	10,454-10,458	6/58-2/61	75,140	--	10,210	10,540	317	12
49-4-27	McCarthy #1 Shelby	Dry hole	10,489	--	--	--	--	10,320	--	--	--
49-4-33	Pan Am. #4 Gilbert	P and A	12,997	10,607-10,613	5/60-3/61	47,679	--	10,370	--	258	8

Appendix A. (cont.)

Well no.	Original operator and well name	Well status	Total depth	Perforated interval(s) [§]	Production period (1st production to date plugged) [§]	Gas production (Mcf) [§]	Condensate produced after 1/1/66 (bbls)* [§]	Structure top lower Hackberry interval	Structure top Hackberry Main sand	Net sand lower Hackberry interval	Net gas sand
49-4-36	Halbouty #2 Rosen	P and A	11,448	10,584-10,606	3/58-2/71	12,931,470	17,226	10,260	10,585	470	35
49-4-37	Halbouty #5 Rosen	P and A	10,805	10,614-10,624	1/59-11/60	--	--	--	10,615	--	--
49-4-37s	Halbouty and Pan Am #5 Rosen	Shut in	10,725	10,680-10,685	11/60-	2,999,901	--	10,290	--	--	6
49-4-38	Halbouty and Pan Am #1 Shelby	P and A	11,470	10,532-10,538, 10,630-10,644	5/58-6/70	9,469,098	5,297	10,320	10,630	415	41
49-4-39	Meredith #1 Shelby	P and A	10,750	10,637-10,656	1/58-6/72	8,438,626	1,177	10,280	10,623	--	30
49-4-40	Pan Am. #2 Gilbert Fee	P and A	10,800	10,650-10,654, 10,670-10,683	2/59-3/61	44,805	--	10,360	10,674	--	3
49-4-41	Meredith #1 Edwards	P and A	11,801	10,625-10,635	8/57-6/72	8,467,217	--	10,280	10,573	--	65

* Plugged and abandoned

** Condensate for the entire field cumulative to 1/1/66 is 8,558,247 bbls (International Oil Scouts, 1966).

‡ This well produced from the Hackberry 10,450 reservoir only. All other producing wells in this table produced from the Hackberry Lower (10,600) reservoir.

§ Data from Dwight's Energydata Co. (1985b,e).

Appendix B. Ellis field well statistics and geological data.

Well no.	Original operator and well name	Well status	Total depth	Reservoir	Perforated interval(s) [‡]	Production period [‡]	Gas production (Mcf) [‡]	Structure top Nod. 3	Net gas sand Nod. 3
1	Sun Oil Co. #A-2 Leonards	P and A*	11,748	Nod. 3 [§]	11,664-11,680	11/61-4/72	5,133,176	11,640	23
2	Pel-Tex Oil Co. #2 M. M. Kerr	Dry	12,670	Other	--	--	--	11,670	19
3	Peltex Oil #1 M. M. Kerr	--	12,560	Other	--	--	--	11,726	--
4	Sun Oil Co. #B-2 Leonard	--	13,400	Nod. 3 oil	11,582-11,603	7/64-	--	11,855	--
5	Sun Oil Co. #1A Leonards redrill	Inactive	12,502	Nod. 3	11,698-11,706	9/70-	264,394	--	4
6	Petro-Lewis Corp. #6 Kerr	Inactive	12,650	Nod. 3	11,590-11,606	2/79-	227,600	11,590	92
7	Forest Oil Corp. et al. #4 A. C. Kerr	--	13,261	Other	--	--	--	11,667	58
8	J. P. Owen et al. #1-A Colan Daigle	--	12,643	Other	--	--	--	--	--
9	Sun Oil Co. #A-3 Leonards	--	12,887	Other	--	--	--	11,902	--
10	Forest Oil Corp. #5 A. C. Kerr	Inactive	11,795	Nod. 3	11,682-11,702	10/64-	1,659,710	11,682	35
11	J. P. Owen #B-1 E. J. Kerr	Inactive	11,758	Nod. 3	11,615-11,620	5/55-	15,409,805	11,590	42
13	Forest Oil Corp. #3-D A. C. Kerr	Active	11,813	Nod. 3	11,574-11,584	11/70-	2,362,404**	11,563	87
14	Jefferson Lake Sul. Co. #1 B. M. Van Meter	P and A	11,847	Nod. 3	11,706-11,712 11,718-11,722	9/60-12/64	27,084	11,708	8
15	Forest Oil & Midstates #1 B. M. Van Meter	--	12,032	Other	--	--	--	11,720	5
17	Forest Oil & Midstates #1 Almina C. Kerr	Inactive	11,783	Nod. 3	11,683-11,691	9/53-	15,248,657	11,615	58
18	The Preston Oil Co. #2 C. Daigle	--	11,027	Other	--	--	--	--	--
19	Midwest Oil Corp. #1-A Stakes Estate	--	12,174	Other	--	--	--	--	--
20	Midwest Oil Corp. #1 J. W. Lawson	--	12,792	Other	--	--	--	--	--
22	Midwest-Owen and Petrol. #1 Zaunbrecher	--	13,700	Other	--	--	--	--	--
28	Forest Oil & Midstates #1 B. M. Stewart	--	12,025	Other	--	--	--	11,880	0
29	American Republics Corp. #1 Almina Kerr	--	12,129	Other	--	--	--	11,700	18

§ Nodosaria 3

* Plugged and abandoned

** 1,204 bbls condensate produced since 1-1-73; no other Nodosaria 3 gas wells have produced condensate since 1-1-73.

‡ Data from Dwight's Energydata Co. (1985g).

Appendix C. Esther field well statistics and geological data.

Well no.	Original operator and well name	Well status	Total depth	Perforated interval(s) [‡]	Producing horizon	Production period (1st production to date plugged) [‡]	Gas production (Mcf) [‡]	Condensate produced after 1/1/66 (bbls) [‡]	13,700 sand			14,060 sand
									Structure on top	Net sand	Net gas sand	Net gas sand
6	Texas Crude, Inc. #1 Sagrera Heirs	Active	14,267	13,799-13,820	14,060 sand	6/79-	7,510,200	71,417	13,588	33	17	7
7	Texas Crude, Inc. #1 Paul Mayard	Active	13,682	13,570-13,582	13,700 sand	9/79-	7,503,800	93,996	13,563	33	18	--
11	Amerada Hess - Ethyl Corp. #1 Caroline Lee	Active	14,205	13,728-13,753	13,700	10/77-	2,281,300	30,510	13,709	57	13	6
12	Amerada Hess - Ethyl Corp. #1 Sagrera Heirs	Active	14,602	14,065-14,093	14,060	3/79-	5,528,200	57,746	13,797	44	0	14
13	Amerada Hess - Ethyl Corp. #2 Sagrera Heirs	Active	14,819	13,914-13,940	14,060	7/79-	8,078,500	79,018	13,760	52	12	19
14	Amerada Hess - Ethyl Corp. #3 Sagrera Heirs	Dry hole	14,180	--	P and A*	--	--	--	13,744	25	6	--
15	Amerada Hess - Ethyl Corp. #4 Sagrera Heirs	Active	14,525	14,092-14,112	14,060	6/81-	3,420,800	32,358	13,820	36	0	30
18	Amerada Hess - Ethyl Corp. #1 Louis Mayard	Active	14,069	13,678-13,713	13,700	6/80-	6,563,700	87,918	13,670	43	23	21
36	Buchanan - Ethyl Corp. #1 Kuehling	Active	14,610	13,956-13,962	14,060	11/84-	550,500	6,937	13,630	77	24	17

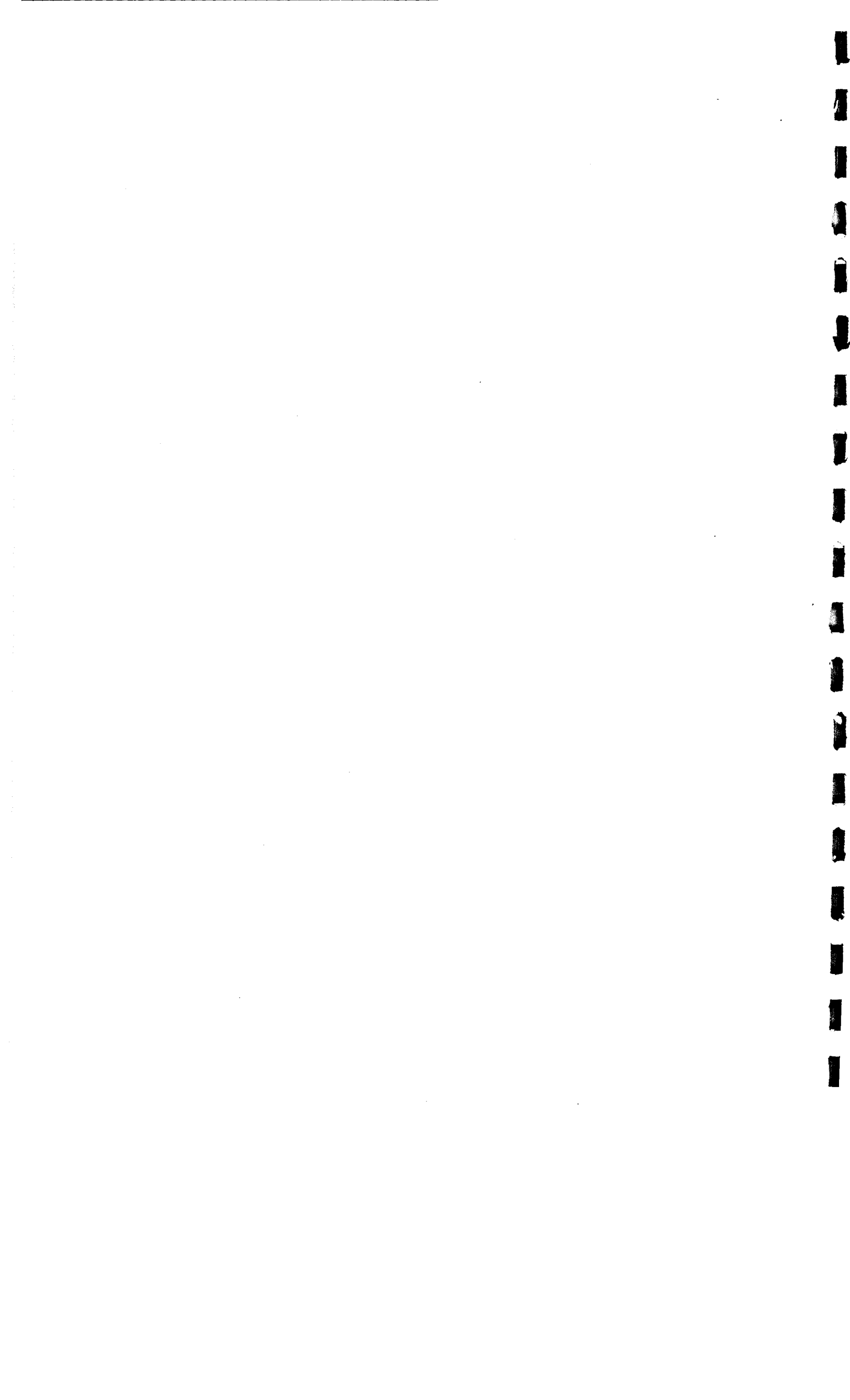
[‡] Data from Dwight's Energydata Co. (1985g).

* Plugged and abandoned.

181



Appendix 2



LOGGING RESEARCH

by Henry F. Dunlap

Introduction

Our logging research effort has been directed toward the following problems: (1) estimation of effect of several high neutron-capture cross-section trace elements on the neutron log, particularly on the pulsed neutron log; (2) resistivity measurements at elevated pressures and temperatures and at intermediate rock wettabilities; (3) continued study of short-term variation in mud-filtrate resistivity and the causes thereof; and (4) consultation on logging programs for the Gas Research Institute co-production project. The status of each of these is discussed briefly below. Logging progress reports to GRI may be referred to for more detailed information.

(1) Estimation of effect of several high neutron-capture cross-section elements on the neutron log. This project is important since estimation of water saturation in cased wells using the pulsed neutron log can be badly in error if certain trace elements such as boron, cadmium, gadolinium, or a few others are present in the reservoir rock in substantial amounts. For example, if more than 25 ppm of gadolinium, 100 ppm of boron, or 300 ppm of cadmium are present, the neutron log porosity will be wrong by a factor of 2 in a 30 percent porosity sandstone. For lower porosities, even smaller trace-element concentrations give 100 percent errors in porosity. Thus far, data on about a dozen Gulf Coast samples have been obtained for cadmium, and in every case the concentration was less than 2 ppm, which is small enough to neglect. Instrumental difficulties with the Bureau of Economic Geology I.C.P. mass spectrometer have prevented

further trace-element analysis. This problem is being worked on and we hope to have results for other trace elements soon.

(2) Variation of saturation exponent, n , and cementation exponent, m , in the Archie equation relating rock resistivity to water saturation is poorly understood. We are interested in the effects of high pressure, high temperature, and varying rock wettability on m and n . We have reviewed the literature and find that wettability changes are reported to change n very drastically, from the commonly used value of $n = 2$ for a water-wet system to as high as $n = 20$ to 25 for a completely oil-wet system. Most natural reservoir rocks are of intermediate wettability (only partially water wet). Changes of n by even a fraction of 2 (from $n = 2$ to $n = 4$, say) would lead to very different estimates of rock-water saturation for a given rock resistivity, so it is important to understand what can be expected here.

We have obtained equipment to measure m and n at high pressure and temperature and for varying wettability. We are beginning experimental work with glass beads of known intermediate wettability but have no results to report as yet.

(3) We have published a paper in the most recent issue of Log Analyst, the journal of the Society of Professional Well Log Analysts, describing an improved method of estimating mud-filtrate resistivity from known values of mud resistivity and mud density. This paper resulted from work carried out with GRI support.

We are continuing our studies in this area, attempting to quantify the effect of variations in mud makeup water resistivity on mud-filtrate resistivity. We have data on three wells where daily values of makeup water resistivity were obtained along with mud data. It appears that a significant part of the mud-filtrate resistivity variation (20 percent or more) can be attributed to variation in the mud makeup water. If this tentative conclusion holds up it will be an

important result, since it means that some reduction in mud-filtrate variation can be achieved by better control of mud makeup water resistivity.

(4) Consultation on co-production logging programs. We participated in planning the logging package run in the Port Arthur Unit 1-6, Port Arthur field, Texas (along with Ercill Hunt and his associates at Res. Tech.). Dr. Myron Dorfman participated in log analysis of the pulsed neutron log run in this well and recommended completion in the lower C zone, which came in flowing 5 MMcf/d plus 350 bbl/d water and 250 bbl/d condensate.



ESTIMATION OF MUD FILTRATE RESISTIVITY
IN FRESH WATER DRILLING MUDS

Tom A. Lowe and H. F. Dunlap

Center for Energy Studies
The University of Texas at Austin
10100 Burnet Road
Austin, Texas 78758

(This paper has been submitted to Log Analyst,
a publication of the Society of Professional Well Log Analysts)



Estimation of Mud Filtrate Resistivity

in Fresh Water Drilling Muds

Tom A. Lowe and H. F. Dunlap
University of Texas, Austin, Texas

ABSTRACT

Accurate values of R_{mf} as a function of depth are needed when calculating formation water resistivity from the S.P., when calculating formation factor and porosity from short investigation resistivity logs, and when interpreting the results of the repeat formation tester. Recent work has shown that the commonly used values for R_{mf} obtained from log header data are unreliable, due to large short term variations in R_m and R_{mf} . The best way to obtain R_{mf} is to measure it daily, but this is almost never done, and cannot be done on wells which have already been drilled. In some wells, however, daily measured values of R_m and mud density, but not R_{mf} , are available from mud logging units. Such data is also available from an increasing number of wells using "measurement while drilling" (MWD) systems. For these wells, we have found that accurate values of R_{mf} can be obtained using a modified form of Overton & Lipson's correlation, $R_{mf} = C(R_m)^{1.07}$, where C is an empirical function of mud density, provided that measured values of R_m and mud density are used rather than log header derived values. Overton's original correlation was for non-lignosulfonate muds, but we find that it works about as well for today's widely used ligno-sulfonate muds. The correlation which we recommend, based on Overton's original, non-lignosulfonate data plus considerable new data we have obtained for lignosulfonate muds, is

$$\log_{10} \left(\frac{R_{mf}}{R_m} \right) = .396 - .0475 \rho_m \dots\dots\dots(1)$$

where ρ_m is mud density in pounds per gallon. For $.1 < R_m @ 75^\circ F < 2.0 \Omega M$, this correlation gives a lower % std deviation relative to measured values of R_{mf} (26%) than other commonly used methods of estimating R_{mf} such as estimating it from log header R_{mf} data, (34%); using $R_{mf} = .75 R_m$, (69%); and using the Overton correlation with log header R_m and ρ_m data, (67%). In the two wells where we believe we have the best data, our correlation gives a standard deviation of only 13% relative to measured values of R_{mf} . This approaches the accuracy of the basic R_m and R_{mf} measurements.

INTRODUCTION

It is necessary to know the value of the mud filtrate resistivity, R_{mf} , to be able to calculate the formation water resistivity from the S.P. log; or to calculate formation factor and/or porosity from short investigation resistivity logs; or to interpret the fluid recovery from the repeat formation tester. Due to the large effect of spurt loss, which occurs while the formation is being drilled, as compared to filtrate loss, occurring days and weeks later, as the hole is deepened, it is important to know R_{mf} as a function of time (depth). This will allow the best estimate of R_{mf} for a given formation of interest.

In the past the variation of R_{mf} with time (depth) has been inferred from log header values of R_{mf} for the several logging depths in a well. The assumption is that R_{mf} varies smoothly between logging

depths. Recent work has shown the assumption above is not valid; R_{mf} and R_m vary considerably from day to day. In several wells where R_{mf} and R_m were measured daily, the standard deviation of the values estimated from the log header values relative to the daily measured values was 30% to 40%.^{1,2,3}

Cause of this variation is complex, but certainly includes such factors as variation in amount and salinity of make up water additions to the mud; variations in amount of mud additives used such as bentonite, lignosulfonate, caustic soda, etc.; and contributions of dissolved salts and drilled up solids from new hole being made. Regardless of the causes, R_{mf} does vary considerably from day to day, and the log analyst must recognize this, and take it into account when interpreting the logs.

The ideal solution would be to measure R_m and R_{mf} daily, and to try to control some of the variables affecting R_{mf} , such as resistivity of the makeup water, in order to reduce the variation in R_{mf} . In practice, R_{mf} is not measured except when making a logging run; sometimes only once, or at most, a few times during the drilling of a well. Some mud logging units measure R_m (but not R_{mf}) daily. Also, the technique of "measurement while drilling" (MWD) is gaining wider use, and some of these systems measure R_m (but not R_{mf}) continuously. Mud engineers usually measure many properties of the mud daily, such as mud density, viscosity, pH, and filtrate loss, but not R_m or R_{mf} . A reliable method of estimating R_{mf} from R_m and mud density would be of considerable value to companies offering MWD and/or mud logging services.

Two methods have been proposed for estimating R_{mf} , given R_m . These are: Overton & Lipson's empirical correlation for non-lignosulfonate muds, $R_{mf} = C(R_m)^{1.07}$, where C is an empirical function of mud density^{4,5}; and an empirical correlation given in the Schlumberger chart book, $R_{mf} = .75 R_m$, mud type not specified.⁵ Overton & Lipson's work was done in 1958, before lignosulfonate muds came into the wide use they enjoy today and no lignosulfonate muds are included in their data set.

This paper will evaluate the accuracy of R_{mf} estimates relative to measured R_{mf} values for Overton and Lipson's correlation; the $R_{mf} = .75 R_m$ correlation; values of R_{mf} inferred from log header R_{mf} data; and a new correlation we have developed based on data given in Overton & Lipson's original paper, plus a large amount of new data we have gathered for lignosulfonate muds.

DATA AND ANALYSIS

We started our work with study of Overton & Lipson's paper.⁴ It quickly became apparent that Table 1 of this paper, supposedly consisting of R_m , R_{mf} and mud density data for 94 field muds, actually contains considerable duplicated data. With a few exceptions (entries 54, 67, and 71, for example), all the data for R_m , R_{mf} and mud density for entries 1 through 45 are repeated line for line for entries 46 through 94! No such duplication was noted for the data on 47 laboratory muds, given in Table 2. Five of the entries in Table 2 were incomplete, however, lacking data for R_m , mud density, or both.

We also did not understand the need for the exponent 1.07, rather than 1.0, in Overton & Lipson's correlation, $R_{mf} = C(R_m)^{1.07}$. In an

empirical relation such as this it should be possible to choose slightly different values of C as a function of mud density, and use the simpler relation $R_{mf} = K_m R_m$, without significant loss of accuracy.

We began by choosing sets of Overton's data with constant mud density (mainly from their Table 2, supplemented where possible with a few points from their Table 1), and then calculated C and the R_m exponent, m' , for a given constant mud density using a linear regression to fit the logarithmic form of their relation,

$\log c = \log R_{mf} - m' \log R_m$. The results are shown in Table 1. We see that both C and m' vary erratically. In fact, the weighted mean of m' for these 48 sets of (mostly) lab' data is not 1.07 but 1.01. This encouraged us to search for a correlation including lignosulfonate muds similar to Overton's, but using an exponent of 1.0 instead of 1.07 for R_m .

Our experimental work was done both in the field and the laboratory. Mud densities were measured with a conventional Baroid mud balance; filtrate was obtained using a conventional 100 psig, lab temperature Baroid filter press; and R_m and R_{mf} measured with a Baroid Resistivity Meter (2 electrode) or a Schlumberger EMT-D meter (4 electrode). Both of the resistivity meters were calibrated using a series of NaCl solutions of varying salinity. We estimate the standard error of our resistivity measurements at 11%.

Figure 1 shows a plot of $K_m = R_{mf}/R_m$ versus mud density for Overton's non-lignosulfonate mud data. Figure 2 shows a similar plot for lignosulfonate muds used in six wells recently drilled in the Texas-Louisiana Gulf Coast area. The solid curves are "eyeball" fits to the data. Although the fitted curves are different in detail, Fig.

3, showing only the two curves superimposed, demonstrates that they actually track rather well.

Figure 4 shows the lignosulfonate data using a semilog plot of K_m versus mud density, and Fig. 5 is a similar plot which includes both the lignosulfonate and non-lignosulfonate data. A fit to the data of Fig. 5 resulted in the equation

$$\log_{10} K_m = \log_{10} \left(\frac{R_{mf}}{R_m} \right) = .396 - .0475 \rho_m \dots\dots(1)$$

where ρ_m is mud density in pounds per gallon. This equation is plotted on both figures 4 and 5 as a solid curve, and seems a reasonable fit to both sets of data.

Table 2 gives the results of our comparison of the different commonly used methods of estimating R_{mf} from R_m . For each method, we show the % standard deviation of estimated R_{mf} , as compared to the known (measured) value of R_{mf} . We see that the results fall into three classes, regardless of mud type. The two worst methods for estimating R_{mf} are: Overton & Lipson's correlation using log header R_m data; and $R_{mf} = .75 R_m$. These show standard deviations of about 68%. A better method is to estimate R_{mf} from log header R_{mf} values. This shows a standard deviation of 34%. The last two methods are best, namely: Overton & Lipson's original correlation using measured values of R_{mf} and mud density instead of log header data; and the new correlation given by equation (1) above, also using measured R_{mf} and mud density values. Use of equation (1) also avoids interpolation from a table. These correlations both show a standard deviation of 26%.

In only two wells were the authors directly involved in gathering the mud samples and making the measurements of R_m , R_{mf} and mud density. These were the TXO Bruce #1 well, and the Secondary Oil & Gas De Lee #1 well, both in Galveston County, Texas. For these two wells, where we are most confident of the data, the results when using our new correlation are excellent - a standard deviation of only 13% between estimated and known (measured) R_{mf} values. This approaches the accuracy of the measured R_m and R_{mf} values themselves.⁶ Figures 6 & 7 show just how well the estimated and measured R_{mf} values agree for these two wells.

DISCUSSION OF RESULTS

Most of the lignosulfonate mud data we have discussed have measured R_m values between .1 and 2.0 ohm meters at 75°F. In one well however, the Republic Energy D & M Cattle Co. #1, Grimes County, Texas, nearly all the measured R_m values were greater than 2.0 ohm meters at 75°F. For this well, the correlation we have developed does not predict the measured R_{mf} values well. (See Fig. 8.) The estimated R_{mf} values track the relative changes of measured R_{mf} modestly well, but the quantitative match of estimated and measured R_{mf} is very poor, with errors approaching 100%. We don't know whether this poor result is due to bad data, or a failure of our correlation for these high R_m values. For now, we must assume the latter. Similarly, we have very little data on very saline muds. At present, we recommend use of the correlation given by equation (1) only for $.1 < R_m < 2.0$ ohm meters at 75°F. Fortunately, this includes most "fresh water" mud systems.

CONCLUSIONS

1. The exponent 1.07 is not justified in Overton and Lipson's correlation, $R_{mf} = C(R_m)^{1.07}$. Using an exponent of 1.0 with slightly different values for C works just as well and is easier to apply.
2. Both Overton & Lipson's correlation, and a new one we have developed,

$$\log_{10} \left(\frac{R_{mf}}{R_m} \right) = .396 - .0475 \rho_m \dots\dots\dots(1)$$

work well in all types of fresh water muds, provided that:

- a) $.1 < R_m < 2.0$ ohm meters' at 75°F, and
 - b) measured values of R_m and ρ_m are used rather than values inferred from log header data.
3. Use of the correlation $R_{mf} = .75 R_m$ is not advisable.
 4. Use of R_{mf} values estimated from log header R_{mf} data is not advisable.
 5. If possible, R_m , R_{mf} , and ρ_m should be measured daily, since they vary rapidly.
 6. If measurement of R_{mf} daily is not practical, R_m & ρ_m should be measured daily, and R_{mf} estimated using equation (1).

SYMBOLS

R_m = mud resistivity; ohm meters

R_{mf} = mud filtrate resistivity; ohm meters

ρ_m = mud density; pounds per gallon

K_m = R_{mf}/R_m ; dimensionless

C = $R_{mf}/(R_m)^{1.07}$; (ohm meters)^{-0.07}

ACKNOWLEDGEMENTS

Financial support from Dept. of Energy, Div. of Geothermal Energy; Gas Research Institute; and Chevron Oil Co. is gratefully acknowledged. We also thank Texas Oil & Gas Co., Chevron Oil Co., Secondary Oil & Gas Recovery, Inc., and Republic Energy Co. for supplying data used in this research.

REFERENCES

1. Williams, H. and Dunlap, H.F., 1984. "Short Term Variations in Drilling Fluid Parameters; Their Measurement and Implications". Log Analyst, Sept.-Oct., 1984; 3-9.
2. Dunlap, H.F., Dupree, Jr., J.H., and Lowe, T.A., 1985. "Effect of Makeup Water and Mud Additives on Drilling Fluid Resistivity". Proc. 6th U.S. Gulf Coast Geopressured Energy Conf., Feb., 1985 (In Press).
3. Dunlap, H.F. and Dorfman, M.H., 1981. "Problems & Partial Solutions in Using the S.P. Log to Predict Water Salinity in Deep, Hot Wells". Trans. Geo. Res. Council, Vol. 5, Oct., 1981 283-286.
4. Overton, H.L. and Lipson, L.B., 1958. "Correlation of Electrical Properties of Drilling Fluids with Solids Content". Pet. Trans. AIME, Vol. 213, 1958; 333-336.
5. Schlumberger Chart Book, Gen. 7, 1985.
6. Moore, C.V. and Kaufman, R.L., 1981. "Your Unsuspected Problems: Fluid Resistivity and Water Analysis". SPWLA Proceedings, 1981.

Mud Density (ppg)	Number of Samples (n)	C	m'
8.9	13	0.763	0.89
9.0	10	0.878	1.04
9.5	13	0.855	1.07
9.7	4	0.796	1.00
10.0	8	0.814	1.10
Weighted average of m' for all samples =			1.01

Table 1.

C and m' for several constant mud density values, Overton & Lipson (non-lignosulfonate) data.

Well Name, Number, and Location or Other Source of Data	Number of Samples (n)	Log Header R_{mf}	$R_{mf} = .75R_m$	Overton and Lipson's Correlation Using Log Header R_m	Overton and Lipson's Correlation Using Mea- sured R_m	R_{mf} Calculated by equ. (1)
Chevron Jose Rodriguez #1 Cameron County, Texas	98	33%	61%	106%	23%	23%
Chevron W.S. Moothart #1 Cameron County, Texas	71	35%	113%	36%	22%	25%
Chevron Cameron Park #1 Cameron County, Texas	63	31%	51%	33%	24%	18%
TXO Production Bruce #1 Galveston County, Texas	40	34%	31%	40%	21%	13%
Chevron State Lease 932 #32 Grand Isle Block 26, Louisiana	24	40%	40%	21%	24%	31%
Secondary Oil & Gas Inc DeLee #1	15	no openhole well logs	20%	no openhole well logs	16%	13%
Laboratory Muds Studied by Overton and Lipson (1958)	42	---	31%	---	40%	39%
Field Muds Studied by Overton and Lipson (1958)	46	---	91%	---	34%	36%
All Muds studied by Overton and Lipson (Non-Lignosulfonate)	88	---	68%	---	37%	38%
All Lignosulfonate Muds (from the six wells listed)	311	34% (n=296)	69%	67% (n=296)	23%	22%
All Muds (includes the six wells plus Overton and Lipson's data)	399	34% (n=296)	69%	67% (n=296)	26%	26%

Table II. Percent Standard Deviations for Various Methods of Estimating R_{mf}

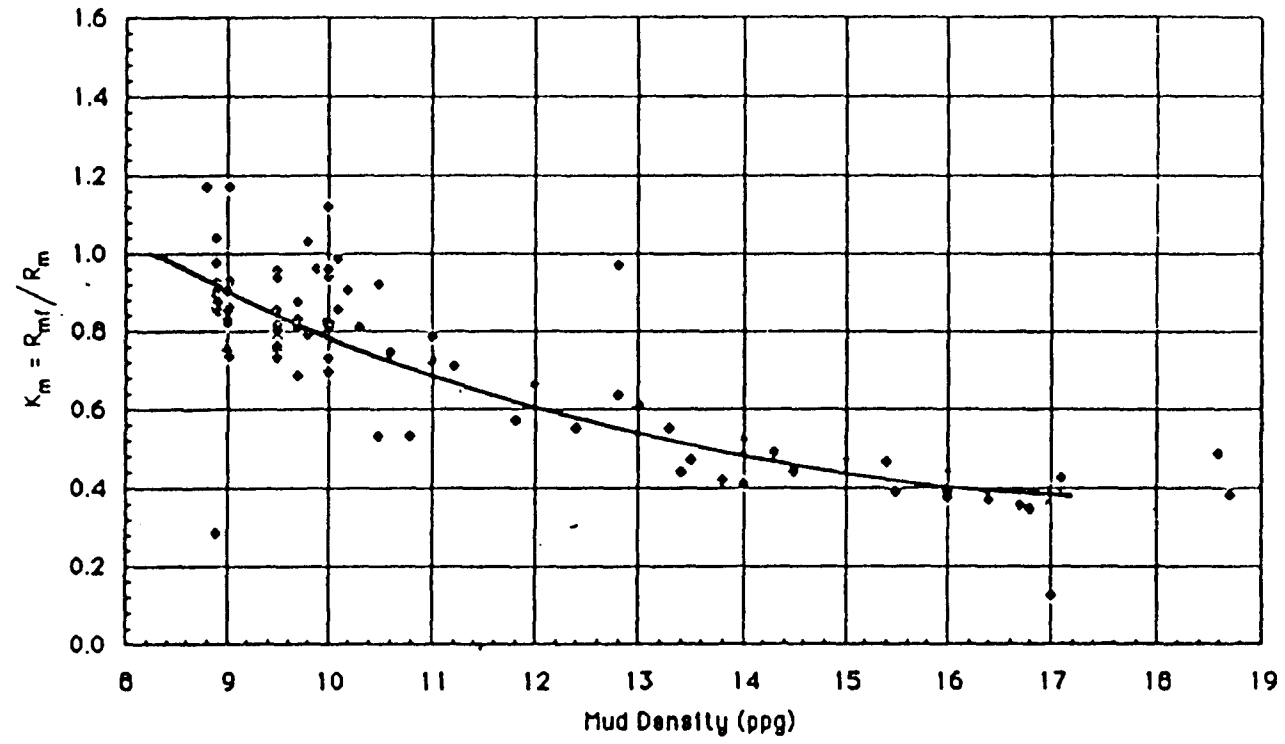


Figure 1

Km Vs Mud Density
Non Lignosulfonate Data (Overton)

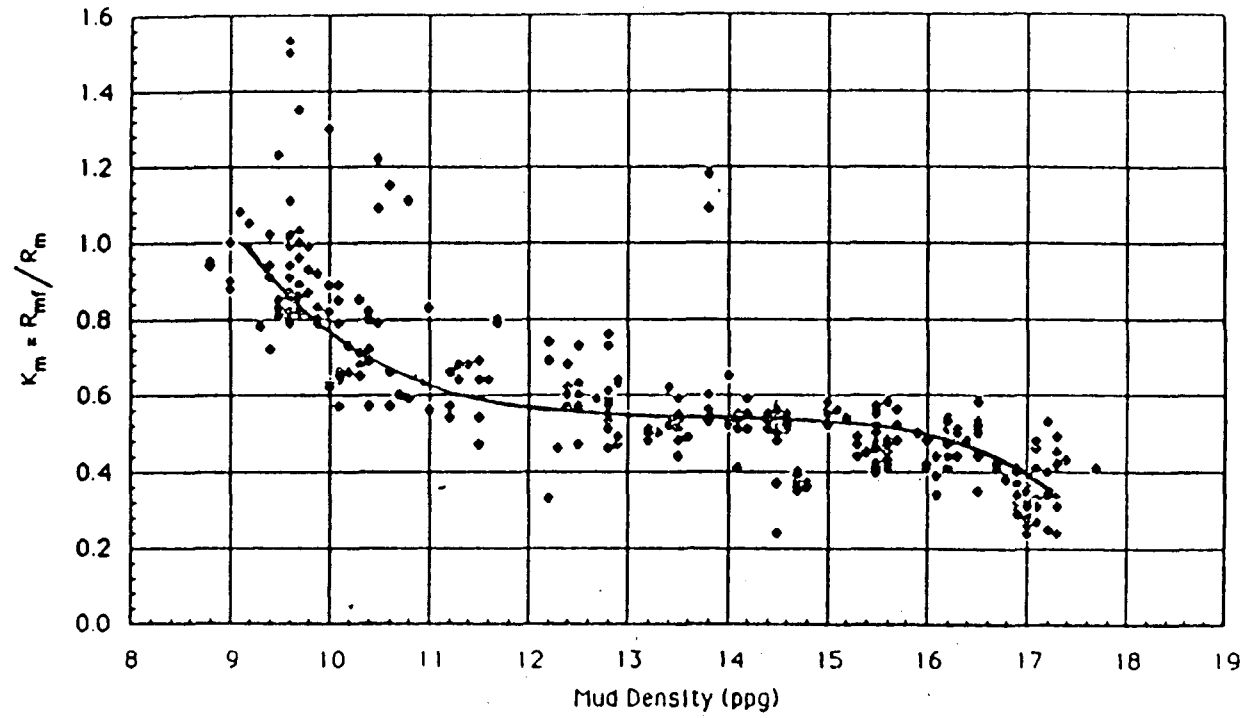


Figure 2
Km Vs Mud Density
Lignosulfonate Data (Lowe)

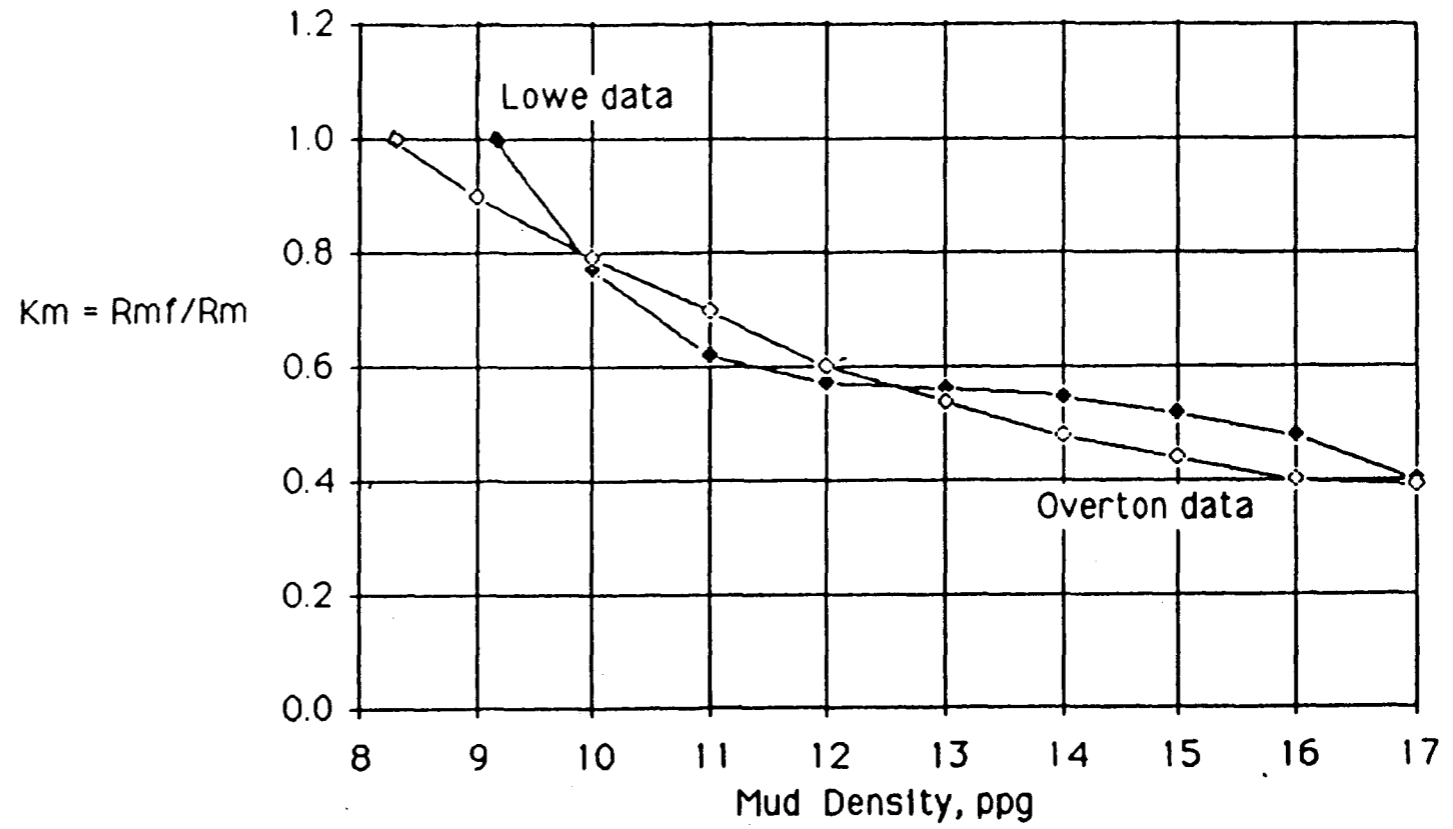


Figure 3. K_m Vs Mud Density

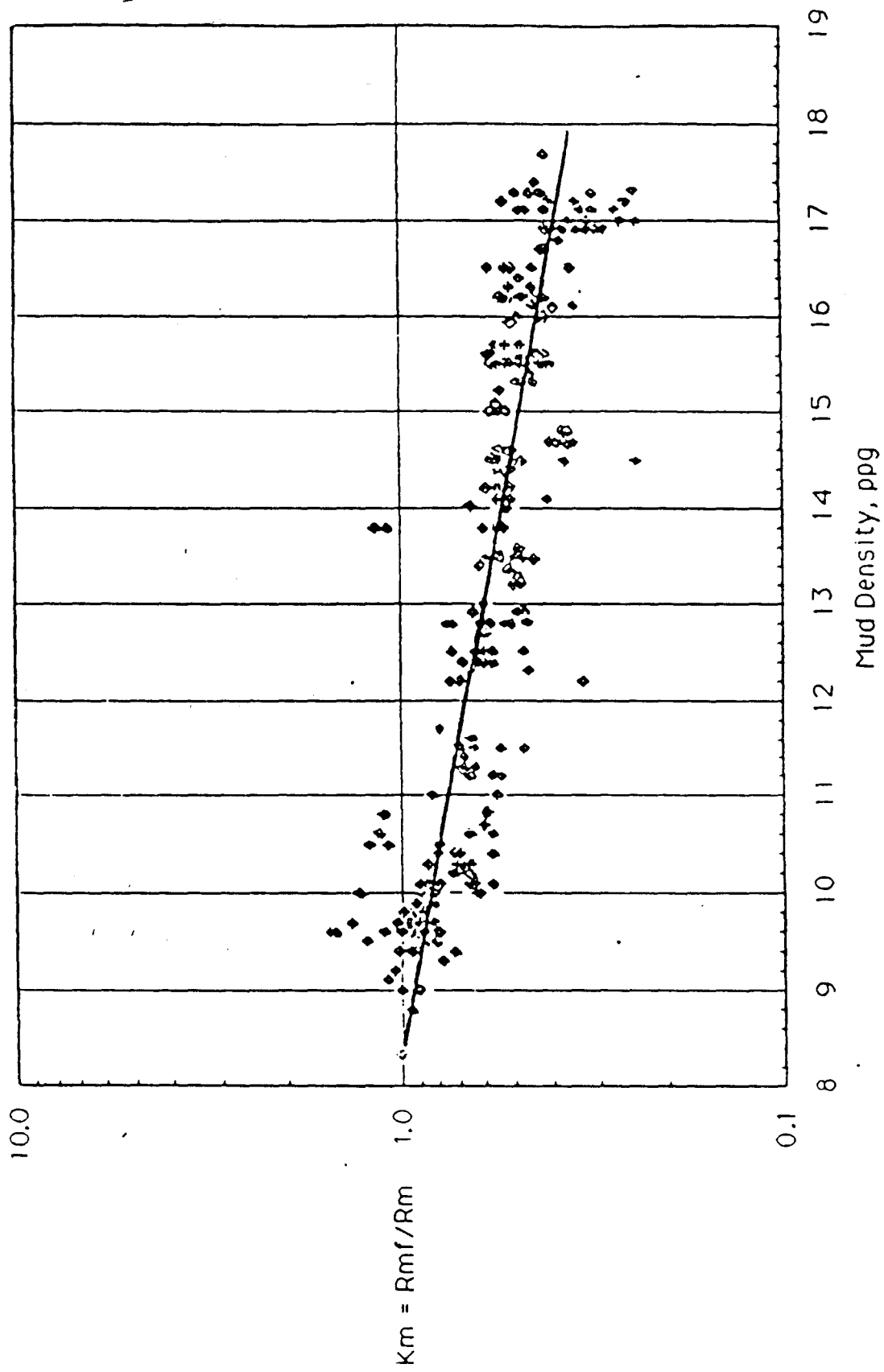


Figure 4 Km Vs Mud Density, Lignosulfonate Muds

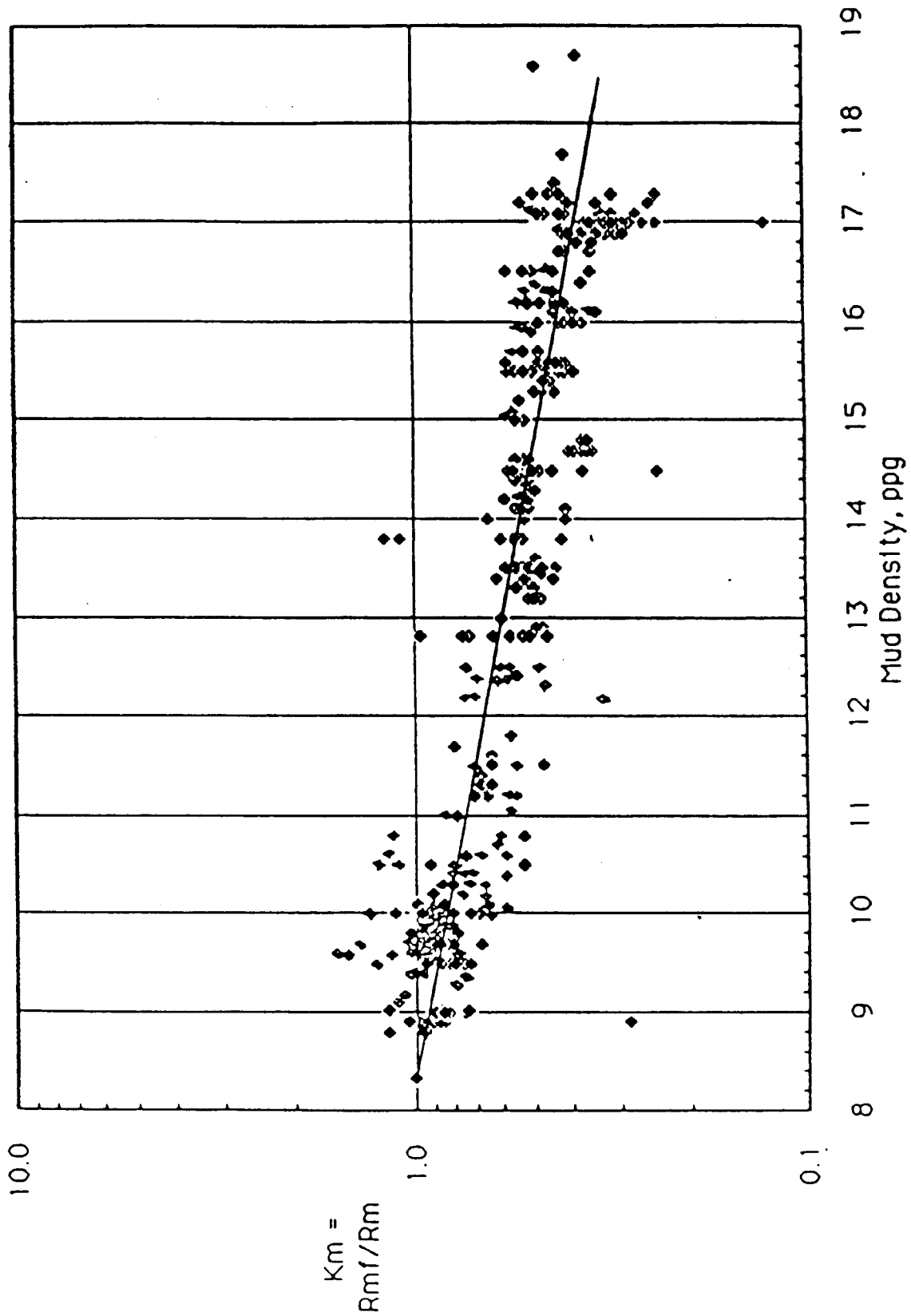


Figure 5 Km Vs Mud Density, All Muds

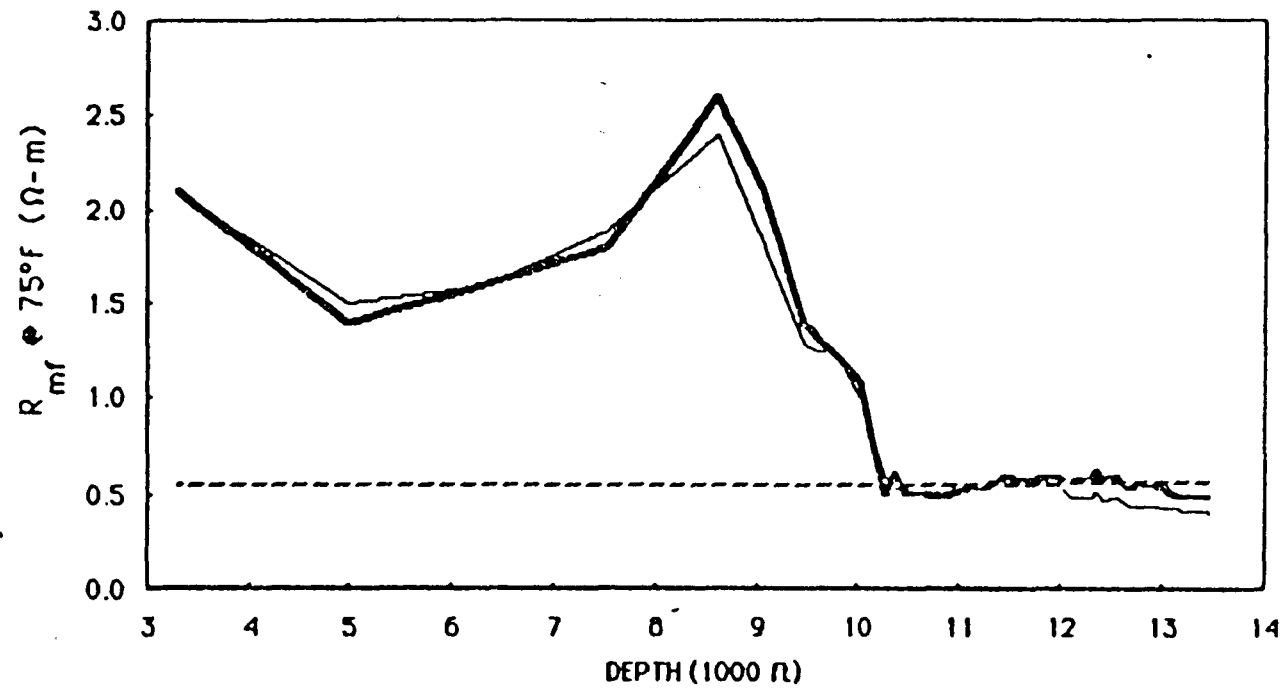


Figure 6

Rmf Vs Depth, Bruce #1 Well

Bold: Measured Rmf
Thin: Rmf from Eq. (1)
Dashed: Log header Rmf

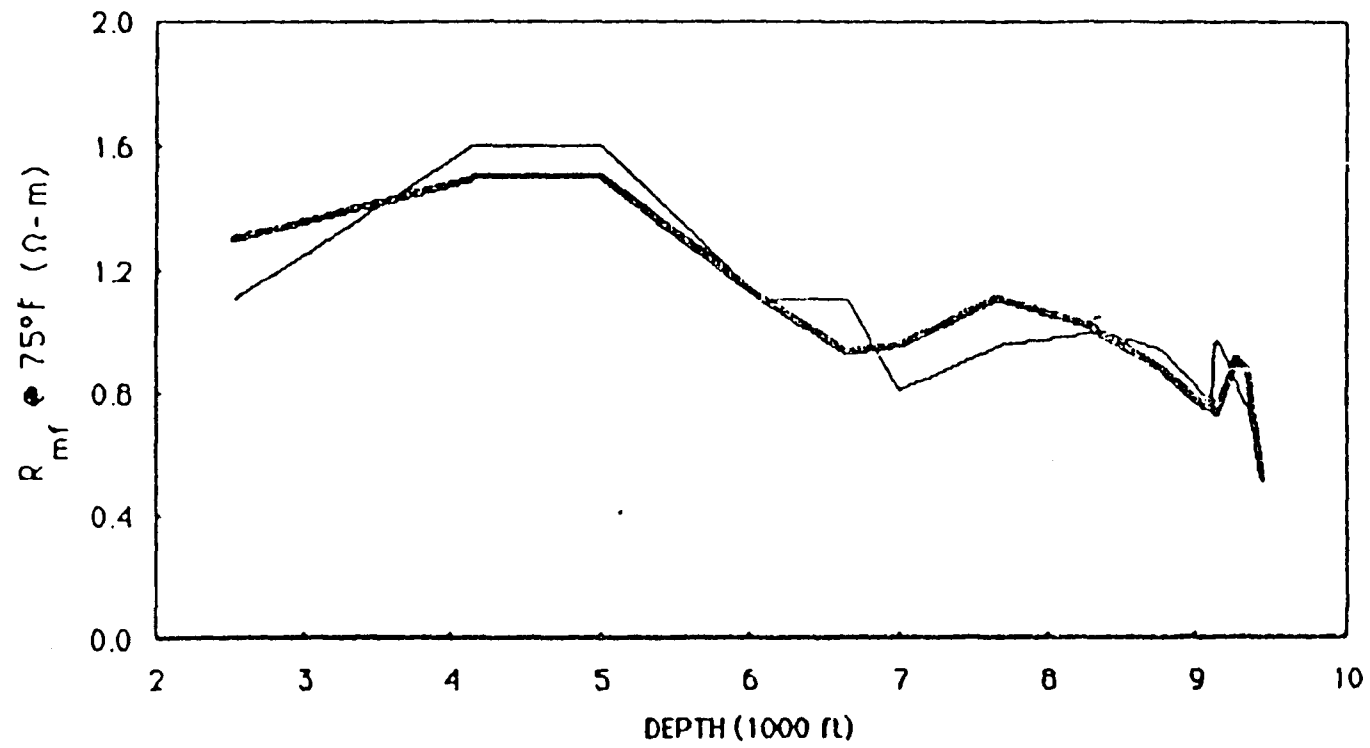


Figure 7

Rmf Vs Depth, De Lee #1 Well

Bold: Measured Rmf
Thin: Rmf from Eq. (1)
No log header Rmf

609

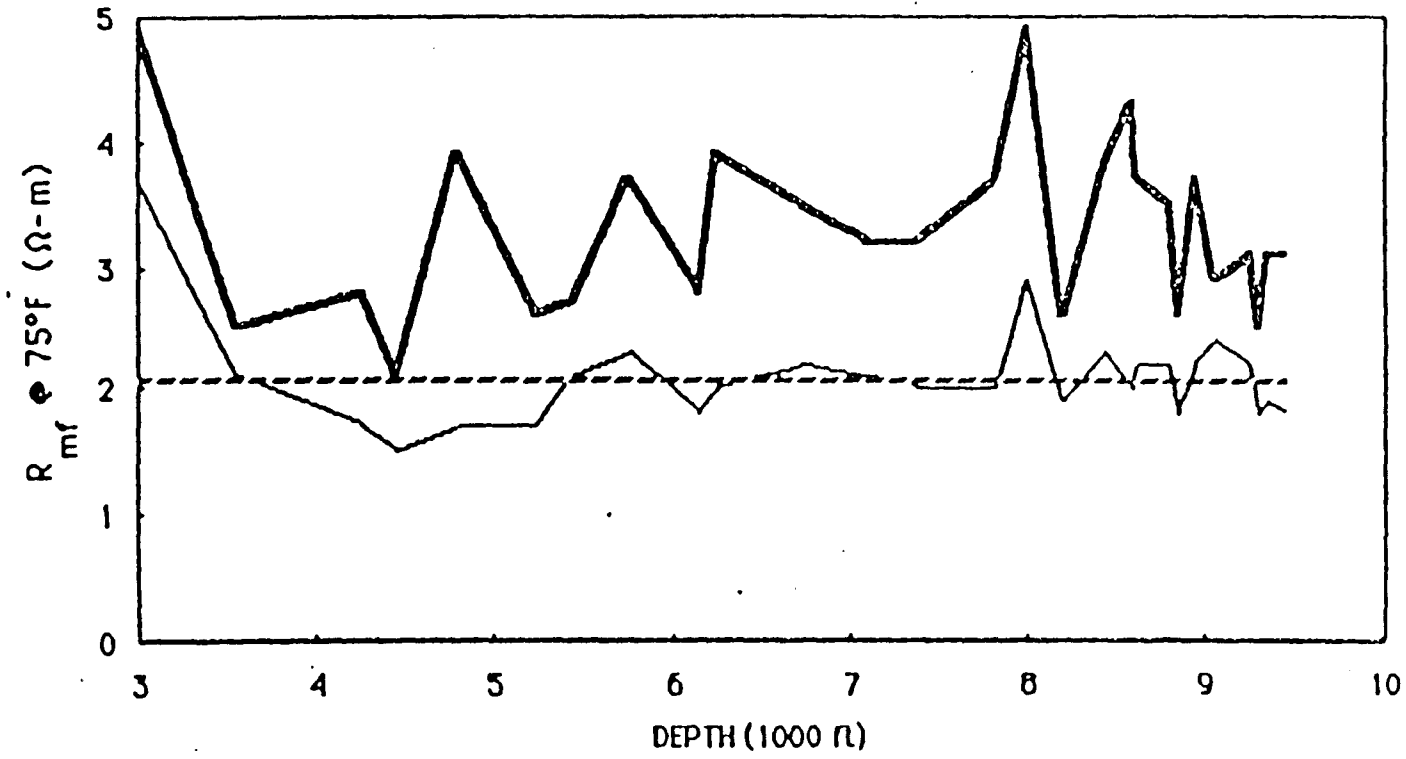


FIGURE 8

Rmf Vs Depth, D & M Cattle Co., #1

Bold: Measured Rmf

Thin: Rmf from Eq. (1)

Dashed: Log Header Rmf

About the Authors

H. F. Dunlap received his B.A. in 1938, M.A. in 1939, and Ph.D. in 1941 from Rice Institute, where he majored in physics. During World War II, he worked at the Carnegie Institution and the University of New Mexico in weapons research. From 1945 through 1975, he held various positions in the production research department of Atlantic Refining Company (now Atlantic Richfield), retiring in 1975. From 1976 to the present, he has served as Adjunct Professor in the Petroleum Engineering Department at the University of Texas at Austin.

Tom A. Lowe received his B.A. in anthropology from the University of California at San Diego in 1982, and his M.S. in petroleum engineering from the University of Texas at Austin, in 1985. He has accepted a position in the international division of Schlumberger.

Appendix 3





GeoChem Laboratories, Inc.

RESULTS OF GEOCHEMICAL EVALUATION
ON SAMPLES PROVIDED BY
UNIVERSITY OF TEXAS AT AUSTIN

Prepared for

UNIVERSITY OF TEXAS AT AUSTIN
Bureau of Economic Geology
Dr. Malcolm Light
University Station, Box X
Austin, Texas 78713-7508

GeoChem Job No. 3013

Prepared by

DOUGLAS A. MUCKELROY
GEOCHEM LABORATORIES, INC.



TABLE I

CRUDE OIL ANALYSIS RESULTS

GeoChem Sample No.: 3013-041
Client Identification No.: N.E. Hitchcock Field

GROSS COMPOSITION

Less than C₁₅₊ 58.3%
C₁₅₊ 41.7%

C₁₅₊ COMPOSITION

Asphaltene (ASPH) 1.0%
Paraffin-Naphthene Hydrocarbons (P-N) 81.3%
Aromatic Hydrocarbons (AROM) 16.7%
Eluted NSO Compounds (NSO) 0.5%
Noneluted NSO Compounds (NSO) 0.5%

RATIOS

$$\frac{P-N}{AROM} = 4.86$$

$$\frac{ASPH}{NSO} = 1.00$$

TABLE II

CRUDE OIL ANALYSIS RESULTS

GeoChem Sample No.: 3013-044
Client Identification No.: Delee #1

GROSS COMPOSITION

Less than C₁₅₊ 37.5%
C₁₅₊ 62.5%

C₁₅₊ COMPOSITION

Asphaltene (ASPH) 1.2%
Paraffin-Naphthene Hydrocarbons (P-N) 72.3%
Aromatic Hydrocarbons (AROM) 23.0%
Eluted NSO Compounds (NSO) 2.3%
Noneluted NSO Compounds (NSO) 1.2%

RATIOS

$$\frac{P-N}{AROM} = 3.14$$

$$\frac{ASPH}{NSO} = 0.34$$

TABLE III
 DETAILED C4-C7 HYDROCARBON ANALYSES
 (NORMALIZED PERCENT)

GEOCHEM SAMPLE NUMBER CLIENT I.D.	3013-041 N.E. Hitchcock Field	3013-044 DELEE #1
ISOBUTANE	4.0	6.7
N-BUTANE	5.6	8.6
ISOPENTANE	8.1	9.4
N-PENTANE	7.6	8.6
2,2-DIMETHYLBUTANE	1.0	1.0
CYCLOPENTANE	0.7	1.0
2,3-DIMETHYLBUTANE	1.6	1.6
2-METHYLPENTANE	6.1	6.1
3-METHYLPENTANE	3.7	3.6
N-HEXANE	8.2	7.7
METHYLCYCLOPENTANE	3.7	4.0
2,2-DIMETHYLPENTANE	0.6	0.6
BENZENE	1.3	3.4
2,4-DIMETHYLPENTANE	0.9	0.9
2,2,3-TRIMETHYLBUTANE	0.3	0.2
CYCLOHEXANE	6.4	7.3
3,3-DIMETHYLPENTANE	0.4	0.3
1,1-DIMETHYLCYCLOPENTANE	0.7	0.7
2-METHYLHEXANE	4.6	2.9
2,3-DIMETHYLPENTANE	0.0	1.1
1, CIS-3-DIMETHYLCYCLOPENTANE	0.7	0.7
3-METHYLHEXANE	3.7	2.8
1 TRANS-3-DIMETHYLCYCLOPENTANE	0.3	0.7
1 TRANS-2-DIMETHYLCYCLOPENTANE	1.3	1.3
3-ETHYLPENTANE	0.3	0.2
2,2,4-TRIMETHYLPENTANE	0.0	0.0
N-HEPTANE	6.5	5.6
1, CIS-2-DIMETHYLCYCLOPENTANE	0.2	0.2
METHYLCYCLOHEXANE	10.0	10.3
1,1,3-TRIMETHYLCYCLOPENTANE *	0.4	0.3
2,2-DIMETHYLHEXANE	0.3	0.2
ETHYLCYCLOPENTANE	0.4	0.3
TOLUENE	10.3	1.6

MOLECULAR RATIOS

2-METHYLPENTANE/3-METHYLPENTANE	1.66	1.65
ISOPENTANE/N-PENTANE	1.07	1.10
CYCLOHEXANE/METHYLCYCLOPENTANE	1.70	1.80
METHYLCYCLOPENT/METHYLCYCLOHEX	0.38	0.40

* C8 COMPOUNDS

** PPM VALUES ARE EXPRESSED AS VOLUMES OF GAS PER MILLION VOLUMES OF CUTTINGS

TABLE IV-A

Saturate Hydrocarbon Analyses

Summary of Paraffin-Naphthene Distribution

Geo Chem Sample Number	Client Identification	% Paraffin	% Isoprenoid	% Naphthene	C-P Index A	C-P Index B	ip19/ip20
3013-041	N. E. Hitchcock Field	36.3	5.6	58.1	1.06	1.08	2.69
3013-044	DELEE #1	37.2	4.9	57.9	1.03	1.09	3.06

TABLE IV-B

Saturate Hydrocarbon Analyses

Normalized Paraffin Distribution

218

Geo Chem Sample Number	Client Identification	% nC15	% nC16	% nC17	% ip19	% nC18	% ip20	% nC19	% nC20	% nC21	% nC22	% nC23	% nC24	% nC25	% nC26	% nC27	% nC28	% nC29	% nC30	% nC31	% nC32	% nC33	% nC34	% nC35
3013-041	N.E. Hitchcock Field	14.1	12.5	9.4	9.8	8.2	3.6	7.2	6.3	5.5	4.4	4.0	3.4	2.9	2.3	1.9	1.3	1.1	0.7	0.5	0.4	0.2	0.2	0.1
3013-044	DELEE #1	12.2	11.4	9.3	8.8	8.7	2.9	7.8	6.9	6.1	5.5	4.8	4.0	3.3	2.5	2.2	1.4	1.2	0.8	0.3	0.1	0.0	0.0	0.0

TABLE V

NICKEL/VANADIUM

<u>GeoChem Sample No.</u>	<u>3013-041</u>	<u>3013-044</u>
Total Nickel	0.23 ppm	0.29 ppm
Total Vanadium	<0.5 ppm	<0.5 ppm

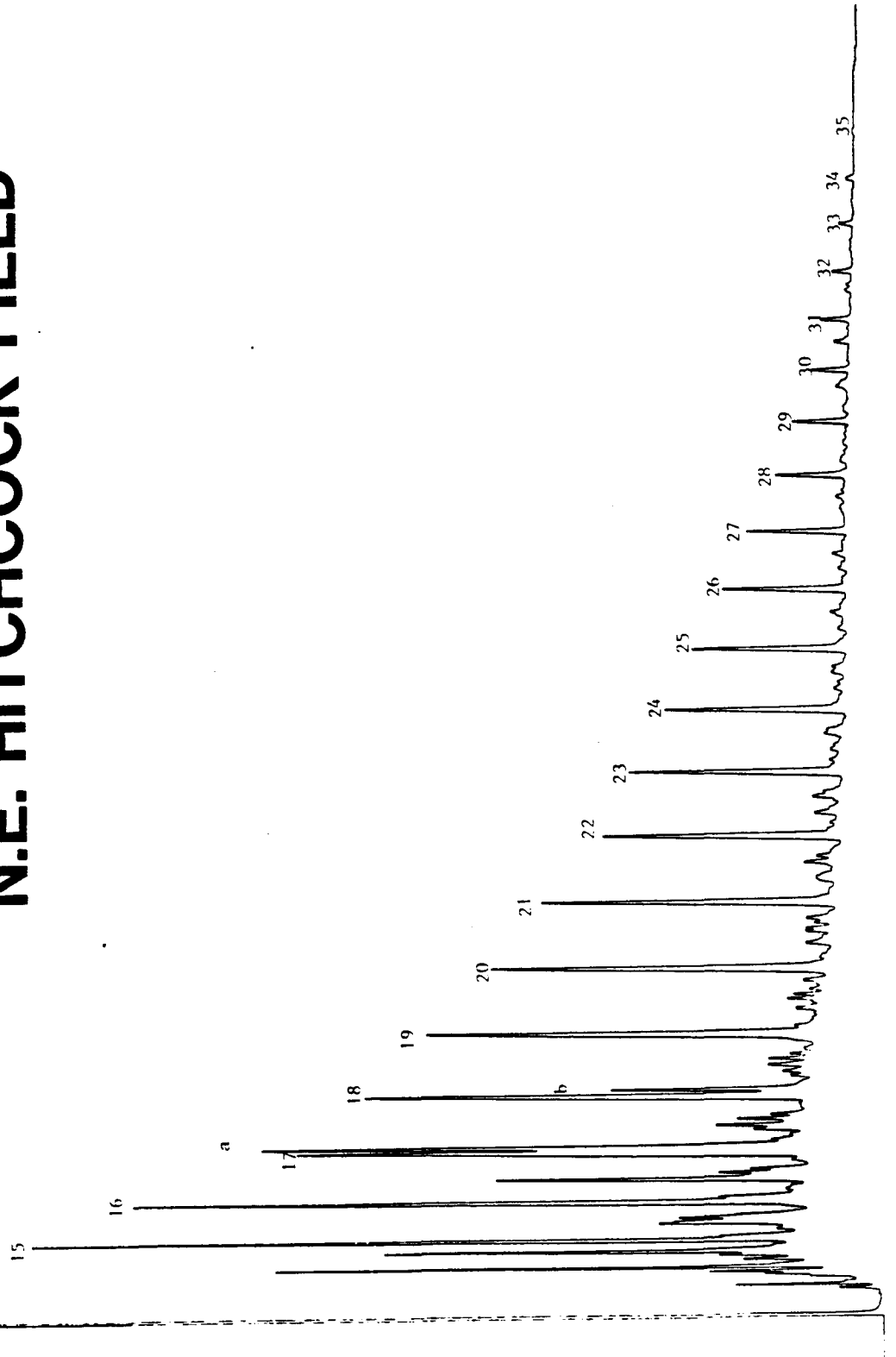
API GRAVITY @ 60°F

<u>GeoChem Sample No.</u>	<u>3013-041</u>	<u>3013-044</u>
API Gravity @ 60°F	42.16	38.6

Quality Assurance: These analyses are performed in accordance with EPA guidelines for quality assurance. These procedures include the following as a minimum requirements: comparisons against known standards in each run, one in ten sample splits, and a quarterly method review against known spike samples.

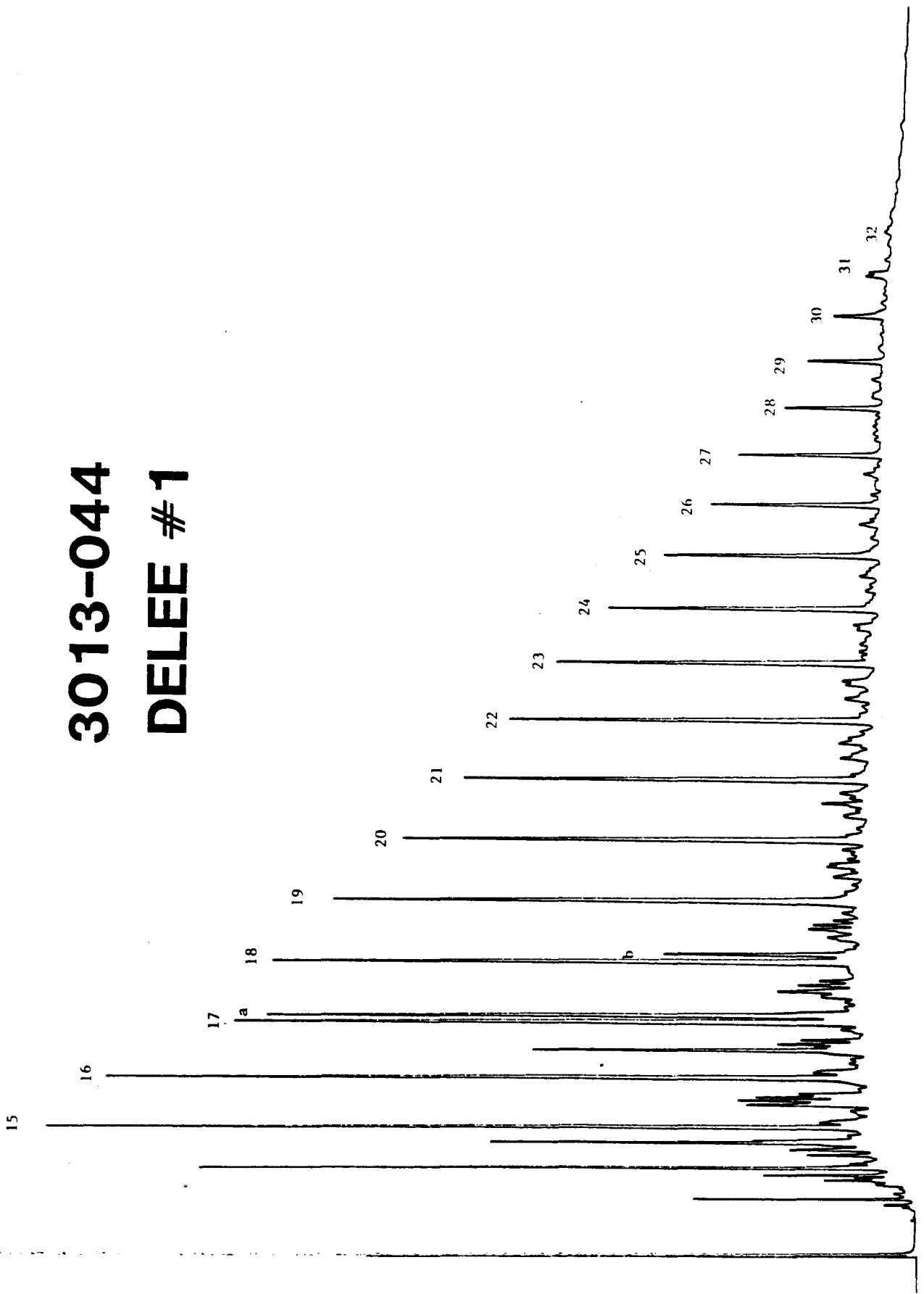
3013-041

N.E. HITCHCOCK FIELD



3013-044

DELEE #1



Biomarker/Aromatic Analyses

Performed For
The University of Texas
Austin, Texas

by
GeoChem Research, Inc.
Houston, Texas

and
GeoChem Laboratories, Inc.
Houston, Texas

I. Introduction

Two (2) samples were submitted for triterpane/sterane biomarker examination using GC/MS selected ion monitoring techniques. Two (2) additional samples were submitted for aromatic analyses using GC/MS full scan techniques. The identification and description of samples appears in Table I.

II. Gas Chromatography/Mass Spectrometry

Aromatic fractions were analyzed with a Finnigan OWA-30 mass spectrometer which was equipped with a 30 m DB-5 fused silica column. Helium was used as a carrier gas and the gas chromatograph was temperature programmed from 50°C to 300°C at 8°C/minute. Splitless injection technique was used. Full scan spectra were recorded from m/z 50 to m/z 400 every one second at an ionization potential of 70eV. Samples were spiked with naphthalene- d_8 , phenanthrene- d_{10} and chrysene- d_{12} for use as internal standards.

Saturate fractions were analyzed with the same instrument and column. The gas chromatograph was temperature programmed from 50°C to 230°C at 15°C/minute, then 230°C to 300°C at 2°C/minute. Ions monitored in the multiple ion detection mode (MID) were: 177; 191; 205; 217; 218; 259. Ions monitored for the analyses of monoaromatized steranes were m/z 239 and m/z 253. In addition, m/z 231 was monitored for the presence of methyl steranes.

III. Results

Using deuterated analogs of naphthalene, phenanthrene and chrysene, the concentrations (in parts per million) of various aromatic species in the total oil samples were calculated from the mass chromatograms (Table II and Table III). A relative response factor of 1 was used for all isomers. The mass chromatograms for the analyses are shown in Figures 1-10.

A sterane/triterpane fingerprint was observed in the samples analyzed by GC/MS/MID. Table IV gives key target steranes which are labeled on the fragmentograms. Due to the weak signal, steranes were not labeled for R785-218. Table V gives key target triterpanes. The sets of mass chromatograms are arranged in ascending mass order for each sample (Figures 11-24). Sample identifications can be found in the left corner of each fragmentogram.

The monoaromatized sterane fingerprint (Figures 25-29 and Figures 32-36) and methyl sterane pattern (Figures 30, 31, 37 and 38) are also presented.

Table 1. Sample Identifications

<u>GRI</u> <u>Sample</u> <u>Number</u>	<u>GLI</u> <u>Sample</u> <u>Number</u>
R785-215	3013-041(S)
R785-217	3013-044(S)
R785-218	3013-044(A)
R785-220	3013-041(A)

TABLE II
CONCENTRATION (PPM) AROMATICS IN OIL

SAMPLE ID: R785217
 WT SAMPLE (MG) 52.61
 VOLUME INJECTED: 1
 VOLUME EXTRACTED: 2
 PERCENT MOISTURE: 1

 STD: NAPHTHALENE-D8 136
 AREA: 30080
 CONC (NG): 20

COMPOUND	RF	AREA	CONC
NAPHTHALENE 128	.993	0	0
METHYLNAPHTHALENE-2 142	.936	0	0
METHYLNAPHTHALENE-1 142	1	0	0
C-2 ALKYLNAPHTHALENE ISOMERS	1	800	.02
C-3 ALKYLNAPHTHALENE ISOMERS	1	6477	.164
C-4 ALKYLNAPHTHALENE ISOMERS	1	6800	.172

 STD: PHENANTHRENE-D10
 AREA: 18496
 CONC (NG): 20

COMPOUND	RF	AREA	CONC
PHENANTHRENE 178	.925	1632	.073
ANTHRACENE 178	.795	0	0
FLUORANTHENE 202	.948	0	0
METHYLPHENANTHRENE ISOMERS	1	4161	.171
C2-ALKYLPHENANTHRENE ISOMERS	1	5628	.231
C3-ALKYLPHENANTHRENE ISOMERS	1	3352	.138

CONCENTRATION (PPM) AROMATICS IN OIL

SAMPLE ID: 3013-044
 WT SAMPLE (MG) 53.42
 VOLUME INJECTED: 1
 VOLUME EXTRACTED: 2
 PERCENT MOISTURE: 1

STD: NAPHTHALENE-D8 136

AREA: 31712
 CONC (NG): 20

COMPOUND	RF	AREA	CONC
----------	----	------	------

NAPHTHALENE 128	.993	0	0
METHYLNAPHTHALENE-2 142	.936	650	.016
METHYLNAPHTHALENE-1 142	1	1232	.029
C-2 ALKYLNAPHTHALENE ISOMERS	1	19242	.454
C-3 ALKYLNAPHTHALENE ISOMERS	1	34941	.824
C-4 ALKYLNAPHTHALENE ISOMERS	1	13888	.328

STD: PHENANTHRENE-D10

AREA: 19200
 CONC (NG): 20

COMPOUND	RF	AREA	CONC
----------	----	------	------

PHENANTHRENE 178	.925	3580	.151
FLUORANTHENE 202	.948	0	0
METHYLPHENANTHRENE ISOMERS	1	4878	.19
C2-ALKYLPHENANTHRENE ISOMERS	1	3513	.137
C3-ALKYLPHENANTHRENE ISOMERS	1	1842	.072

Table IV

Steranes

Chromatographic ¹ Identifier	Structural Assignment	Number of Carbons	Molecular Weight
A'	13 β ,17 α Diacholestane (20S)	27	372
B'	13 β ,17 α Diacholestane (20R)	27	372
C'	13 α ,17 β Diacholestane ---	27	372
D'	13 α ,17 β Diacholestane ---	27	372
E'	24-Methyl-13 β ,17 α Diacholestane (20S)	28	386
F'	24-Methyl-13 β ,17 α Diacholestane (20S)	28	386
G'	5 α ,14 α ,17 α Cholestane (20S)	27	372
H'	24-Ethyl-13 β ,17 α Diacholestane (20S)	29	400
I'	5 α ,14 β ,17 β Isocholestane (20S)	27	372
J'	5 α ,14 β ,17 β Isocholestane (20R)	27	372
K'	5 α ,14 α ,17 α Cholestane (20R)	27	372
L'	24-Ethyl-13 β ,17 α Diacholestane (20R)	29	400
M'	24-Methyl-5 α ,14 α ,17 α Cholestane(20S)	28	386
N'	24-Methyl-5 α ,14 β ,17 β Isocholestane (20S)	28	386
O'	24-Methyl-5 α ,14 β ,17 β Isocholestane (20R)	28	386
P'	24-Methyl-5 α ,14 α ,17 α Cholestane (20R)	28	386
Q'	24-Ethyl-5 α ,14 α ,17 α Cholestane (20S)	29	400
R'	24-Ethyl-5 α ,14 β ,17 β Isocholestane (20S)	29	400
S'	24-Ethyl-5 α ,14 β ,17 β Isocholestane (20R)	29	400
T'	24-Ethyl-5 α ,14 α ,17 α Cholestane (20R)	29	400

¹ The chromatographic identifiers are labeled for each sample on the applicable fragmentogram.

Table V

Tri- And Pentacyclic Terpanes
(Primarily Hopane Series)

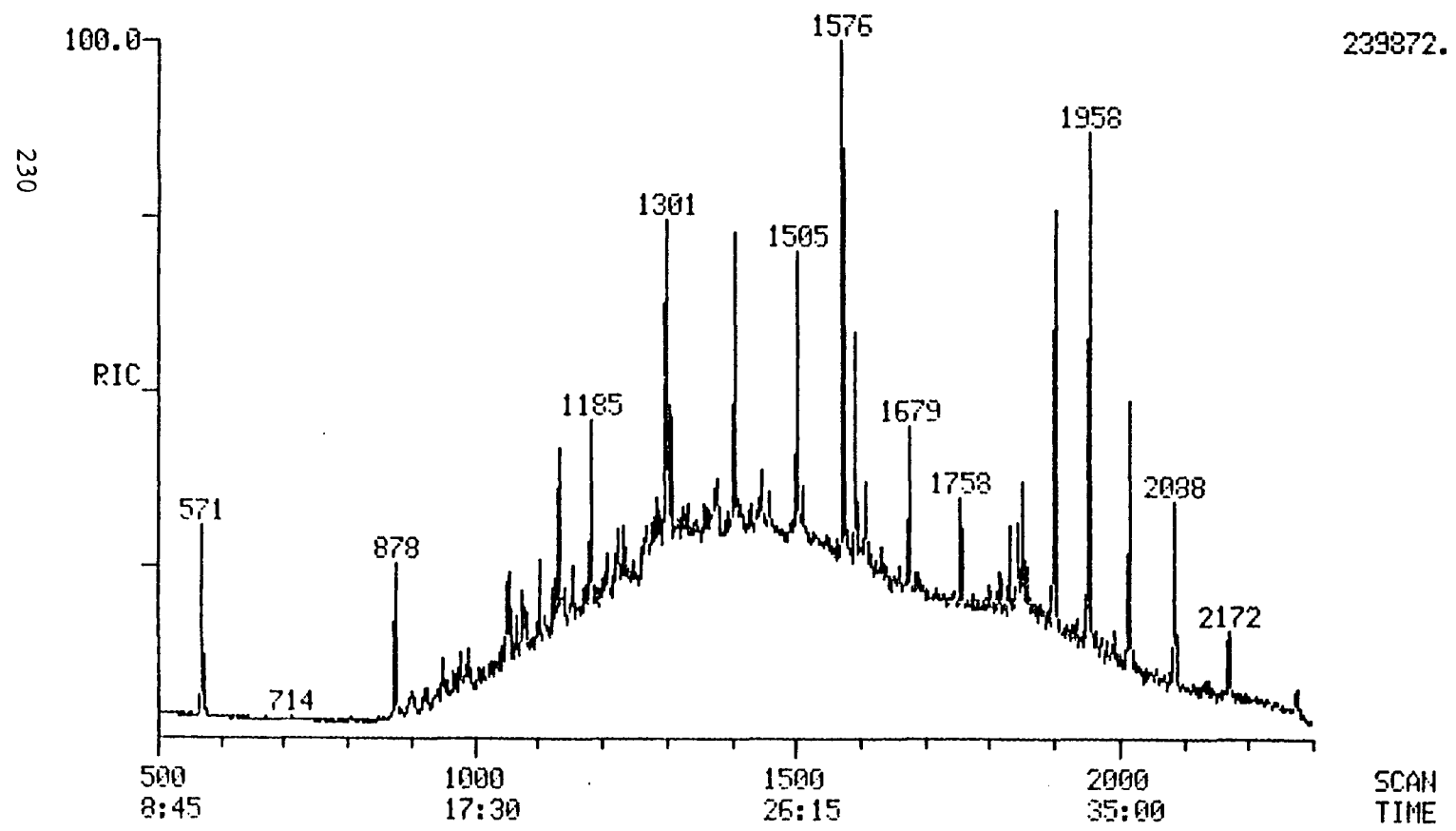
Chromatographic ¹ Identifier	Structural Assignment	Number of Carbons	Molecular Weight
A	Tricyclic Triterpane A	28	388
B	Tricyclic Triterpane B	28	388
C	Tricyclic Triterpane C	29	402
D	Tricyclic Triterpane D	29	402
E	18 α (H)-22,29,30-Trisnorhopane II (Ts)	27	370
F	17 α (H)-22,29,30-Trisnorhopane (Tm)	27	370
G	17 α (H),21 β (H)-30-Norhopane	29	398
H	17 β (H),21 α (H)-30-Normoretane	29	398
I	17 α (H),21 β (H)-Hopane	30	412
J	17 β (H),21 α (H)-Moretane	30	412
K	17 α (H),21 β (H)-30-Homohopane (22S)	31	426
L	17 α (H),21 β (H)-30-Homohopane (22R)	31	426
M	17 α (H),21 β (H)-30,31-Bishomohopane (22S)	32	440
N	17 α (H),21 β (H)-30,31-Bishomohopane (22R)	32	440
O	17 β (H),21 α (H)-30,31-Bishomohopane (22S)	32	440
P	17 β (H),21 α (H)-30,31-Bishomohopane (22R)	32	440
Q	17 α (H),21 β (H)-30,31,32-Trishomo- hopane (22S)	33	454
R	17 α (H),21 β (H)-30,31,32-Trishomo- hopane (22R)	33	454
S	17 α (H),21 β (H)-30,31,32,33-Tetra- kishomohopane (22S)	34	468
T	17 α (H),21 β (H)-30,31,32,33-Tetra- kishomohopane (22R)	34	468

1 The chromatographic identifiers are labeled for each sample on the applicable chromatogram.

RIC
09/19/85 10:19:00
SAMPLE: 3013-041 AROMATIC FRACTION

DATA: R785017

SCANS 500 TO 2300



239872.

FIGURE 1

MASS CHROMATOGRAMS
09/19/85 10:19:00
SAMPLE: 3013-041 AROMATIC FRACTION

DATA: R785017

SCANS 550 TO 1150

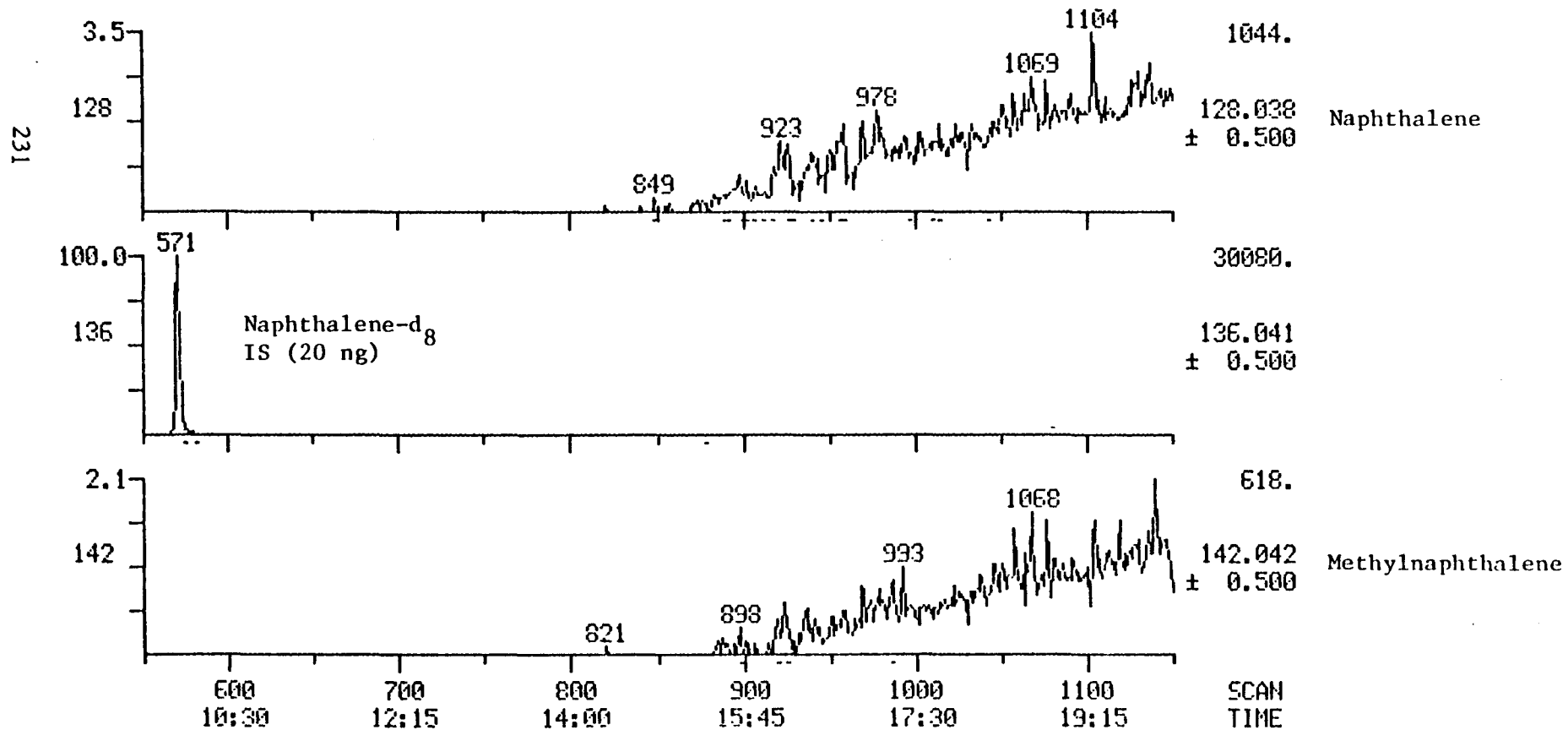


FIGURE 2

MASS CHROMATOGRAMS
09/19/85 10:19:00
SAMPLE: 3013-041 AROMATIC FRACTION

DATA: R785017

SCANS 550 TO 1150

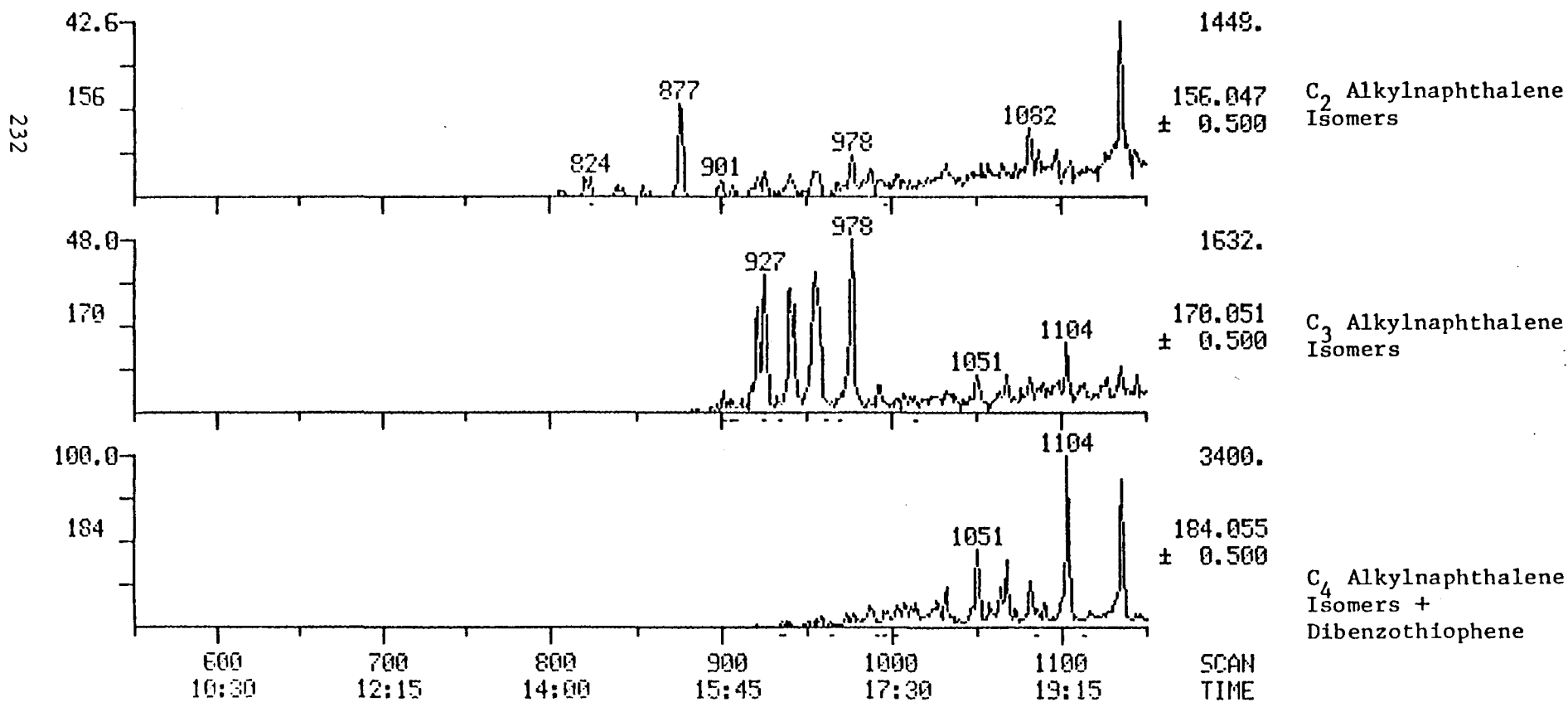


FIGURE 3

MASS CHROMATOGRAMS
 09/19/85 10:19:00
 SAMPLE: 3013-041 AROMATIC FRACTION

DATA: R785017

SCANS 1100 TO 1500

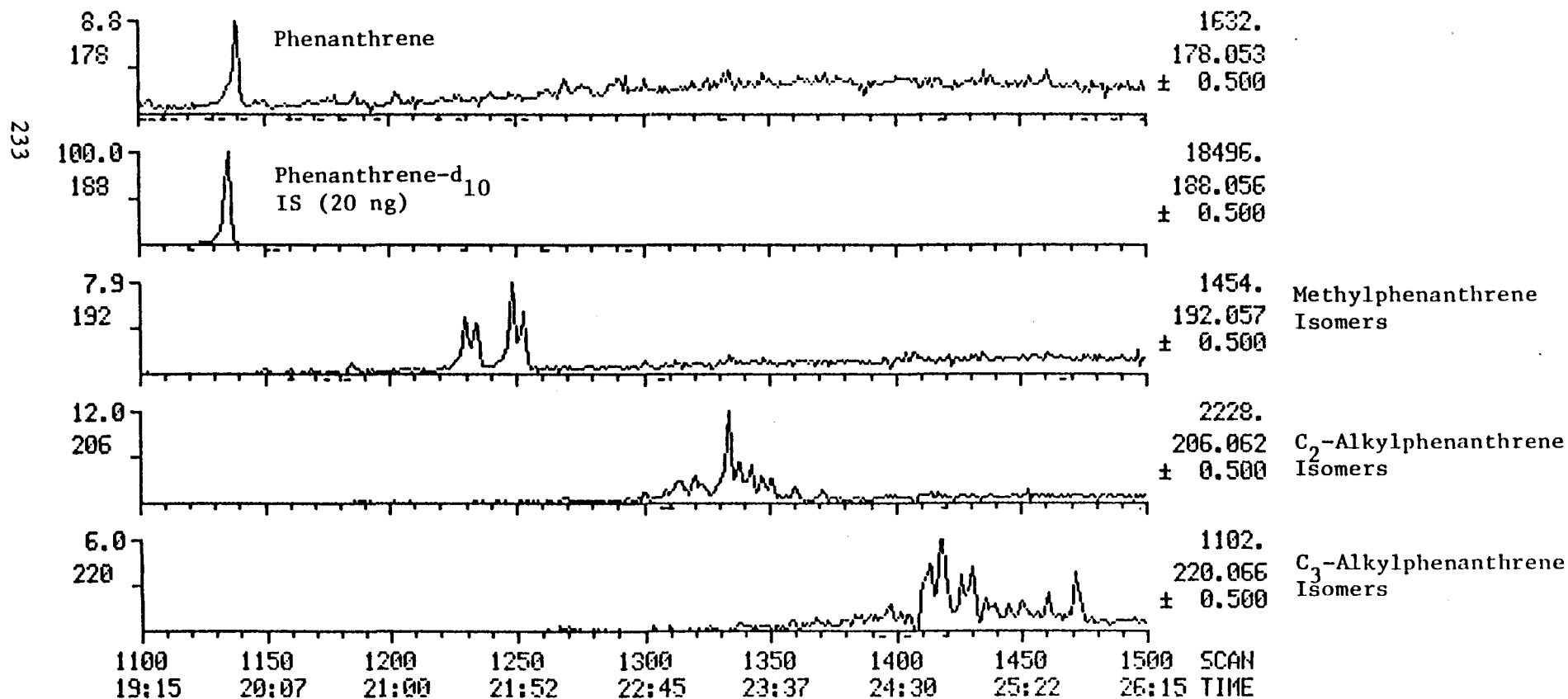


FIGURE 4

MASS CHROMATOGRAMS
09/19/85 10:19:00
SAMPLE: 3013-041 AROMATIC FRACTION

DATA: R785017

SCANS 1500 TO 1800

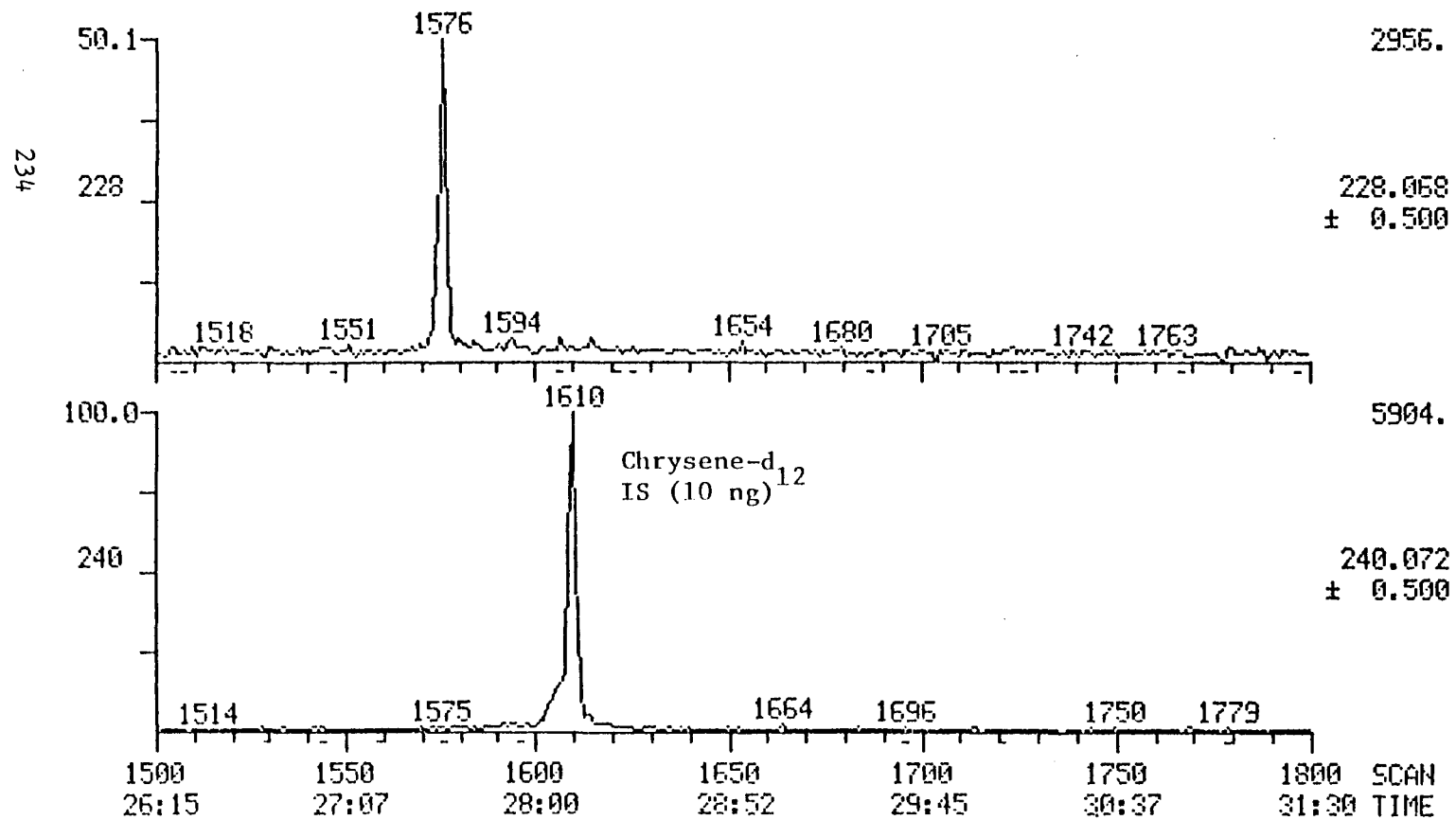


FIGURE 5

RIC
09/19/85 11:19:00
SAMPLE: 3013-044 AROMATIC FRACTION

DATA: R785022

SCANS 500 TO 2300

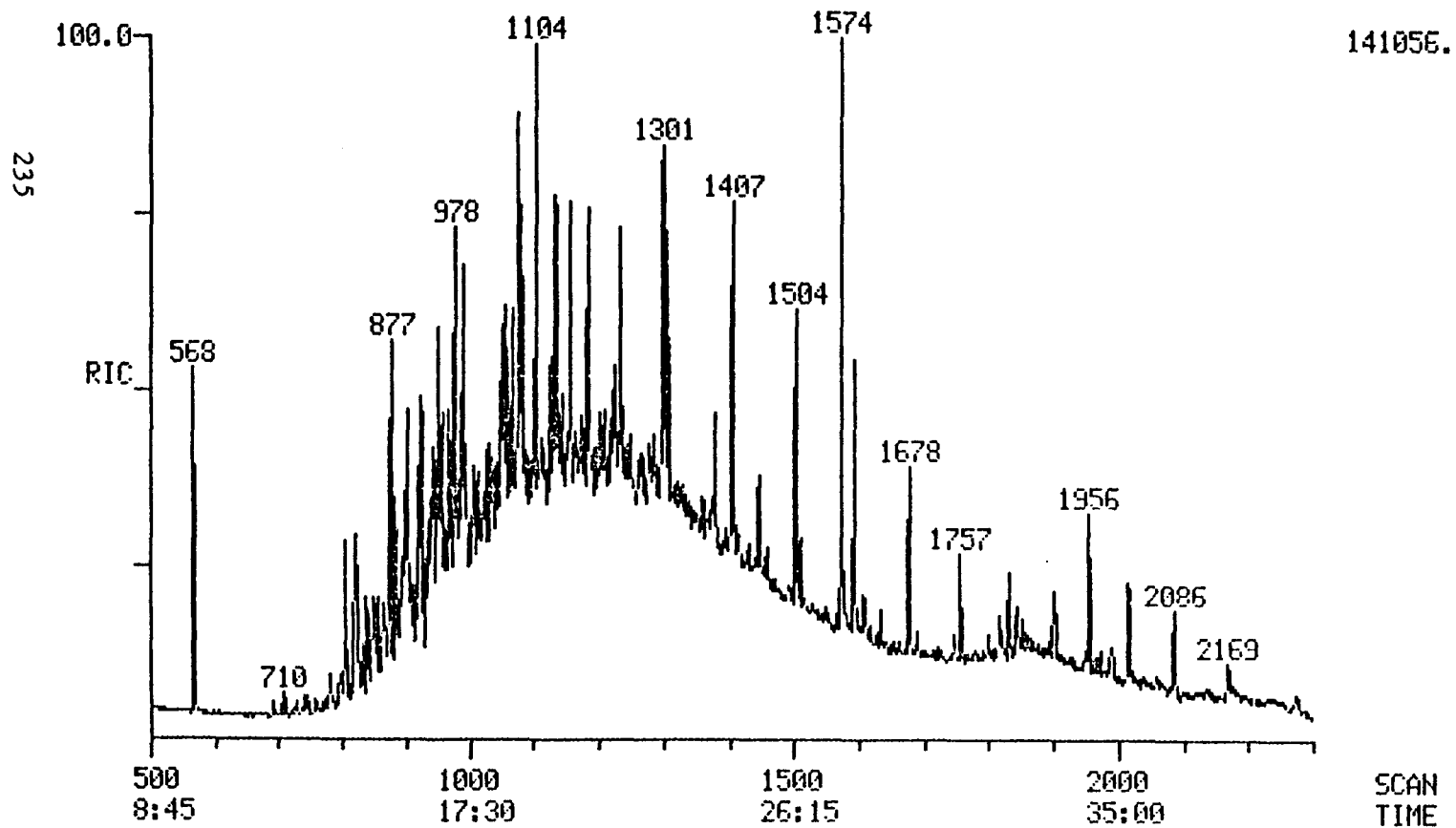


FIGURE 6

MASS CHROMATOGRAMS
09/19/85 11:19:00
SAMPLE: 3013-044 AROMATIC FRACTION

DATA: R785022

SCANS 550 TO 1150

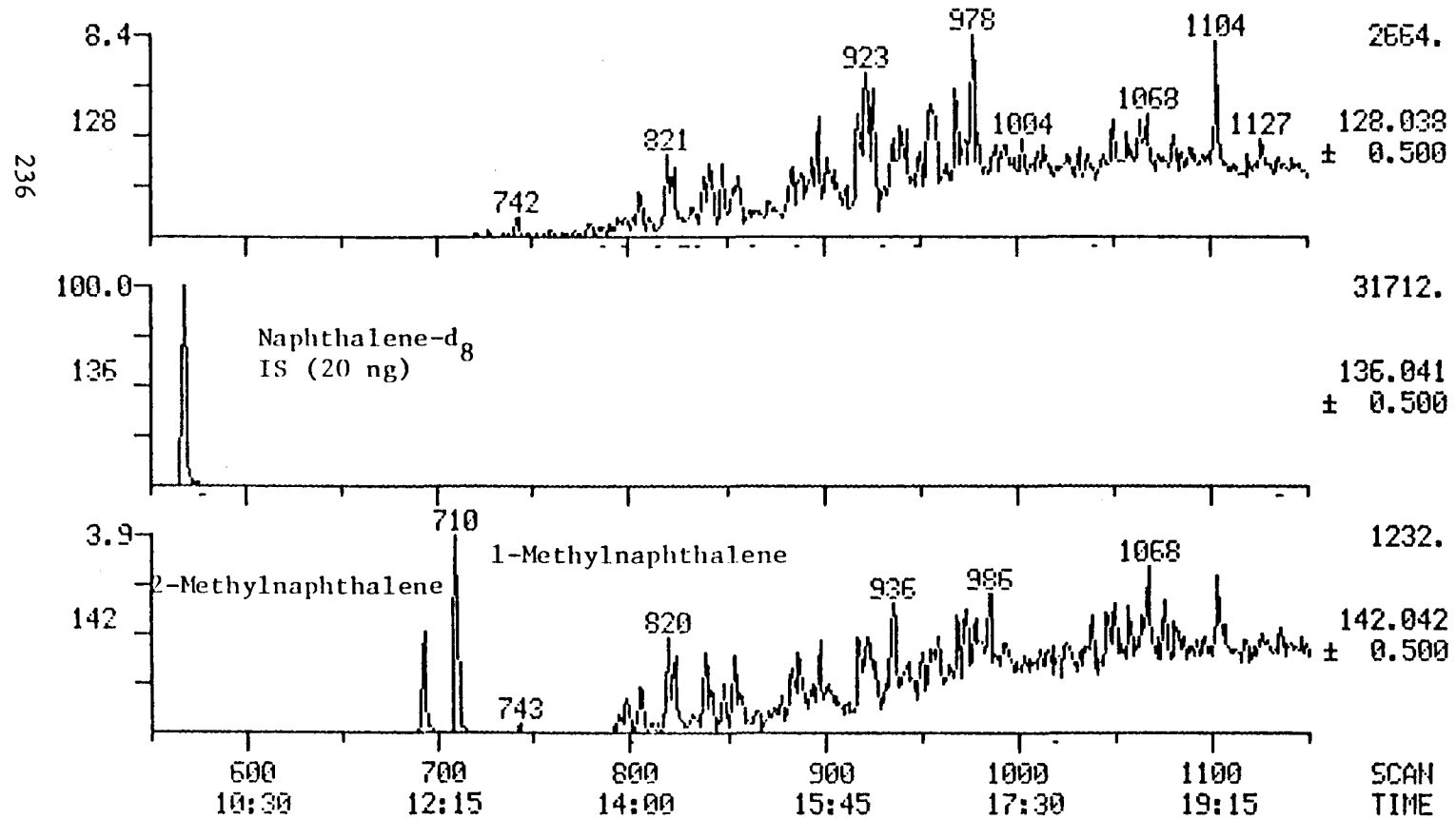


FIGURE 7

MASS CHROMATOGRAMS
09/19/85 11:19:00
SAMPLE: 3013-044 AROMATIC FRACTION

DATA: R785022

SCANS 550 TO 1150

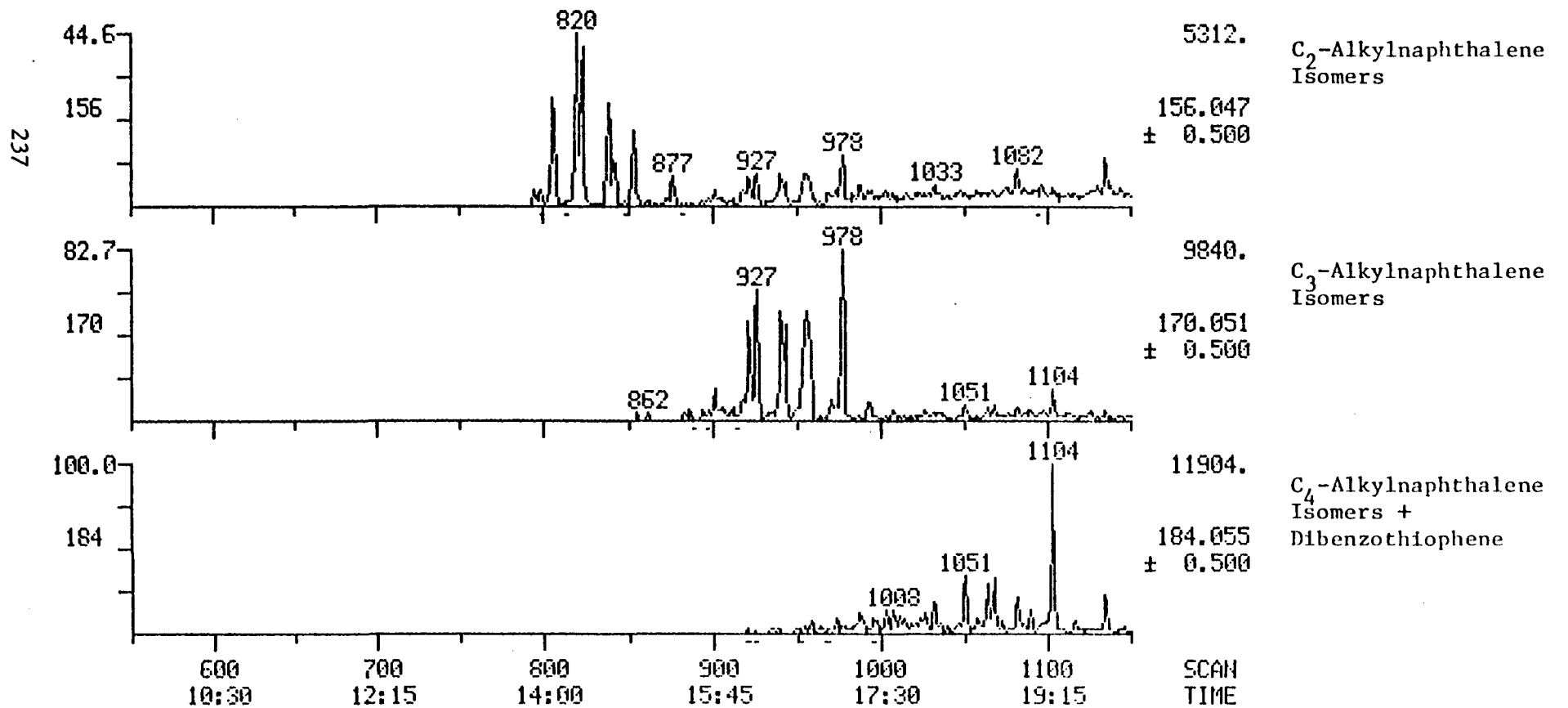


FIGURE 8

MASS CHROMATOGRAMS
 09/19/85 11:19:00
 SAMPLE: 3013-044 AROMATIC FRACTION

DATA: R785022

SCANS 1100 TO 1500

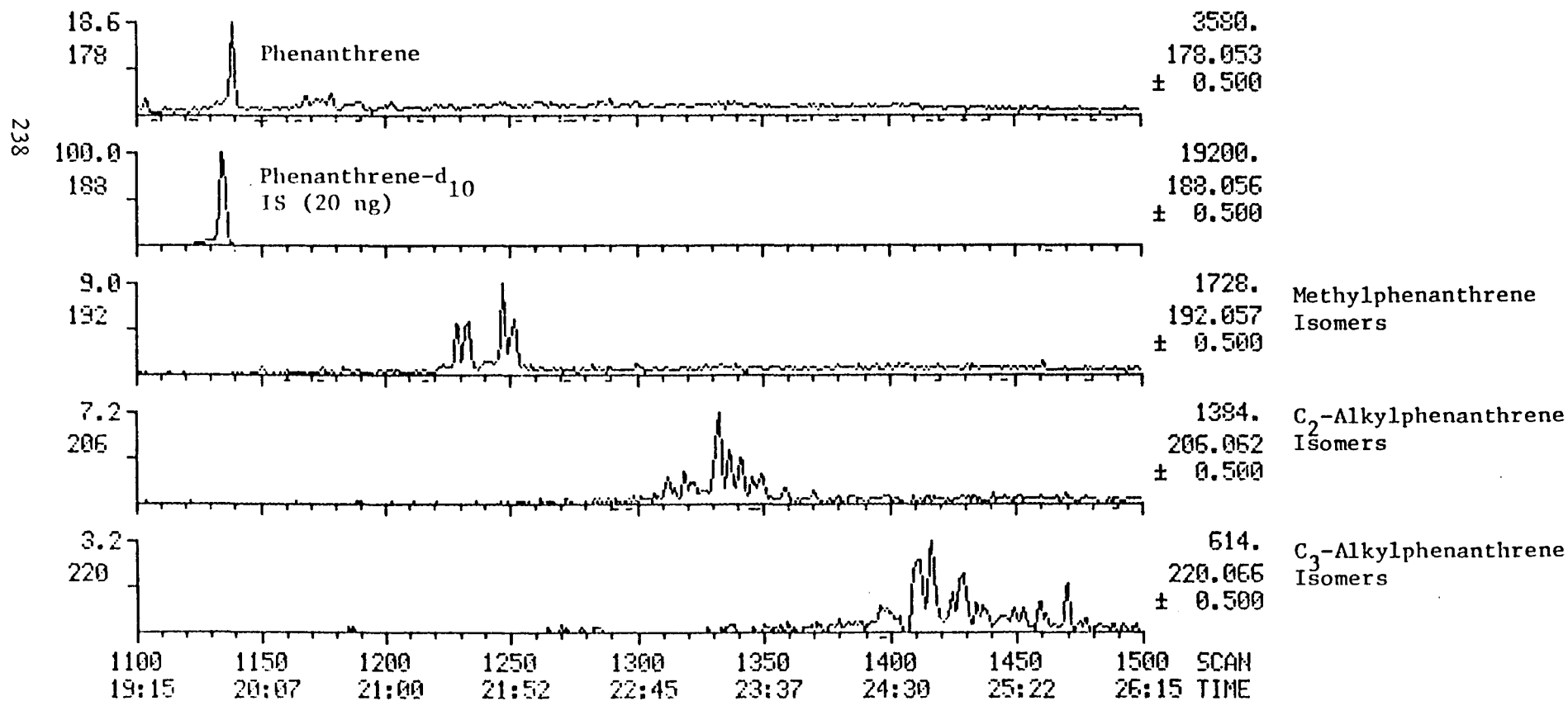


FIGURE 9

MASS CHROMATOGRAMS
09/19/85 11:19:00
SAMPLE: 3013-044 AROMATIC FRACTION

DATA: R785022

SCANS 1500 TO 1800

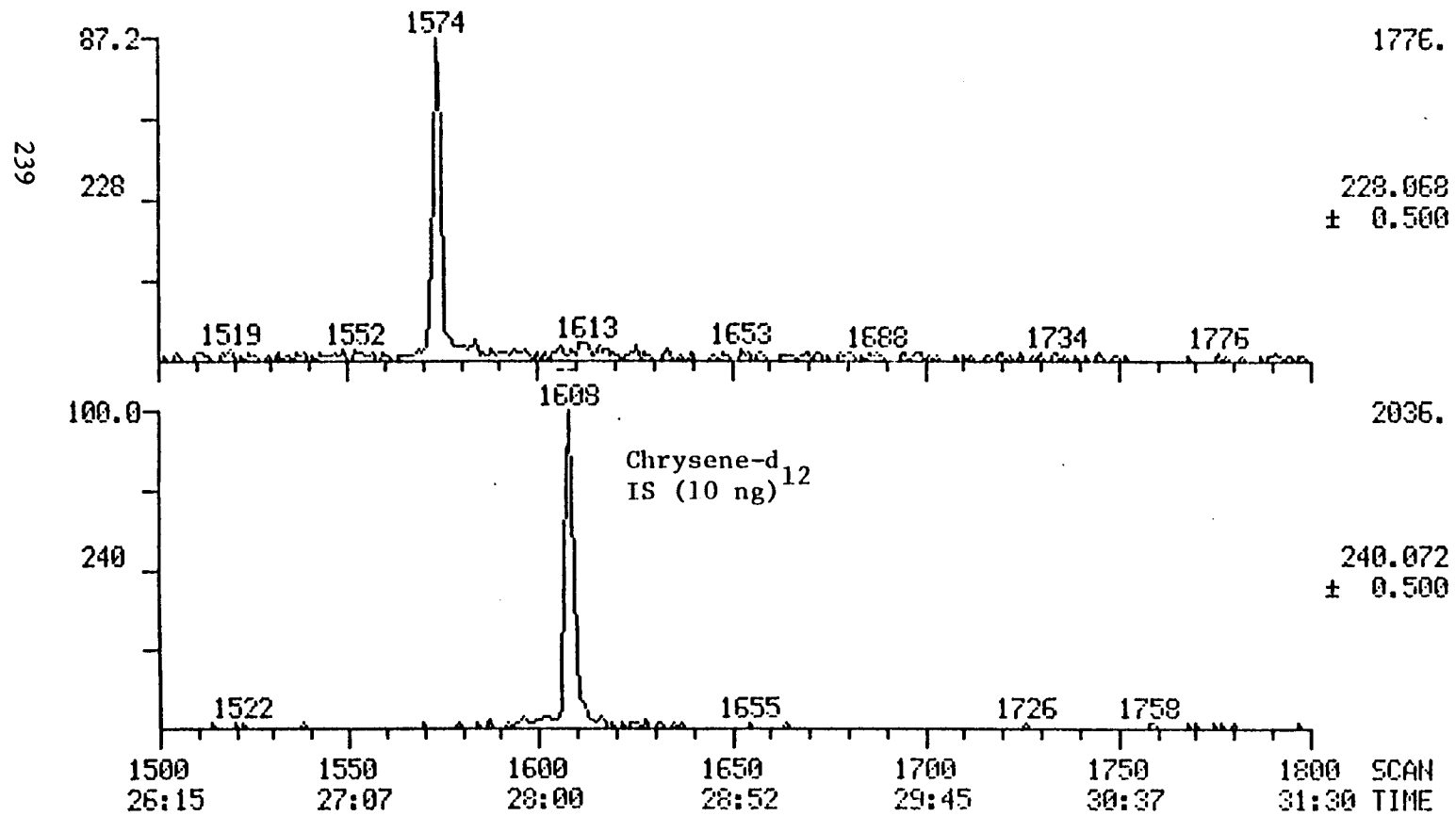


FIGURE 10

RIC
09/19/85 13:50:00
SAMPLE: 3013-041 SAT FRAC

DATA: R785215

SCANS 1 TO 1100

670720.

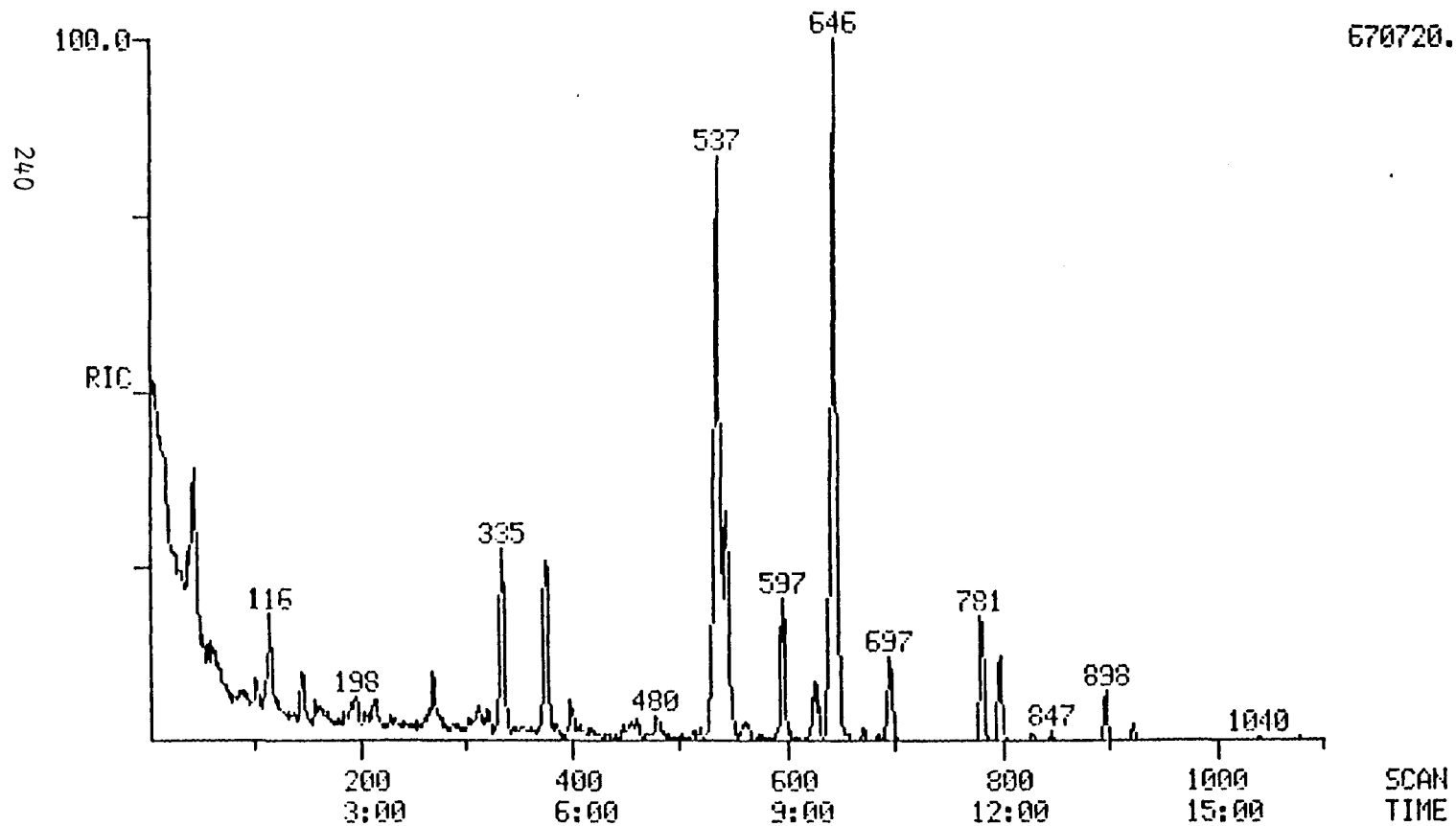


FIGURE 11

MASS CHROMATOGRAM
09/19/85 13:50:00
SAMPLE: 3013-041 SAT FRAC

DATA: R785215

SCANS 200 TO 1200

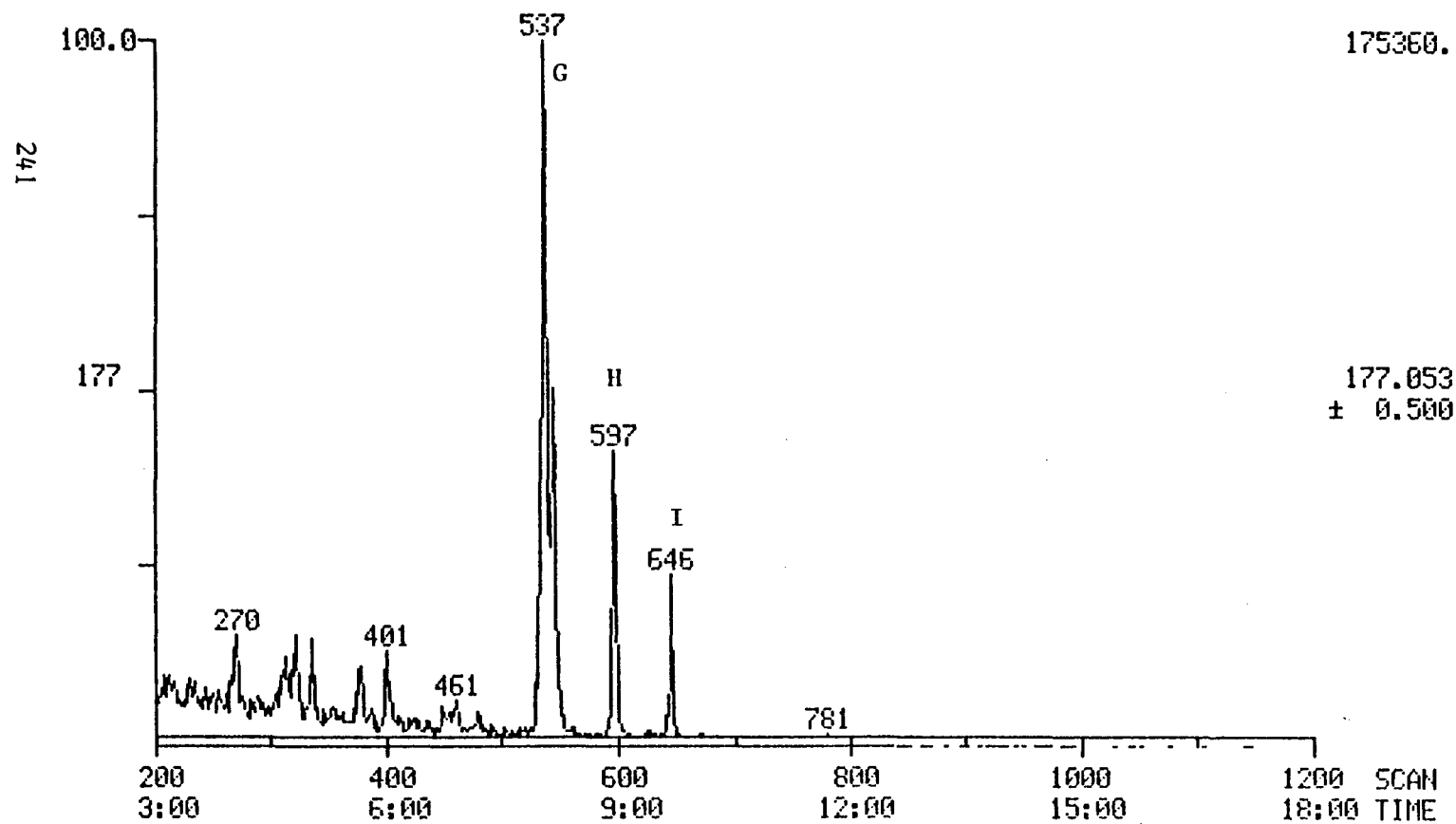


FIGURE 12

MASS CHROMATOGRAM
09/19/85 13:50:00
SAMPLE: 3013-041 SAT FRAC

DATA: R785215

SCANS 200 TO 1200

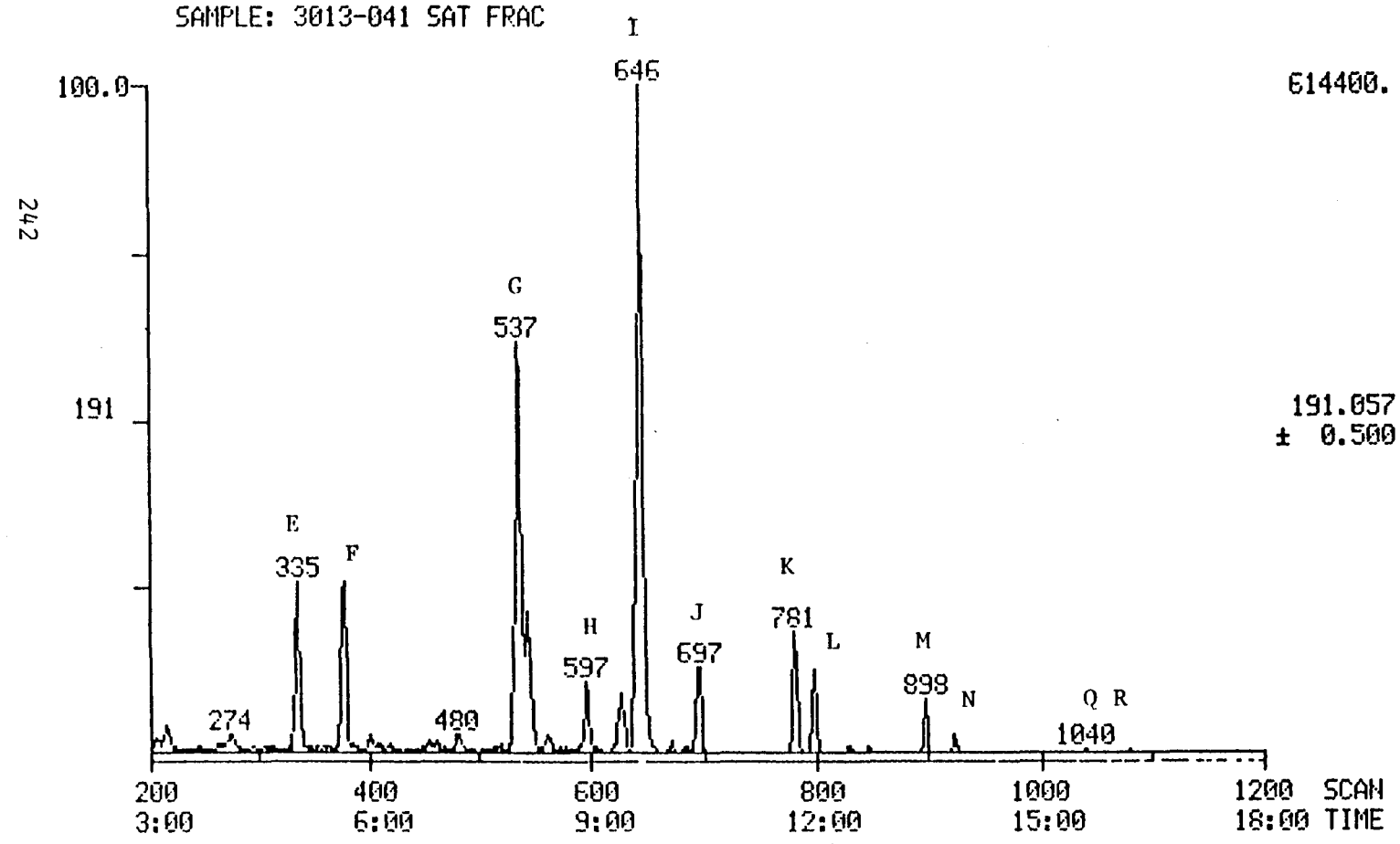


FIGURE 13

MASS CHROMATOGRAM
09/19/85 13:50:00
SAMPLE: 3013-041 SAT FRAC

DATA: R785215

SCANS 200 TO 1200

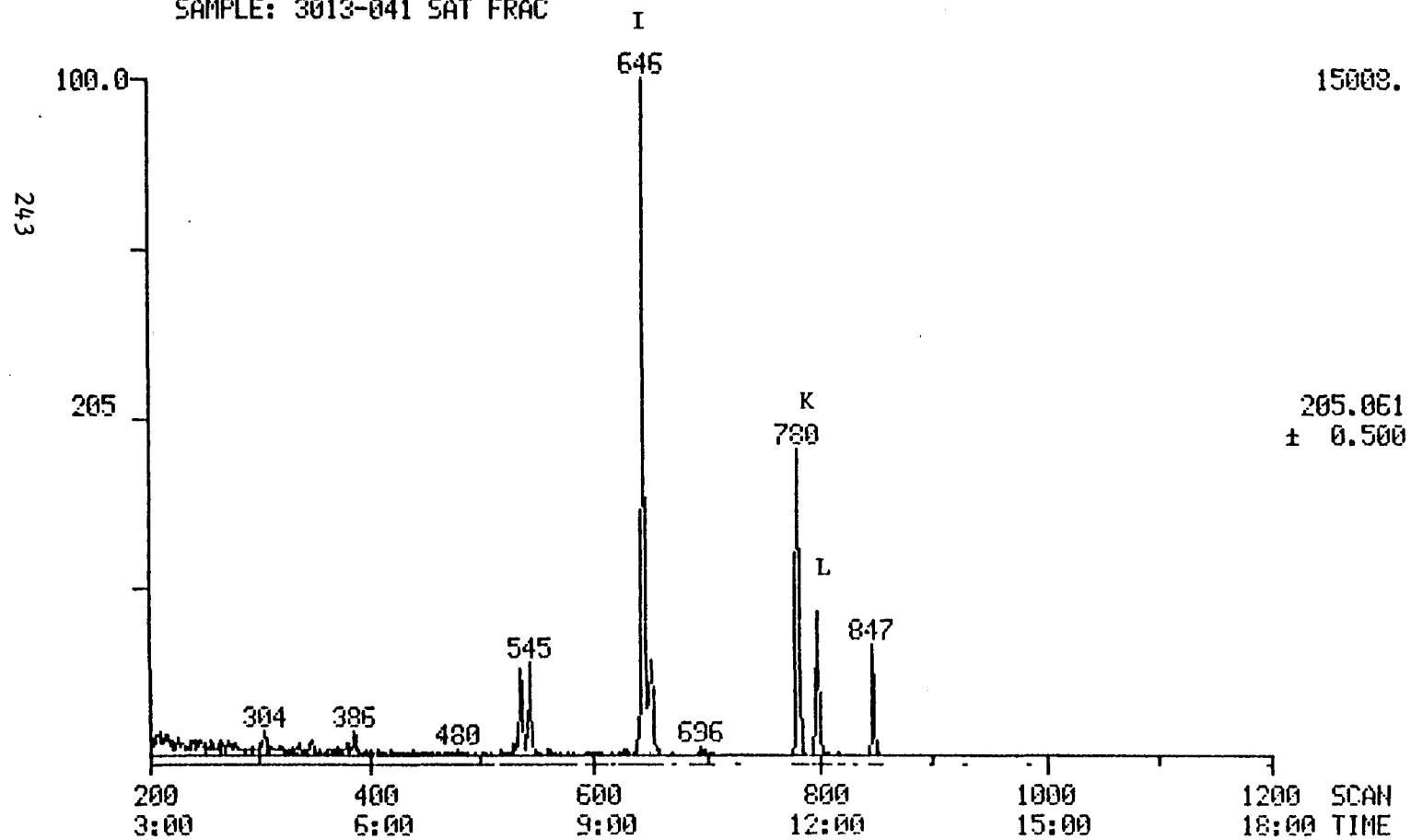


FIGURE 14

MASS CHROMATOGRAM
09/19/85 13:50:00
SAMPLE: 3013-041 SAT FRAC

DATA: R785215

SCANS 1 TO 800

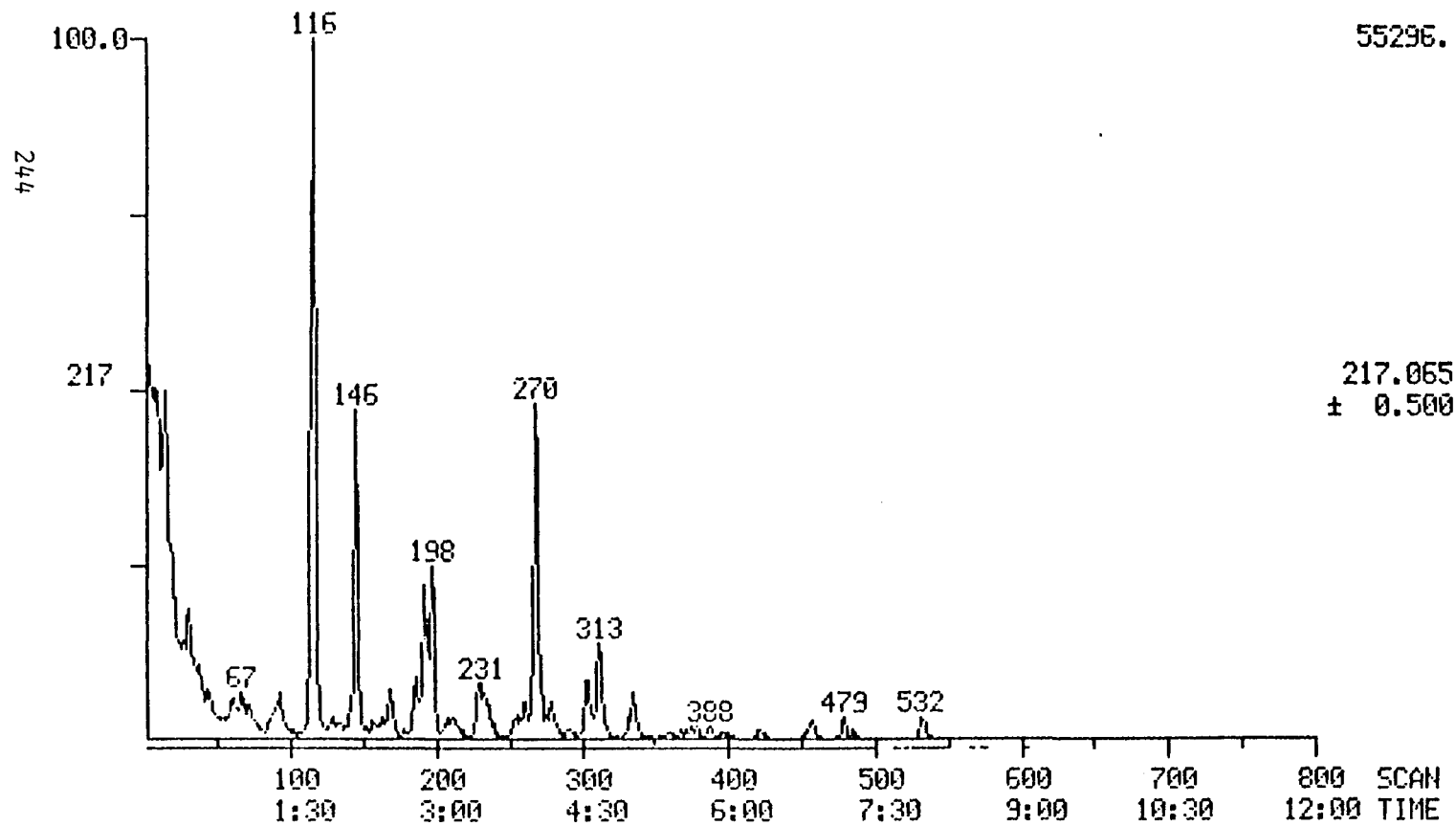


FIGURE 15

MASS CHROMATOGRAM
09/19/85 13:50:00
SAMPLE: 3013-041 SAT FRAC

DATA: R785215

SCANS 1 TO 800

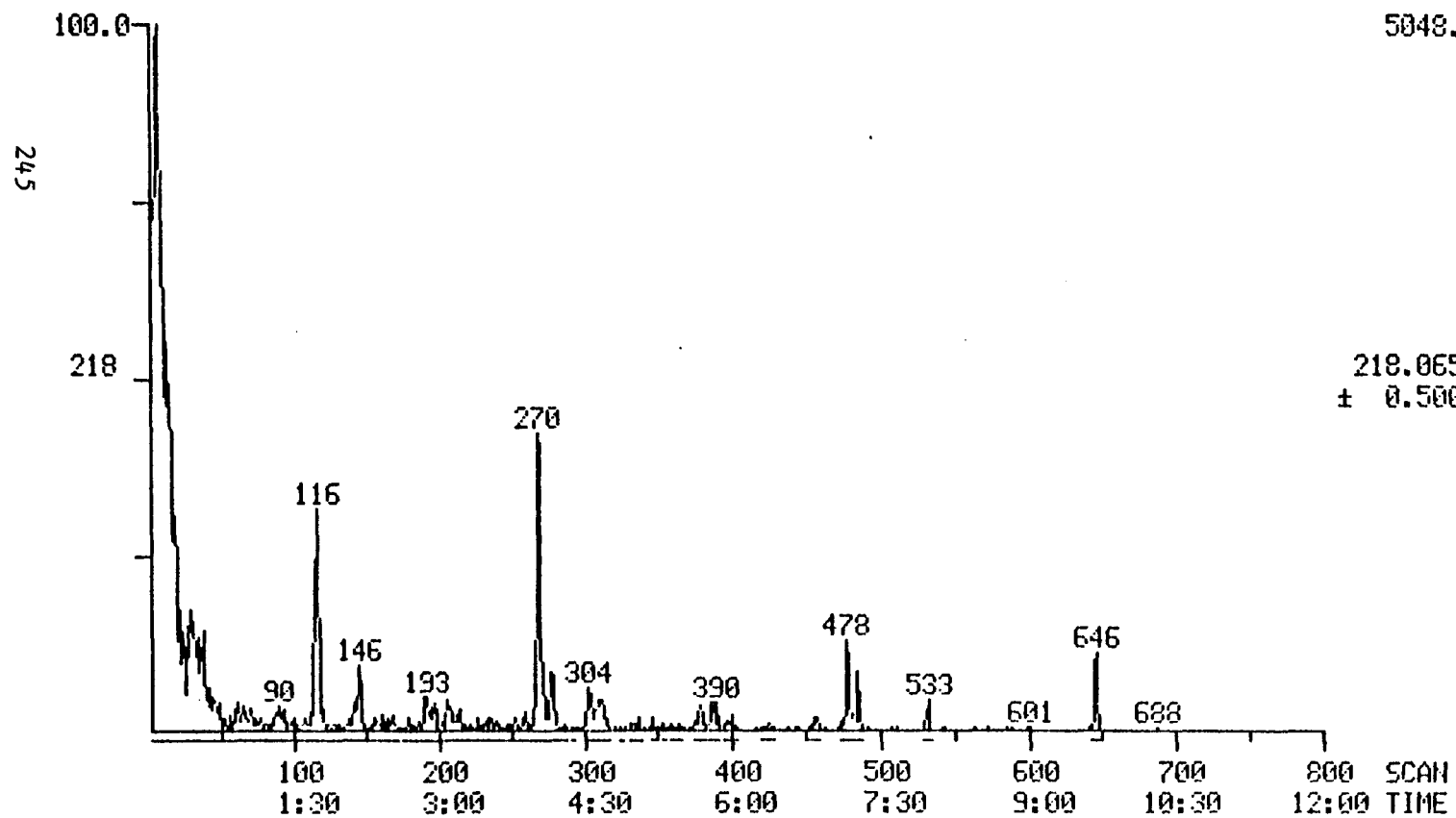


FIGURE 16

MASS CHROMATOGRAM
09/19/85 13:50:00
SAMPLE: 3013-041 SAT FRAC

DATA: R785215

SCANS 1 TO 800

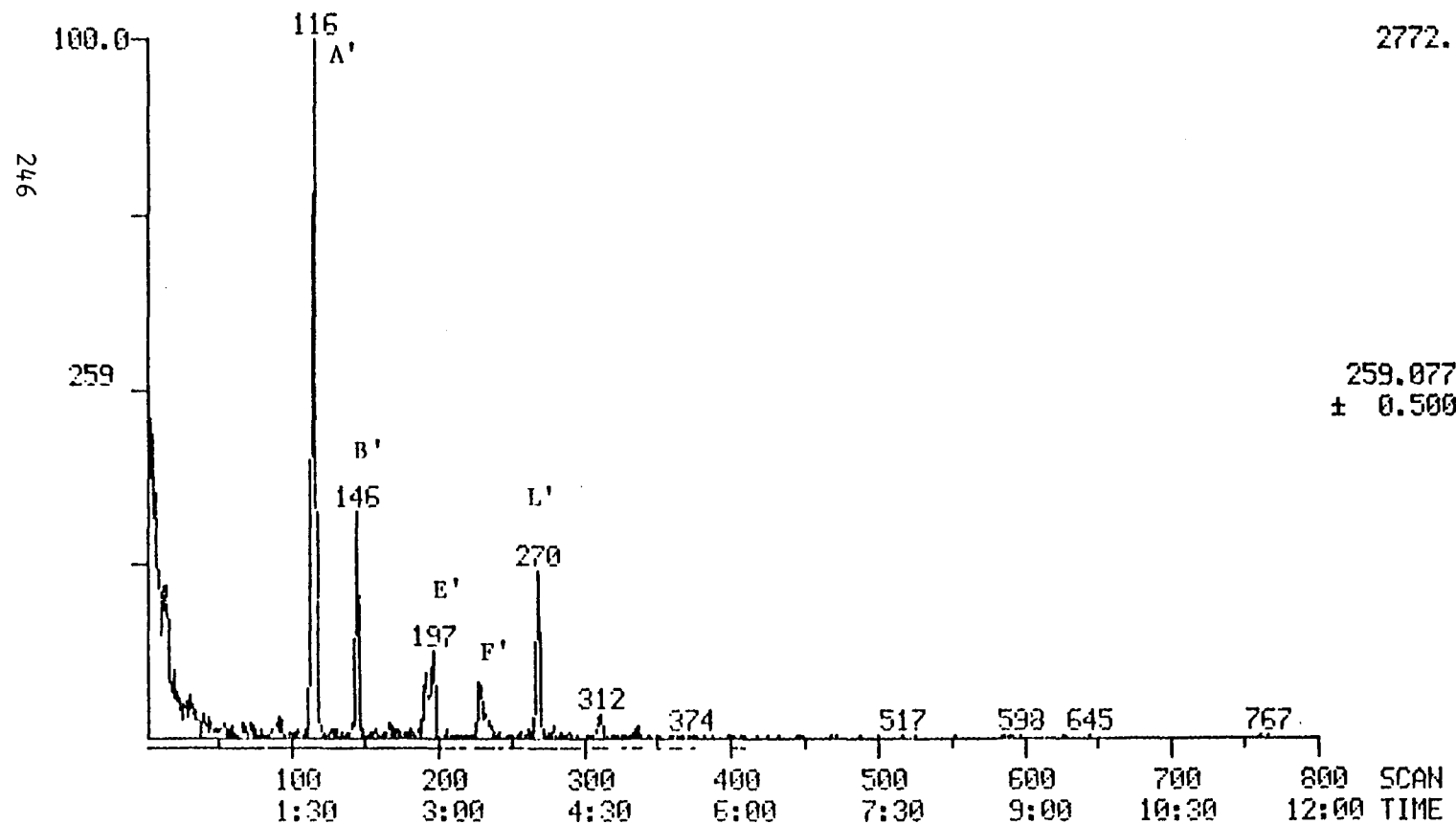


FIGURE 17

RIC
09/19/85 15:00:00
SAMPLE: 3013-044 SAT FRAC

DATA: R785218

SCANS 50 TO 1150

1200120.

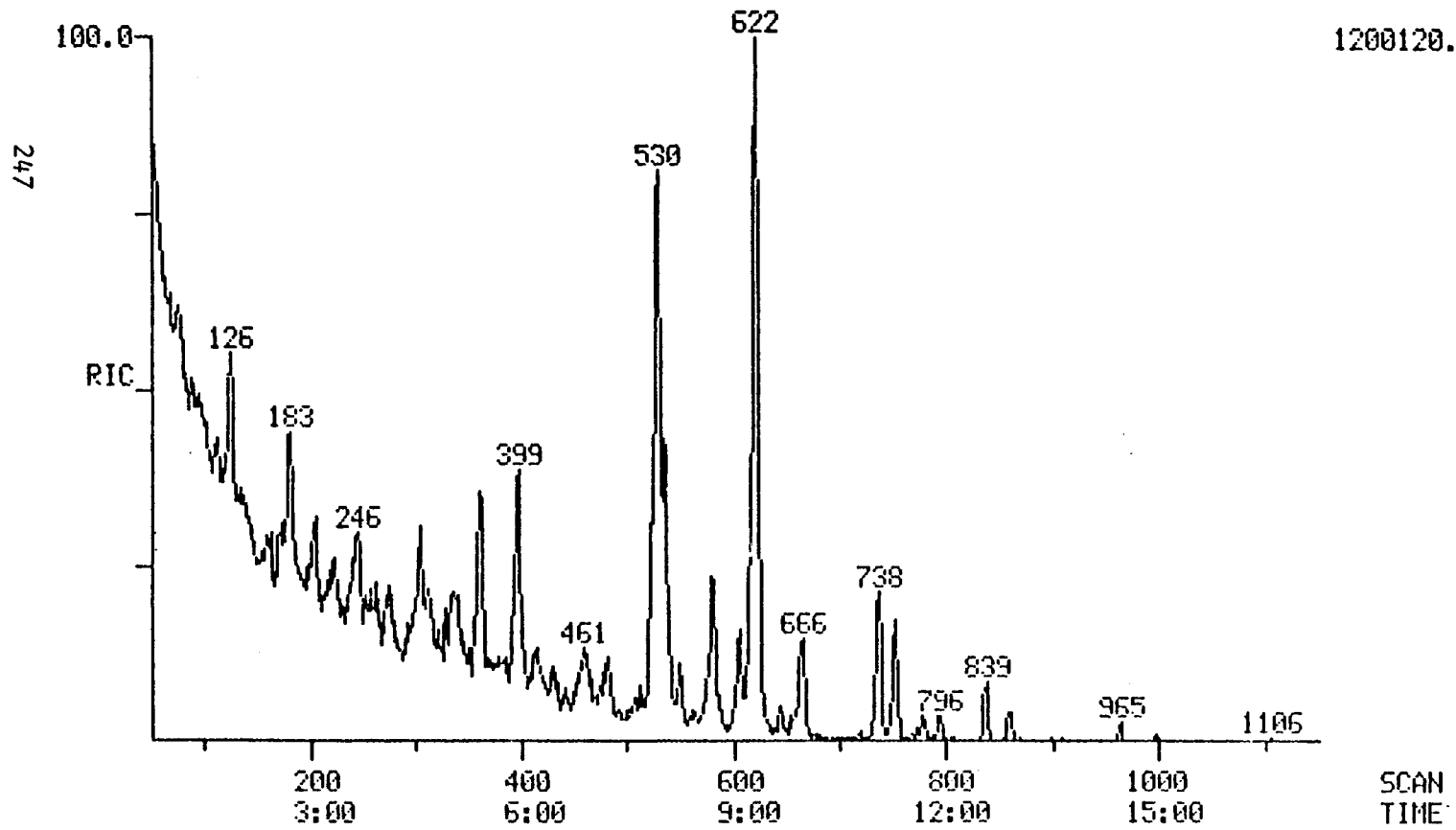


FIGURE 18

MASS CHROMATOGRAM
09/19/85 15:00:00
SAMPLE: 3013-044 SAT FRAC

DATA: R785218

SCANS 200 TO 1200

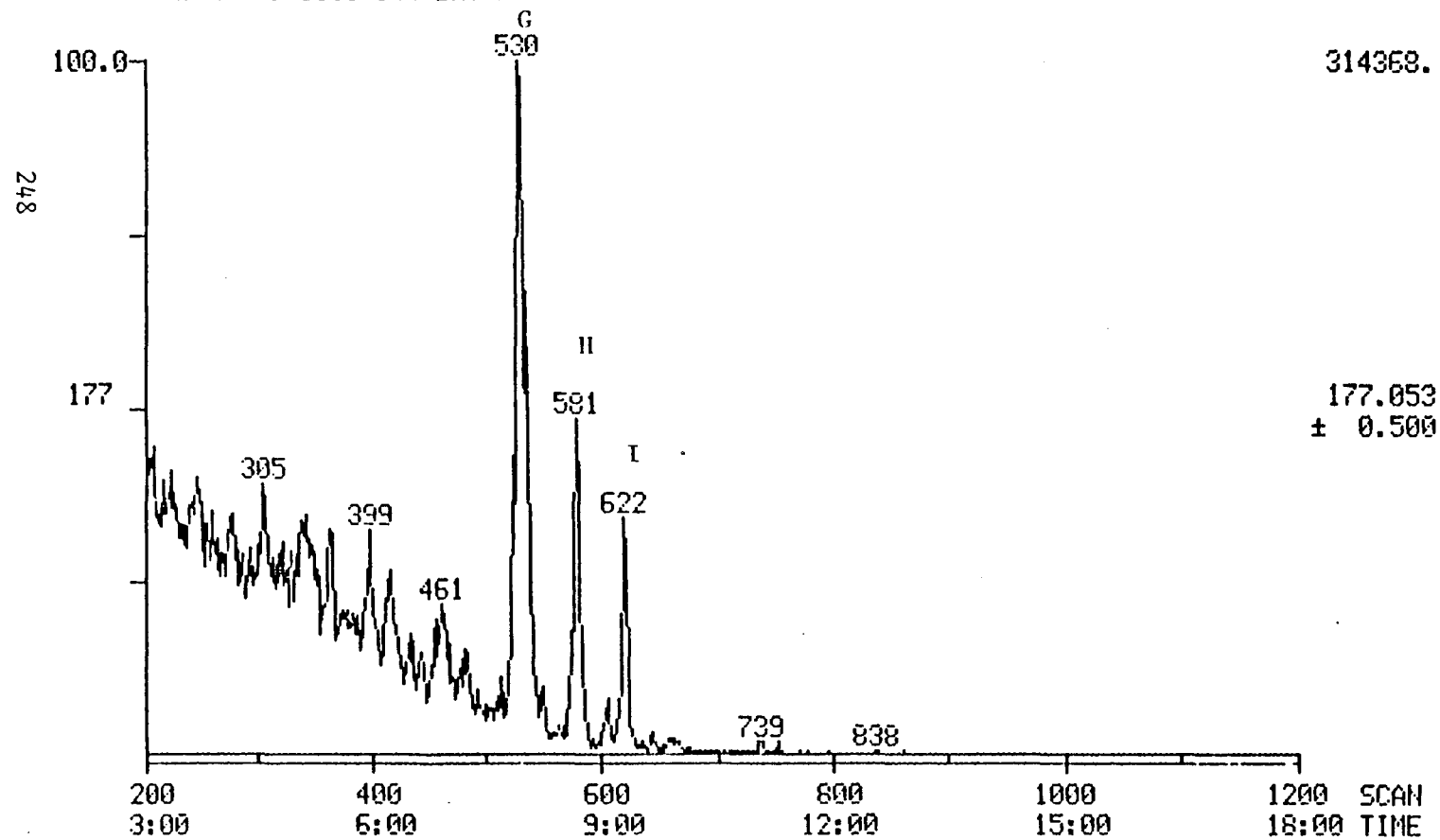


FIGURE 19

MASS CHROMATOGRAM
09/19/85 15:00:00
SAMPLE: 3013-044 SAT FRAC

DATA: R785218

SCANS 200 TO 1200

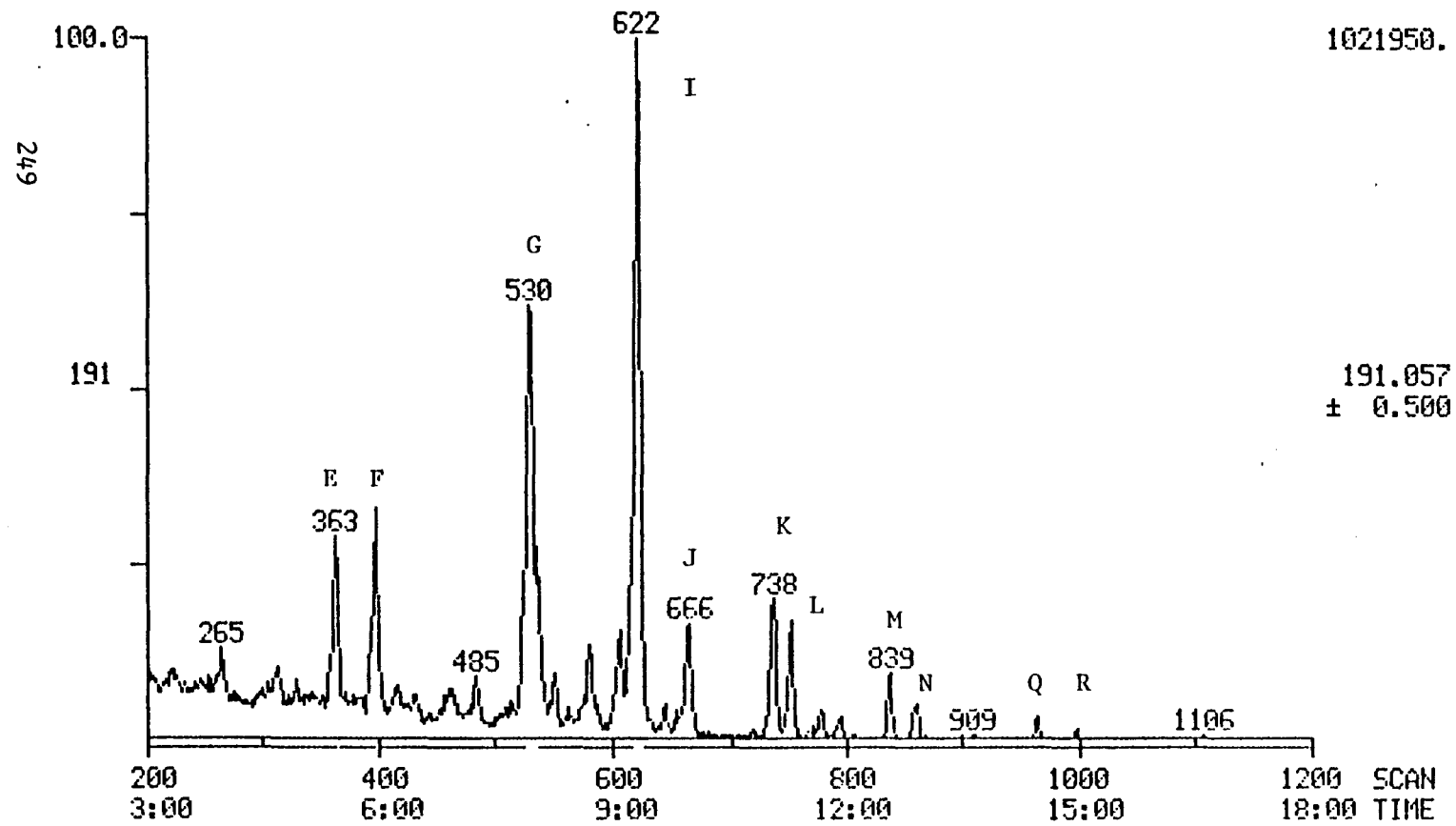


FIGURE 20

MASS CHROMATOGRAM
09/19/85 15:00:00
SAMPLE: 3013-044 SAT FRAC

DATA: R785218

SCANS 200 TO 1200

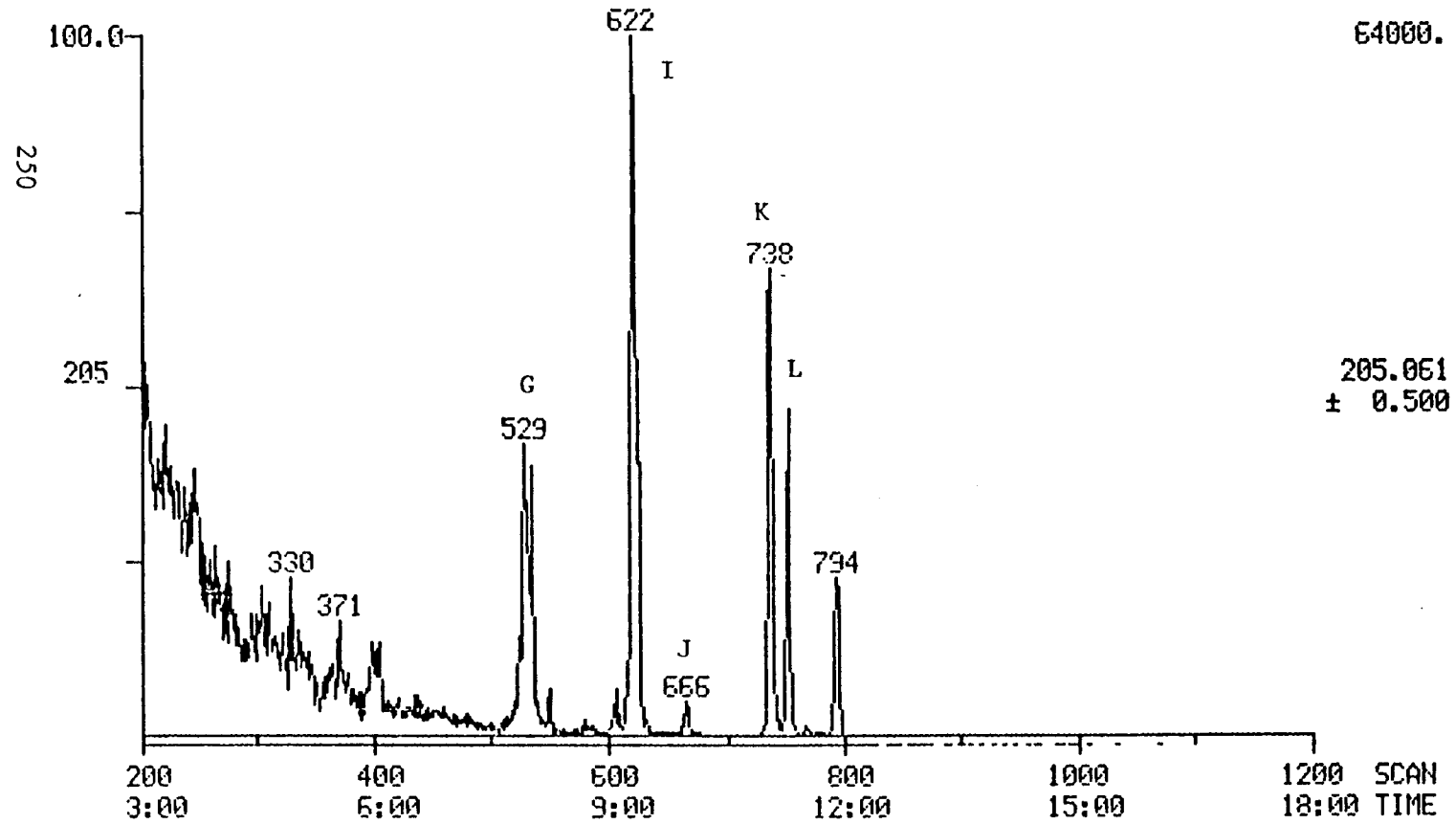


FIGURE 21

MASS CHROMATOGRAM
09/19/85 15:00:00
SAMPLE: 3013-044 SAT FRAC

DATA: R785218

SCANS 1 TO 800

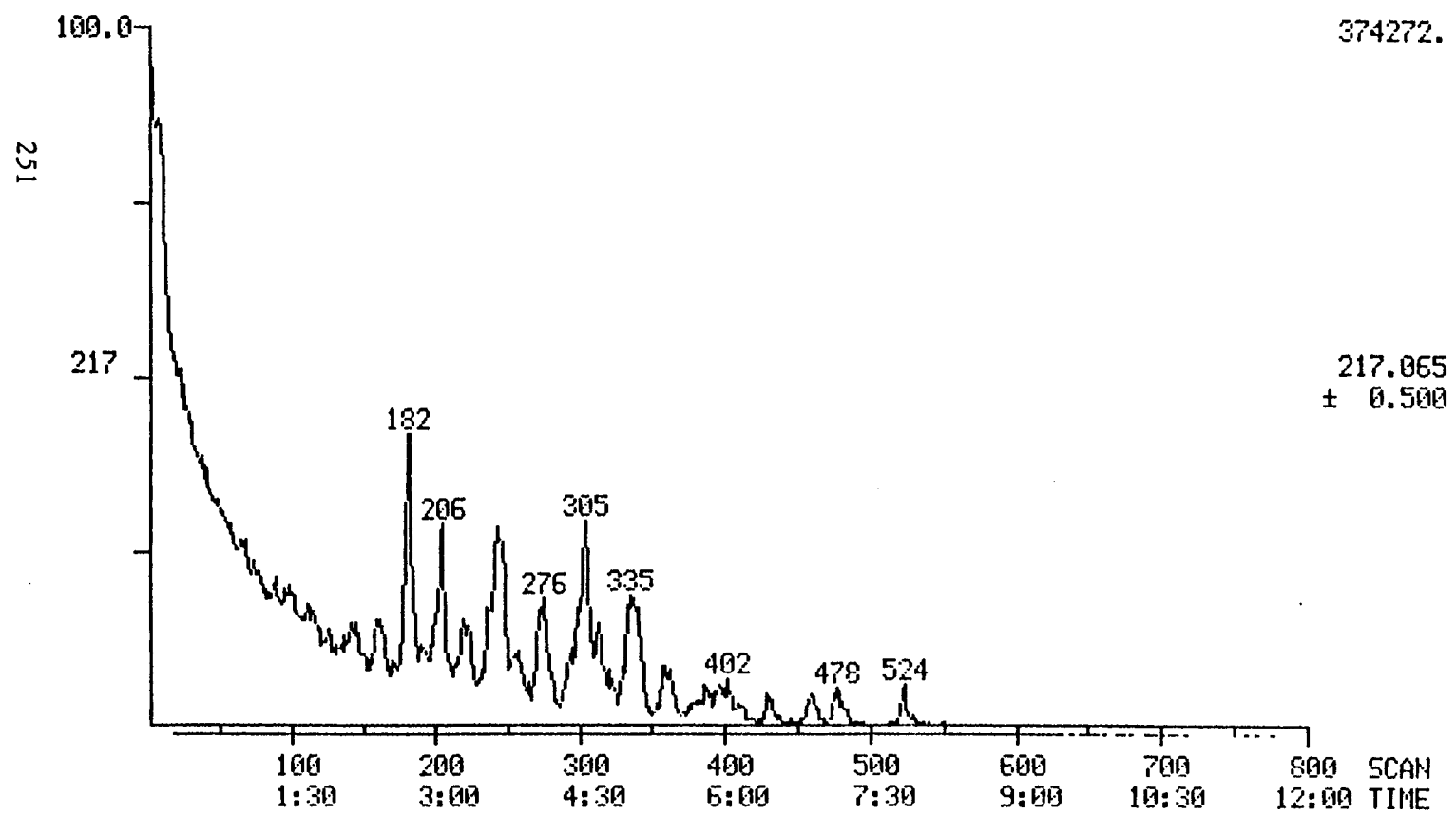


FIGURE 22

MASS CHROMATOGRAM
09/19/85 15:00:00
SAMPLE: 3013-044 SAT FRAC

DATA: R785218

SCANS 1 TO 800

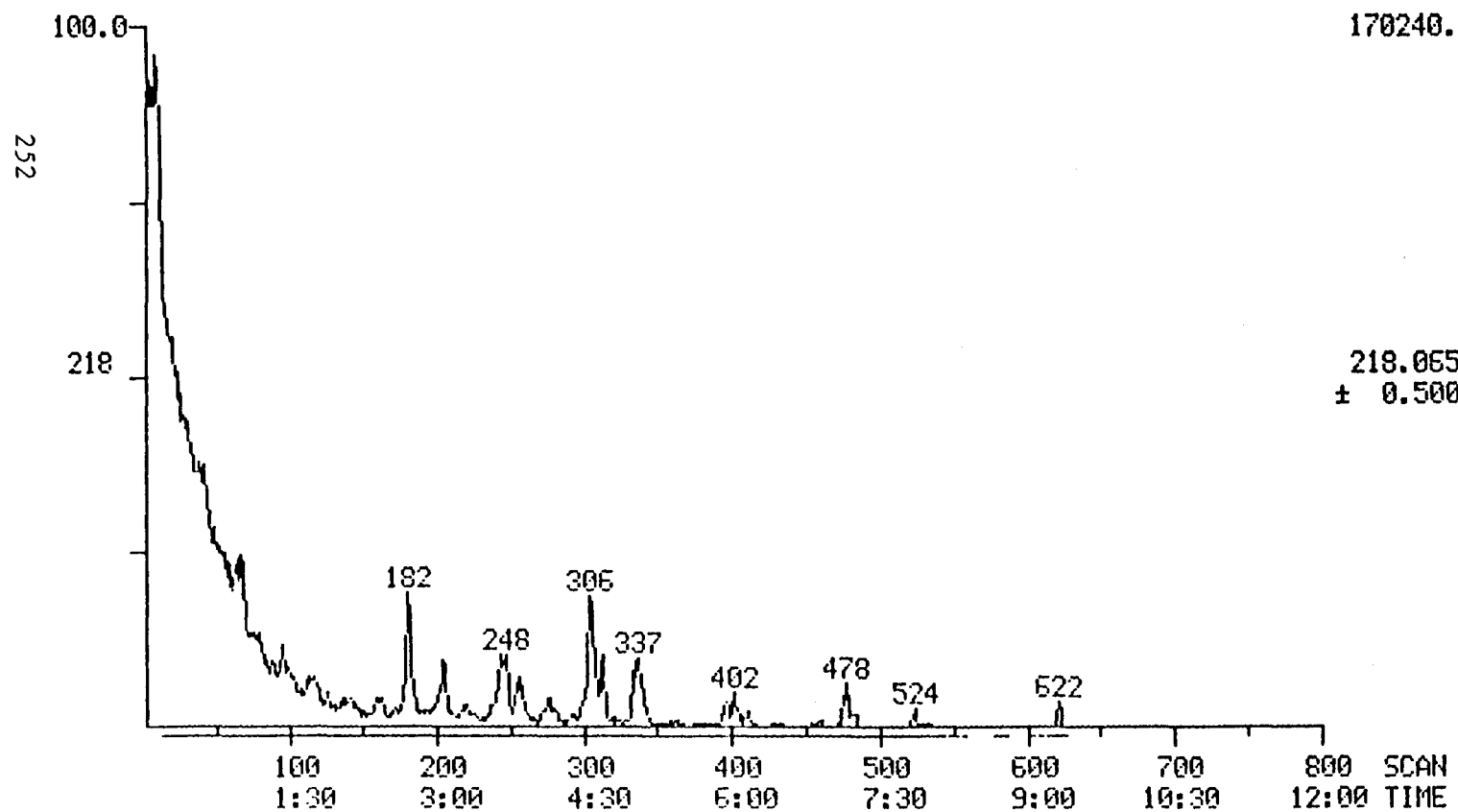


FIGURE 23

MASS CHROMATOGRAM
09/19/85 15:00:00
SAMPLE: 3013-044 SAT FRAC

DATA: R785218

SCANS 1 TO 800

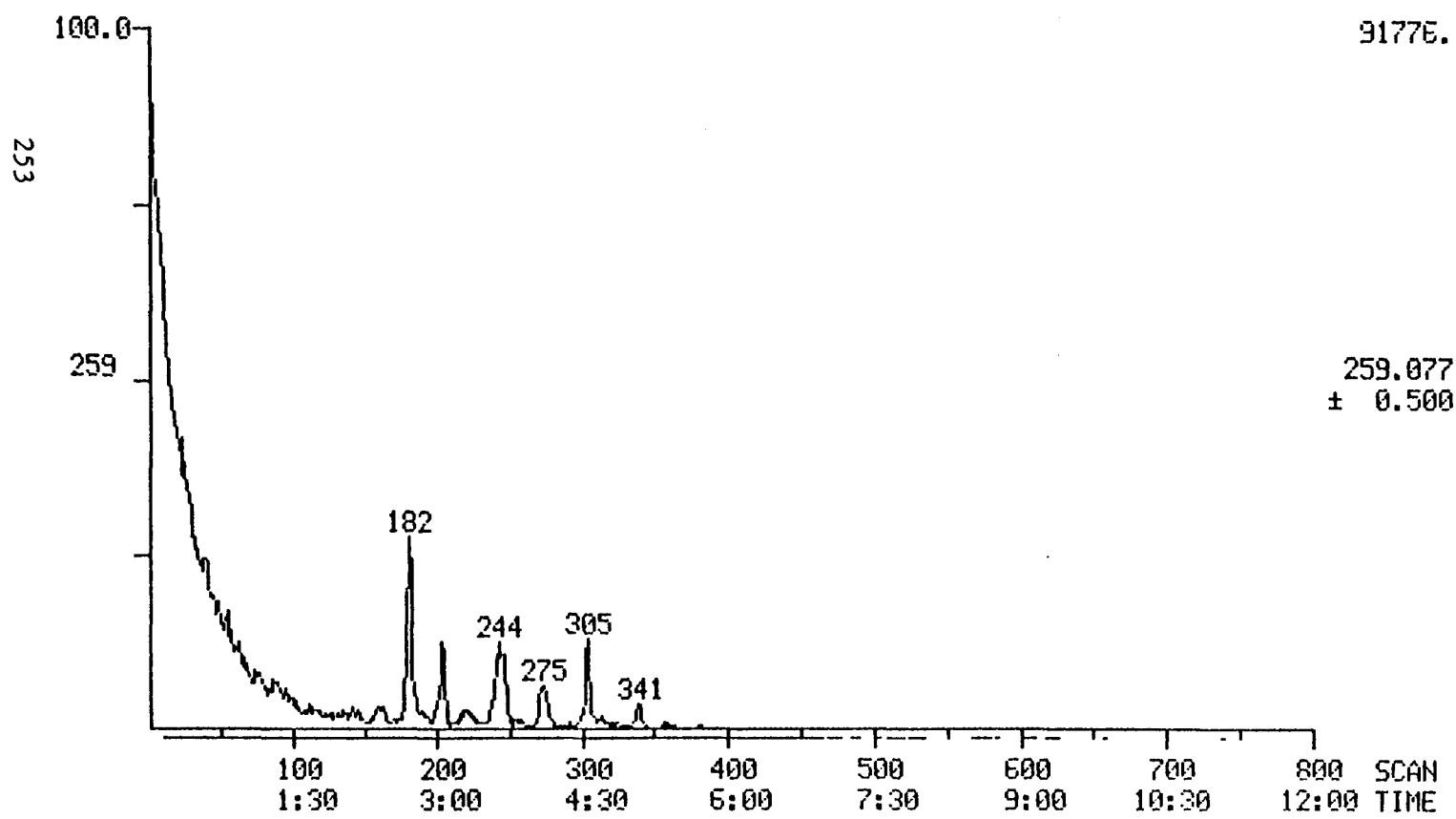


FIGURE 24

RIC
09/20/85 13:23:00
SAMPLE: 3013-041 MONO AROMATIC STERANES

DATA: R785217A

SCANS 1 TO 2144

527350.

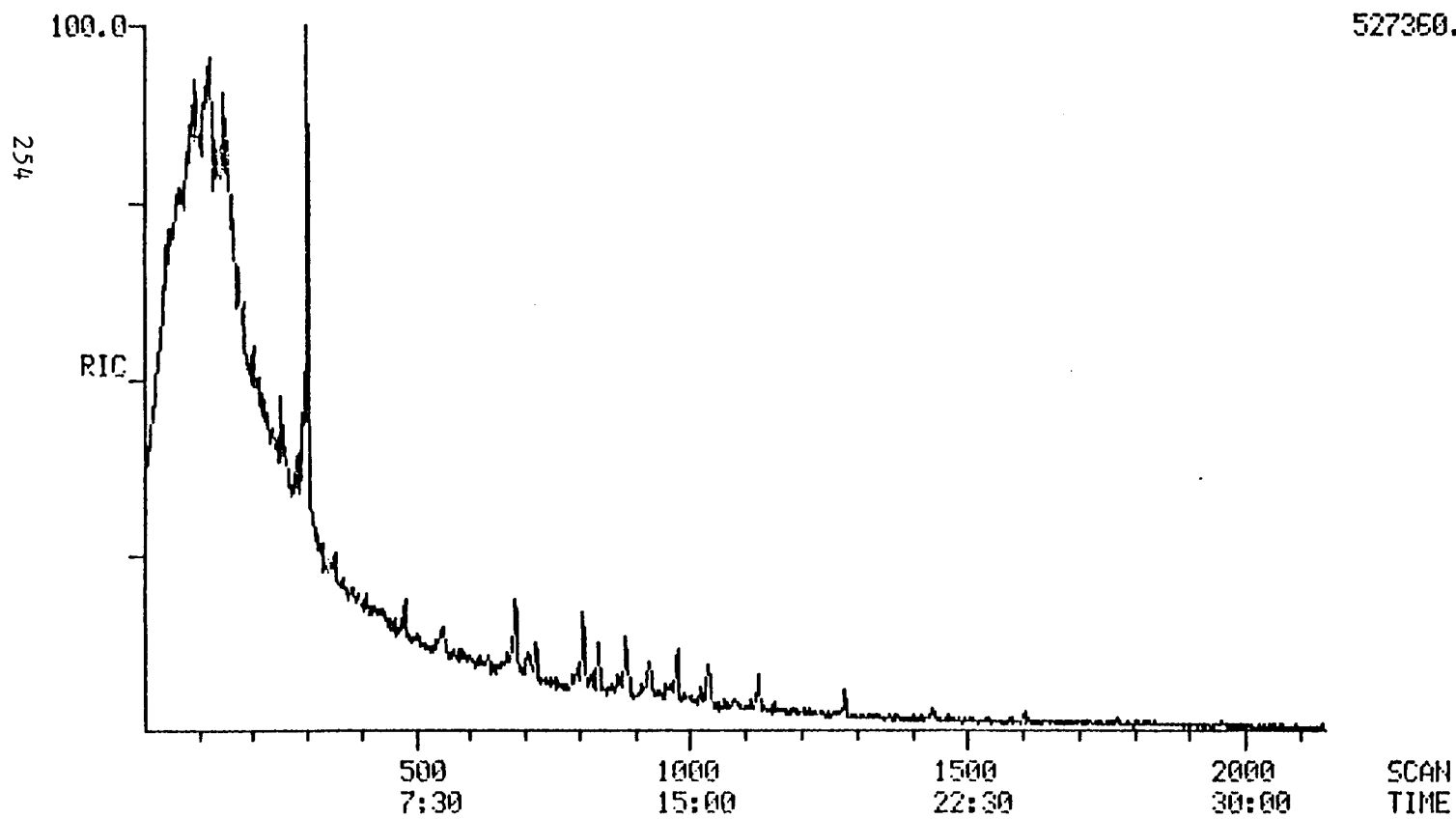


FIGURE 26

MASS CHROMATOGRAM
09/20/85 13:23:00
SAMPLE: 3013-041 MONO AROMATIC STERANES

DATA: R785217A

SCANS 144 TO 1216

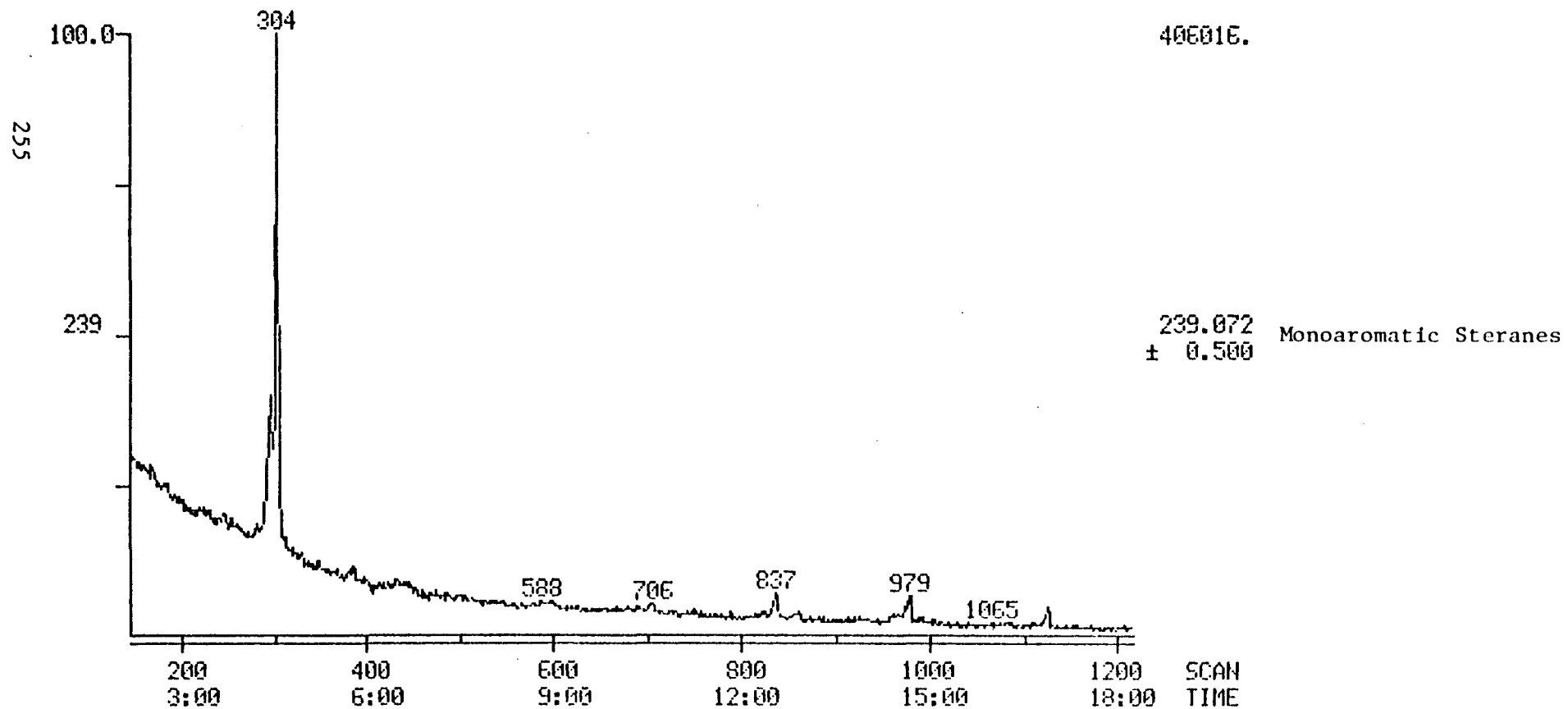


FIGURE 27

MASS CHROMATOGRAM

DATA: R785217A

SCANS 1216 TO 2144

09/20/85 13:23:00

SAMPLE: 3013-041 MONO AROMATIC STERANES

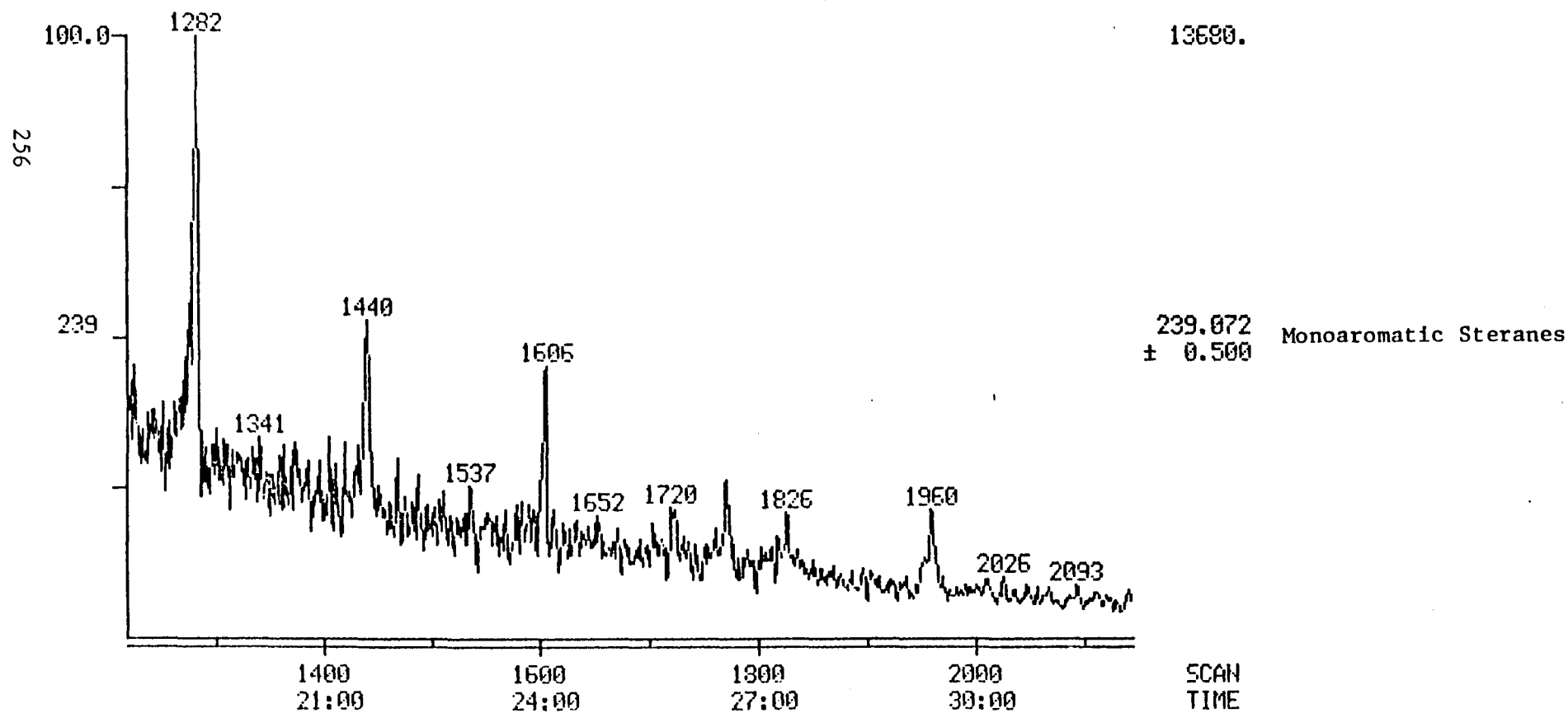


FIGURE 28

MASS CHROMATOGRAM
09/20/85 13:23:00
SAMPLE: 3013-041 MONO AROMATIC STERANES

DATA: R785217A

SCANS 1216 TO 2144

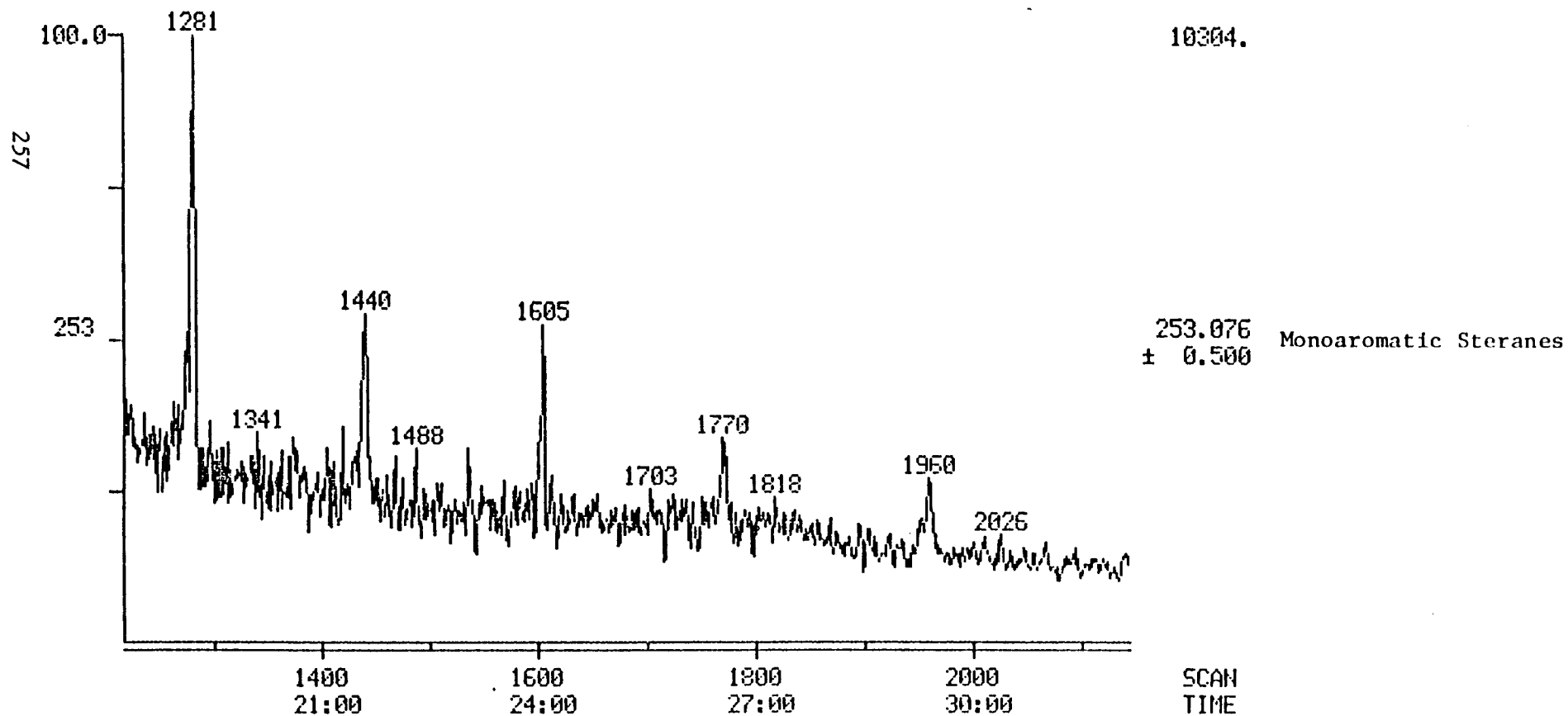


FIGURE 29

MASS CHROMATOGRAM
09/20/85 13:23:00
SAMPLE: 3013-041 MONO AROMATIC STERANES

DATA: R785217A

SCANS 144 TO 1216

135424.

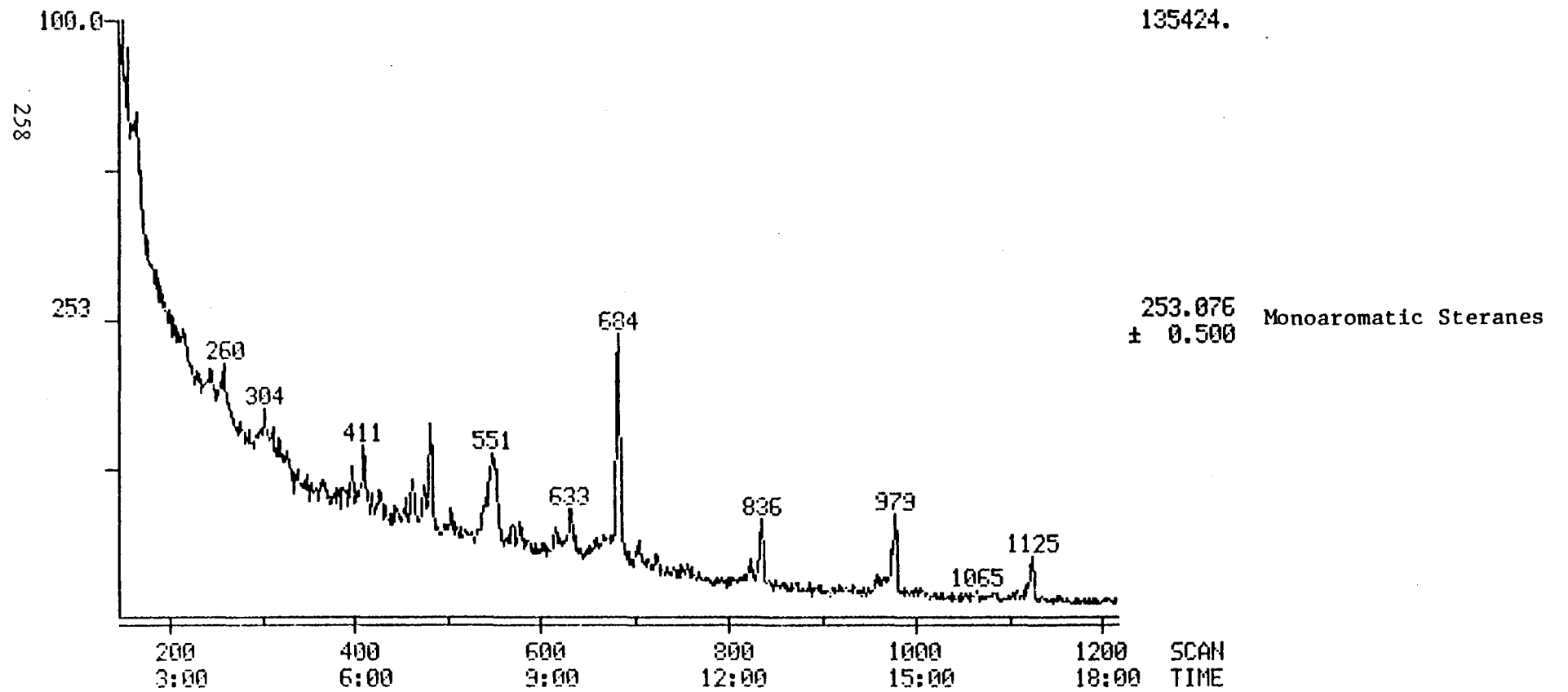


FIGURE 30

MASS CHROMATOGRAM
09/20/85 13:23:00
SAMPLE: 3013-041 MONO AROMATIC STERANES

DATA: R785217A

SCANS 144 TO 1216

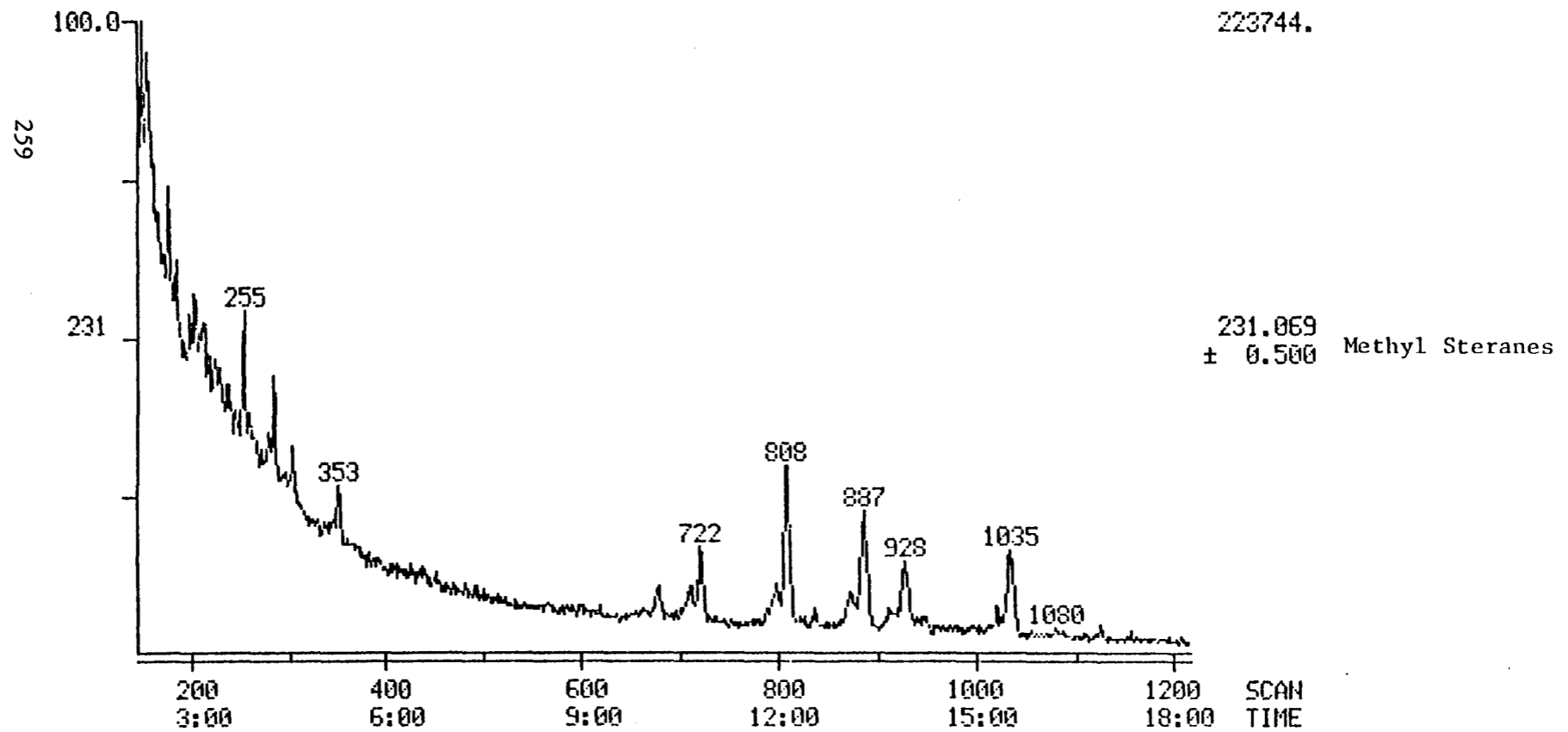


FIGURE 31

MASS CHROMATOGRAM
09/20/85 13:23:00
SAMPLE: 3013-041 MONO AROMATIC STERANES

DATA: R785217A

SCANS 1216 TO 2144

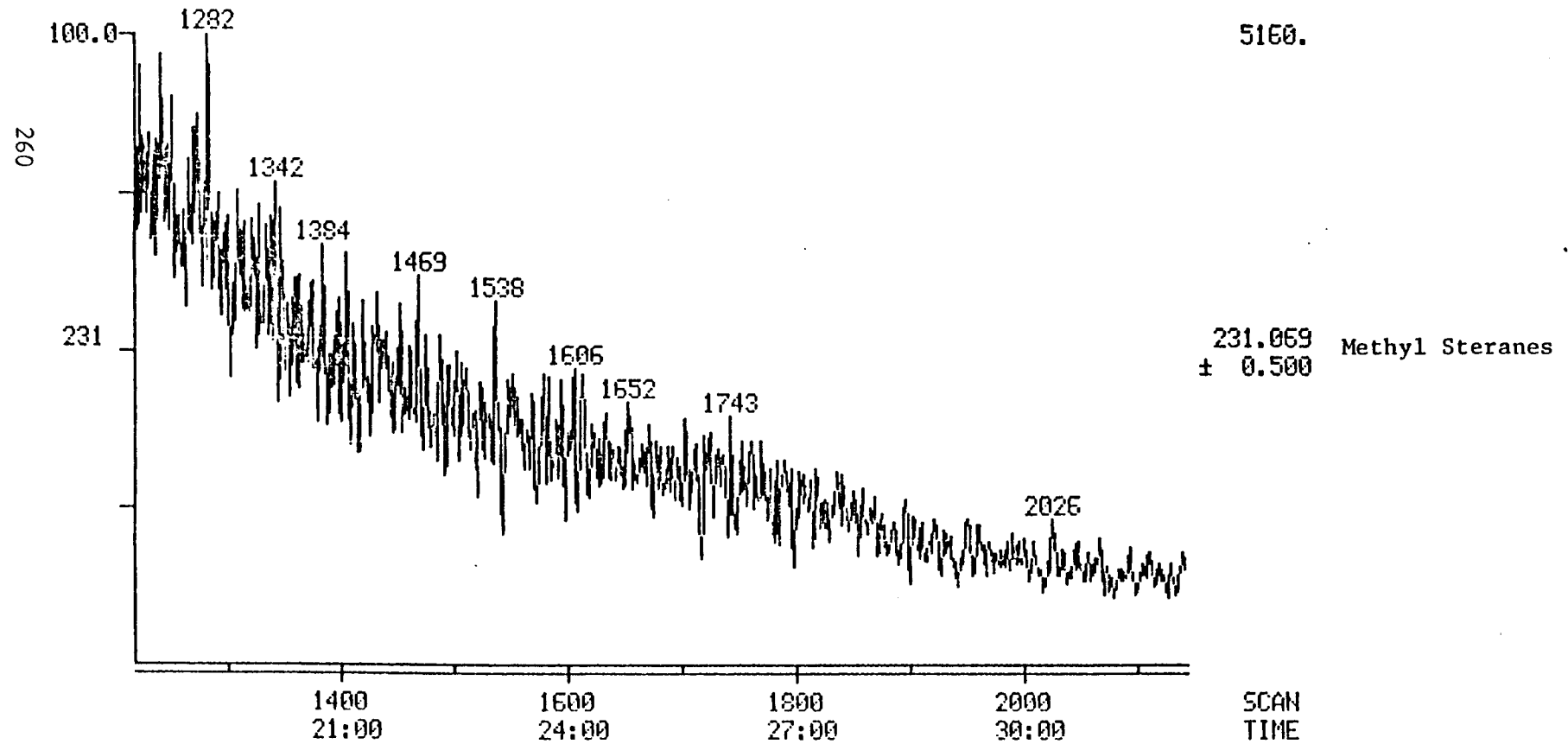


FIGURE 32

RIC
09/20/85 14:53:00
SAMPLE: 3013-044 MONO AROMATIC STERANES

DATA: R785220A

SCANS 1 TO 2645

2756600.

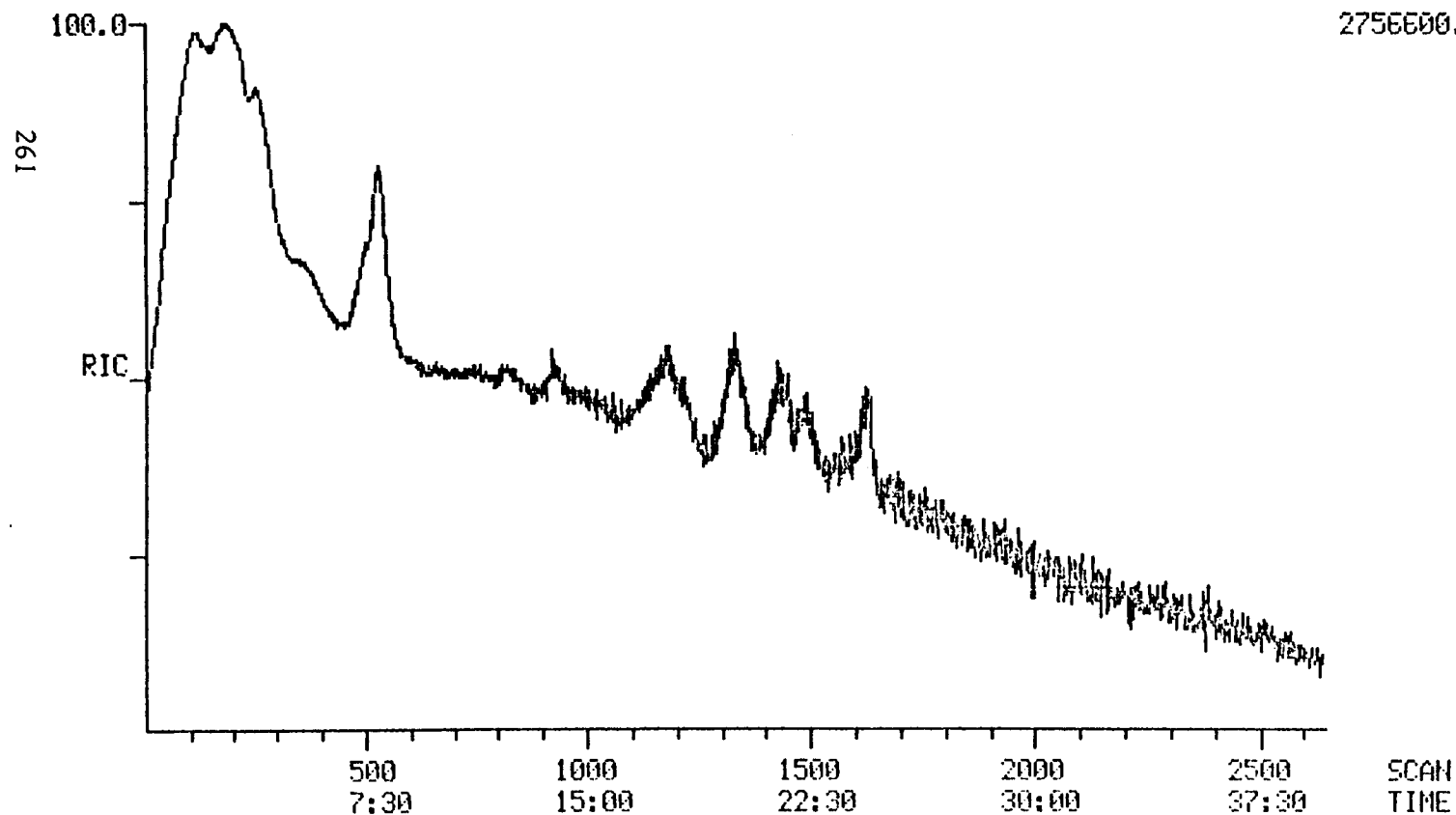


FIGURE 33

MASS CHROMATOGRAM
09/20/85 14:53:00
SAMPLE: 3013-044 MONO AROMATIC STERANES

DATA: R785220A

SCANS 1 TO 1322

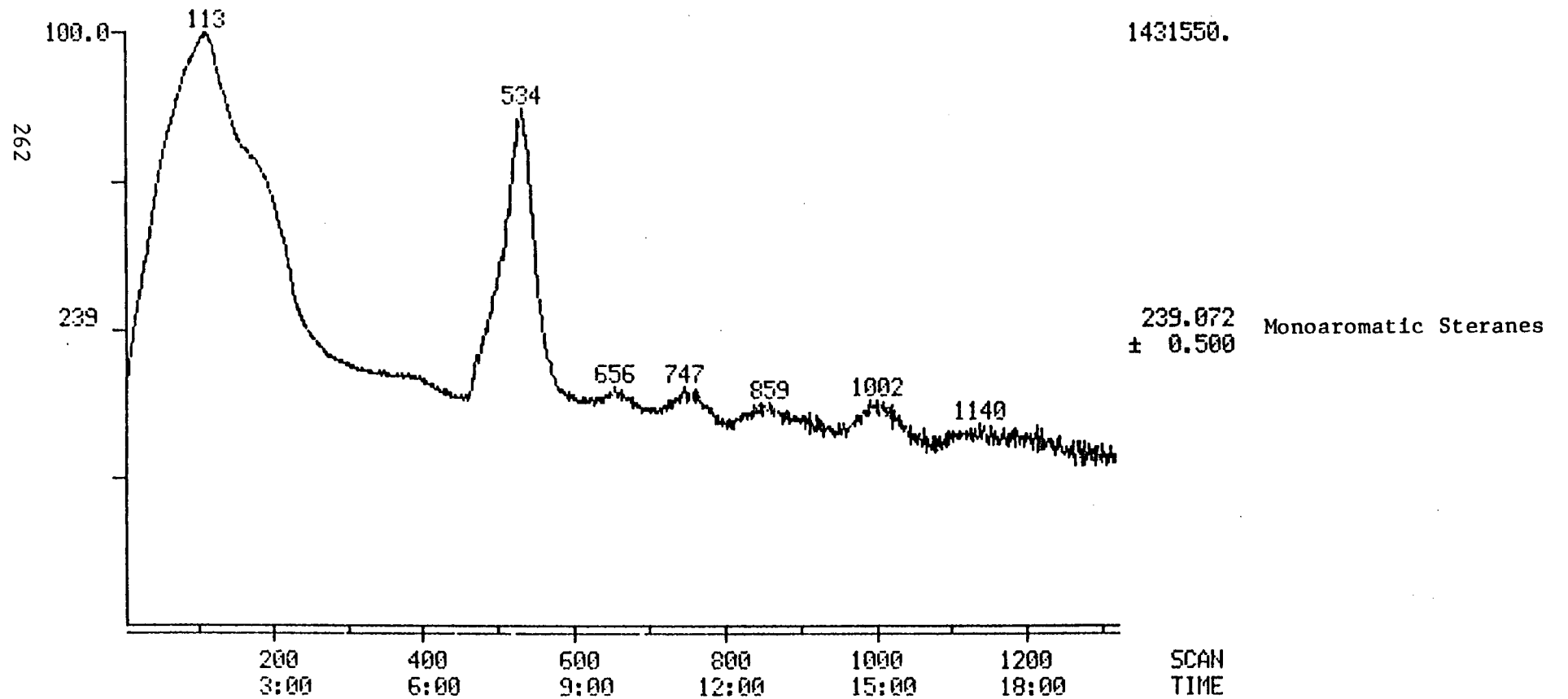


FIGURE 34

MASS CHROMATOGRAM
09/20/85 14:53:00
SAMPLE: 3013-044 MONO AROMATIC STERANES

DATA: R785220A

SCANS 1322 TO 2645

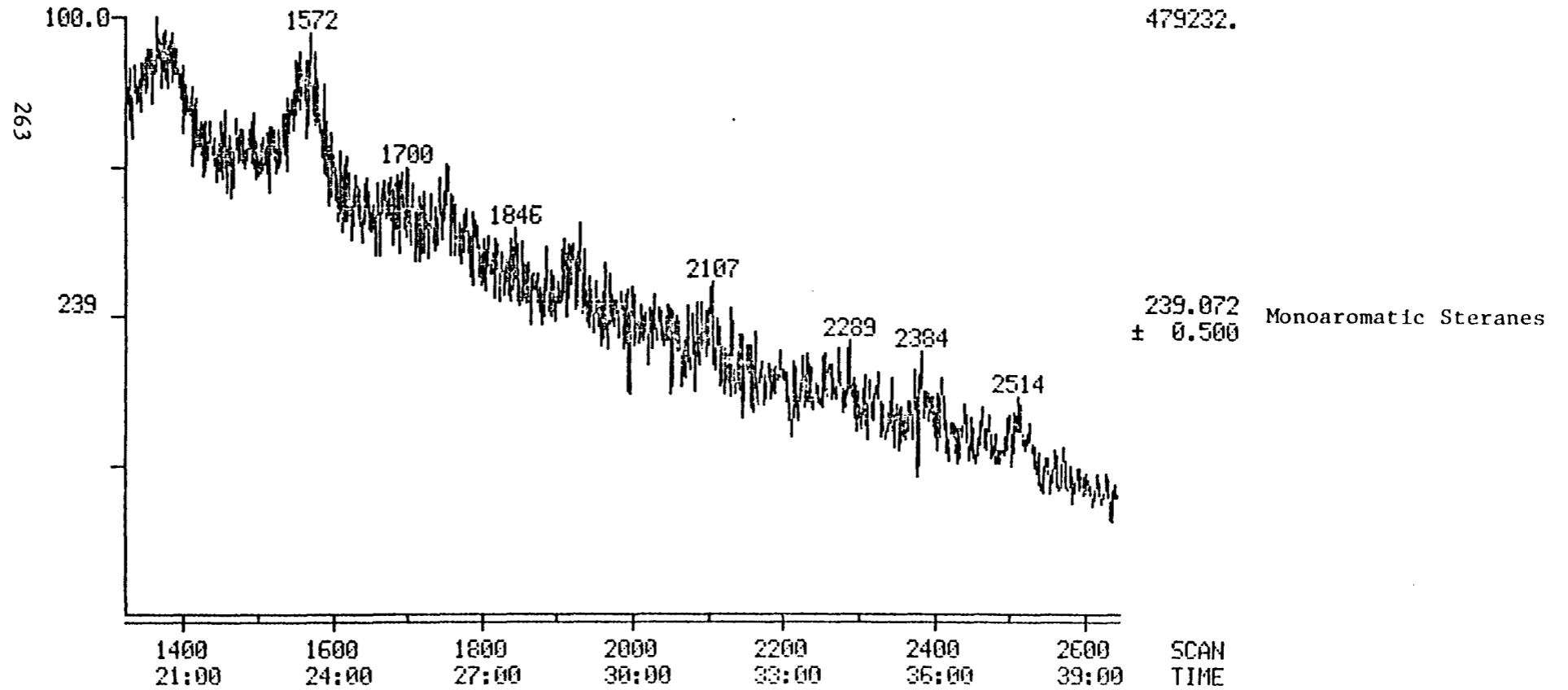
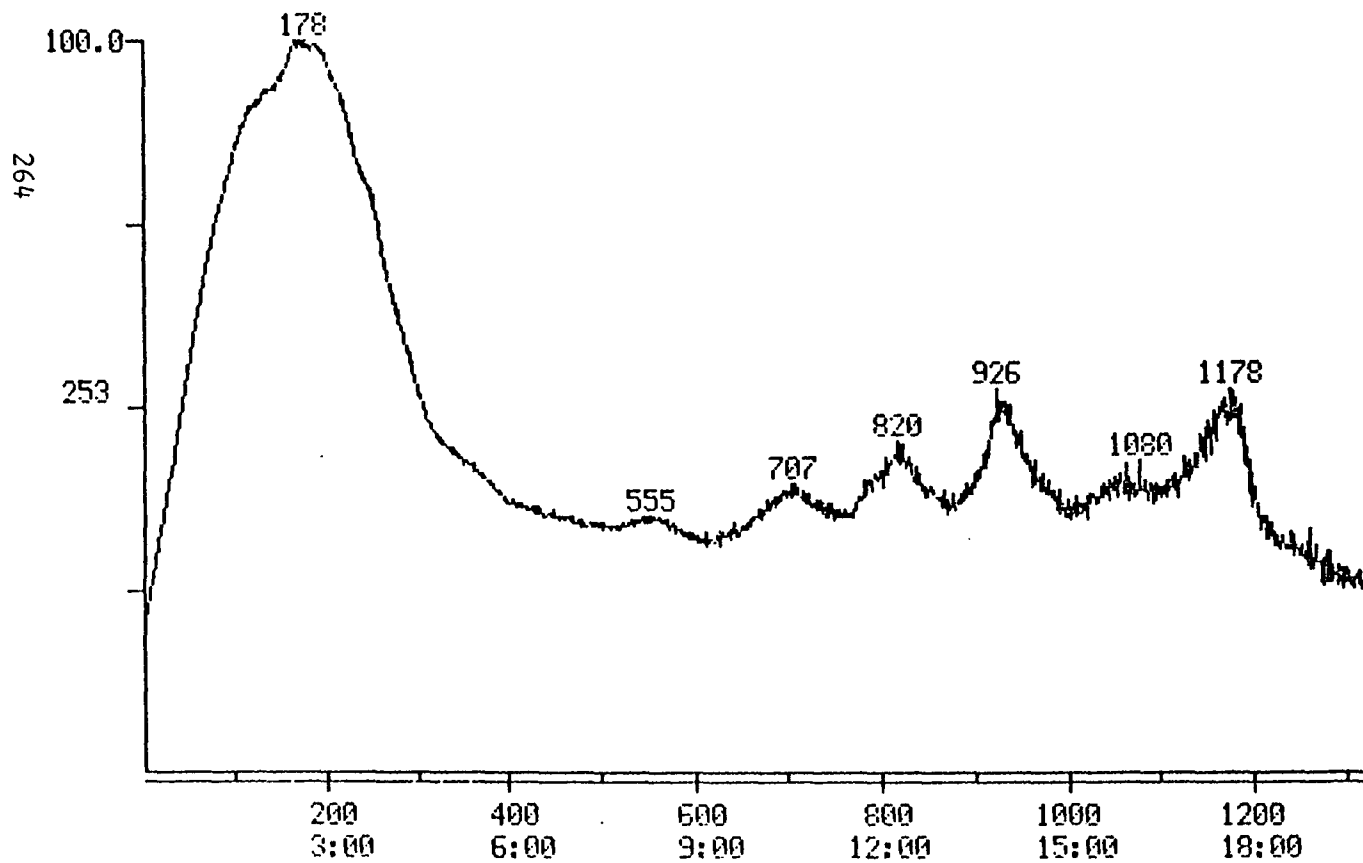


FIGURE 35

MASS CHROMATOGRAM
09/20/85 14:53:00
SAMPLE: 3013-044 MONO AROMATIC STERANES

DATA: R785220A

SCANS 1 TO 1322



1124350.

253.076 Monoaromatic Steranes
± 0.500

FIGURE 36

MASS CHROMATOGRAM
09/20/85 14:53:00
SAMPLE: 3013-044 MONO AROMATIC STERANES

DATA: R785220A

SCANS 1322 TO 2645

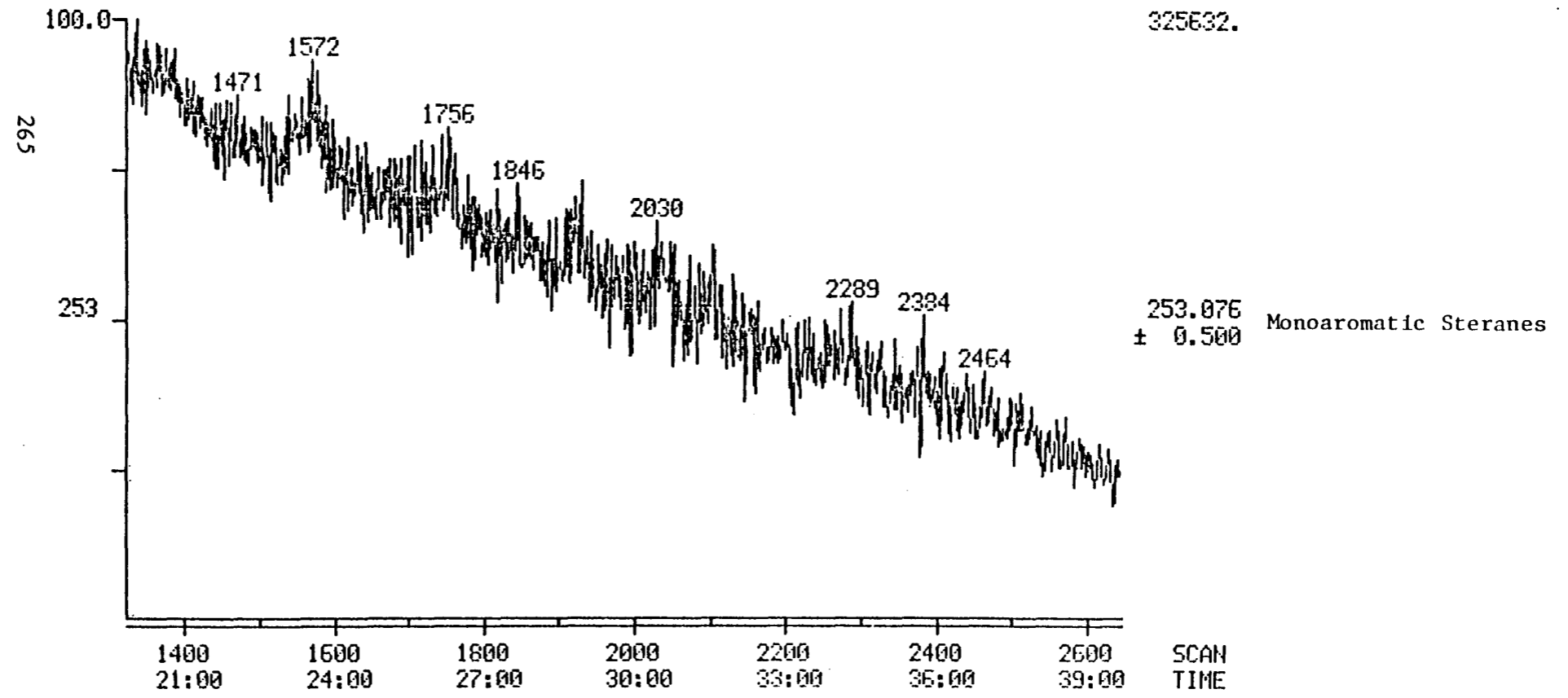


FIGURE 37

MASS CHROMATOGRAM
09/20/85 14:53:00
SAMPLE: 3013-044 MONO AROMATIC STERANES

DATA: R785220A

SCANS 1 TO 1322

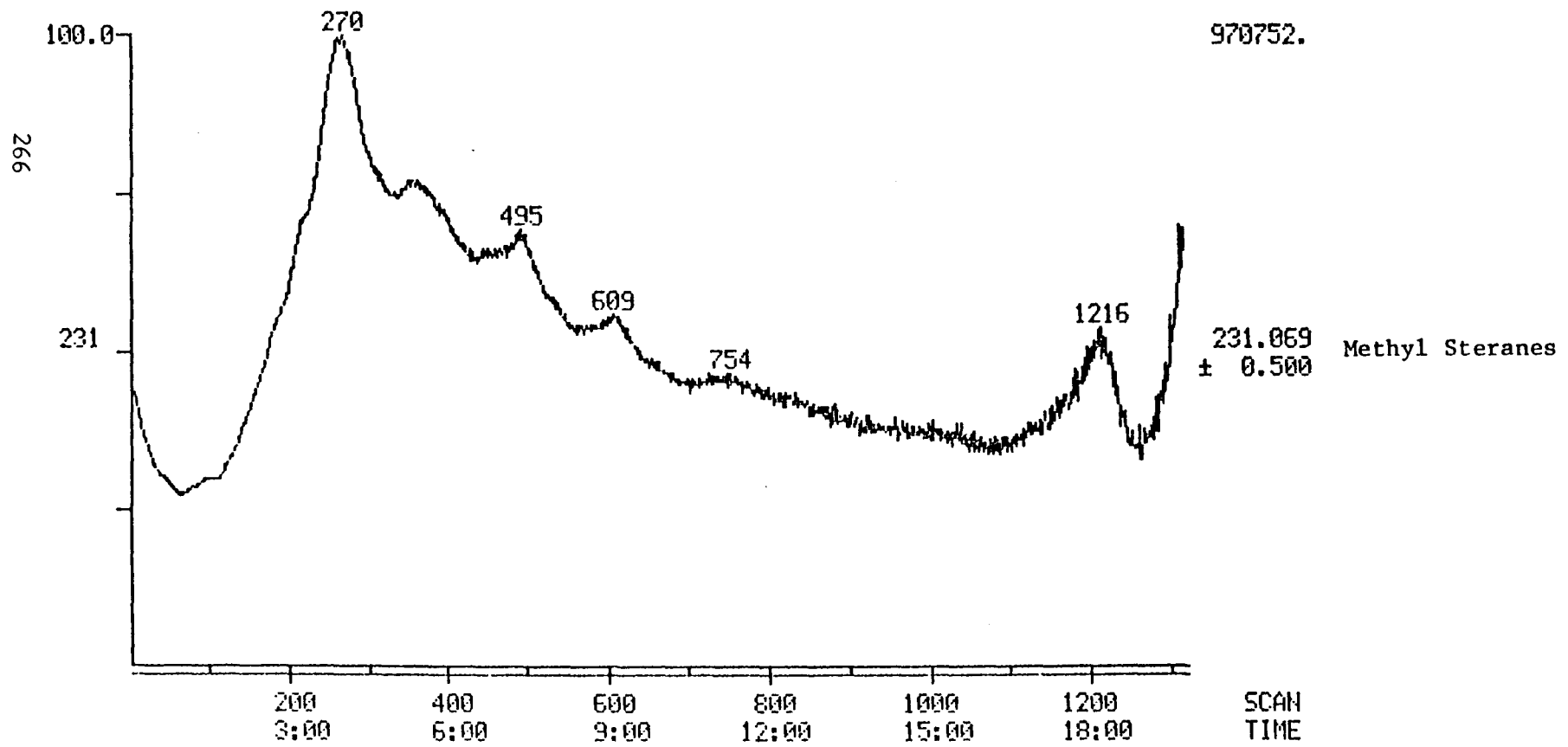


FIGURE 38

MASS CHROMATOGRAM
09/20/85 14:53:00
SAMPLE: 3013-044 MONO AROMATIC STERANES

DATA: R785220A

SCANS 1322 TO 2645

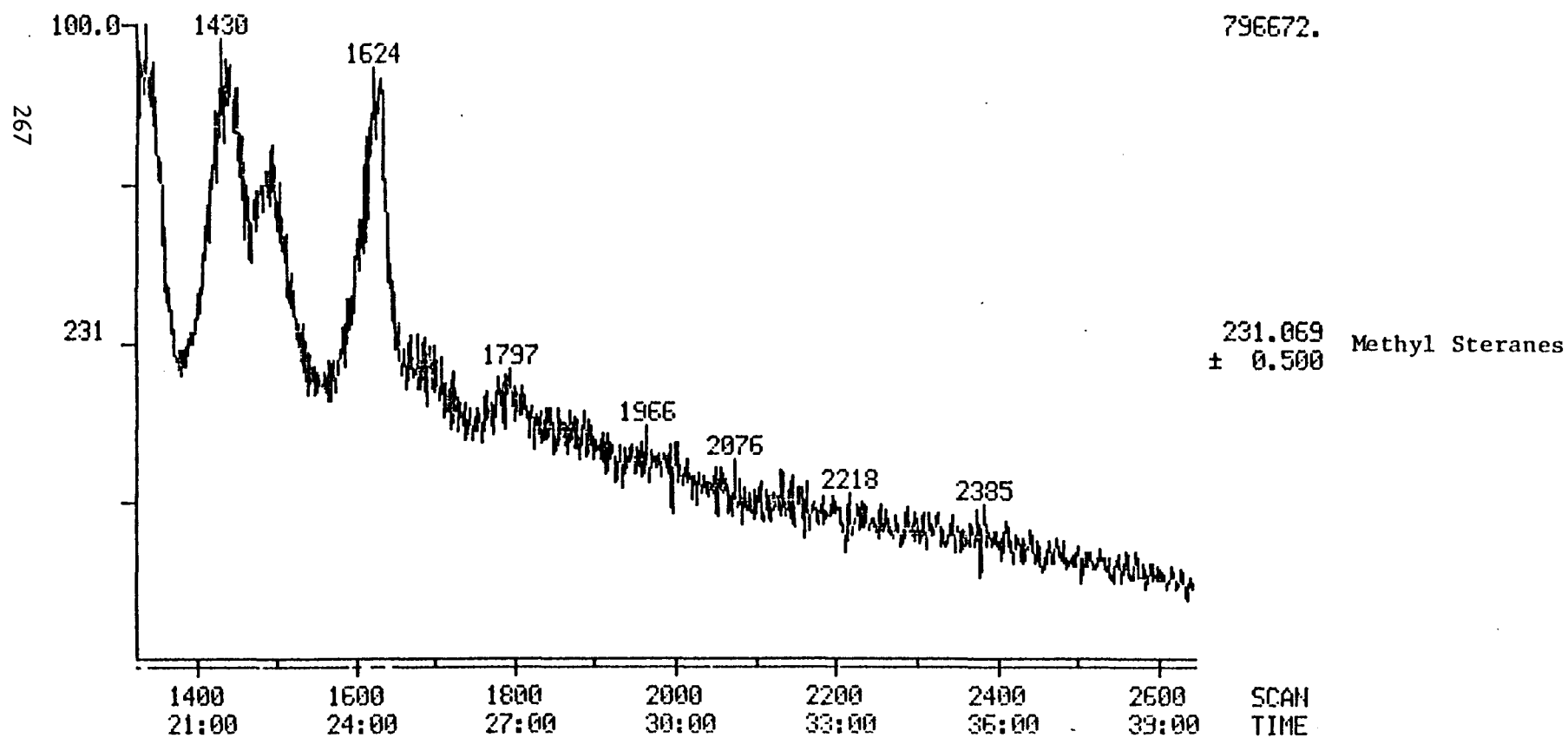


FIGURE 39

